Fundamental studies of the PVD technique.

IVES, Malcolm.

FUNDAMENTAL STUDIES OF THE PVD TECHNIQUE

Malcolm Ives

A thesis submitted in partial fulfilment of the
requirements of
Sheffield Hallam University
for the degree of Doctor of Philosophy

September 1994

Collaborating organisations:
Science and Engineering Research Council
Rolls-Royce plc.

ABSTRACT
Fundamental Studies of the PVD Technique

A study and comparison of two commercially available and competitive physical vapour deposition techniques has been made. Titanium nitride (the most widely used hard and decorative coating) has been deposited by both steered arc and the new Arc Bond Sputter (ABS) magnetron technique under a range of deposition conditions. The coatings have subsequently been analysed by a variety of methods and the results reported here.

The steered arc technique has been identified as the better technique for everyday ease of use in producing mononitride and monocarbide coatings with good batch uniformity and reproducibility in terms of composition and microstructure. However, for versatility the ABS magnetron technique allows the possibility to vary multiple parameters and hence change coating properties at will, albeit with some difficulty to maintain stable and reproducible operation. In this respect, plasma uniformity is discussed and problems with water vapour contamination and gas flow regulation are highlighted and possible solutions suggested.

The coating-substrate interface region is considered, and the merits of metallic interlayers and arc etching are compared. An interlayer achieves good adhesion only at an optimum thickness as confirmed in this work. The good adhesion afforded by the arc etch phase of both processes is addressed and the ion-surface interactions modelled using commercially available computer software. The improvement in adhesion on high speed steel is explained by sputtering of the substrate matrix leaving hard carbide particles standing proud of the surface. When deposition takes place, the carbides mechanically key the coating to the substrate surface, and also possibly act as physical blocks to interfacial crack propagation.

A theoretical contribution to the explanation of preferred crystallographic orientation during coating deposition is proposed derived from experimental results, surface physics and semiconductor growth theory. This attempts to explain the flexibility of sputtering techniques to produce a wide range of orientations, and the reasons why arc evaporation almost always produces {111} orientated coatings.

Finally, a consideration of a comparatively new analytical technique (Glow Discharge Optical Emission Spectroscopy) to the application of PVD coatings evaluation is addressed. The speed and versatility of this technique makes it strategically important in the future research, development and quality control of thin film production.

CONTENTS

CHAPTER 1 INTRODUCTION 1

1.1 Surface Engineering

1.2 Chemical Vapour Deposition

1.3 Physical Vapour Deposition

CHAPTER 2 LITERATURE REVIEW 7

2.1 **Evaporative Techniques** 7

2.1.1 Resistive Heating Evaporation

2.1.2 Inductive Heating Evaporation

2.1.3 Electron-beam Evaporation

2.1.4 Cathodic Arc Evaporation

2.1.4.1 Random Arc

2.1.4.2 Macroparticles

2.1.4.3 Steered Arc

2.2 **Sputtering Techniques** 16

2.2.1 Ion Beam Sputtering

2.2.2 Glow Discharge - Diode Sputtering

2.2.3 Triode Sputtering

2.2.4 Glow Discharge Plasma

2.2.5 Radio-Frequency Sputtering

2.2.6 Magnetron Sputtering

2.2.6.1 Unbalanced Magnetron

2.2.6.2 Closed-Field Systems

2.3 **Coating Deposition** 28

2.3.1 Surfaces and Nucleation

2.3.2 Sputter Etching

2.3.3 Interlayers

2.3.4 Coating Growth

2.3.4.1 Structure-Zone-Models

2.3.5 Low Energy Ion Irradiation

2.3.5.1 Radio-Frequency Biasing

2.3.5.2 Biasing Edge Effects

2.3.5.3 Residual Stress

2.3.6 Reactive Deposition

2.3.6.1 Cathode Poisoning

2.4 **Evaluation Techniques** 41
2.4.1 Colourimetry
2.4.2 Surface Roughness Profiling
2.4.3 Coating Thickness Calotest
2.4.4 X-Ray Fluorescence Thickness Test
2.4.5 Microhardness Test
2.4.6 Rockwell Indentation Adhesion Test
2.4.7 Scratch Adhesion Test
2.4.8 X-Ray Diffraction Analysis
2.4.9 X-Ray Photoelectron Spectroscopy
2.4.10 Scanning Electron Microscopy
2.4.11 Transmission Electron Microscopy
2.4.12 Glow Discharge Spectroscopy

CHAPTER 3 EXPERIMENTAL TECHNIQUE 64
3.1 Sample Preparation for Coating
3.2 Deposition by Steered Arc Evaporation
3.2.1 Process Parameters / Deposition Conditions
3.3 Deposition by ABS Magnetron Sputtering
3.3.1 Process Parameters / Deposition Conditions
3.4 Sample Preparation for Analysis
3.4.1 Additional Notes on XTEM Sample Preparation
3.5 Analysis Techniques

CHAPTER 4 RESULTS 78
4.1 **Parameter Study** 78
4.1.1 Deposition Conditions and Plasma Uniformity
4.1.2 Colour
4.1.3 Surface Roughness and Droplets
4.1.4 Thickness / Deposition Rate
4.1.5 Microhardness and Ultra-microhardness
4.1.6 Adhesion
4.1.7 Structure
4.1.7.1 Scanning Electron Microscopy
4.1.7.2 X-Ray Diffraction
4.2 **GDOES Technique** 107
4.2.1 Composition
4.2.2 Coating Thickness

4.2.3 Sputter Crater Shapes
4.2.4 TiN Calibration
4.2.5 R.F. Depth Profile
4.3 **Interface Region** 119
4.3.1 Glow Discharge Spectroscopy
4.3.2 Scanning Transmission Electron Microscopy
4.3.3 TRIM Program Calculations
4.3.4 Sputter Depth Calculation
4.3.5 X-Ray Photoelectron Spectroscopy
4.3.6 Adhesion vs Interlayer Thickness

CHAPTER 5 DISCUSSION 129
5.1 **Parameter Study** 129
5.1.1 Process Operation
5.1.1.1 Deposition Conditions and Plasma Uniformity
5.1.2 Testing and Analysis
5.1.2.1 Colour
5.1.2.2 Surface Roughness and Droplets
5.1.2.3 Thickness / Deposition Rate
5.1.2.4 Microhardness and Ultra-microhardness
5.1.2.5 Adhesion
5.1.2.6 Structure
5.1.2.6.1 Scanning Electron Microscopy
5.1.2.6.2 X-Ray Diffraction
5.2 **GDOES Technique** 141
5.2.1 Coating Composition and Thickness
5.2.2 Applicability of GDOES to Coating Analysis
5.2.3 Depth Resolution
5.2.4 Quantification
5.2.5 Radio-Frequency Source
5.3 **Interface Region** 146
5.3.1 Sputter Etching
5.3.2 Interlayers
5.4 **Crystallographic Orientation** 149
5.4.1 Preferred Orientation
5.4.2 Film Growth
5.4.3 Crystallite Growth
5.4.4 Bombardment Energy

5.4.5 Arc Evaporated Coatings
5.5 **Atomic Bonding** 158
5.5.1 Interstitial Solid Solutions
5.5.2 Covalent-Ionic Bonding

CHAPTER 6 CONCLUSIONS AND FUTURE WORK 163

ACKNOWLEDGEMENTS 169

APPENDIX 1 PROCESS MONITOR 170

APPENDIX 2 COURSES AND CONFERENCES ATTENDED 187

APPENDIX 3 PUBLICATIONS 188

CHAPTER 1
Introduction

1.1 Surface Engineering

Surface Engineering is the modification of a surface to improve its engineering performance and enhance its properties. The ability to do this allows engineers to take advantage of the bulk properties of a material (such as strength or lightness) and modify the surface to suit its working environment (such as high temperature or a corrosive atmosphere). Aeronautics has utilised surface engineering for many years in gas turbine jet engines, but more recently it has become available to less "high-tech" industrial applications. Surface engineering can take several forms ranging from actual surface modification techniques; in which the existing surface is physically altered by the addition of foreign atoms (usually small atoms of a gas such as carbon or nitrogen) into the material matrix by thermal diffusion or ion implantation, through hard facing by welding or friction surfacing techniques, to various coating technologies; in which a thin layer of material with the desired properties is deposited onto the bulk material. This work is concerned with the latter techniques.

There is rapidly increasing interest in the use of various deposition techniques to create thin films and different types of protective coatings. True thin films, in the angstrom and nanometre thickness range, are used in optical applications such as filters and anti-reflective coatings for lenses; also the electronics industry uses thin film deposition techniques in semiconductor device fabrication. The use of somewhat thicker coatings for protective or decorative purposes is now becoming widespread and it is this class of materials that this work addresses.

An example of an important application is thermal barrier coatings applied to hot-section components in aero gas turbines. Such coatings must provide a protective barrier for the aerofoil blades against the erosive, corrosive and highly oxidising atmosphere within the turbine. Modern aero engine turbines operate at gas temperatures in excess of the melting point of the substrate materials used in the blades. The blades survive because they are internally air cooled through a network of ducts, surface cooled by a stream of air, and surface coated with a material of low thermal conductivity, forming a temperature gradient between the hot atmosphere and the blade. Coating failure is deleterious to turbine blade and engine life, so the thermal barrier coating must also be resistant to erosion from particles entering the compressor during take-off , corrosion from hot salts, and high temperature oxidation [1 2]. The most common thermal barrier coating system currently used

consists of a low thermal conductivity ceramic coat such as partially stabilised zirconia (ZrO_2), deposited over an oxidation and corrosion resistant Co-Ni-Cr-Al-Y bond-coat on the substrate [3] [4]. Such thermal barrier coatings are several hundred microns thick in order to achieve the necessary temperature insulation requirements, but when the thermal barrier properties are not necessary, much thinner coatings can be used that still offer good wear and corrosion resistance [5].

Coatings in aero engines are also extensively used for clearance control purposes in order to achieve good gas path seals so as to ensure gases in the compressor and turbine flow over the blade surfaces with minimum loss between blade tip and engine casing liner [6]. This is achieved by coating the casing liner with an abradable coating, and the blade tip with an abrasive coating. Optimum clearance is obtained when the rotating blades erode a small channel in the casing liner, so achieving maximum sealing. The abrasive coating must exhibit good wear resistance and low friction properties in order to minimize the heat generated during rubbing.

Similar requirements are expected from coatings in industrial applications such as protective coatings used on cutting and forming tools.

Coatings deposited for industrial protective or decorative purposes are normally in the range 1 to 5 μm thick and are most usually binary compounds composed of a transition or refractory metal nitride or carbide [7] (eg. TiN, TiC, CrN, ZrN, etc.) or ternary compounds with either two non-metals (eg. TiCN, TiBN, etc.) or two metals (eg. TiAlN, TiZrN, etc.). Some quaternary compound films have also been deposited (eg. TiAlVN, TiAlHfN, etc.). Of these, the most widely used wear resistant coating today is TiN, which is often described as a ceramic coating, although "pseudo-ceramic" might be a better term, because although there are some similarities with ceramics, such as hardness and brittleness, there are also acute differences, such as good electrical and thermal conductivity.

The protective coatings exhibit extreme properties such as high melting point, high hardness and chemical inertness [8] and would be used for corrosion [9] [10] [11] [12] or wear resistance [13] [14] [15] [16], e.g. increasing the lifetime and / or cutting speed of high speed steel (HSS) drills, end mills and hobs [17]. As well as the above properties, they also offer a smooth surface finish with a low coefficient of friction [18] [19] [20], making them ideal for extrusion dies, deep drawing dies and punches [21]. As decorative coatings they would also exhibit a good surface finish and an attractive colour [22] [23] [24] [25] [26], and might be used in place of more expensive and less well-wearing coatings, e.g. the "gold" coating on watch cases and spectacle frames.

There are a number of deposition technologies currently in use including electro- and electroless plating, ion-assisted coating, laser ablation and plasma spraying, each having a suitability to particular applications. However, the two main deposition

techniques for surface engineering are Chemical and Physical Vapour Deposition.

1.2 Chemical Vapour Deposition (CVD)

Chemical vapour deposition was the first of the vacuum-based techniques to be used widely for ceramic deposition, particularly for tool coating [27 28]. In this process a stream of gas containing volatile compounds of the element or elements to be deposited is introduced into a reaction chamber. The conditions within the chamber are controlled to enable an appropriate chemical reaction to take place which leads to the formation of a coating on the substrate surface. The volatile reaction products are removed from the chamber during the process. CVD can take place at normal atmospheric pressure or at low pressure (<100 Pa) but generally requires high temperatures (>900°C) for the necessary reactions to take place. This has caused difficulties in the coating of temperature sensitive materials, in particular carbon tool steels which suffer loss of hardness above 550°C. Plasma assisted CVD (PACVD) has lowered the required coating temperatures somewhat by increasing the energy of the gaseous reactants in the chamber using a plasma (excited and ionized gas). However, this has also introduced "field" effects, variable composition and line-of-sight problems. If the substrate can withstand the temperatures needed in CVD then this technique produces very dense and high quality coatings with excellent penetration into holes and re-entrants.

1.3 Physical Vapour Deposition (PVD)

Physical vapour deposition is an expression covering a wide range of coating processes [29 30 31 32 33]. The common feature of which is that they are all carried out under partial vacuum conditions in which at least one of the depositing species is atomised from solid within the chamber. The process may be plasma assisted (PAPVD), and is characterised by its low deposition temperature (<500°C), making it ideal for the coating of temperature sensitive materials. This process allows the deposition of metals, alloys and ceramics onto a wide range of substrates, with unprecedented control over the coating-substrate interface and growth characteristics. Normally conducting materials would be used for the cathode, but non-conductors can also be deposited by using a radio-frequency (rf) power supply. Atomization of the depositing species in PVD is realised by one of two different methods: evaporation or sputtering.

Evaporative PVD is a process in which the coating material is heated by resistive, inductive, electron beam or arc techniques, until it evaporates into the vapour phase.

Sputter PVD is a process in which the coating material is bombarded with high kinetic energy ions and neutrals such that there is a momentum transfer that removes or sputters the surface atoms of the source material. This may be achieved by diode, triode, magnetron or ion beam techniques.

With both methods, the atomised species can be mixed with a reactive gas for ceramic deposition.

In PAPVD the substrate is also subjected to bombardment by high kinetic energy ions and neutrals which increases adatom mobility of the depositing species and is reported to result in denser structures [27].

Of the various PVD techniques, this work will concentrate on just two; cathodic arc evaporation and magnetron sputtering. These are representative of their individual atomization methods, are the most recent methods respectively, have undergone extensive development, and are the least well understood.

Also, advancements in each technique have led to the realisation of confined or "steered" arc, and unbalanced planar magnetron technologies. The cathode constructions of these are technically similar, and readily lend themselves to integration into a single cathode unit capable of operating in either mode, with just a magnetic re-arrangement and different power supply characteristics [34]. This is the principle behind the Arc Bond Sputter (ABS) system [35 36], which claims to offer a "hybrid" deposition process, utilising the confined arc to "etch" the substrate surface prior to coating, thus causing "implantation" of the depositing species and enhancing adhesion, followed by the droplet-free versatility of unbalanced magnetron sputter coating. This process thus effectively joins the two branches (evaporation and sputtering) of the PVD "family tree" (see figure 1).

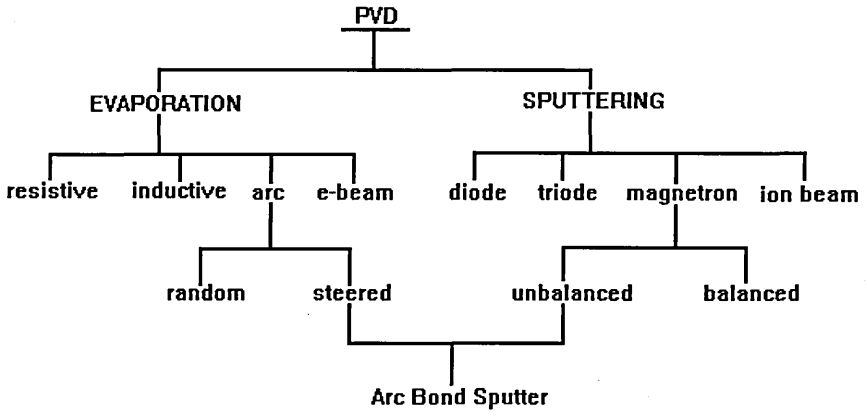

Figure 1. PVD Family Tree

References

[1] A.E.Weatherill and B.J.Gill, *Met. and Mat.*, 1988,49,551.

[2] T.N.Rhys-Jones, *Surface Stability*, 1989,6,51, Inst. of Met., London.

[3] T.N.Rhys-Jones, *High Temp.Technol.*, 1989,7(2),73.

[4] T.N.Rhys-Jones, *Corrosion Science*, 1989,29(6),623.

[5] V.R.Parameswaran, J.P.Immarigeon and D.Nagy, *Surf.Coat.Technol.*, 1992,52,251.

[6] T.N.Rhys-Jones, *Surf.Coat.Technol.*, 1990,42(1),1.

[7] H.Holleck, *Surf.Coat.Technol.*, 1990,43/44,245.

[8] R.F.Bunshah, *Phys. and Chem. of Protective Coatings*, 1986,149,131.

[9] A.Schroer, W.Ensinger and G.K.Wolf, *Mat.Sci.Eng.*, 1991,A140,625.

[10] J.Aromaa, *Mat.Sci.Eng.*, 1991,A140,722.

[11] I.M.Penttinen, A.S.Korhonen, E.Harju, M.A.Turkia, O.Forsen and E.O.Ristolainen, *Surf.Coat.Technol.*, 1992,50,161.

[12] H.A.Jehn and M.E.Baumgartner, *Surf.Coat.Technol.*, 1992,54/55,108.

[13] D.S.Rickerby and P.J.Burnett, *Surf.Coat.Technol.*, 1987,33,191.

[14] K.H.Habig, *Tribology Int.*, 1989,22(2),65.

[15] T.S.Eyre, *Metals and Materials*, 1991,3,143.

[16] W.Konig, R.Fritsch and D.Kammermeier, *Surf.Coat.Technol.*, 1991,49,316.

[17] P.Hedenqvist, M.Olsson, P.Wallen, A.Kassman, S.Hogmark and S.Jacobson, *Surf.Coat.Technol.*, 1990,41,243.

[18] K.H.Habig, *Surf.Coat.Technol.*, 1990,42,133.

[19] S.J.Bull, D.S.Rickerby and A.Jain, *Surf.Coat.Technol.*, 1990,41,269.

[20] S.J.Bull and P.R.Chalker, *Surf.Coat.Technol.*, 1992,50,117.

[21] J.Vogel, *Adv.Tech.Plasticity, 1987,1,103.*

[22] R.Buhl, H.K.Pulker and E.Moll, *Metallurgical and Protective Coatings*, 1981/82,265.

[23] H.Erhart, S.Bastian and H.Petersen, *Plasma Surf.Eng.*, 1989,1,603.

[24] G.Reiners, H.Hantsche, H.A.Jehn, U.Kopacz and A.Rack, *Surf.Coat.Technol.*, 1992,54/55,273.

[25] H.Randhawa and H.M.Gabriel, *Plasma Surf.Eng.*, 1989,1,547.

[26] B.Zega, *Surf.Coat.Technol.*, 1989,39/40,507.

[27] W.V.Turennout and N.Reiter, *Cutting Tool Eng.*, 1986,38(1),16.

[28] E.Horvarth, *Surmetal Surf.Met.*, 1987,333.

[29] P.J.Martin, *Materials Australasia*, 1986,18(5),11.

[30] P.W.Hatto, *Trans IMF*, 1988,66,55.

[31] A.Matthews, *Adv.Mat.Man.Proc.*, 1988,3(1),91.

[32] E.Bergmann and E.Moll, *Plasma Surf.Eng.*, 1989,1,521.

[33] E.Moll, R.Buhl, H.K.Pulker and E.Bergmann, *Surf.Coat.Technol.*, 1990,39/40,475.

[34] P.Robinson and A.Matthews, *Surf.Coat.Technol.*, 1990,43/44,288.

[35] W.D.Munz, D.Schulze and F.J.M.Hauzer, *Surf.Coat.Technol.*, 1992,50,169.

[36] W.D.Sproul, P.J.Rudnik, K.O.Legg, W.D.Munz, I.Petrov and J.E.Greene, *Surf.Coat.Technol.*, 1993,56,179.

CHAPTER 2
Literature Review

2.1 Evaporative Techniques

Evaporation is the conversion of a substance, usually a metal, into a vapour at high temperatures, either from the liquid state or by sublimation from the solid metal. By evaporating in a vacuum environment, a flux of atomistic material may be produced that can be used for coating a substrate.

2.1.1 Resistive Heating Evaporation

In the resistive heating process [1 2 3], the evaporant (often in powder or chip form) is held on a filament or in a crucible or "boat" made from a high melting point resistive material such as a refractory metal, eg. tungsten, molybdenum or tantalum. To prevent reaction between the crucible and the evaporant, the crucible may be coated or made out of a refractory metal oxide or nitride (Al_2O_3, BeO, BN, etc.) with the resistive tungsten wire coiled round the outside. On application of a current through the resistive wire, heat is liberated by the Joule effect, the material is melted and eventually evaporates (see figure 2).

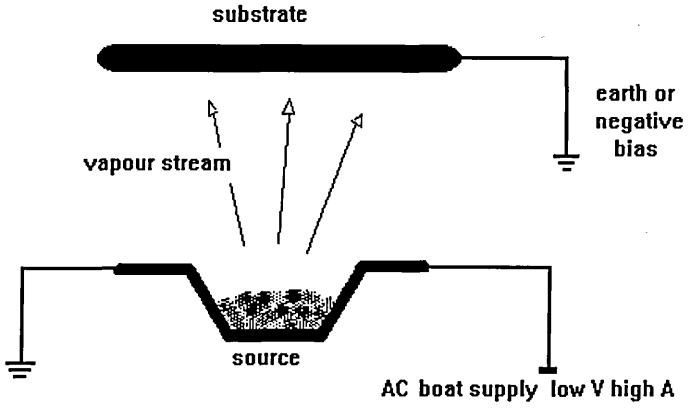

Figure 2. Resistive Heating

2.1.2 Inductive Heating Evaporation

An alternative method is the inductively heated source [4]. This is again often used with refractory metal oxide or nitride crucibles, but has the advantage that no direct thermal coupling between evaporant and heating coil is necessary, thus the crucible temperature stays lower. This method employs the application of a radio frequency (rf) alternating current to the coil which causes a varying magnetic field and induces eddy currents in the conducting evaporant material. This current flow in the evaporant causes heating due to the Joule effect. When the metal has melted, the eddy currents set up circulatory movements that stir the melt and so ensure even evaporation (see figure 3).

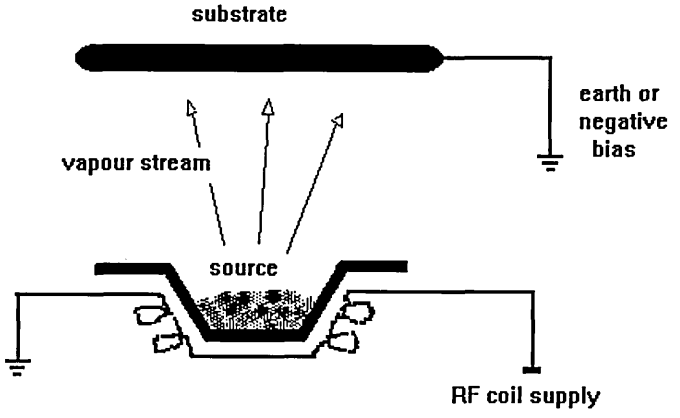

Figure 3. Inductive Heating

2.1.3 Electron-beam Evaporation

A more technologically advanced method is the electron beam evaporation source [5 6 7 8]. This is very versatile in the range of materials that can be evaporated, and also the electron beam causes ionization of the gas and vapour species so forming a plasma that assists the deposition process. The conventional electron gun involves heating a tungsten filament to incandescence by application of an electric current such that thermionic electron emission occurs. The problem with using a hot filament is that low pressures are required to prevent oxidation, and so the electron gun must be differentially pumped separate from the main deposition chamber. The electron beam is then magnetically deflected onto the crucible containing the evaporant material. The crucible is normally made of copper and is water cooled so

that the molten pool sits within a solid shell of evaporant material. This provides a barrier to evaporant-crucible interaction and ensures high purity vapour is produced (see figure 4). An alternative electron source is the "plasma" electron beam gun. This source uses a hollow cathode arrangement in which a glow discharge and plasma are generated. Inert gas ion bombardment within the hollow cathode causes electron emission (either secondary, thermionic or both) and a beam is magnetically or electrostatically extracted. The advantage of this type of gun is that higher pressures can be used, and so differential pumping is no longer necessary.

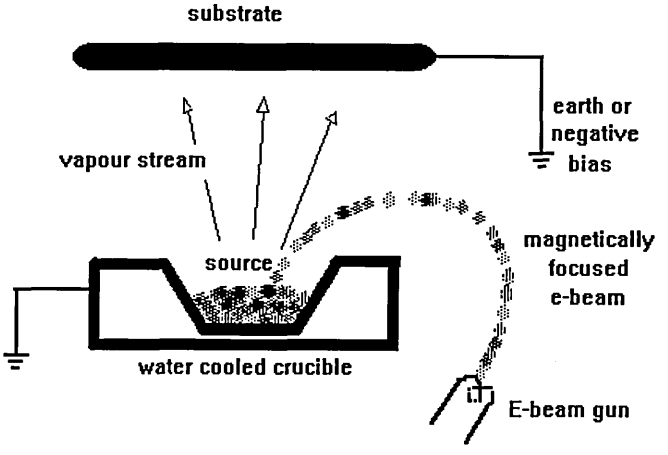

Figure 4. E-beam Evaporation

All of the above techniques cause the evaporating material to undergo bulk melting such that a vapour is liberated from a large molten pool. This severely restricts the orientation and hence positioning of the evaporation source in the PVD chamber and may not be suitable for coating large objects. Also, apart from the electron beam method, the above techniques require some form of ionization enhancement in order to generate a plasma. The cathodic arc evaporation technique does not suffer from such limitations.

2.1.4 Cathodic Arc Evaporation

Original work on arc evaporation appeared in the literature as far back as 1939 [9], and modifications and developments are still being made today. It is, however, only in recent years that commercially useful deposition systems have become available. The arc PVD coating technique is essentially an ion-plating process that was pioneered and then further developed in the USA [10 11] and Soviet Union [12 13] during the early 1970's. More recent development in the late 1980's [14] has seen the

innovation of the steered arc process which has considerably improved coating quality. The main difference between the arc process and the more traditional ion-plating technologies is the means of producing the evaporated species.

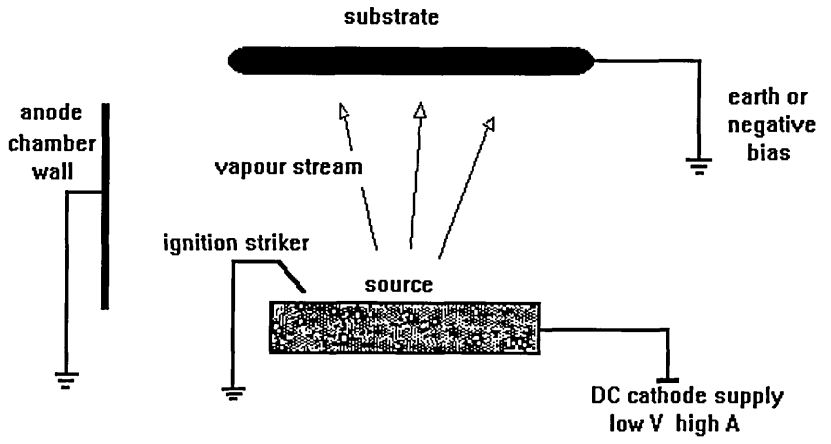

Figure 5. Cathodic Arc Evaporation

In this coating process, an electric arc is struck on the surface of the material to be evaporated (the cathode), while the work chamber, which is usually grounded, acts as the anode (see figure 5). The arc "triggering" can be either mechanical (by momentarily bringing a grounded probe into contact with the cathode surface) or it can be electrical (by relying on the thermal breakdown of a thin, poorly conducting film between the cathode and the "ignition" wire on application of a current pulse). Once initiated, the arc is self-sustaining and operates in a low-voltage, high-current mode (the voltage drop to the source being typically -20 to -60 V at a discharge current of 50 to 400 A) (see figure 6). The arc is supported in the generated flux, and can therefore be maintained under high vacuum conditions. Normally, however, the evacuated chamber is back-filled with either an inert gas to help sustain the arc, or a reactive gas such as nitrogen so that compound films may be deposited.

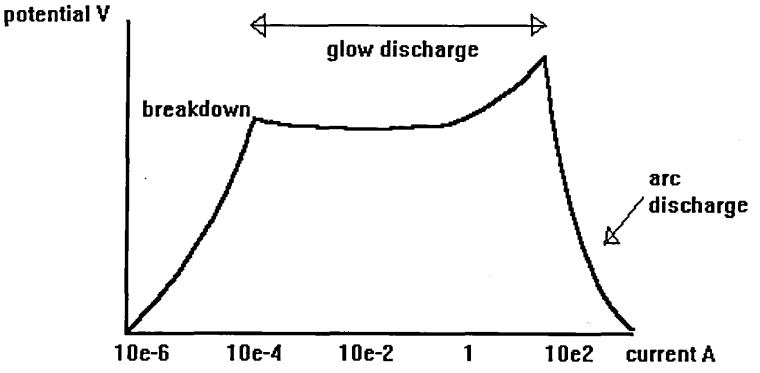

Figure 6. Characteristics of Arc Discharge

2.1.4.1 Random Arc

There are various descriptions and theories about the nature and operation of the arc and its one or more cathode "spots" (the areas of intense plasma initiated at the cathode surface) [15 16 17 18 19 20]. These spots are only a few microns in diameter, and so each has a high current density of typically 10^7 A cm^{-2}, but only exists for a fraction of a second (10^{-7} s) before another spot forms immediately adjacent to it, and the discharge moves. The direction of movement is influenced by asperities on the cathode surface, with the arc showing preference for microscopic protuberances or gullies. Given adequate cooling of the cathode, material may pass into the vapour phase at each spot without the cathode undergoing bulk melting. Thus the evaporation sources may be mounted in any desired orientation within the chamber, even upside-down.

The cathode spots and hence the arc move rapidly and at random across the surface of the cathode, evaporating microscopic points and producing a high velocity jet or flux of atomistic material, both highly ionized and neutral, and various sized clusters of atoms and ions. At the cathode spot a minute liquid pool of molten cathode material is produced which is vigorously evaporated. Electrons are emitted by a combination of thermionic and field emission mechanisms, and are accelerated away from the cathode surface. These electrons rapidly collide with the evaporating neutral atoms and ionize them, thus creating a dense, hot plasma just above the spot. The plasma of ions and electrons expands rapidly, but the electrons can move much faster due to their lower mass, leaving behind a positive space charge that retards further electrons and accelerates the ions in all directions (see figure 7).

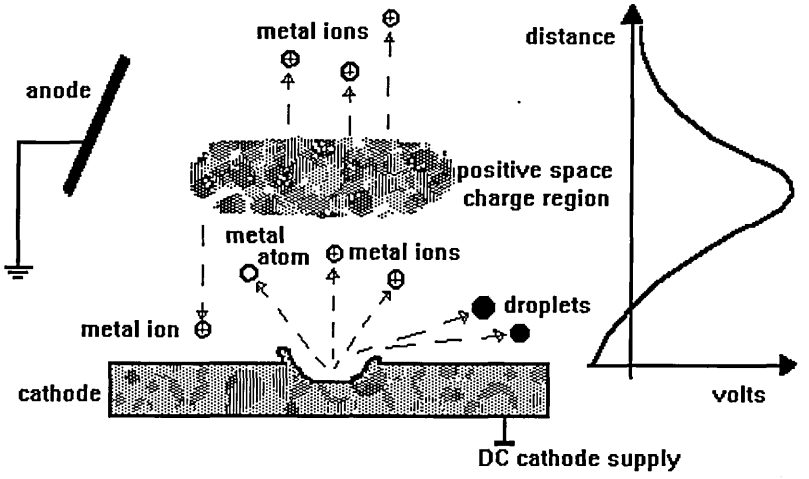

Figure 7. Cathode Spot Region

The plasma jet peaks in the direction normal to the cathode surface and is of a highly ionized nature (some 90% of the evaporated species) with a high kinetic energy (up to 100 eV). For refractory metals the evaporated species are multiply ionized with, for example, a charge distribution of typically 27% Ti^{+}, 70% Ti^{2+} and 3% Ti^{3+} for titanium [21]. This makes an ideal source for use in ion-plating [22], although the highly ionized nature of the depositing species can cause uniformity problems when coating onto odd-shaped components due to bias charge distribution effects (see section 2.3.5.2).

2.1.4.2 Macroparticles

During operation, the random arc spots show a tendency to dwell in certain areas, producing comparatively large, localised molten pools. The positive space charge that accelerates ions away from the cathode, also accelerates some ions towards the cathode. The impingement of this ionic jet on the liquid pool surface may cause the ejection of droplets or macroparticles that are several tens of microns in diameter [23 24 25 26]. These droplets are undesirable due to their detrimental effect on surface quality and adhesion of the deposited film, and also wastage of cathode material.

Macroparticle formation occurs mainly during the heating and sputtering phases of a PVD process when an inert gas is present. During the actual coating phase, providing there is sufficient reactive gas, then contamination or "poisoning" of the cathode surface occurs (nitriding in the case of nitrogen). This raises the melting point of the cathode material, so reducing the size of the molten pools, and also

increases arc velocity due to liberation of the contaminant gas when intensely heated by the arc. This results in less macroparticle formation. Deliberately providing excess reactive gas so as to cause cathode poisoning is known as the "modified arc process" [27].

Macroparticle formation can also be reduced during all phases (but not eliminated) by increasing the speed at which the arc traverses the cathode surface using magnetic confinement or steering (confined or steered arc) [28 29]; or by filtering the produced flux using a magnetic coil (plasma duct) [30 31]. The latter method has proved to be the most effective at eliminating macroparticles, but can suffer from plasma losses and reduced ion flux density at the substrate surface.

2.1.4.3 Steered Arc

A magnetic field can be used to confine or steer the arc due to the fact that the arc sits preferentially at the point on a cathode surface where the normal component of an applied magnetic field is zero [32] (see figure 8).

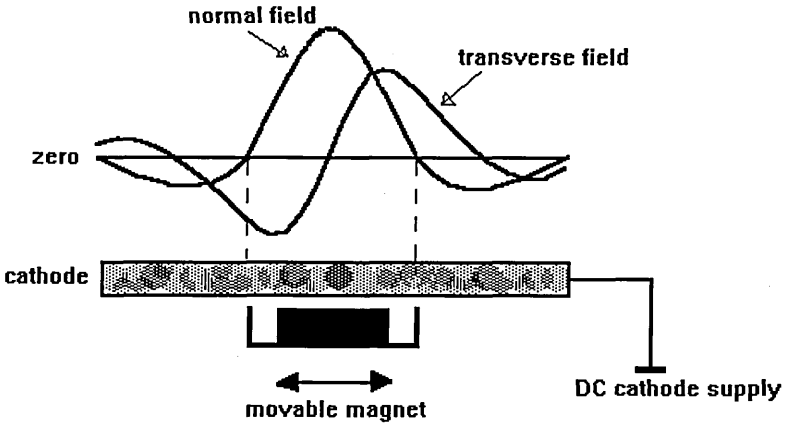

Figure 8. Magnetically Steered Arc

The magnetic field due to a magnet or coil will be circular or oval in shape and so there will be a "racetrack" of zero normal field on which the arc may reside. Due to the "Hall effect" of the transverse field component, the arc will travel around this racetrack at high velocity. However, there is an unexpected phenomenon regarding the direction of arc motion.

Ampere's rule states that all matter carrying an electric current density **J**, in the presence of a magnetic flux density **B**, is subject to a force density **J** ^ **B** (the Hall effect). The arc behaves as a current carrying conductor and should not be an exception to this rule. However, high-speed photography has revealed that the arc does in fact move in the opposite direction. This phenomenon is known as "retrograde motion" [33]. The Hall effect is a consequence of the Lorentz force acting on the charge carrying particles, which are normally the electrons. The Lorentz force is given by :

$$\mathbf{F} = q(\mathbf{E} + \mathbf{v} \wedge \mathbf{B}) \qquad \text{..... (1)}$$

where **F** is the force, q is the moving charge, **E** is the electric field and **v** ^ **B** is the vector product of the particle's velocity and the magnetic flux density.

A sideways drift is imposed on the motion of the electrons by their passage through the magnetic field. However, in the case of the magnetically-steered low pressure (vacuum) arc, electrons are partially confined to cycloidal paths in the magnetic field, and many return to the cathode without constituting a net current flow. Due to the intense flux jet of highly ionized cathode material, the current is mainly carried away by positive charge carriers instead, and the Hall field is thus reversed. At higher pressures (not found in PVD) the arc motion reverts to the proper Ampere direction. This is explained by a shorter mean free path for the ion flux, resulting in kinetic energy loss collisions such that fewer positive ions escape the cathode. Thus the current is mainly carried by the electrons as in the normal situation. The exact mechanisms of this phenomenon are not well understood, but fortunately it does not unduly affect the use of magnetically steered arcs in PVD.

Mechanical or electrical changes in the magnetic field profile allow precise control of the arc motion and the ability to steer the arc in a predetermined closed-path of variable radius on the cathode surface. Confinement or steering can be implemented by either permanent magnets or electromagnets. The early steered arc method used a small permanent magnet attached to a rotating arm behind the cathode. Rotation of the arm during evaporation, caused the arc to follow a circular path on the cathode surface, the width of the path being a function of the strength of the magnetic field. Later methods have used stationary magnetic field coils behind the cathode to both guide the arc and increase its velocity. By varying the current in the coils, and hence the magnetic field strength, the path radius could be altered. With both methods, the resultant motion of the arc spot has improved cathode erosion uniformity, reduced frequency and size of macroparticles, and reduced arc quenching due to travel beyond the cathode edge. The steered arc technique also offers the possibility to exactly control the evaporation area (arc path) and hence lead to the use of

segmented cathodes for the deposition of graded and multi-layered coatings [34].

Confinement of the arc to the cathode surface is also possible using a "passive border" with predetermined electronic characteristics. The requirement of passive confinement is that the border material should have a very low secondary electron emission. This will result in reduced ionization and a weakened plasma jet, causing the arc to veer in the opposite direction. The passive border does not extinguish the arc, nor does the arc spontaneously extinguish; hence the evaporation source is much more stable and operates for a longer period of time without re-ignition. The preferred material for passive confinement is boron nitride, and it is normally used in addition to magnetic confinement.

2.2 Sputtering Techniques

Sputtering is a process by which atomistic material can be ejected from a solid surface through energetic ion and neutral bombardment. The concept that a solid surface could be eroded by an impinging flux of accelerated positive ions dates back to 1842 [35], but the process was not utilised until some hundred years later. In the 1950's it was discovered that a radio frequency (rf) glow discharge could be used to sputter insulating materials [36], which opened up a vast range of possibilities, most notably utilised by the semiconductor industry. In the 1970's the development of magnetron sputtering [37] with its higher deposition rate allowed sputtering to compete with other ion-plating processes across the field. Further significant improvement came in the mid-1980's with modifications resulting in the unbalanced magnetron sputtering process [38 39 40].

2.2.1 Ion Beam Sputtering

Sputtering involves the bombardment of a cathode surface by energetic ions and neutrals. These species may originate from an external source such as a plasmatron or a Penning gun which contain a plasma produced by an arc or a glow discharge respectively. The ions are extracted electrostatically and magnetically directed as a beam onto the cathode surface. Alternatively, the glow discharge may be generated directly in front of the cathode so that it is uniformly bombarded by ions rather than by a focused beam. Ion beams are most commonly used for implantation and surface modification treatments rather than as a sputtering source for PVD [41 42 43 44].

2.2.2 Glow Discharge - Diode Sputtering

The simplest arrangement of sputtering is the well known dc (direct current) glow discharge [45 46 47]. A glow discharge can be created by introducing an inert "working gas" (usually argon) into a vacuum chamber and applying a high potential (300 to 5000 V) between two electrodes (diode arrangement - normally a cathode of the material to be deposited, with the grounded chamber walls forming the anode) (see figure 9).

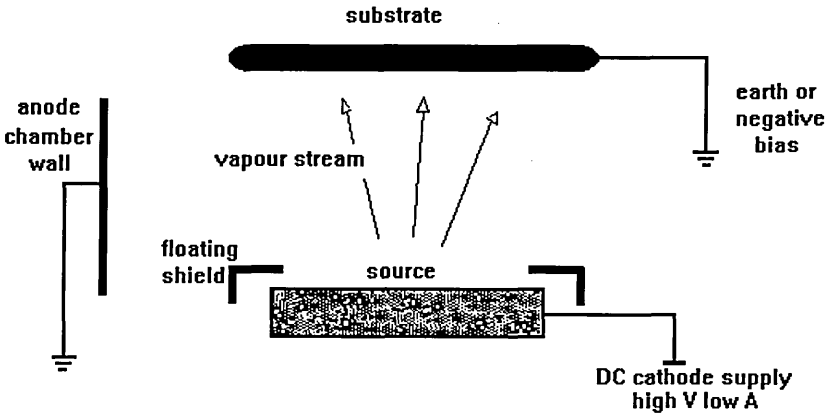

Figure 9. Diode Sputter Source

Providing that the potential is greater than the "breakdown" voltage of the gas, then an electric current will start to flow. This is initiated by the acceleration of naturally occurring gas ions (or ions caused by cosmic radiation) towards the cathode, and electrons towards the anode. When the accelerated ions collide with the cathode surface most of their kinetic energy is lost. They also lose their charge and are either elastically recoiled or implanted. Some of their incident energy is transferred to the cathode atoms as momentum, causing a "collision cascade" within the cathode surface.

The energy E_t transferred in such binary collisions is given by :

$$E_t = 4m_i m_t / (m_i+m_t)^2 \qquad \text{..... (2)}$$

where m_i and m_t are the masses of the incident and target atoms respectively. The collision cascade may travel deep into the cathode, dissipating its energy ultimately as lattice vibrations (heat), or it may recoil to the surface where, if the collision energy is greater than the surface binding energy of the lattice, it may result in the ejection (sputtering) of an atom or sometimes clusters of atoms of the cathode material (see figure 10).

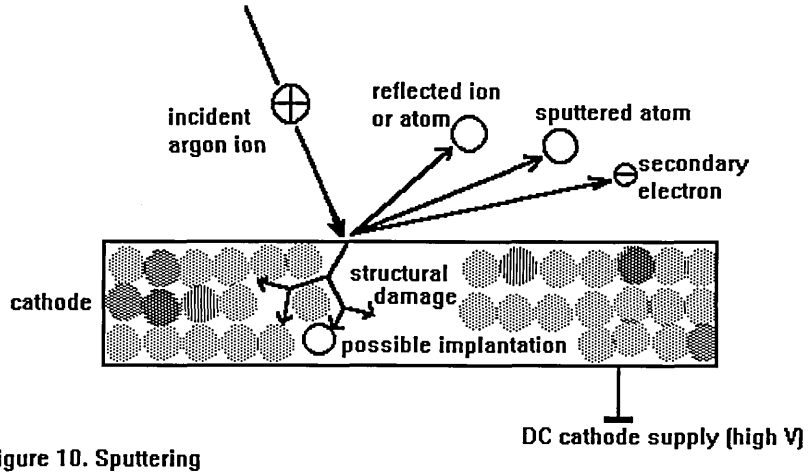

Figure 10. Sputtering

Clearly, this is a very inefficient process where typically only 1% of the incident energy reappears as the energy of the sputtered atoms [48] [49]. The ejected atoms are mainly neutral (more than 90%) and of low kinetic energy (5 to 20 eV). The number of atoms removed per incident ion is termed the "sputtering yield". The yield is dependent on the incident ion energy and mass, as well as the characteristics and geometry of the cathode material. In general, however, the variation in sputter yields of different materials is less than the variation in evaporation rates found in other processes. The sputtering yield S can be obtained from [50]:

$$S = 3E_t \alpha E_i / 4\pi^2 U_o \qquad \text{..... (3)}$$

where E_t is the energy transferred in a binary collision, α is a function of the colliding atom masses, E_i is the energy of the incident ion, and U_o is the surface binding energy of the cathode.

The energetic bombardment may also cause secondary electron emission, X-ray emission, photon generation and desorption of gas atoms from the cathode surface.

The most important of these, in terms of the glow discharge, is the secondary electron emission. These electrons are accelerated rapidly away from the cathode, gaining kinetic energy, and colliding with the working gas and other gas atoms causing ionization events, dissociation and excitation, thus creating a "plasma". Provided that each secondary electron produces a sufficient number of ions to cause the release of a further secondary electron at the cathode, then the glow discharge will be self-sustaining. This requirement can be expressed by the following

relationship for the minimum potential V_{min} to sustain a discharge :

$$V_{min} = E_o / \varepsilon_i \Gamma_i I_e \quad \text{..... (4)}$$

where E_o is the average energy required for producing ions (about 30 eV for Ar^+), ε_i is the ion collection efficiency of the cathode, Γ_i is the number of secondary electrons emitted per incident ion, and I_e is the fraction of the total ions V/E_o that is produced by an average secondary electron before it is lost from the system.

The number of secondary electrons emitted per incident ion Γ_i is termed the "secondary electron yield". Typically for a pure metal cathode, with argon working gas, and -500 V cathode potential, the secondary electron yield will be 10%.

2.2.3 Triode Sputtering

By utilising a third electrode to enhance ionization, the discharge becomes no longer dependent solely on the generation of secondary electrons at the cathode to sustain it. This electrode may be a simple positively biased conductor, or a thermionic electron emitter (see figure 11). With an electron source, it becomes possible to vary the discharge current independently of the discharge voltage, making higher ion densities at the cathode and substrate possible [51]. Such an arrangement allows lower discharge voltages and pressures to be used, and leads to higher deposition rates and independent control of plasma density. However, there are several disadvantages, such as contamination from the thermionic source, substrate overheating due to direct electron bombardment or indirectly by radiation from the heated chamber walls (the anode), and complications of use, especially when scaled up in size.

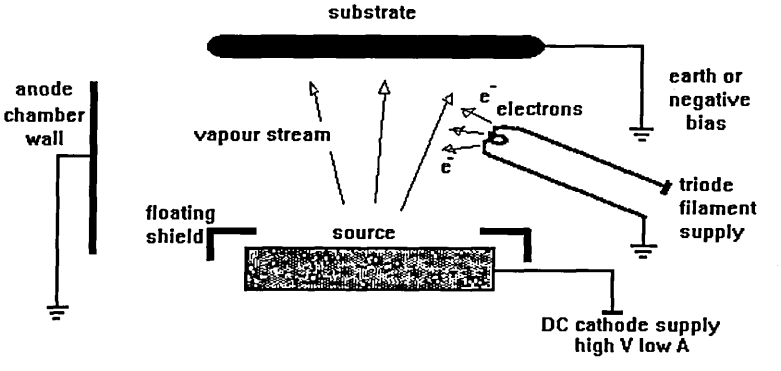

Figure 11. Triode Sputter Source

2.2.4 Glow Discharge Plasma

The type of dc discharge used in sputtering processes is known as an "abnormal glow discharge". At lower applied voltages and consequently lower currents, a discharge results that is characterised by its constant voltage and constant current density, utilising a small area of the cathode. This is known as a "normal glow discharge". As the power is increased, the region of the cathode carrying current increases in size (current increases, current density and voltage remain constant) until the whole cathode is used. At this point, any increase in power will result in an increase in current and current density, with a sharp increase in voltage. This is known as an "abnormal glow discharge" (see figure 12).

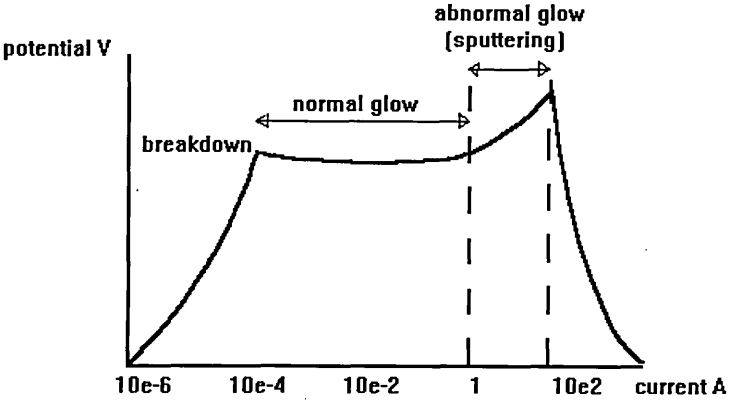

Figure 12. Characteristics of Glow Discharge

The glow discharge plasma can be separated into several distinct regions, though in practice they are not all clearly observed. Directly in front of the cathode is the "cathode glow region" which is luminous due to ion neutralisation at the cathode surface. In front of this is the "dark space", "sheath", or "cathode fall region". It is across this region that most of the applied potential is dropped, providing the accelerating force for the impinging working gas ions and the emitted secondary electrons.

The dark space region originates when the plasma makes contact with a surface. If the surface is electrically isolated, then the flux of electrons to the surface tends to exceed that of the ions due to the electrons having typically higher random velocities. The surface thus acquires a negative potential relative to the plasma. If the surface is a powered cathode, then this negative potential is considerably enhanced. This results in a redistribution of the ion and electron densities in the vicinity of the

surface and the charge separation induces an electric field that retards the electron flux and enhances the positive ion flux incident upon the surface. This creates a region of depleted electron density (the dark space region) adjacent to the surface.

The thickness of the dark space region is quite small compared to the dimensions of the bulk plasma and can be approximated from the Child-Langmuir space charge limited current flow equation [52] :

$$L = (4\varepsilon_0/9J)^{0.5} (2q/m)^{0.25} V^{0.75} \quad \text{..... (5)}$$

where L is the cathode fall length, ε_0 is the permittivity of free space, J is the cathode current density, q is the ion charge, m is the ion mass, and V is the potential drop across L.

Although the dark space region is localised, a fully consistent model must treat the plasma as a whole which is computationally intensive and beyond the scope of this work. A simpler approach is to treat it in isolation as with the Child-Langmuir law above, but this makes a number of incorrect assumptions such as zero incoming ion velocity, zero electric field at the plasma-dark space boundary and no collisions within the dark space [53]. Fortunately, in surface engineering a simplistic understanding of the plasma and dark space is all that we require as we are using the plasma purely as a tool for coating deposition.

Thus the dark space region provides the accelerating force for the incident positive ions in the plasma and, depending on the mean free path for charge exchange, collisions can take place within the dark space resulting in high kinetic energy neutrals that also impinge on the cathode surface. Thus sputtering can occur by both ion bombardment and fast atom bombardment [54 55].

Next is the "negative glow region" which in PVD processes normally fills the rest of the chamber. It is this negative glow which is often referred to as the plasma, and in this region the electrons expend most of their energy creating additional ions and exciting atoms. Relaxation of the excited gas atoms in the plasma results in photon emission which heats the plasma and gives rise to the visible glow. The colour and intensity of the plasma will be characteristic of the gas species, target material, pressure and excitation. It is thus possible to detect the presence of certain components by monitoring the characteristic spectral wavelengths.

Under appropriate conditions, beyond the negative glow are the "Faraday dark space", the "positive column" and the "anode dark space" (see figure 13), but these are not normally observed in the pressure ranges used in sputtering processes.

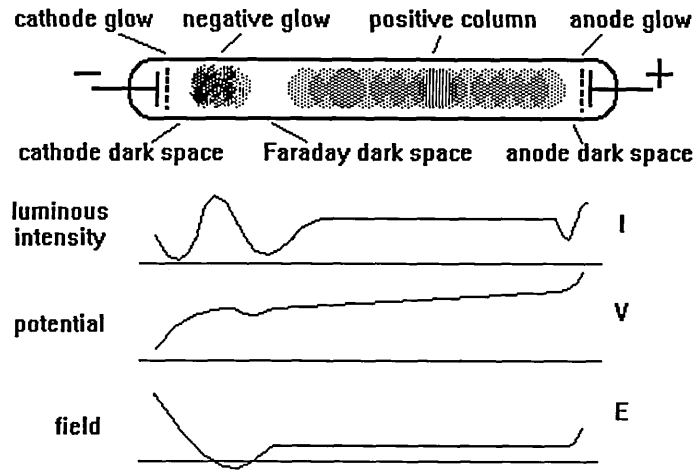

Figure 13. Glow Discharge Plasma

2.2.5 Radio-Frequency Sputtering

A large range of single, alloyed or multi-component cathode materials can be used for dc glow discharge sputtering, the only requisite being that they are electrically conductive. When it is required to sputter non-conducting material then a radio frequency (rf) oscillating power source is necessary.

If an insulator is used as a cathode in the dc glow discharge, then its surface will charge up to the floating potential of the plasma such that the fluxes of ions and electrons to the surface become equal. These ions and electrons recombine on the surface so that there is no current flow. By using an oscillating source an alternating current (ac) discharge is set up that neutralises the positive charge accumulated during one half-cycle by electron bombardment during the next half-cycle. At low frequencies this results in a pulsed discharge because the insulator charges up in a shorter time than the period of the half-cycle, and for the remainder of the period the discharge is off. If however, the oscillating frequency is above 1 MHz (radio frequency), then the ions, due to their relatively large mass, are no longer able to follow the alternating potential on the electrodes at the rate the electrons can and so the electrodes effectively become negative because they are never fully neutralised (see figure 14).

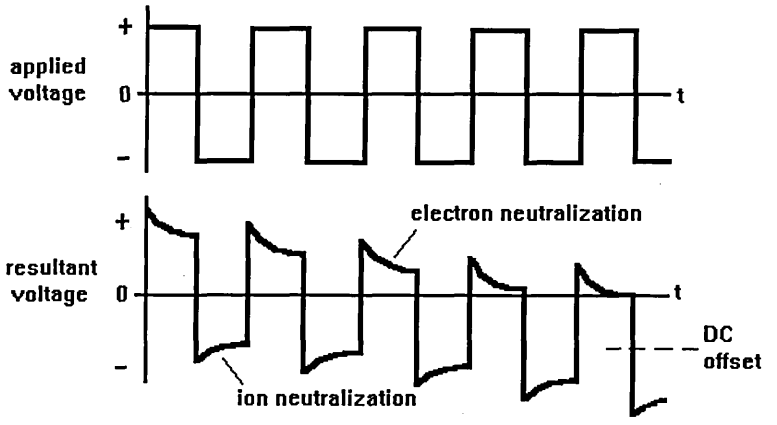

Figure 14. RF biasing

In order to sputter only the "cathode", this electrode is the only one that is effectively powered by the rf supply, while the other electrode is grounded. Also, the "cathode" must be made significantly smaller than the "anode". In this way, the dark space around the "cathode" will be thicker and ions will be sufficiently accelerated to cause sputtering. If the "anode" is once again the grounded chamber walls, then the dark space will be spread very thinly and provide insufficient kinetic energy to the ions for sputtering to occur.

2.2.6 Magnetron Sputtering

In a conventional glow discharge, electrons are quickly lost by recombination at the anode. To minimize this loss a magnetic field can be used that makes more efficient use of the electrons causing them to produce more ionization [56 57 58]. The "magnetron" is such a system that employs magnets behind the cathode whose field lines penetrate the dark space and produce a magnetic field parallel to the cathode surface and hence perpendicular to the electric field of the dark space (see figure 15)

The magnetic fields used are quite weak, so that only the electrons are affected; the ions being too massive. A secondary electron emitted from the cathode will be acted upon by the crossed electric and magnetic fields and deflected by the Lorentz force.

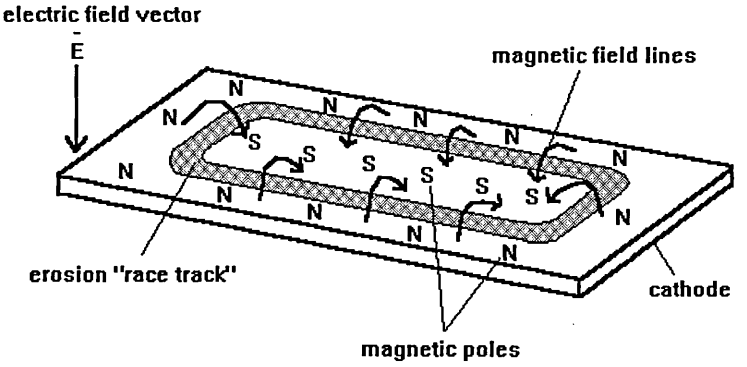

Figure 15. Magnetron Cathode

For a charged particle moving at angle θ to a magnetic field, this force will cause the particle to move in an orbital path. Thus the electron will describe a semicircle of radius *r* given by :

$$r = m_e v.\sin\theta / Be \qquad \text{..... (6)}$$

where m_e is the electron mass, v.sinθ is the component of velocity perpendicular to the magnetic field, **B** is the magnetic field, and *e* is the electron charge.

Coupled with the component of velocity v.cosθ parallel to **B**, which is unaffected by the magnetic field, then providing there are no collisions, the electron will describe a cycloidal or helical path before returning to the cathode surface. Thus secondary electrons are trapped close to the cathode and spend more time in the discharge. As a result, more ionizing collisions occur which allow the electrons to escape confinement, but also produce a greater number of ions to sustain the glow. The more ions that are produced, then the more sputtering that is possible, and so a higher deposition rate can be realised, and lower discharge voltages and pressures used. Also, electron trapping provides the additional advantage that fewer electrons are free to bombard the substrate surface and chamber walls, resulting in a "cooler" deposition process, which for temperature sensitive materials can be very important [59 60 61].

The application of magnetic fields to enhance ionization in glow discharges dates back to 1936 [62], but not until the 1970's has the principle of crossing electric and magnetic fields been effectively applied to sputtering systems. Three conventional magnetron designs have emerged: cylindrical or post magnetrons, circular magnetrons, and planar magnetrons. This work is concerned with the latter design as

the most applicable to large scale PVD coating systems [63]. Typical cathode size is 600 x 200 mm using a central magnet pole and outer magnet pole configuration resulting in a "looping" magnetic field that restricts the sputtering area to an elliptical "racetrack". Thus the planar magnetron makes a stable line source, with substrate rotation required for coating uniformity. The magnetic field causes very effective concentration of the glow and so localised erosion in the racetrack area can be a problem [64]. This leads to variation in deposition rate with time, and necessitates frequent cathode replacement.

2.2.6.1 Unbalanced Magnetron

The conventional magnetron system, although a considerable improvement over the dc glow discharge process, still suffers from a poor "throwing distance" of the depositing species when compared to other ion-plating techniques [65 66]. This has severely restricted the coating range and the size and shape of possible substrates. However, a simple modification to the magnet configuration has resulted in an extremely versatile source called the "unbalanced magnetron" [67 68 69].

In a conventional magnetron, the inner pole and outer pole magnets behind the cathode are of equal strength, and so the field lines loop between them, returning via the steel yoke on which the magnets are fixed. By strengthening one set of magnets (either with additional magnets or by using an electromagnetic coil) the magnetron becomes magnetically unbalanced, hence the name. There are two unbalancing options; strengthen the inner pole or the outer pole. Strengthening the inner pole results in increased secondary electron confinement and draws the glow region in more tightly to the cathode with no obvious advantage. However, if the outer pole is strengthened, then the magnetic field lines, as well as looping on the cathode surface, curve away on all sides (see figure 16). Clearly, some of the secondary electrons follow these lines and are no longer confined to the cathode surface, but also the plasma glow is expanded outward towards the substrate and considerably increases substrate bombardment intensity such that it is comparable with other high deposition rate techniques [70]. The unbalanced magnetron has the additional benefit that the ion energy and flux can be varied almost independently of one another, giving a further controllable process parameter.

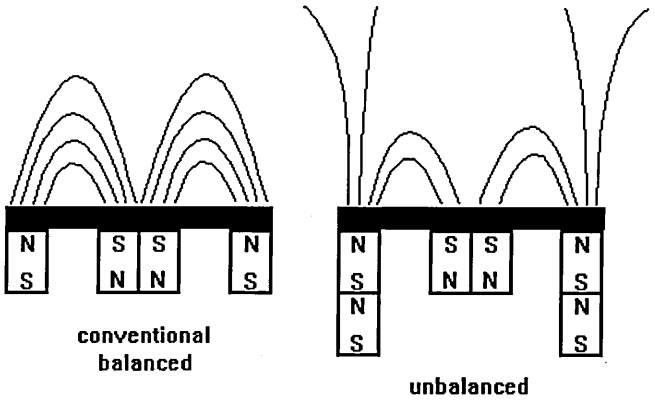

Figure 16. Unbalanced Magnetron

2.2.6.2 Closed-Field Systems

The use of unbalanced magnetrons with uncontained field lines gives rise to various possible magnetic field geometries when two or more cathodes are used in the same system [71 72 73]. Such multi-cathode systems generally have only two distinct configurations : the "mirrored" arrangement where the outer magnetic poles of the cathodes are alike (ie. all north, or all south), or the "opposed" arrangement where each alternate cathode has like outer poles and adjacent cathodes are opposite (ie. north, south, north, south, etc.). Due to the bi-polar nature of magnets, only even numbers of cathodes may be used in an opposed arrangement without upsetting the repeating pattern (unless "dummy" magnets are used). The opposed magnet configuration gives rise to field linking between the north and south outer poles of adjacent cathodes which serves to reconfine the escaped secondary electrons and distribute them and the plasma intensity evenly around the multi-cathode system. The increased travelling distance of the secondary electrons between cathodes creates more ionization events and increased sputtering. Also the closed magnetic field helps confine the plasma to the substrate region thus enhancing deposition conditions [74 75 76]. In contrast, the mirrored magnet configuration has none of the above advantages and will probably reduce the unbalancing efficiency by restricting the reach of the uncontained field lines to half the inter-cathode distance (see figure 17).

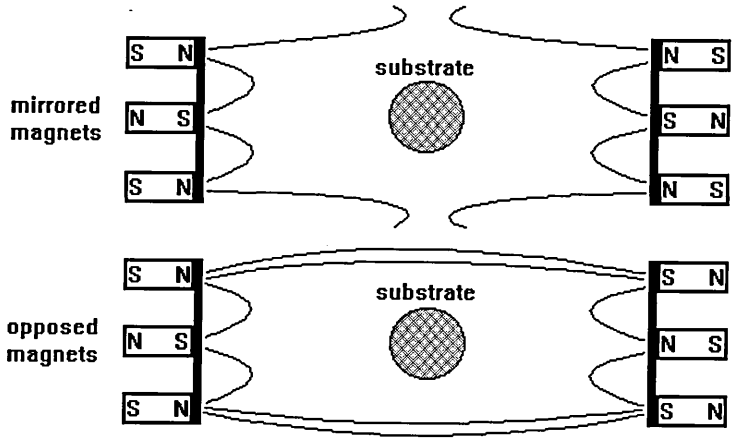

Figure 17. Field Linking

2.3 Coating Deposition

2.3.1 Surfaces and Nucleation

The nucleation stage is a critical step in any PVD process, since it can strongly affect adhesion, crystallographic orientation, grain size, defect density, etc., and so have a significant influence on overall coating properties.

Nucleation and initial deposition of any coating must take place onto a substrate surface, often of a material that is dissimilar to that of the coating. The surface is considered to be the top few atomic layers of a solid and it is likely that it will have different properties from that of the bulk material [77]. This is because many electronic properties of the bulk solid depend upon the three-dimensional periodicity of the potential within it. Any loss of this periodicity in one or more dimensions (ie. due to the existence of a surface), will result in a change in the electronic states and properties near and at the surface. Also, the lack of adjacent neighbours on one side of the surface atoms may make available chemical bonds for possible reactions.

Thus the surface of the substrate material is likely to affect the nucleation and initial deposition of a coating. It may increase the "driving force" of the deposition process in the early stages while it is exposed to the depositing vapour, and indeed continue affecting the growth rate until a film of sufficient thickness (several atomic layers) has been produced such that it has its own bulk and surface properties. An increased driving force (ie. increased nucleation probability) will result in a greater nucleus density, higher deposition rate and finer grain structure at the start of coating [78]. For subsequent growth, secondary nucleation occurs without the substrate influence, the deposition rate decreases and larger grains are obtained. In practice this is what is observed in TEM cross-sections [79 80 81].

Possible nucleation sites on a surface are significantly increased by the existence of defects in the otherwise flat atomic layers [56]. Both monocrystalline and polycrystalline solid surfaces exhibit "steps" on an atomic level [82]. A polycrystalline surface consists of many individual crystals or grains of different crystallographic orientations and surface steps exist within each grain. The steps are formed from new atomic layers building up on the layers below. Between each step is a perfectly flat face called a "terrace". The terraces and the steps may contain further defects such as dislocations and vacancies. They also contain adsorption sites for atoms and molecules (see figure 18).

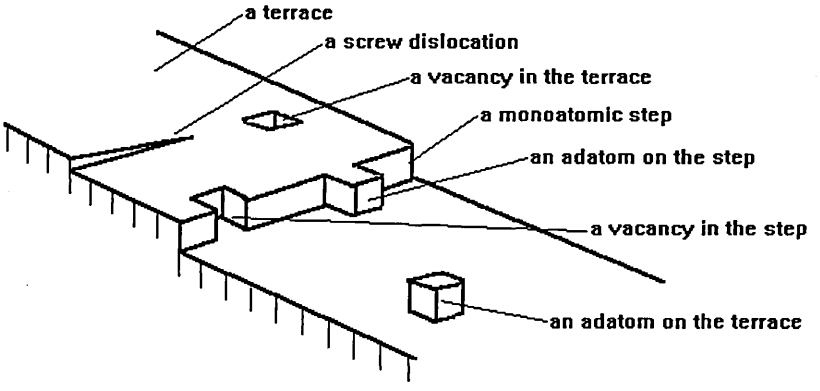

Figure 18. Surface Defects

At any finite temperature above absolute zero the atoms of a solid are vibrating, particularly those at the surface, in their own individual potential energy wells. If an atom receives sufficient thermal energy it may overcome the potential energy barrier so that it can leave its initial site in the surface and become an adatom in a neighbouring position of potential energy minimum [83]. This process is known as "surface diffusion" and gives rise to "adatom mobility". A somewhat higher thermal energy is required for diffusion into the bulk solid. The time that a surface atom stays at one site is called the "residence time" and depends on the bond strength or the depth of the potential well in addition to the amount of thermal energy input. In surface diffusion, atoms or molecules jump between adsorption sites. Generally, the adsorption is much stronger at the steps or in defects than it is on the flat terraces [84]. Hence the residence time is longer, and adatoms tend to diffuse to and coalesce at these points that form primary nucleation sites for coating growth (see figure 19).

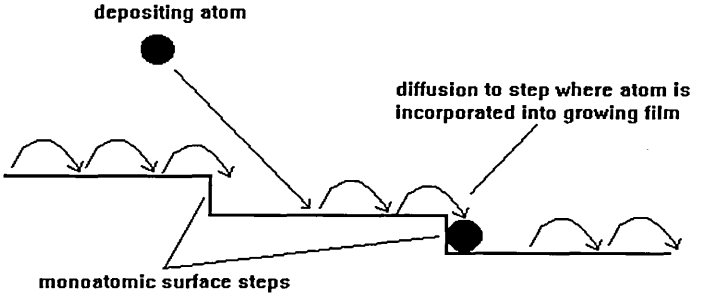

Figure 19. Surface Diffusion

Clearly a surface containing a greater density of surface defects (ie. one that has incurred radiation damage by ion bombardment, or is simply orientated such that a larger number of steps are present at the surface) will have a higher nucleus density, greater deposition rate and possibly better adhesion and finer grain structure. This defect and step structure is fundamental to both nucleation and later to coating growth, since at any time during deposition the growing film will have its own surface layer consisting of steps, defects and related adsorption sites, all of which will influence the condensation process.

2.3.2 Sputter Etching

By applying a large negative bias (eg. -1000 V) to the substrate during the phase prior to coating, and introducing a working gas (eg. argon), then the substrate will behave like a cathode in a dc diode discharge. The gas will break down into a plasma and positive argon ions will be accelerated towards the substrate. The ionization may be enhanced by operating the "real" cathodes simultaneously. When the accelerated ions impinge on the substrate surface they lose their kinetic energy by transfer of momentum to the surface atoms, which in turn cause a collision cascade within the substrate surface. The cascade may travel deep into the substrate dissipating its energy as heat, or it may recoil and cause sputtering of surface atoms. The required effect of the bombardment is to remove the surface atoms of the substrate along with any contaminants, thus cleaning the surface ready for deposition [85]. Additionally it is required that the incident bombardment energy heats the substrate to the desired temperature for deposition (if no auxiliary heating method is employed).

One of the effects of sputtering is a roughening of the substrate surface and the introduction of lattice defects, particularly if the sputter cleaning / heating phase is prolonged. This may be due to preferential sputtering (of particular species or along grain boundaries), angular dependence of sputtering yield, or sub-surface collision cascades causing dislocations. Clearly, for polished decorative surfaces, roughening cannot be tolerated and the sputtering phase would be minimized. However, for other coating purposes, this "etching" of the substrate surface provides a high density of possible nucleation sites for the depositing film, as well as a "mechanical keying" effect. The result is an improvement in the adhesion of the coating to the substrate [56].

Another possible effect of sputtering is ion implantation. This does not occur to any great extent at the energies involved in PVD systems but may be positively utilised if the cathodes are powered during the sputter etching phase so that the plasma contains metal ion species. The implantation will be enhanced (or over-

shadowed) by metal atoms depositing on the substrate surface and diffusing in, due to the heat energy of the ion bombardment. Additionally, part of the substrate surface may be sputtered by the intense ion bombardment, and then redeposited along with incident cathode metal ions producing a mixed layer (for example Ti-Fe). The substrate will thus contain some of the depositing metal which is thought to improve coating adhesion [18].

It is possible to model these sputtering effects using the Monte Carlo program TRIM (TRansport of Ions in Matter) [86]. This program models collision cascades within a surface after bombardment by ions. The incident ions and the recoil atoms are followed throughout their slowing-down processes until their energy falls below a predetermined level (5 eV for the incident ion, and the surface binding energy for the recoil atoms). By recording the number of recoil atoms that reach the surface with sufficient energy to overcome the binding energy, and so leave the solid, the sputter yield can be calculated. Comparisons of TRIM program results with experimental data have shown good agreement [87].

2.3.3 Interlayers

Where surface roughening by sputtering is not acceptable, then the use of a metal interlayer (where the metal is one of the components of the coating, ie. titanium) has been shown to lead to a substantial increase in adhesion [88 89 90 91 92 93]. The improvement may result from a number of factors including chemical gettering effects, where the titanium reacts with and dissolves weak oxide layers at the interface, and mechanical effects, where the titanium acts as a soft, compliant layer that reduces shear stresses across the interface and hinders crack propagation. Stress has been shown to peak in the substrate-coating interface region, particularly as coating thickness increases, and so stress relaxation by this softer interlayer allows the substrate to support much thicker films without spallation than would normally be possible [94 95 96].

Additionally, the titanium interlayer may act as a graded interface between the substrate and coating after diffusion along each of its boundaries (for example, to produce TiC with carbon from the steel, and Ti_2N with nitrogen from the nitride coating). This may improve adhesion by reducing the acute step difference in material properties at the interface.

2.3.4 Coating Growth

Once nucleation sites have been established the film will begin to grow (or condense from the vapour phase) about these sites as "islands" which will expand both vertically and laterally (across the surface) until they meet adjacent islands (see figure 20).

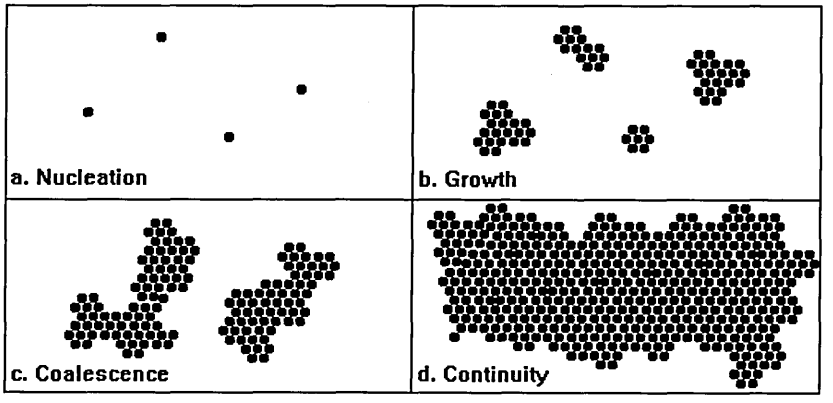

Figure 20. Island Growth

As the islands expand and their growth fronts meet, a grain boundary defect is generated and growth can then only continue vertically. Each island grain will be orientated so as to match, as nearly as possible, the underlying surface grain orientation at the adsorption site, and so initially on the substrate surface all possible orientations will be present. However, what follows is competitive growth between adjacent grains, where a particular orientation (as favoured by the incident bombardment energy and reactive gas pressure) takes precedence [97]. Those grains with the favoured orientation will flourish, growing upwards and sideways at a greater rate than the grains orientated differently. As the film thickens, so these dendritic columns cluster together into larger features with the dominant orientation, and produce the commonly observed columnar structure [98] (see figure 21).

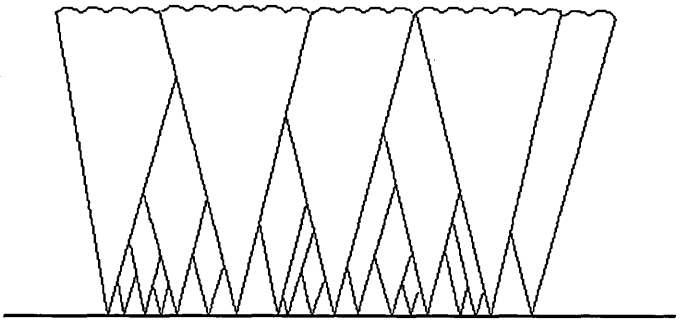

Figure 21. Columnar growth

2.3.4.1 Structure-Zone-Models

The exact nature of the columnar structure varies with different deposition conditions from a porous, open-structure through a fine-grained, fibrous structure to re-crystallised densely packed columns. These structures have been depicted in various structure-zone-models along with the conditions under which they were observed [99] [100]. Movchan and Demchishin [101] were the first to classify these structures, and they identified three distinct zones as a function of substrate temperature over melting point. The low-temperature zone 1 structure corresponds to low adatom mobility and consists of widely spaced columns with domed or angular tops. The mid-temperature zone 2 structure corresponds to significant surface diffusion effects and consists of densely packed columns with a smooth surface. For the high temperature zone 3 structure, bulk diffusion becomes the dominant process and the structure is equiaxed.

For most PVD processes, only the first two structure zones are observed. The half-melting-point limit is normally only exceeded by the very high deposition temperatures found in CVD processes.

Later work by Thornton [102] demonstrated that the presence of a working gas such as argon could modify this model and a further region called zone T or the transition zone was slotted in between zones 1 and 2. Zone T consists of densely packed but poorly defined fibrous grains, and the interesting point to note on the structure-zone-models is that this zone is skewed relative to the bias axis such that at high bias, the fibrous structure is obtainable at a lower temperature than would normally be possible. Thus, as an alternative to increasing deposition temperature, the zone 1 structure can be overcome by subjecting the growing film to ion bombardment.

Messier *et al.* [103] have modified the structure-zone-model to account for these substrate biasing and ion bombardment effects (see figure 22).

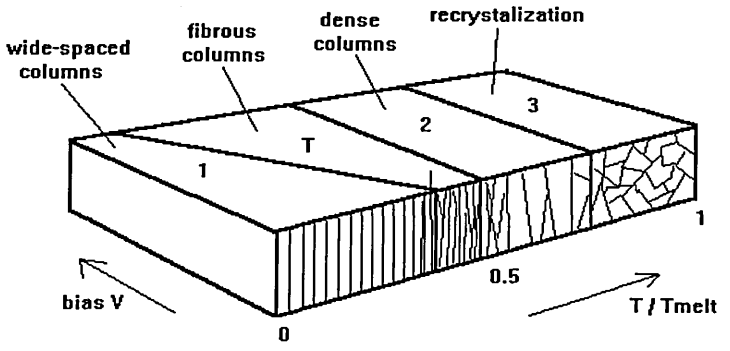

Figure 22. Structure Zone Model

2.3.5 Low Energy Ion Irradiation

By applying a small negative bias (<-250 V) to the substrate material during a coating process that involves the use of a plasma (ionized gas), then the growing film will be subjected to low-energy ion irradiation [48]. The deposition technique then comes under the generic title of "ion-plating". In general, the ion current density J_i depends on the space charge limited ion extraction from the plasma, which is a function of the applied bias. In the case of parallel current emitting and collecting areas, this can be approximated from the Child Langmuir law [52] :

$$J_i = 0.44\varepsilon_o (2Ze/m_i)^{0.5} V^{1.5}/L^2 \qquad \text{..... (7)}$$

where ε_o is the dielectric constant, Z is the average number of charges per ion, e is the electron charge, m_i is the ion mass, V is the potential drop between the plasma and substrate, L is the dark space length between the plasma and substrate.

The effect of this bombardment is to increase depositing adatom mobility due to an input of kinetic energy from the bombarding species, generate point defects in the film structure, and raise the surface temperature. The result of this bombardment, is a densification of the depositing film, similar to the effect of raising the overall process temperature, or lowering the operating pressure such that there are fewer energy-loss collisions. The growing film thus has a higher packing density and smaller grain size [104 105 106 107].

2.3.5.1 Radio-Frequency Biasing

If an unbiased substrate is placed in the glow discharge, then it will still be subjected to bombardment, but by very low energy ions and electrons that exist within the plasma. This will cause some heating and cleaning by desorption of impurities from the substrate surface, but may also result in contamination by other species adsorbing on the surface, so some biasing is usually preferred. If the substrate is a non-conductor, then dc biasing cannot be used, as the substrate will charge up to the floating potential of the plasma and become effectively unbiased. In this case, a radio frequency (rf) oscillating bias supply is necessary to achieve suitable ion bombardment, as with the situation of sputtering an insulating cathode. Once again, the oscillating frequency should be above 1 MHz (radio frequency) in order to obtain a continuous discharge [108] [109] [110].

2.3.5.2 Biasing Edge Effects

A problem encountered with substrate biasing is that it is difficult to ensure uniform ion bombardment and heating on odd-shaped or differently sized components that are being coated simultaneously [111] [112]. Since the substrate behaves as a cathode in the plasma, then it will have an associated dark space region around it, over which most of the applied bias potential will be dropped. At edges or corners, or on small components, the ratio of dark space surface area to substrate surface area increases, causing a localised increase in ion current density on the substrate (see figure 23). The greater ion bombardment can cause overheating, and these areas may also experience different coating growth conditions, resulting in different properties or appearance from the bulk . If the bias is near a critical threshold, these areas may even be subject to re-sputtering of the depositing coating.

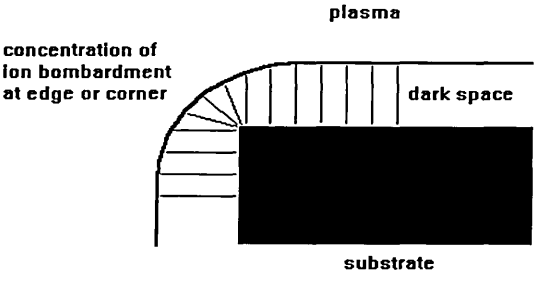

Figure 23. Bias Edge Effects

2.3.5.3 Residual Stress

Residual or internal stresses occur in virtually all hard coatings deposited using PVD techniques, but particularly where some form of ion irradiation has been employed. The levels of residual stress present in a coating are important since they relate to coating adhesion and dictate the maximum coating thickness that can be deposited before spallation occurs [94]. Measurements generally show high compressive stresses in the coating material, attaining values up to several gigapascals (GPa) in both evaporated and sputtered coatings [95]. The creation of these stresses is attributable to either thermal expansion mismatch of the substrate and coating materials, or to growth-induced stresses occurring during the condensation process. Total residual stress is the sum of these two stress types [113].

Thermal expansion mismatch occurs when the lattice of the substrate material expands (or contracts) by a different amount to that of the coating material, when subjected to a temperature change. This temperature change may occur if there is a fluctuation in the deposition process temperature, or as the samples cool after the process, or heat as a result of friction during use. Hence, if minimum residual stress is required during use, then the deposition temperature should be kept constant and should match the working temperature that the coating will be subjected to. Thermally induced stress can be calculated by :

$$\sigma = E \Delta\alpha \Delta T / 1-\nu \qquad \text{..... (8)}$$

where σ is the stress, E is Young's modulus of the coating, $\Delta\alpha$ is the difference between the thermal expansion coefficients, ΔT is the difference between room temperature and the deposition temperature, and ν is Poisson's ratio of the coating.

Growth-induced stresses are a function of the microstructure and ion bombardment during the deposition process. A dense coating with close-packed columns tends to have high compressive stresses as the column boundaries "press" against each other. A less dense coating with an open columnar structure tends to have much lower stresses as the columns can relax by expansion into the voids. Ion bombardment often generates compressive stresses by the "ion-peening mechanism", in which the surface region of the depositing film undergoes plastic deformation in order to accommodate the defects produced by the bombardment process. The impacting ions themselves can also cause an expansion in the surface region by a process known as "ion stuffing", in which the bombarding ions, such as argon, are "forced" into the depositing structure and become trapped [114]. Clearly, any forced expansion of the coating structure results in a state of compressive stress. Ion bombardment induced

stress σ can be calculated by :

$$\sigma = K R E^{0.5} \quad \text{..... (9)}$$

where K is a material-dependent constant, E is the ion energy, and R is the ion-to-atom arrival ratio.

2.3.6 Reactive Deposition

Reactive deposition involves the introduction of a reactive gas that combines with the metal vapour flux to produce a compound film on the substrate surface [115 116]. The choice of reactive gas depends on the desired compound, for example nitrogen (to form a nitride), methane or acetylene (to form a carbide), or a mixture of both (to form a carbo-nitride). Introduction of the gas into a plasma, subjects the gas molecules to electron and ion bombardment which results in dissociation, excitation and ionization of the gas atoms. The use of a plasma is important if high deposition rates are to be attained in PVD as it governs one of the rate-limiting steps. For the formation of a compound by any chemical reaction, the appropriate thermodynamic and kinetic constraints must be realised and the rate-controlling steps of such a reaction are :

1. Adequate supply of reactants.
2. Adequate collision frequency.
3. Adequate energy to activate the reaction.
4. Adequate rate of removal of reaction by-products.

In a vapour deposition system these steps are resolved as follows :

1. Adequate supply of reactants is attained by ensuring a high flow rate of reactive gas and high evaporation or sputtering rate of the cathode material.
2. Adequate collision frequency is attained by ensuring a sufficient pressure in the reaction chamber of reactive gas and metal vapour flux.
3. Adequate activation energy is attained by high temperature or by plasma assistance.
4. Adequate rate of removal of reaction by-products is attained by high pumping speed of the vacuum system.

The use of high temperature to activate a reaction is normal for CVD systems, but one of the virtues of PVD is the low deposition temperature. Thus activation by a plasma is normally used. Sputtering systems that employ a glow discharge automatically generate a plasma, as do arc and electron beam evaporation. Other systems will often include an electron source to provide ionization assistance. Thus the "activated" gas promotes reaction kinetics and accelerates the rate of compound film formation.

The pressure in a deposition chamber is governed by the reactive gas flow rate and metal vapour production rate, and the pumping speed of the vacuum system. Normally the latter will be fixed, but will be sufficiently high so as not to unduly constrain the reaction. Thus the main rate-limiting step in a PVD system will be the adequate supply of reactants. The evolution of metal vapour flux is controlled by the power input to the cathode and would appear to be the only constraint since the chamber could be easily saturated with reactive gas. However, if that were done, most PVD systems would function quite inefficiently due to a reduction in the cathode output and reduced mean free path length of the depositing species.

All PVD systems require a low pressure environment such that a useful metal vapour may be liberated, and also to allow many of the evaporation and sputtering mechanisms to operate. Reactive gas enters the chamber at one or more points, and metal vapour will be produced from one or more cathodic sources. The reactive gas will tend to diffuse all around the chamber, and so the partial pressure must be low enough to allow a similar impingement rate of both reactants upon the substrate simultaneously (for maximum efficiency). The impingement rate of reactive gas atoms on the substrate surface is largely independent of the cathode-to-substrate distance [117], so the flux density of the metal vapour is once again the limiting factor. The metal vapour will leave the source with a high kinetic energy which will promote adhesion to the substrate. If the partial pressure of reactive gas is too high, then the metal vapour flux will undergo a significant number of energy loss collisions due to mean free path considerations, before reaching the substrate. If the partial pressure is too low, then the metal vapour flux will not be scattered at all, and line-of-sight coating problems will arise. In addition to this, over- or under-stoichiometric coatings will also be produced.

Thus a basic operating pressure for PVD systems is dictated that is a product of the reactive gas flow rate and metal vapour production rate, the two being mutually linked due to reaction of the former with the latter. The matter is further complicated by the fact that the compound film only forms on a surface and not in the gas phase (due to dissociation by the energetic plasma), and that this surface need not necessarily be that of the substrate.

2.3.6.1 Cathode Poisoning

A compound film may also form on the surface of the solid metal source or cathode. This is known as "poisoning" and will almost always reduce the cathode's efficiency. In the case of evaporation, the rate at which metal vapour is liberated is dependent on the melting point and heat of vapourization of the source material. For a ceramic coating, this will be higher (often by a factor of two or three times) than that of the pure metal, and hence the rate of evaporation will be proportionally lower. Since most evaporative sources are in a continuously molten state that is heated from within or below, this is not a problem. Only the arc source remains predominantly solid, but even for this technique, poisoning is not so critical due to the high intensity of the cathode spot. In fact, poisoning is sometimes actively encouraged in order to reduce droplet emission [27].

In the case of sputtering, the effect of poisoning is more profound since the cathode is always in the solid state. Again, the energy input requirements for sputtering a ceramic are somewhat higher than those for a pure metal, hence the yield per incident ion will be lower [109 118]. A drop in metal vapour yield at the onset of poisoning results in an excess of reactive gas which will cause more poisoning and thus exacerbate the problem. The extent of poisoning will increase until the whole cathode is poisoned, at which point the yield will stabilise at its minimum level. Additionally, the evolved vapour will not be a pure metal, but instead will be a mixture of the compound constituents. It is therefore necessary for the reactive gas flow to be reduced accordingly in order to maintain a stoichiometric coating.

Thus if poisoning is allowed to occur, the deposition rate will fall dramatically and the coating process will no longer be economically viable.

It is, however, possible to "recover" a poisoned cathode by reducing the reactive gas flow below the 50:50 ratio such that the compound coating is sputtered away, so returning to the pure metal cathode situation. At this point the sputter yield will rise once more and the reactive gas flow will again need to be adjusted accordingly.

The poisoning effect can be illustrated graphically by plotting sputter rate or deposition rate against reactive gas flow (see figure 24). A hysteresis loop effect is observed where the flow rate for cathode recovery is lower than the flow rate for the onset of poisoning. Clearly the optimum operating flow for maximum sputter rate is at a point just prior to the onset of poisoning. This should not be confused with an identical flow rate just prior to the onset of recovery, that corresponds to a much lower sputter rate. The operating flow should thus be approached from a low value on the hysteresis curve.

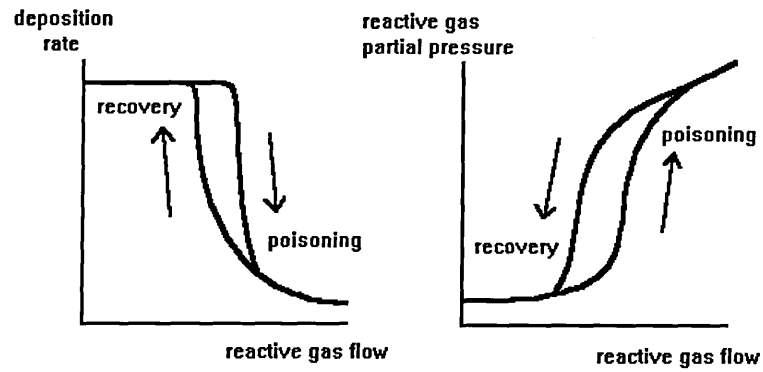

Figure 24. Hysteresis Loops

A similar hysteresis loop can be plotted for reactive gas partial pressure against reactive gas flow (see figure 24). As before, the flow rate for cathode recovery is lower than the flow rate for the onset of poisoning. The graph, however, is reversed, and partial pressure rises at the onset of poisoning. This is because as a solid compound is formed from a gas and a vapour, the volume occupied by the constituents is reduced, and hence so is the pressure. As the cathode becomes poisoned, there is less metal vapour to react with the gas and become solid. Thus there is more gas in the system and the pressure rises.

Clearly the use of a sensitive and fast-response gas flow controller is required that monitors the relative levels of reactants in the chamber and thus maintains stoichiometry without allowing cathode poisoning. It should also be capable of effecting a rapid recovery if poisoning should occur. The use of high pumping speeds helps in this respect by rapidly removing excess reactants from the chamber.

It is possible to identify the onset of cathode poisoning by monitoring the reactive gas partial pressure, or the intensity of the metal vapour flux in the plasma (using optical emission spectroscopy), or the relative amounts of both reactants (using mass spectrometry). All methods have been used in practice [119] [120] [121]. The monitored signal is used as a closed-loop feedback to some form of automatic gas flow controller that is preferably of a proportional type that will not induce it's own oscillations and instabilities into an otherwise erratic system.

2.4 Evaluation Techniques

2.4.1 Colourimetry

Colourimetry is the quantitative measurement of perceived colour, which encompasses illumination, reflectance (or transmission) of the sample, and visual response of the observer. The colourimeter is an instrument that senses tristimulus (X, Y, Z - red, green, blue) values and converts them to chromaticity (hue and intensity) components of colour. It can detect minute variations in the surface colour of a sample in a quantitative and objective manner, whilst human colour perception is both subjective and of variable sensitivity over the visible spectrum (400-700 nm wavelength).

It has particular application to the decorative coatings industry for providing colour description and matching, but some workers also believe it can give an indication of composition and stoichiometry [122 123 124].

Colour determination involves illuminating the sample surface with a standard light source (eg. a xenon flash tube) and detecting the reflected light with photocells, individually filtered to accept one each of the primary colours; red, green or blue. The detected signal values are compared to reference calibration values and the deviation calculated. Thus a "colour difference" measurement is made based on the CIELAB Colour Space standard established by the Commission Internationale de l'Eclairage (CIE) in 1976. The CIELAB Colour Space has the co-ordinates L^*, a^*, b^*, which correspond to Lightness or reflectance (black-white), red-green, and blue-yellow differences [125 126] (see figure 25).

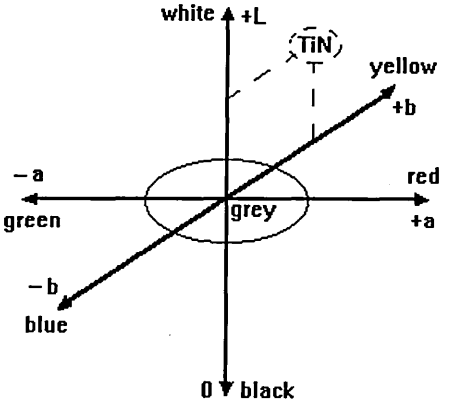

Figure 25. $L^*a^*b^*$ Colourspace Diagram

2.4.2 Surface Roughness Profiling

The surface roughness of a coated component can be a very important parameter, whether the coating is used solely for decorative purposes or if it is required to enhance engineering performance. The surface finish of PVD coatings are claimed to mimic the underlying surface finish of the uncoated substrate [43]. In practice the coating surface is always rougher, due to non-uniform coverage, defects or voids in the growing film, and inclusion of droplets (macroparticles) from the cathodes [29] [127]. These result in an increase in roughness of typically around 1 μm, or more in the case of droplets. For decorative coatings the loss of surface finish is clearly detrimental from an aesthetic point of view and so is undesirable. For engineering components, the quality of surface finish can have a more far reaching effect. One of the reasons that ceramic coatings extend tool life is that as well as being very hard, they also have a low coefficient of friction. This means that the tool can be operated at higher speeds, requires less cooling, and is more resistant to cold welding between itself and the workpiece [128]. Obviously, if the surface roughness of the coating is high, then this low friction advantage will be reduced [129].

Surface roughness measurement usually involves moving a stylus across the surface of the sample. The minute vertical displacement of the stylus is monitored and a trace profile of the surface produced. Several statistical values are normally quoted to describe the roughness measurement over a set distance :

R_{max} - the max. full stylus deflection from peak to valley.
R_z - the average of all deflections from peak to valley.
R_a - the arithmetic mean of all deflections from the mean line.

It is also possible to measure roughness profiles without any physical contact with the sample surface. The "laser stylus" profilometer focuses an infrared laser beam on the sample surface, and detects the reflected beam. The sharp focus of the beam is maintained by automatically varying the position of the objective lens in the instrument. The displacement of the objective lens is linearly proportional to the surface roughness of the sample, and so detection of this displacement by a sensitive transducer, allows the surface roughness to be recorded.

2.4.3 Coating Thickness Calotest

Coating thickness can affect the validity of both hardness and adhesion tests, and is also likely to affect the actual coating performance itself. Thus a knowledge of the

thickness is vital. An obvious way to measure the thickness is to cut up the coated component, examine a cross-section in a SEM and measure directly. In practice, particularly in an industrial environment, such a method would be too time consuming, laborious and expensive, not to mention destructive to the component.

A somewhat quicker method, though still partially destructive, is the calotest [130] [131]. This involves eroding a hemispherical crater in the coated sample using a rotating steel ball-bearing (10-50 mm diameter) and standard metallographical diamond lapping paste. This is known as "ball-cratering" (see figure 26).

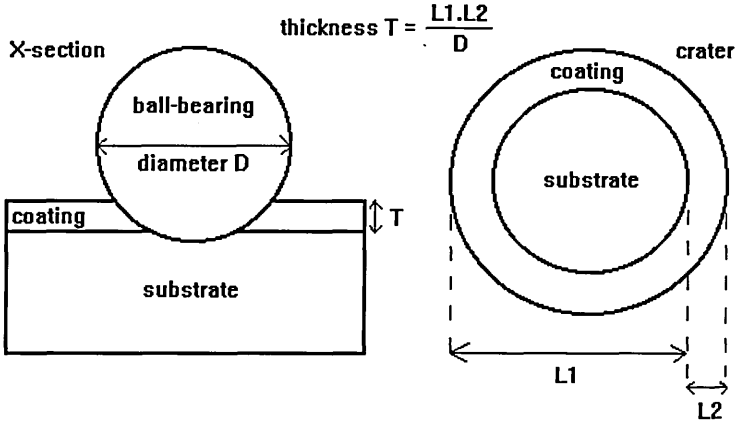

Figure 26. Calotest

The diameters of the coating ring and substrate crater of the shallow hemispherical taper section are then measured under an optical microscope. By relating these two measurements to the ball diameter, a value for the coating thickness can be easily obtained.

2.4.4 X-Ray Fluorescence Thickness Test

A totally non-destructive coating thickness test involves the use of the X-ray fluorescence (XRF) technique [132] [133].

When a sample is bombarded by X-rays, the incident photon energy is absorbed by an inner shell electron of a constituent atom. If this energy is sufficient, it will lead to the ejection of the electron from the atom. The atom will thus become unstable and the vacancy will be filled by the transfer of an electron from an outer shell. In transferring to the inner shell, the electron will lose energy, which will appear as an emitted X-ray photon characteristic of the atomic transition. The overall process, of absorption of an X-ray beam followed by emission of a set of secondary X-rays, is

known as X-ray fluorescence (see figure 27).

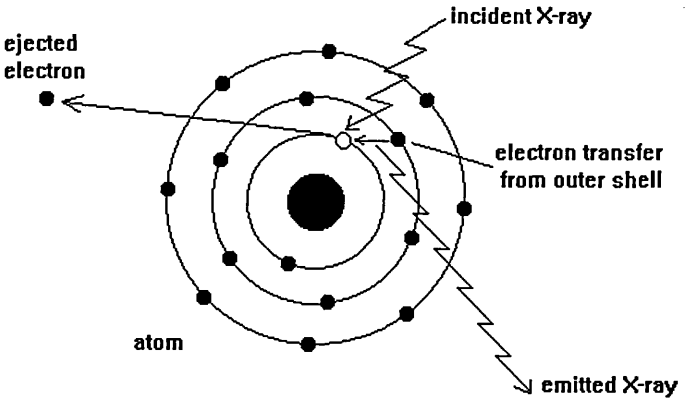

Figure 27. X-Ray Fluorescence

XRF can be used to identify the elemental composition of a sample, but may also be used to determine coating thickness from the emission intensity, by assuming that the thickness, composition and density of the coating are all uniform. Either the characteristic X-rays of the substrate or the coating may be used.

If X-rays from the coating are used, then the emission intensity will be approximately proportional to the coating thickness, due to the emission area density, but must be corrected for self-absorption effects. Calibration curves or mathematical relationships can be prepared from standards of known thicknesses and compared with the measured intensities to determine the film thickness.

If X-rays from the substrate are used, then the emission intensity will be attenuated by the beam passing through the coating. The attenuation will be proportional to the film thickness, which may be determined by comparison with calibration curves of known thicknesses, or calculated directly using absorption equations if the density of the coating is known.

Beer's Law defines X-ray absorption as :

$$I/I_0=\exp(-x\rho\mu/\rho) \qquad \text{..... (10)}$$

where I is intensity following absorption, I_0 is intensity of incident X-rays, x is thickness (cm), ρ is density (g/cm^3) and μ/ρ is mass absorption coefficient.

2.4.5 Microhardness Test

The hardness of a solid material is defined as its resistance to penetration by another body under load [134]. Hardness is often used as a guide to the suitability of a coating for any application requiring high abrasive wear resistance. The term "microhardness" usually refers to indentation hardness tests with loads not exceeding 1000 g. Some tests may use loads as low as 1 g, but for ceramic coatings, the majority are in the 25-100 g range.

The test involves pressing a diamond indenter, of known geometry, into a sample surface for a fixed time duration using a known force. A dimensional measurement of the indentation in the surface is then made visually, and a "microhardness number" is calculated (usually in the units kg/mm^2). Two common measurement scales are in use; Vickers and Knoop [135]. These differ principally in the shape of the diamond indenters; the Vickers is a square-base pyramid, while the Knoop is a rhombic-base pyramid with a ratio between the long and short diagonals of about 7:1. Consequently, the Knoop indenter offers a longer indent diagonal than the Vickers for the same penetration depth, making it much more suitable for the measurement of thin films. For direct hardness measurement, the coating thickness should be at least ten times the indentation depth so that there is no contribution to the measured hardness from the substrate material. The indentation depth can be reduced by lowering the loading force, but there is a corresponding reduction in the indentation size. This makes it more difficult to accurately measure the length of the diagonal and leads to increased subjective measurement errors [136].

Two alternative solutions are possible. One is a modelling approach where the composite coating and substrate hardness is deconvoluted to approximate the actual coating hardness alone [137]. The other is a direct approach using a depth-sensing hardness tester called a "ultra-microhardness indenter" or "nano-indenter" [138]. This is computer-controlled and can make very small indents since no visual measurement is required. Hardness is determined from the depth of penetration of the indenter. It has three distinct advantages; use of very low loads, no subjective error, no "shrinkage" of the indentation prior to measurement due to elastic recovery after removal of the indenter [139].

2.4.6 Rockwell Indentation Adhesion Test

Adhesion is the state in which two surfaces are held together by interfacial forces. For any coating application, the minimum acceptable requirement is that the coating should remain adhered to the substrate throughout its specified use. One method of

assessing this is to excessively load the coating-substrate system to a greater extent than would normally occur. Such a method is the Rockwell indentation test [106] [140] [141].

Using a conventional Rockwell-C hardness indenter with the usual 150 kg load, a mechanically stable crack is introduced into the coating-substrate system. The resistance to propagation of the crack along the interface is then used as a measure of the adhesion. The test is observed visually as cracking or spallation of the coating at the surface (see figure 28). Depending on the extent of the failure, the coating may be classed as either acceptable or not acceptable, but no specific value is normally assigned.

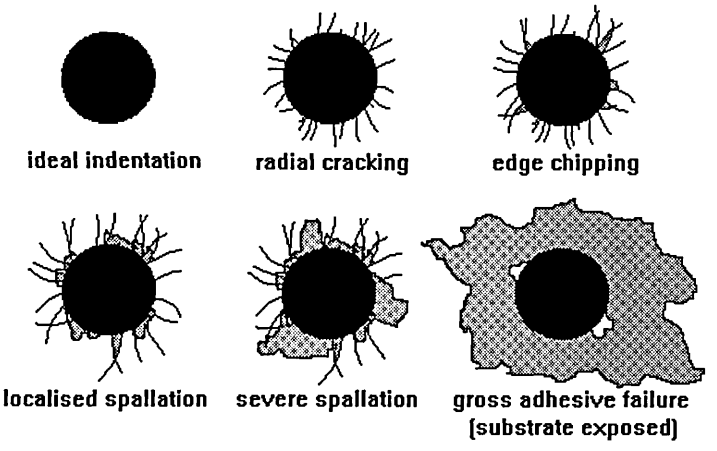

Figure 28. Rockwell Adhesion

The test makes the assumption that the interface is the weak point in the coating-substrate system, resulting in adhesive failure under load. When the fracture occurs within the coating or substrate itself then cohesive failure has occurred and it may be concluded that the interface is at least as tough as the weaker of the film or substrate.

2.4.7 Scratch Adhesion Test

Adhesion is more directly measured mechanically in terms of the minimum force per unit area required to separate the coating from its substrate. The scratch test is the most widely used technique for this [142] [143] [16]. It involves drawing a Rockwell-C diamond over the sample surface under a stepwise or continuously increasing normal force until the coating detaches (see figure 29). In practice the film is seldom removed completely from within the scratch channel, but as patches along its length.

At low loads, small areas may spall due to isolated flaws in the coating surface. A critical load L_c is usually quoted which corresponds to the load at which the coating is removed in a regular way along the whole channel.

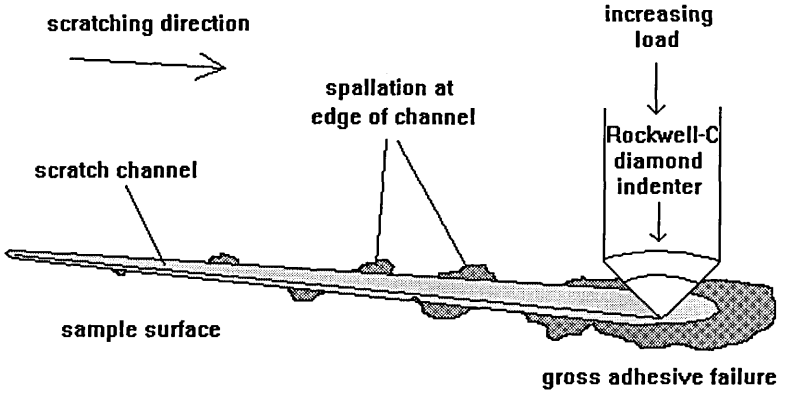

Figure 29. Scratch Adhesion

Adhesive failure can be detected in several ways. The best, but unfortunately the slowest method is visual observation by optical or scanning electron microscopy [144] [145] [146]. This is done after the scratches have been made and allows identification of the type of failure mode. Detection may also take place whilst the scratches are being made, by monitoring the acoustic emission (vibration) generated when a brittle coating cracks [147]. Finally, detection may occur by monitoring the frictional force of the diamond moving against the sample surface [148] [149]. There will be a change in friction between the diamond and the coating, and the diamond and the substrate, and so the point of coating removal may be determined.

With all the detection methods, the critical load L_c is determined by the operator and so the quoted load for adhesive failure will be subjective. In addition, there are a number of other parameters that can affect the result. These are coating thickness, substrate hardness, residual stress and indenter wear. The outcome of this is that absolute scratch adhesion results cannot be reliably quoted, though the test can be very useful for relative comparisons of similar coating-substrate systems produced by the same process for internal standardisation purposes.

2.4.8 X-Ray Diffraction Analysis

X-Ray Diffraction (XRD) is an analytical technique that provides structural information about the crystal lattice and grain orientation of a solid sample [133 150]. It relies on diffraction of a beam of X-rays by atomic planes lying in the surface of the sample.

Diffraction is essentially a scattering phenomenon in which a large number of atoms co-operate. X-rays are used because, in general, diffraction will only occur when the wavelength of the incident radiation is of the same order of magnitude as the repeat distance between the scattering centres (around 0.3 nm for most crystals). Diffraction is a phase relationship between two or more waves from an incident X-ray beam that have been scattered by a periodically repeating array of atoms in a lattice. When these waves interact there will be constructive interference if they are in phase (ie. if their path lengths are equal or if they differ by a whole number of wavelengths). However, in most directions of scattering, these waves will be out of phase and so destructive interference will occur and the waves will cancel out.

If an X-ray beam is incident on an atomic array with interplanar spacing d (see figure 30), and is diffracted at an angle θ (the Bragg angle) by atoms K and L lying in parallel planes (A, B, C, ...), then the path difference between the diffracted rays is given by :

$$ML + LN = d.\sin\theta + d.\sin\theta \qquad \text{..... (11)}$$

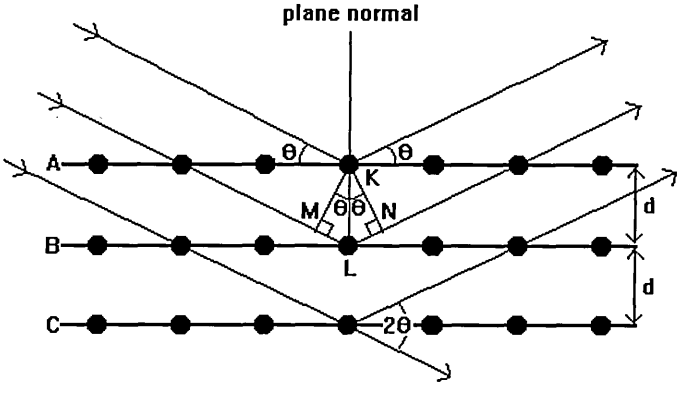

Figure 30. Diffraction of X-Rays by a Crystal

The two rays will be completely in phase if the path difference is equal to a whole number of wavelengths $n\lambda$. Hence, constructive interference and a diffracted beam

of X-rays will occur when the Bragg equation is satisfied :

$$n\lambda = 2d.\sin\theta \qquad \text{..... (12)}$$

The diffractometer consists of an X-ray source emitting radiation of a known wavelength, and a movable detector (counter). The sample, positioned at the centre of the apparatus, can rotate about its axis through an angle θ. The detector rotates about the same axis but through an angle 2θ from the source, so as to maintain the Bragg conditions (see figure 31).

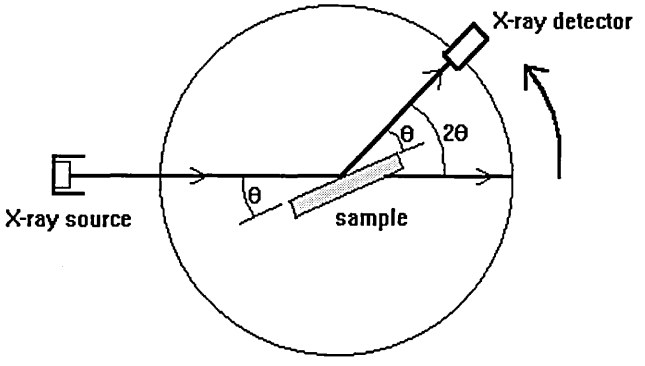

Figure 31. X-Ray Diffractometer

The output from the detector (X-ray intensity) is plotted against the diffraction angle 2θ and is represented as a series of peaks characteristic of the unit cell of each chemical phase present in the crystalline solid. The positions of the peaks provides information about the size and shape of the unit cell, and the intensities provide information about the positions of the atoms within the unit cell [151]. The peak widths can be used to evaluate the size and strain of the polycrystalline grains, and for determination of residual stresses [114 152 153 154].

2.4.9 X-ray Photoelectron Spectroscopy

X-ray Photoelectron Spectroscopy (XPS) is a near-surface (top few atomic layers) analytical technique, although depth profiling is also possible in association with an auxiliary ion gun which sputters away progressively deeper layers between successive measurements [84 155 156 157].

XPS relies on the ionization of atoms within the sample being analysed. An incident beam of monoenergetic X-rays interacts with the sample surface and is "photoabsorbed", ie. the energy of the X-ray photon is transferred to the electrons in the atom thus placing them in an excited state. If the quantum of supplied energy is sufficient (greater than the first ionization energy) then an electron will be emitted and the atom will be said to be ionized. This mechanism is called the "photoelectric effect" and the emitted electron is called a "photoelectron" (see figure 32).

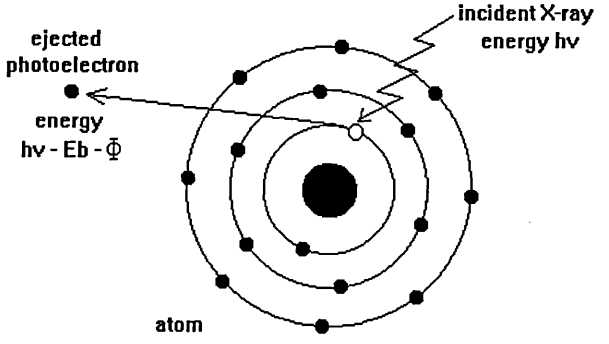

Figure 32. X-Ray Photoelectron Spectroscopy

Depending on the energy absorbed, the photoelectron may originate from a core or valence electron orbital. The kinetic energy E_k of the photoelectron is related to the electronic binding energy (or ionization energy) E_b of the sample atoms :

$$E_k = hv - E_b - \Phi \qquad \text{..... (13)}$$

where h is Planck's constant, v is the frequency of the incident X-rays, Φ is the work function of the sample.

Thus the binding energies of the sample atoms may be determined, and since the patterns of binding energies of all the elements are uniquely different, the elemental species may be identified. Estimates of composition can be made by consideration of peak intensities in the energy spectrum obtained. XPS is particularly sensitive to small differences in atomic binding levels corresponding to different valence states which manifests itself as peak shifts and gives an indication of chemical bonding.

2.4.10 Scanning Electron Microscopy

Scanning Electron Microscopy (SEM) depends on the interaction of a finely focused electron beam with a sample [130 158 159]. The incident electrons will either be undeviated or they will be scattered and then absorbed, reflected or transmitted.

In the SEM an electron gun provides a stable source of electrons which is used to form the electron beam. The electron beam passes through several electromagnetic lenses whose function is to demagnify and focus an image of the electron source (the gun-crossover) onto the sample surface. Demagnification is necessary to reduce the electron beam probe diameter for higher resolution imaging. The final "probe-forming" lens also comprises scan coils for rastering the focused electron beam across the sample surface.

An image of the sample is formed either from the reflected (back-scattered) electrons or from emitted secondary electrons, principally the latter. Secondary electrons are produced through inelastic collisions of the incident electron beam with the loosely bound outer electrons of the atoms in the sample. The electrons are detected by a scintillation photomultiplier detector and converted into an electrical signal. This signal is used to control the intensity of output (brightness) of the electron gun in a cathode ray tube (CRT). An image is formed by synchronising the rastering of the electron beam across the CRT screen with the rastering (or scanning) of the SEM electron beam across the sample surface.

As well as secondary and back-scattered electrons, the interaction of the incident electron beam in an SEM will produce, among other things, characteristic X-rays (see figure 33).

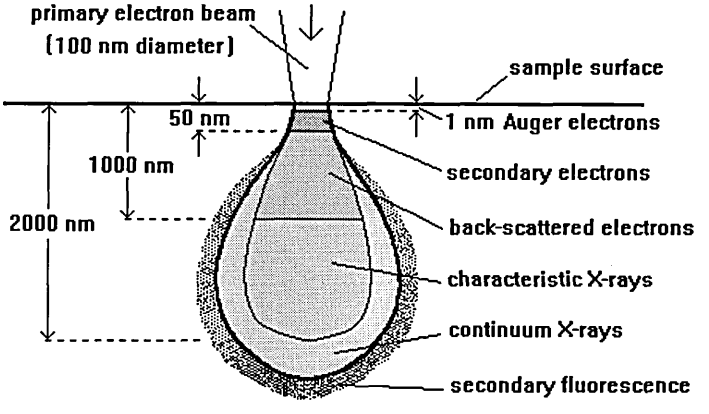

Figure 33. Electron Beam Interaction Volume and Analysis Resolution

When an electron is ejected from an inner atomic shell by inelastic collision with the high energy electron beam, the result is an ion in an excited state. The ion "relaxes" to its ground state by the transition of an electron "dropping" from an outer shell into the vacancy in the inner shell. Energy must be emitted during this transition in the form of a photon of electromagnetic radiation (an X-ray in the case of high energy transitions involving inner shells). The energy of radiation is characteristic of the element from which it came, hence the name "characteristic X-ray". The SEM is usually fitted with an X-ray detector (either energy-dispersive (EDX) or wavelength-dispersive (WDX) or both) thus allowing it to perform chemical analysis as well as imaging of the sample [160].

2.4.11 Transmission Electron Microscopy

Transmission Electron Microscopy (TEM), as the name suggests, depends on a sample being sufficiently thin (less than 100 nm) so as to allow electrons to be transmitted through it [161] [162]. This type of electron microscope is analogous of the optical variety, but with a much higher resolution, and hence possible magnification, that is associated with using radiation of a shorter wavelength for imaging. In optical microscopy, differences in absorption in the sample are normally responsible for image contrast whereas in the case of electrons, contrast is obtained by utilising differences in scattering power.

The electron beam accelerating voltage in the TEM is somewhat higher than that of an SEM electron gun (up to 200 kV as opposed to less than 50 kV) so as to increase the electron energy, thereby reducing the wavelength and increasing sample penetration.

The electron beam passes through several electro-magnetic lenses whose function is to demagnify, focus and render parallel the rays forming an image of the electron source (the gun-crossover) onto the thinned sample surface. The scattered and transmitted electrons which pass through the sample will then be recombined by the objective lens to form a diffraction pattern in the back focal plane and a magnified image in the image plane (see figure 34). A further series of electro-magnetic lenses projects either the diffraction pattern or the image onto a fluorescent screen for observation, or onto a photographic plate for recording. By varying the current in these final lenses, the magnification can be altered from 1,000 times to over 1,000,000 times.

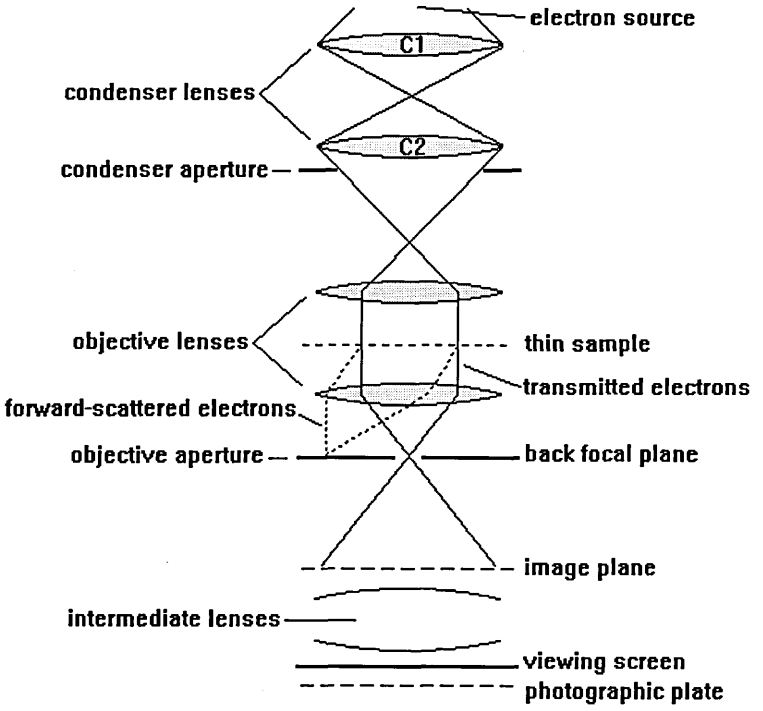

Figure 34. Transmission Electron Microscope

An extension to the conventional TEM (CTEM) is the Scanning Transmission Electron Microscope (STEM) [163] [164]. It is so named because it combines features of both SEM and TEM. Essentially it consists of an electron gun and a series of electro-magnetic lenses which focus a fine electron beam probe onto a thin sample and scan it across the surface. The electrons are transmitted and forward scattered through the sample before the objective lens recombines them in the back focal plane. Further lenses direct these electrons towards a detector and the electrical signal is used to modulate the display of a CRT to produce an image of the sample.

The STEM will operate as a conventional TEM, however it is also possible to operate it as a conventional SEM using secondary or back-scattered electrons, but with much greater resolution. In addition, it is possible to perform chemical analysis by energy dispersive (EDX) detection of X-rays generated by inelastic electron collisions within the sample.

2.4.12 Glow Discharge Spectroscopy

Glow Discharge Optical Emission Spectroscopy (GDOES), like any atomic emission spectroscopy, relies on excitation of atoms within the sample being analysed [165].

When energy is transferred to an atom, providing it is sufficient, it will increase the energy of an electron such that it can move to a higher energy level or orbital. This will be an unstable state since there will be a vacancy in the lower energy level

which the electron will prefer. Thus the electron will move back to this lower energy level, dissipating its excess energy as it does so (see figure 35).

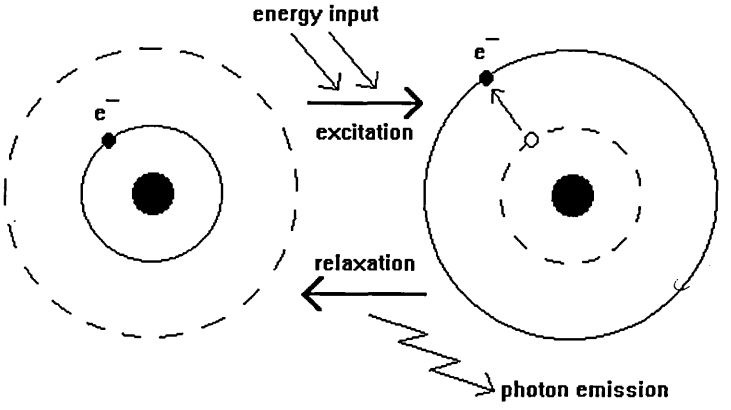

Figure 35. Principle of Excitation and Emission

This excess energy is emitted as a photon whose wavelength λ corresponds to the energy E emitted :

$$E = hc/\lambda \qquad \text{..... (14)}$$

where h is Planck's constant and c is the speed of light.
Any transition of an electron between two quantised energy levels corresponds to the absorption or emission of energy as electromagnetic radiation. Because each element atom has different electron orbital energy levels, then the possible electron transitions for each element will also differ. Hence excitation of different elemental atoms will give rise to the emission of characteristic spectral lines by which those elements may be identified. The intensities of the lines are proportional to the number of emitted quanta, and hence to the element concentration. This is the essence of atomic emission spectroscopy [166].

For line spectra to be produced in this way the atoms must be in the form of a low pressure gas, since an excited or hot solid will produce a continuum of energy due to thermal radiation and lattice vibrations. So, the solid must be volatilised into an evacuated chamber. A glow discharge plasma is the volatilisation method used in this technique [167].

Glow discharge spectroscopy has a number of advantages over more commonly used analysis methods [168] :

1. Little or no sample preparation is required for bulk solids.
2. It naturally separates the removal of atoms from the solid surface (atomization), from the subsequent excitation and ionization of those atoms, thus reducing matrix effects and normalising sample-to-sample inconsistencies.
3. Because successive surface layers are removed the technique offers compositional depth profiling.
4. Due to the small cathode to anode distance, sputtering occurs over a narrow volume resulting in uniform sample erosion over the analysed area giving good resolution when used for depth profiling.
5. The excitation and emission layer is also thin, minimising self-absorption and giving a linear relationship between intensity and concentration, with sharp emission lines.

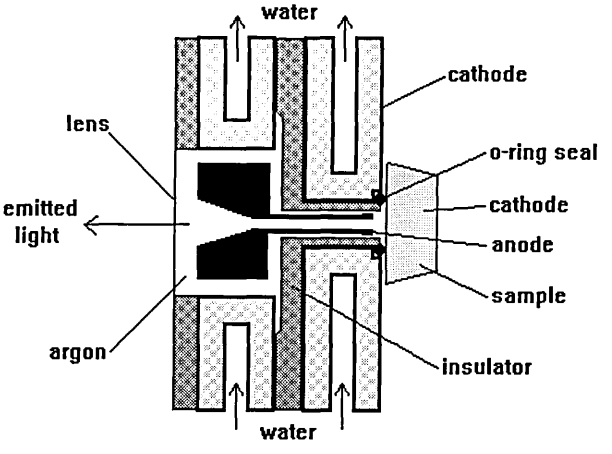

Figure 36. Glow Discharge Lamp

The analysing chamber or glow discharge lamp used in this technique is based on a design by Grimm in 1968 [169] (see figure 36). It consists of a small vacuum chamber with a hollow cylindrical anode typically 4 or 8 mm in diameter with the sample to be analysed forming the cathode at one end. The outside of the anode cylinder is vacuum pumped and bled with a working gas (argon). The other end of the cylinder contains a window through which the photon emission is detected via a polychromator. Typical operating conditions are 500 to 1500 V and 20 to 200 mA, giving a sputtering rate in the range 10 to 100 nm per second.

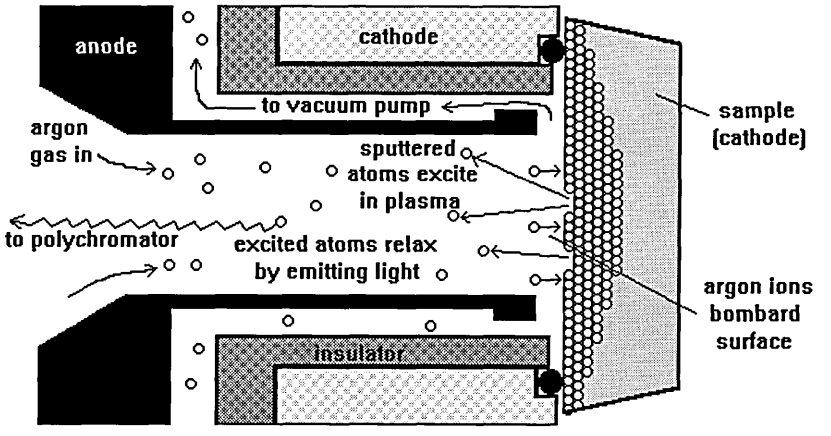

Figure 37. Sputtering in the Glow Discharge Lamp

The glow discharge sputtering process in the lamp operates conventionally [170] (see figure 37). A voltage is applied across the anode and cathode that causes breakdown of the working gas, whose ions are then accelerated across the dark space towards the cathode. On impact, kinetic energy is transferred (so conserving momentum) that causes the ejection (or sputtering) of neutral cathode atoms and secondary electrons. The secondary electron emission accelerates rapidly away from the cathode and upon collision with working gas atoms, causes ionization thus sustaining the discharge. The sputtered cathode atoms diffuse across the dark space into the negative glow region and are excited or ionized by collisions with secondary electrons or working gas ions. These excited cathode atoms will emit characteristic line spectra as described previously. Most of the sputtered material and argon working gas are then pumped out through the vacuum system. However, some sputtered material is deposited on the anode and some at the edge of the eroded crater, forming a slight lip. This can cause the glow discharge lamp to short circuit on long analyses, thus limiting the maximum depth of profiling to between 50 and 100 μm depending on the sputter rate of the material. Between analyses, the anode is automatically cleaned using a reamer.

At one end of the glow discharge lamp is a window through which the emitted photons pass into a polychromator for detection. The polychromator is based on the Rowland focusing property that enables a range of spectral wavelengths to be focused on a surface (the Rowland circle) simultaneously [171] (see figure 38).

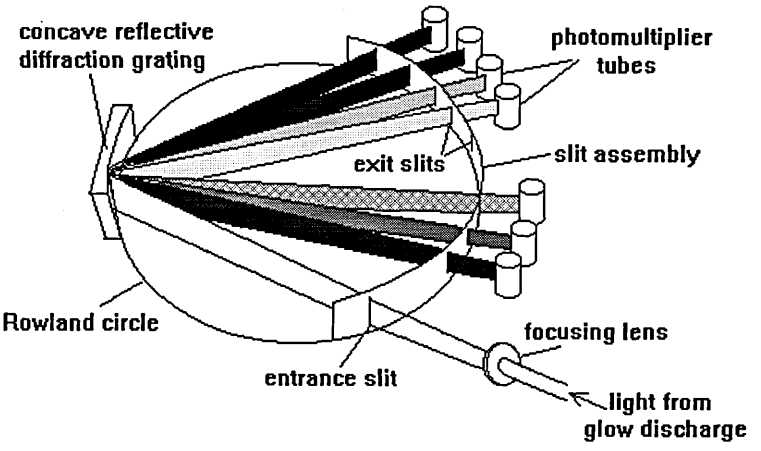

Figure 38. Polychromator

The GDOES polychromator contains pre-etched exit slits for all the possible elements in the periodic table. However, the number of elements that can be detected is limited to a maximum of 44 due to the physical size requirements of the photomultiplier tubes placed behind these slits.

Quantification of GDOES results can be split into two parts: determination of the sputtered depth from the sputtering time and sputter rates of individual elements; and determination of the chemical content from the emission line intensities.

Sputter rates can be calibrated from sputter depth measurements using a surface profilometer or derived directly from available sputter yield data. The quantification of depth can also be subsequently checked by surface profiling the sputter erosion craters after analyses and comparing with the glow discharge plots.

The emission line intensities are dependent on the voltage, current, and sputtering rates, as well as the chemical composition. By operating in constant current or voltage mode the dependence of intensity on the variable parameter can be found, leading to an empirical formula relating all the parameters [172]. Intensity calibration is performed using certified reference materials of known chemical composition. During depth profile quantification the analysed composition is normalised to 100%, so it is important to know all the major elements present in the sample, otherwise misleading results can occur.

References

[1] A.Matthews, *Adv.Mat.Man.Proc.*, 1988,3(1),91.

[2] L.Holland, *Vacuum Deposition of Thin Films*, 1966, Chapman & Hall, London.

[3] R.F.Bunshah, *Deposition Technologies for Films and Coatings*, 1982, Noyes Data Corporation, New Jersey.

[4] D.S.Rickerby, A.Matthews, A.Leyland and A.S.James, *Advanced Surface Coatings*, 1991, Blackie & Son Ltd., Glasgow.

[5] S.Schiller, U.Heisig, M.Neumann and G.Beister, *Vakuum-Technik*, 1986,35,35.

[6] A.Matthews, *Surface Engineering*, 1985,1(2),93.

[7] H.K.Pulker, *Coatings on Glass*, 1984, Elsevier, Amsterdam.

[8] T.S.Sudarshan, S.Schiller, U.Heisig and P.Frach, *Surface Technologies Handbook*, 1988, Marcel Dekker, New York.

[9] A.Burkhardt USP 2157478/1939

[10] A.A.Snaper USP 3625848/1971

[11] A.A.Snaper USP 3836451/1974

[12] L.P.Sablev USP 3783231/1974

[13] L.P.Sablev USP 3793179/1974

[14] S.Ramalingam USP 4673477/1987

[15] R.L.Boxman and S.Goldsmith, *Surf.Coat.Technol.*, 1987,33,153.

[16] E.Erturk and H.J.Heuvel, *Thin Solid Films*, 1987,153,135.

[17] E.Erturk, *VDI-Z Bd.*, 1987,129,89.

[18] P.C.Johnson, *Physics of Thin Films*, 1989,14,129

[19] D.M.Sanders, D.B.Boercker and S.Falabella, *IEEE Trans.Plasma Sci.*, 1990,18,883.

[20] P.J.Martin, R.P.Netterfield, D.R.McKenzie, I.S.Falconer, C.G.Pacey, P.Tomas and W.G.Sainty, *J.Vac.Sci.Technol.*, 1987,A5,22.

[21] B.Rother, *Surf.Eng.*, 1988,4,335.

[22] P.W.Hatto and D.G.Teer, *Vacuum*, 1986,36,67.

[23] R.L.Boxman and S.Goldsmith, *Surf.Coat.Technol.*, 1992,52,39.

[24] C.N.Tai, E.S.Koh and K.Akari, *Surf.Coat.Technol.*, 1990,43/44,324.

[25] A.Wahab Baouchi and A.J.Perry, *Surf.Coat.Technol.*, 1991,49,253.

[26] J.E.Daalder, *J.Phys.D:Appl.Phys.*, 1976,9,2379.

[27] H.D.Steffens, M.Mack, K.Moehwald and K.Reichel, *Surf.Coat.Technol.*, 1991,46,65.

[28] S.Boelens and H.Veltrop, *Surf.Coat.Technol.*, 1987,33,63.

[29] E.Erturk, H.J.Heuvel and H.G.Dederichs, *Surf.Coat.Technol.*, 1989,39/40,455.

[30] P.J.Martin, R.P.Netterfield, A.Bendavid and T.J.Kinder, *Surf.Coat.Technol.*,

1992,54/55,136.

[31] P.J.Martin, D.R.McKenzie, R.P.Netterfield, P.Swift, S.W.Filipczuk, K.H.Muller, C.G.Pacey and B.James, *Thin Solid Films*, 1987,153,91.

[32] P.D.Swift, D.R.McKenzie and I.S.Falconer, *J.Phys.D:Appl.Phys.*, 1989,66,505.

[33] J.Vyskocil and J.Musil, *Surf.Coat.Technol.*, 1990,43/44,299.

[34] P.Jewsbury, S.Ramalingam and R.F.Chang, proceedings of *Eng.Mat.for Adv.Friction and Wear App. Conference 1988,107.*

[35] W.R.Grove, *Phil.Trans.Roy.Soc.London*, 1842,142,87.

[36] G.K.Wehner, *Adv.in Electronics and Electron Phys.*, 1955,7,239.

[37] Airco Temescal, USP 4166018

[38] B.Window and N.Savvides, *J.Vac.Sci.Technol.*, 1986,A4(2),196.

[39] B.Window and N.Savvides, *J.Vac.Sci.Technol.*, 1986,A4(3),453.

[40] N.Savvides and B.Window, *J.Vac.Sci.Technol.*, 1986,A4(3),504.

[41] P.Sioshani, R.W.Oliver and F.D.Matthews, *J.Vac.Sci.Technol.*, 1985,A3(6),2670.

[42] P.A.Dearnley, *Proc.of ASM Conf. Ion Plating and Implantation*, 1986,31.

[43] B.Garside and R.Sanderson, *Metals and Materials*, 1991,3,165.

[44] R.A.Kant and B.D.Sartwell, *J.Vac.Sci.Technol.*, 1985,A3(6),2675.

[45] K.S.Fancey and A.Matthews, *Surf.Coat.Technol.*, 1987,33,17.

[46] G.Mohan Rao and S.Mohan, *J.Appl.Phys.*, 1991,69(9),6652.

[47] L.I.Maissel, *Physics of Thin Films*, 1966,3,61.

[48] R.P.Howson, H.A.J'afer and A.G.Spencer, *Thin Solid Films*, 1990,193/194,127.

[49] G.N.Jackson, *Thin Solid Films*, 1970,5,209.

[50] P.Sigmund, *Phys.Rev.*, 1969,184,383.

[51] J.M.Molarius, A.S.Korhonen and E.O.Ristolainen, *J.Vac.Sci.Technol.*, 1985,A3(6),2419.

[52] B.N.Chapman, *Glow Discharge Processes*, 1980,Wiley, New York.

[53] R.T Farouki and M.Dalvie, *J.Appl.Phys.*, 1990,68(12),6106.

[54] K.S.Fancey and A.Matthews, *Vacuum*, 1990,41,2196.

[55] H.Bingsen and C.Zhou, *Surf.Coat.Technol.*, 1992,50,111.

[56] J.A.Thornton, *Metal Finishing*, 1979,5,83.

[57] J.A.Thornton, *J.Vac.Sci.Technol.*, 1978,15(2),171.

[58] R.K.Waits, *J.Vac.Sci.Technol.*, 1978,15(2),179.

[59] M.Ahern, *Surf.Coat.Technol.*, 1990,43/44(1-3),279.

[60] M.Y.Al-Jaroudi, H.T.G.Hentzell, S.E.Hornstrom and A.Bengston, *Thin Solid Films*, 1989,182,153.

[61] O.Knotek, M.Atzor and F.Jungblut, *Plasma Surf.Eng.*, 1989,1,579.

[62] F.M.Penning, *Physica III*, 1936,9/10,873.

[63] J.Almeida, *Vacuum*, 1989,39,717.

[64] W.Yao, S.Tung, W.Shi and Z.Qi, *Plasma Surf.Eng.*, 1989,1,633.
[65] W.D.Munz, *Vakuum Technik*, 1981,30,78.
[66] S.Schiller, *J.Vac.Sci.Technol.*, 1987,A5,2188.
[67] S.Kadlec and J.Musil, *Surf.Coat.Technol.*, 1990,39/40,487.
[68] S.Kadlec, J.Musil, V.Valvoda, W.D.Munz, H.Petersein and J.Schroeder, *Vacuum*, 1990,41,2233.
[69] D.Monaghan and R.D.Arnell, *Vacuum*, 1992,43,77.
[70] R.P.Howson, H.A.J'Afer and A.G.Spencer, *Thin Solid Films*, 1990,193/194,127.
[71] M.S.Wong, W.D.Sproul and S.L.Rohde, *Surf.Coat.Technol.*, 1991,49,121.
[72] S.L.Rohde, I.Petrov, W.D.Sproul, S.A.Barnett, P.J.Rudnik and M.E.Graham, *Thin Solid Films*, 1990,193/194,117.
[73] M.J.Murphy, D.C.Cameron, M.Z.Karim and M.S.J.Hashmi, *Surf.Coat.Technol.*, 1993,57,1.
[74] W.D.Sproul, P.J.Rudnik, M.E.Graham and S.L.Rohde, *Surf.Coat.Technol.*, 1990,43/44,270.
[75] W.D.Sproul, *Surf.Coat.Technol.*, 1991,49,284.
[76] I.Efeoglu, R.D.Arnell, S.F.Tinston and D.G.Teer, *Surf.Coat.Technol.*, 1993,57,61.
[77] A.H.Cottrell, *An Introduction to Metallurgy*, 1967, Edward Arnold, London.
[78] R.E.Reed-Hill, *Physical Metallurgy Principles*, 1964, Van Norstrand, New Jersey.
[79] L.Hultman, G.Hakansson, U.Wahlstrom, J.E.Sundgren, I.Petrov, F.Adibi and J.E.Greene, *Thin Solid Films*, 1991,205,153.
[80] A.Erdemir and C.C.Cheng, *Surf.Coat.Technol.*, 1989,39/40,285.
[81] G.Hakansson, L.Hultman, J.E.Sundgren, J.E.Greene and W.D.Munz, *Surf.Coat.Technol.*, 1991,48,51.
[82] A.Zangwill, *Physics at Surfaces*, 1988, Cambridge University Press, Cambridge.
[83] P.G.Shewmon, *Diffusion in Solids*, 1963, McGraw-Hill, New York.
[84] M.Prutton, *Surface Physics*, 1983, Oxford University Press, Oxford.
[85] G.Kuznetsov and V.Delian, *Surf.Coat.Technol.*, 1992,54/55,96.
[86] J.P.Biersack and L.G.Haggmark, *Nucl.Instrum.Methods*, 1980,174,257.
[87] J.P.Biersack and W.Eckstein, *Appl.Phys.*, 1984,A34,73.
[88] S.Vuorinen, E.Niemi and A.S.Korhonen, *J.Vac.Sci.Technol.*, 1985,A(3),2445.
[89] D.S.Rickerby and R.Newbury, *Vacuum*, 1988,38,161.
[90] D.S.Rickerby and P.J.Burnett, *Thin Solid Films*, 1988,157,195.
[91] C.C.Cheng, A.Erdemir and G.R.Fenske, *Surf.Coat.Technol.*, 1989,39/40,365.
[92] S.J.Bull, P.R.Chalker, C.F.Ayres anf D.S.Rickerby, *Mat.Sci.Eng.*, 1991,A139,71.
[93] K.A Pischow, L.Eriksson, E.Harju, A.S.Korhonen and E.O.Ristolainen, *Surf.Coat.Technol.*, 1993,58,163.

[94] D.S.Rickerby, G.Eckold, K.T.Scott and I.M.Buckley-Golder, *Thin Solid Films*, 1987,154,125.

[95] O.Knotek, R.Elsing,G.Kramer and F.Jungblut, *Surf.Coat.Technol.*, 1991,46,265.

[96] W.Herr, B.Matthes, E.Broszeit and K.H.Kloos, *Surf.Coat.Technol.*, 1993,57,43.

[97] L.D.Schepper, M.D'Olieslaeger, G.Knuyt, L.M.Stals, M.V.Stappen, B.Malliet, J.P.Celis and J.R.Roos, *Thin Solid Films*, 1989,173,199.

[98] P.Ding, Z.Ni, S.Zhou and F.Pan, *Surf.Coat.Technol.*, 1991,49,203.

[99] J.Musil, S.Kadlec, V.Valvoda, R.Kuzel and R.Cerny, *Surf.Coat.Technol.*, 1990,43/44,259.

[100] S.Kadlec, J.Musil and J.Vyskocil, *Surf.Coat.Technol.*, 1992,54/55,287.

[101] B.A.Movchan and A.V.Demchishin, *Fiz.Met.Metalloved.*, 1969,28,653.

[102] J.A.Thornton, *Ann.Rev.Mater.Sci.*, 1977,7,239.

[103] R.Messier, A.P.Giri and R.A.Roy, *J.Vac.Sci.Technol.*, 1984,A(2),500.

[104] L.Hultman, W.D.Munz, J.Musil, S.Kadlec, I.Petrov and J.E.Greene, *J.Vac.Sci.Technol.*, 1991,A9(3),434.

[105] I.Petrov, L.Hultman, U.Helmersson, J.E.Sundgren and J.E.Greene, *Thin Solid Films*, 1989,169,299.

[106] W.D.Munz, *Surf.Coat.Technol.*, 1991,48,81.

[107] J.A.Thornton, *J.Vac.Sci.Technol.*, 1974,11,666.

[108] M.I.Ridge, *Thin Solid Films*, 1981,80,31.

[109] J.E.Sundgren, B.O.Johansson and S.E.Karlsson, *Thin Solid Films*, 1983,105,353.

[110] Y.Kubo and M.Hashimoto, *Surf.Coat.Technol.*, 1991,49,342.

[111] K.S.Fancey and A.Matthews, *Plasma Surf.Eng.*, 1989,1,61.

[112] K.S.Fancey and A.Matthews, *Thin Solid Films*, 1990,193/194,171.

[113] S.J.Bull, A.M.Jones and A.R.McCabe, *Surf.Coat.Technol.*, 1992,54/55,173.

[114] A.J.Perry, M.Jagner,W.D.Sproul and P.J.Rudnik, *Surf.Coat.Technol.*, 1990,42,49.

[115] W.Fleiscer, D.Schulze, R.Wilberg, A.Lunk and F.Schrade, *Thin Solid Films*, 1979,63,347.

[116] J.Vyskocil, J.Musil, S.Kadlec and W.D.Munz, *Plasma Surf.Eng.*, 1989,1,661.

[117] F.Richter, H.Kupfer, H.Giegengack, G.Schaarschmidt, F.Scholze, F.Elstner and G.Hecht, *Surf.Coat.Technol.*, 1992,54/55,338.

[118] G.P.Georgiev and D.N.Popov, *Plasma Surf.Eng.*, 1989,1,587.

[119] S.Schiller, *Thin Solid Films*, 1982,96,235.

[120] W.D.Sproul, *Surf.Coat.Technol.*, 1987,33,73.

[121] W.D.Sproul, P.J.Rudnik, C.A.Gogol and R.A.Mueller, *Surf.Coat.Technol.*, 1989,39/40,499.

[122] J.Stanislav, J.Sikac and M.Cermak, *Thin Solid Films*, 1990,191,255.

[123] B.Zega, *Surf.Coat.Technol.*, 1989,39/40,507.

[124] P.J.Martin, *Materials Australasia*, 1986,6,11.

[125] G.J.Chamberlin and D.G.Chamberlin, *Colour, its measurement, computation and application.*, 1980, Heyden & Son, New York.

[126] G.Reiners, H.Hantsche, H.A.Jehn,U.Kopacz and A.Rack, *Surf.Coat.Technol.*, 1992,54/55,273.

[127] K.Akari, H.Tamagaki, T.Kumakiri, K.Tsuji, E.S.Koh and C.N.Tai, *Surf.Coat.Technol.*, 1990,43/44(1-3),312.

[128] K.H.Habig, *Tribology International*, 1989,22(2),65.

[129] T.S.Eyre, *Met.& Materials*, 1991,3,143.

[130] H.Schwarz, *Pract.Met.*, 1987,24,257.

[131] A.Schulz, H.R.Stock and P.Mayr, *Mat.Sci.Eng.*, 1991,A140,639.

[132] B.B.Joffe, *Plating Surf.Finish.*, 1983,9.

[133] C.Whiston, *X-Ray Methods*, 1987, John Wiley & Sons, Chichester.

[134] H.E.Boyer, *Hardness Testing*, 1987, ASM International, Metals Park, Ohio.

[135] P.J.Blau, *Phys.&Chem.Protective Coatings*, 1986,149,1.

[136] P.K.Mehrotra and D.T.Quinto, *J.Vac.Sci.Technol.*, 1985,A3(6),2401.

[137] S.J.Bull and D.S.Rickerby, *Surf.Coat.Technol.*, 1990,42(2),149.

[138] D.S.Stone, K.B.Yoder and W.D.Sproul, *J.Vac.Sci.Technol.*, 1991,A9(4),2543.

[139] P.C.Jindal and D.T.Quinto, *Surf.Coat.Technol.*, 1988,36,683.

[140] W.D.Munz, D.Schulze and F.J.M.Hauzer, *Surf.Coat.Technol.*, 1992,50,169.

[141] W.D.Munz, K.Vannisselroy, R.Tietema, T.Hurkmans and G.Keiren, *Surf.Coat.Technol.*, 1993,58,205.

[142] P.R.Chalker, S.J.Bull and D.S.Rickerby, *Mat.Sci.Eng.*, 1991,A140,583.

[143] J.Valli, U.Makela and A.Matthews, *Surf.Eng.*, 1986,2(1),49.

[144] S.J.Bull, *Surf.Coat.Technol.*, 1991,50,25.

[145] P.Hedenqvist, M.Olsson, S.Jacobson and S.Soderberg, *Surf.Coat.Technol.*, 1990,41,31.

[146] M.Bromark, M.Larsson, P.Hedenqvist, M.Olsson and S.Hogmark, *Surf.Coat.Technol.*, 1992,52,195.

[147] A.J.Perry, *Thin Solid Films*, 1983,107,167.

[148] S.J.Bull, D.S.Rickerby, A.Matthews, A.Leyland, A.R.Pace and J.Valli, *Surf.Coat.Technol.*, 1988,36,503.

[149] J.Valli, U.Makela, A.Matthews and V.Murawa, *J.Vac.Sci.Technol.*, 1985,A3(6),2411.

[150] B.D.Cullity, *Elements of X-Ray Diffraction*, 1978, Addison-Wesley, Massachusetts.

[151] A.H.Windle, *A First Course in Crystallography*, 1977, G.Bell & Sons, London.

[152] J.A.Sue, *Surf.Coat.Technol.*, 1992,54/55,154.

[153] D.S.Rickerby, *J.Vac.Sci.Technol.*, 1986, A4(6),2809.

[154] T.Hirsch and P.Mayr, *Hart.-Tech.Mitt.*, 1988,43(4),212.

[155] T.A.Carlson, *Photoelectron and Auger Spectroscopy*, 1975, Plenum Press, New York.

[156] R.K.Wild, *Characterisation of High-Temp.Mat.*, 1989,6,241.

[157] D.P.Woodruff and T.A.Delchar, *Modern Techniques of Surface Science*, 1986, Cambridge University Press, Cambridge.

[158] D.K.Bowen and C.R.Hall, *Microscopy of Materials*, 1975, Macmillan Press, London.

[159] A.R.Gabriel, *SEM:A User's Manual for Materials Science*, 1985, ASM, Ohio.

[160] G.Lawes, *Scanning Electron Microscopy and X-Ray Microanalysis*, 1987, John Wiley & Sons, Chichester.

[161] P.J.Goodhew, *Specimen Preparation in Materials Science*, 1972, North-Holland Publishing, Amsterdam.

[162] P.J.Goodhew, *Thin Foil Preparation for Electron Microscopy*, 1985, Elsevier, Amsterdam.

[163] D.B.Williams, *Practical Analytical Electron Microscopy in Materials Science*, 1984, Philips Electronic Instruments Electron Optics Publishing Group, New Jersey.

[164] P.J.Grundy and G.A.Jones, *Electron Microscopy in the Study of Materials*, 1976, Edward Arnold, London.

[165] J.Murphy, *Characterisation of High-Temperature Materials*, 1988,2,14.

[166] H.A.Strobel, *Chemical Instrumentation*, 1977, Addison-Wesley, Massachusetts.

[167] J.A. Broekaert, *Journal of Analytical Atomic Spectrometry*, 1987,2(9),537.

[168] W.W.Harrison, *Journal of Analytical Atomic Spectrometry*, 1992,7(3),75.

[169] W.Grimm, *Spectrochimica Acta*, 1968,23B,443.

[170] A.Bengston and M.Lundholm, *Journal of Analytical Atomic Spectrometry*, 1988,3(9),879.

[171] J.F.James and R.S.Sternberg, *The Design of Optical Spectrometers*, 1969, Chapman & Hall, London.

[172] A.Bengston, *Spectrochimica Acta*, 1985,40B(4),631.

CHAPTER 3
Experimental Technique

In order to compare the two deposition processes of steered arc evaporation and ABS magnetron sputtering, coatings were deposited by each process onto metallographically prepared substrates under varied operating conditions. The coatings were subsequently analysed by several techniques to assess their properties.

3.1 Sample Preparation for Coating

The sample substrates used for this study consisted of flat blocks (18 x 18 x 9 mm) or cylinders (10 x 30 mm diameter) of M2 high speed steel (HSS), 8 mm HSS drills or 6 mm HSS drill blanks, and rectangular strips (50 x 20 x 1.5 mm) of 316 stainless steel. The blocks and cylinders were mechanically polished to 1 μm diamond finish. Similarly prepared cylinders of titanium and nickel based alloys were also used in certain coating runs.

The substrates were cleaned in a commercially available cleaning line according to the following procedure :

1. Vapour degreasing in freon or Arklone vapour
2. Ultrasonic cleaning in strong alkali at 70-80°C
3. Immersion rinsing in distilled water
4. Ultrasonic degreasing and water displacement in freon or Arklone
5. Spot-free drying in freon or Arklone vapour
6. Hot-air drying

Alkaline detergent based on NaOH was used for the removal of inorganic contaminants. Alkali was used instead of acid, as this has a pacifying effect on the substrate metal, so impeding corrosion during the cleaning process, while acid tends to activate the metal. However, some metals such as aluminium, which are attacked by alkali, would be cleaned in alcohol instead.

After cleaning, all substrates were handled with cotton gloves to prevent re-contamination with oils and salts from the skin.

3.2 Deposition by Steered Arc Evaporation

Coating deposition was performed in a prototype version PVD-S-3 coating unit produced by Interatom / Multi-Arc Europe GmbH. This consisted of an 8000 ls^{-1}

4-stage diffusion-pumped, water-cooled stainless steel vacuum chamber of 740 litres capacity (see figure 39).

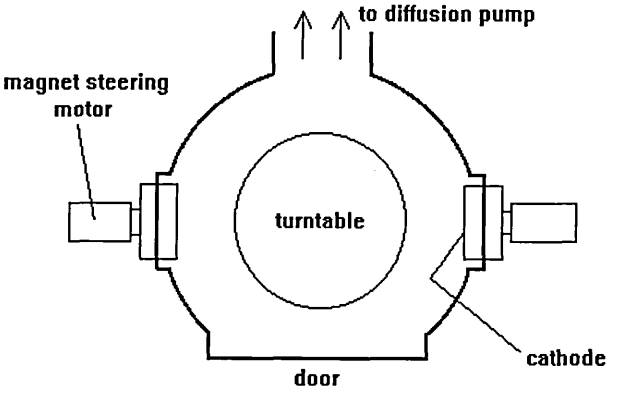

Figure 39. Steered-Arc Deposition Unit

A diffusion pump was used as it is very efficient and has no moving parts, though it may be a source of chamber contamination. Liquid oil at the base of the pump is heated, vaporises, and travels upwards through a central tube until striking a series of metal "umbrellas" that deflect the vapour stream downwards. The vapour stream entraps any gas molecules and carries them towards the base of the pump, where the gas is removed by a conventional rotary pump. The oil vapour condenses on the cooled pump base and flows back to the central heated region to repeat the cycle. The number of umbrellas denotes the number of stages in the pump, with each stage capable of producing a pressure difference of 10^1 Pa.

The chamber was fitted with two water-cooled circular cathodes of 125 mm diameter working area, and 7 mm thickness. The cathodes were fabricated from 99.98% purity titanium and could be operated in steered arc mode only. Each cathode was connected to an individual power supply capable of delivering 100V/300A. Negative bias potentials of -1000 V (for etching) and -50 to -200 V (for coating) were applied to the substrates.

Gas supplies were argon (99.999%) as an arc discharge support gas for sputter etching and nitrogen (99.999%) for reactive deposition. Reactive gas flow was controlled by feedback of gas pressure (reactive gas only) during coating. Substrates were mounted at a nominal distance of 250 mm from the cathode on a rotating turntable, with drills pointing radially in a "hedgehog" style fixturing arrangement (see figure 40). Substrate temperature was monitored by optical infrared pyrometers.

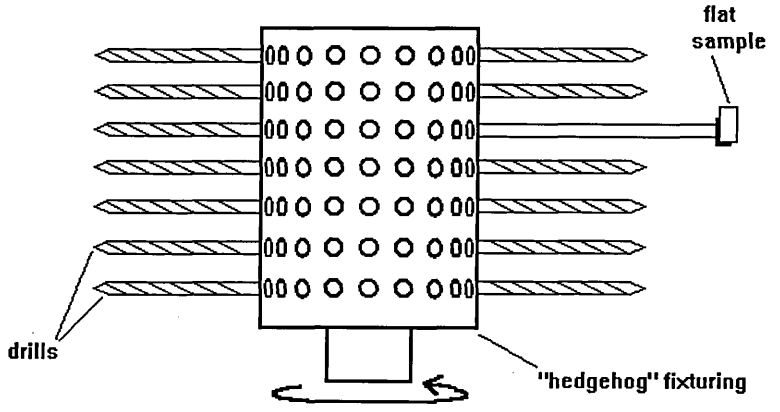

Figure 40. Steered-Arc Turntable Assembly

3.2.1 Process Parameters / Deposition Conditions

The process variables explored were substrate bias voltage and nitrogen pressure during the coating cycle. The substrate voltage was set at -50, -100, -150 and -200 V for processes at each of the nitrogen pressures 0.1, 0.6, 1.1 and 1.6 Pa. These values were chosen around the nominal operating conditions of -150 V bias and 1.1 Pa nitrogen pressure for the substrate load involved.

A typical process run was as follows :

1. Pump down to below $1x10^{-3}$ Pa. This would take typically 30 minutes to 1 hour depending on how long the chamber had been open.
2. Heat and sputter etch substrates with titanium ions in steered arc discharge, argon pressure 0.07 Pa, bias voltage -1000 V, discharge current 130 A per cathode (2 cathodes), approximate time 5 minutes to reach 450°C.
3. Coat substrates with TiN in steered arc discharge, nitrogen pressure variable (0.1 to 1.6 Pa - no argon), bias voltage variable (-50 to -200 V), discharge current 130 A per cathode (2 cathodes), coating time variable (20 to 90 minutes for a 3.5 μm coating, depending on conditions).

Apart from the parameter study, other coating experiments included varying the position of substrates in the chamber to examine deposition uniformity.

3.3 Deposition by ABS Magnetron Sputtering

Coating deposition was performed in a production version HTC 1000-4 ABS coating unit produced by Hauzer Techno Coating Europe BV. This consisted of a 4400 ls^{-1} twin turbo-pumped, water-cooled stainless steel vacuum chamber of 800 litres capacity (see figure 41).

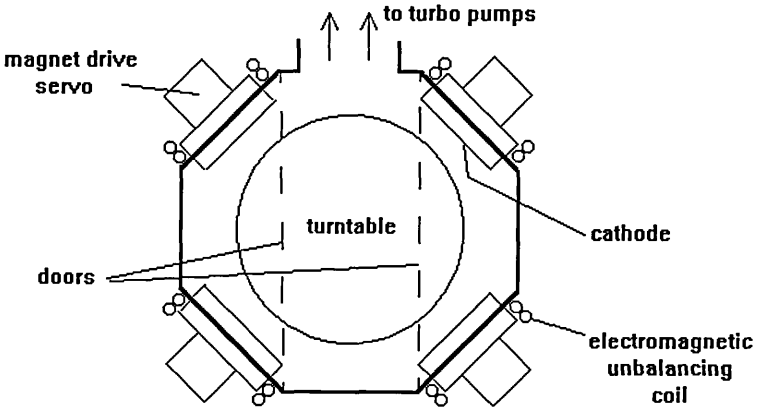

Figure 41. ABS Magnetron Deposition Unit

Turbomolecular pumps were used as they minimize oil contamination of the vacuum chamber. They consist of alternating rows of rotating blades and stationary slotted disks resembling a turbine. When driven at high speed, the rotating blades strike any gas molecules and propel them towards the adjacent disk. A very high pressure ratio is established by the alignment of the disks relative to one another, and the sequence continues through subsequent stages, until the gas is finally removed by a rotary pump.

The chamber was fitted with four water-cooled rectangular cathodes of 600 x 190 mm working area, and 14 mm thickness. The cathodes were fabricated from 99.98% purity titanium and could be operated in confined arc mode or magnetron mode with variable electromagnetic unbalancing in a linked or closed-field configuration. Each cathode was connected to an individual power supply capable of delivering 80V/100A in arc mode and 750V/40A in magnetron mode. Electromagnetic coils around the cathodes supplied a variable magnetic field for unbalancing the cathodes during magnetron operation. Negative bias potentials of -1000 to -1200 V (for etching) and -50 to -200 V (for coating) were applied to the substrates.

Gas supplies were argon (99.999%) as a glow discharge working gas for

magnetron sputtering and nitrogen (99.999%) for reactive deposition. Reactive gas flow was controlled by feedback of total gas pressure (reactive + working) during coating. Substrates were mounted at a nominal distance of 250 mm from the cathodes on a three-fold planetary rotation turntable to ensure uniform coating coverage, with drills pointing vertically (see figure 42). Substrate temperature was monitored by thermocouples.

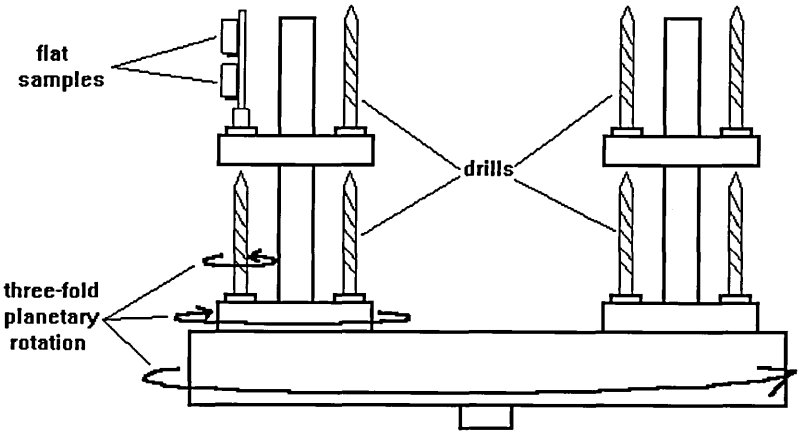

Figure 42. Three-fold Planetary Rotation Turntable Assembly

3.3.1 Process Parameters / Deposition Conditions

The process variables explored were substrate bias voltage and nitrogen partial pressure during the coating cycle. In fact, total pressure was the monitored factor, but argon gas flow was kept constant, so nitrogen partial pressure was effectively controlled. The substrate bias voltage was set at -50, -100, -150 and -200 V for processes at each of the total pressures 0.26, 0.29 and 0.32 Pa. These values were chosen around the nominal operating conditions of -150 V bias and 0.29 Pa pressure for the substrate load involved. This bias voltage was chosen as it maintained substrate temperature stability throughout the deposition process. The pressure was obtained by performing a hysteresis test of gas flow versus pressure and selecting a point prior to the onset of cathode poisoning (see section 4.1).

A typical process run was as follows :

1. Pump down to below $1x10^{-3}$ Pa. This would take typically 2 hours. Overnight pumping may be employed if the chamber had been open a long time. A residual gas analyser was used to monitor the water vapour level in the chamber. After pumping down, the water vapour to nitrogen ratio should be better than 1:10.

2. Heat and sputter clean substrates with argon ions in unbalanced magnetron glow discharge, argon pressure 0.33 Pa, bias voltage -1000 V, discharge voltage -200 V per cathode (4 cathodes), approximate time 30 minutes to reach 450°C.
3. Clean cathode surfaces with argon ions in unbalanced magnetron glow discharge (contaminants sputtered onto shutters closed in front of cathodes), argon pressure 0.16 Pa, bias voltage 0 V, discharge power 5 kW per cathode (4 cathodes), approximate time 15 minutes to fully clean.
4. Heat and sputter clean substrates with argon and titanium ions in confined arc discharge, argon pressure 0.19 Pa, bias voltage -1200 V, discharge current 100 A per cathode (2 cathodes), approximate time 1 minute to reach 450°C, (repeated 10 times with intermittent cooling to 400°C, effective sputter time 10 minutes).
5. Coat substrates with TiN in unbalanced magnetron glow discharge, argon pressure 0.5 Pa, nitrogen pressure variable (total pressure 0.26 to 0.32 Pa), bias voltage variable (-50 to -200 V), discharge power 10 kW per cathode (4 cathodes), approximate time 70 minutes for a 1.5 to 2 μm coating.

Apart from the parameter study, other coating experiments included varying the position of substrates within the chamber to examine deposition uniformity, depositing various thicknesses of titanium interlayers to examine the effect on adhesion and comparing with the arc etched samples, and depositing multilayered coatings (Ti,TiN,Ti,TiN) to examine the effect on nitrogen diffusion and interface mobility with temperature.

It was thought necessary to have some kind of process monitoring system, in order that deposition run details could be recorded for identification of problems and for repetitions of processes if required. To this end, an IBM PC was interfaced to the control cabinet of the ABS magnetron system, and monitoring software written in BASIC. Details and examples of the software can be found in appendix 1.

3.4 Sample Preparation for Analysis

Most of the analytical techniques used did not require any form of sample preparation, other than a quick surface clean with an air jet or a solvent (eg. acetone or methanol) to remove dust and possibly fingerprints. Basically, the less preparation required, the better, since with any mechanical polishing, sectioning or thinning, there is the risk of distorting, damaging or contaminating the sample to be examined. Some analytical instruments (eg. the X-ray diffractometer) could only accept samples of a limited size, and so samples were sectioned accordingly using a

rotary saw. The Calotest technique required ball-cratering in order to obtain a taper-section through the coating and substrate. The electron microscopic techniques were the most demanding in terms of sample preparation, in particular where coating cross-sections were to be examined. This could entail fracturing, sectioning, polishing, etching, dimpling, and ion-beam thinning techniques [1 2 3 4].

1. Ball-cratering

This technique involved eroding a hemispherical crater in a sample surface by means of a rotating steel ball-bearing (10 to 50 mm diameter) coated with a diamond compound paste. The ball was friction driven by an electric motor via a twin-conical axle shaft, such that two points of the ball-bearing rested on the shaft, while the third rested on the sample surface. The action of the diamond-coated ball rotating against the sample caused a small crater to be eroded, and thus a shallow hemispherical taper section of the surface layers to be revealed (see figure 43).

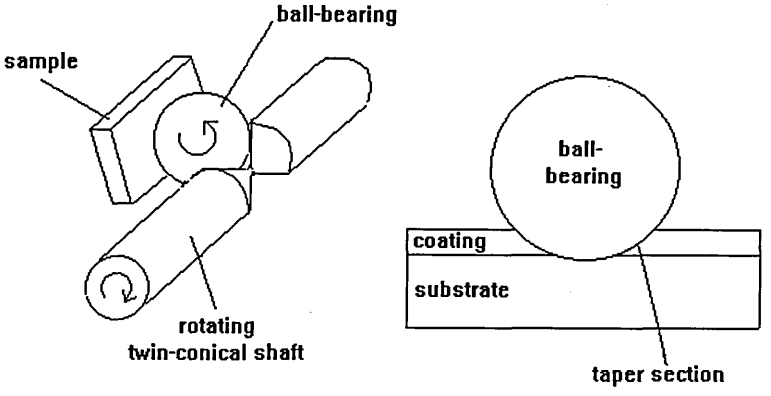

Figure 43. Ball Cratering

Where a dedicated ball-cratering device was not available, a similar erosion crater could be made using a dimple grinder.

The instruments used in this work were a CSEM Calotester, and a Gatan dimple grinder.

2. Fracturing

This technique was used to reveal the grain and column structure of the coatings and was performed on drills and drill blanks, since these were of a convenient shape

and size. The procedure involved cutting a deep slit into the side of the sample opposite to that which was to be examined. The bottom of the sample was then clamped firmly in a vice, and a uniformly distributed load applied to the upper exposed half, causing fracture to occur evenly along the length of the slit. In practice, the load was applied as a sharp blow with a hammer. Fracture naturally occurs along weak points such as grain boundaries and intercolumnar voids, so making them visible for examination

3. Metallographic Sectioning

The most simple and quick method for slicing a large piece of material was by hack-saw or cut-off wheel. It was important not to cut off too fine a slice by these methods as sample damage could easily extend several hundred microns below the surface. The rotating cut-off wheel (made of aluminium oxide) was generally used for sample thicknesses over 3 mm. This was continuously lubricated with distilled water to cool the sample and help prevent clogging.

For finer cuts, and a narrower slit, of smaller pieces of material, or where the sample was particularly fragile (as with glued cross-sections for transmission electron microscopy) a diamond-wire saw was used. This consisted of a fine steel wire (200 μm diameter) embedded with 60 μm sized diamonds that was driven back and forth at low speed and pressure against the sample surface. This was continuously lubricated with distilled water to cool the sample and help prevent clogging. In this way very little stress was applied to the sample. It was important not to cut off too large a slice by this method since the diamond wire was then subject to jamming and snapping.

The instruments used in this work were an Accutom cut-off wheel, and a Well diamond-wire saw.

4. Lapping and Polishing

For scanning electron microscopy, preparation of polished sections by conventional techniques (hand grinding on successively finer wet grit paper (silicon carbide) and polishing on soft felt wheels) led to serious edge-rounding of the samples. Since the edge (ie. the 2 μm coating) was the area of interest, alternative techniques were used. The sectioned samples were automatically ground on cast iron or cermet lapping plates with successively finer diamond compound pastes (typically 14, 6 and 3 μm respectively for 10 minutes each). The plates were hard and flat, and the sample mount ensured a steady pressure (1 kg load) that was central and

perpendicular to the sample face. In this way, the sample edges, and hence the coating, were retained. Further edge retention was possible by mounting two sectioned samples together, face to face. In this way, the two coating layers were sandwiched between the substrates which offered good protection. Polishing was also carried out automatically on napless nylon cloths impregnated with 3 and 1 μm diamond paste respectively. A final short hand polish using 0.2 μm alumina slurry on a felt pad was also performed.

5. Etching

In order to reveal the structure of some samples, the polished sections were etched with acid. This had the effect of removing material selectively from the steel substrate, particularly along the grain boundaries, such that the grains and the coating interface became more apparent. 4% Picral (4% Picric acid in alcohol) was used as the etchant, and the samples were typically treated for about thirty seconds.

6. Dimple Grinding

Samples for transmission electron microscopy (TEM) must be sufficiently thin to allow electrons to pass through, hence the name. This means that for electron transparency, the sample must be thinned to about 100 nm thickness. If the whole sample were this thin, it would be extremely fragile and consequently impossible to handle and examine. Instead, only the central region is thinned, leaving a robust "thick" supporting rim. It was also useful for the final thinning stage to start with a sample containing a depression in its centre, as this ensured that the perforation and transparent region would be central.

A dimple grinder was used to prepare 3mm diameter TEM samples to less than 50 μm thickness in the centre. The dimpler consisted of a rotating turntable onto which the sample was mounted with low melting-point wax. A grinding wheel of 15 mm diameter and orientated perpendicularly to the table, rotated against the sample surface under a 20 g load. The wheel was coated in 14 μm diamond compound paste, and by this dual rotating action, a shallow hemispherical crater was eroded in the sample surface. The grinding wheel was then replaced by a felt polishing wheel impregnated with 1 μm diamond compound paste, and the crater was polished. A final polish with alumina suspension was also possible.

The instrument used in this work was a Gatan dimple grinder.

7. Ion-beam Thinning

Final sample thinning to perforation for TEM analysis, was carried out in an ion-beam thinning mill. This consisted of a small vacuum chamber containing two Penning ion guns positioned on either side of the dimpled sample, and aimed at it with a shallow angle (<15°). A working gas (argon) was bled into the guns and a high potential (5 kV) applied across the hollow anode and cathode. This produced a glow discharge within each gun, and an ion beam was emitted through a small orifice in each cathode with an energy equivalent to the accelerating voltage (5 keV). The ion beams were incident on the sample surface and caused the gentle removal of material by sputtering (see figure 44).

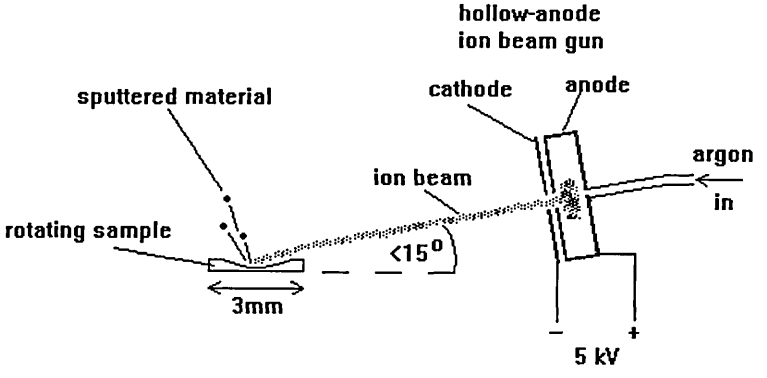

Figure 44. Ion Beam Thinning

The ion energy and angle of incidence were kept low in order to minimize the amount of implantation and depth of damage in the sample. Also, the sputtering yield was greater at glancing angles (15-40°) due to the incident energy being distributed nearer to the surface, than penetrating straight in. Thinning rates were typically of the order of 10 $\mu m\ h^{-1}$.

The instruments used in this work were an Edwards ion beam thinner, and a Gatan Precision Ion Polishing System (PIPS).

3.4.1 Additional Notes on XTEM Sample Preparation

The preparation of cross-sectional samples for TEM analysis (XTEM) required some additional sample handling not mentioned above. The procedure used was as follows :

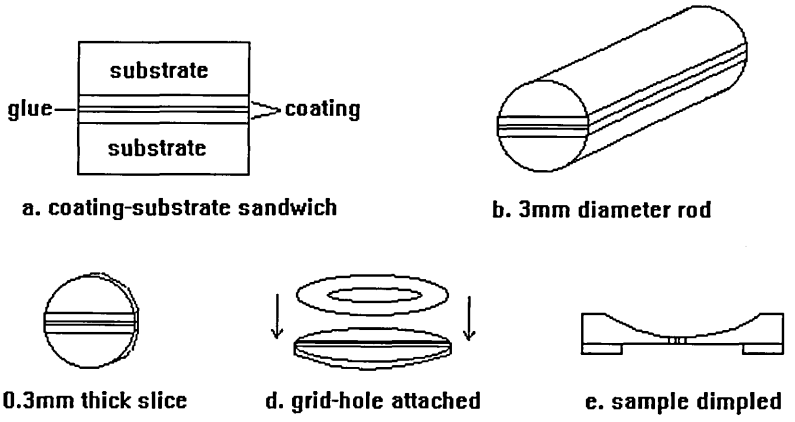

Figure 45. XTEM Sample Preparation

1. Two flat coated samples were joined together face-to-face with epoxy resin and allowed to cure. Thus a sandwich of two coating layers surrounded by two substrate layers was formed (see figure 45a). At first, the epoxy resin used was Araldite, which was mixed with graphite powder to make it conductive. Later, Gatan G1 low viscosity epoxy was used, and the samples were clamped and allowed to cure under vacuum, in order to minimise the glue layer thickness and remove any trapped air bubbles.

2. A rod of 3 mm diameter was then sawn or spark eroded from the sandwich block, such that the sandwich interface ran lengthways down the centre of the rod (see figure 45b). Alternatively, by using coated samples on stainless steel sheet of about 1.5 mm thickness, the production of a rectangular "rod" was possible, which considerably reduced the preparation involved.

3. Thin discs (0.3 mm thickness) were then sawn from the rod (see figure 45c). This required the use of a diamond-wire saw so as not to unduly stress the thin glue interface.

4. Each disc was mounted on a stub with low melting-point wax and hand ground to remove any sawing burrs, before being mechanically polished on a dimpler with a felt wheel.

5. A grid hole (3 mm diameter, 2 mm hole) was then glued to the disc with epoxy resin and allowed to cure (see figure 45d), before the disc was removed from the supporting stub.

6. The disc was reversed and affixed (grid hole side down) to the stub once more with low melting-point wax, and hand ground to remove any sawing burrs.

7. The disc was dimpled with 14 μm diamond paste and 20 g load until within 20 μm central thickness (see figure 45e), then polished with a felt wheel, before removal from the stub and thorough washing in a suitable solvent.

8. The dimpled disc was then mounted in an ion-beam thinner at a glancing incidence angle. Shielding was used to prevent the ion beams impinging perpendicularly on the glue-line and coating surface edge, as this would result in preferential sputtering of this area and effective "etching back" of the region of interest.

3.5 Analysis Techniques

The following techniques and instrumentation were used for coating analysis :

1. Colourimetry using a Minolta CR-100 colorimeter and an Applied Colour Systems Chroma Sensor-3.

2. Surface roughness profiling using a Mahr Perthen profilometer, a Rank-Taylor Hobson Form Talysurf-120L and a Rodenstock RM600-3D Laserstylus.

3. Coating Thickness Calotest using a CSEM Calotester and a Gatan dimple grinder.

4. X-Ray Fluorescence Thickness Test using a Fischerscope XRF Coating Thickness Computer.

5. Microhardness Test using a Tukon (model M0) microhardness tester with a Knoop diamond indenter and a Fischer H100 ultra-microhardness tester with a Vickers diamond indenter.

6. Rockwell Indentation Adhesion Test using a Rockwell-C hardness tester with 150kg load.

7. Scratch Adhesion Test using a CSEM Revetest and a VTT Technology Inc. (type ST105) scratch tester.

8. X-Ray Diffraction Analysis using a Philips 1710 based Automated Powder Diffractometer with Cu Kα radiation.

9. Glow Discharge Spectroscopy using a Leco GDS-750 QDP glow discharge spectrometer.

10. X-ray Photoelectron Spectroscopy using a VG Scientific Microlab 500.

11. Scanning Electron Microscopy using a Jeol 840A, a Philips SEM500 and a Philips XL40 ASEM.

12. Transmission Electron Microscopy using a Philips CM20 STEM.

References

[1] A.B.Smith and R.Williams, *Powder Metallurgy*, 1988,31(2),127.

[2] G.Hakansson, *Growth of Compound and Superlattice Thin Films*, 1991, Linkoping University, Sweden.

[3] P.J.Goodhew, *Specimen Preparation in Materials Science*, 1972, North-Holland Publishing, Amsterdam.

[4] P.J.Goodhew, *Thin Foil Preparation for Electron Microscopy*, 1985, Elsevier, Amsterdam.

CHAPTER 4
Results

4.1 Parameter Study

This section presents typical results from repeated analyses of the effects of changing two variable parameters : reactive gas pressure and substrate bias voltage. A third dependent variable parameter, that of substrate temperature, is also presented. This was inextricably linked to the ion bombardment intensity, which was in turn dependent on bias and pressure conditions during deposition. Any variations from the typical values shown are also reported. The steered arc parameter range covered the full operating range of the instrument. However, the ABS magnetron parameter range was restricted to a pressure range close to the optimum in order to avoid cathode poisoning or pure metal deposition. This optimum pressure was obtained by performing a hysteresis test of gas flow versus pressure and operating at the "knee" of the increasing gas flow plot (shown by an arrow below) which is the point just prior to the onset of cathode poisoning.

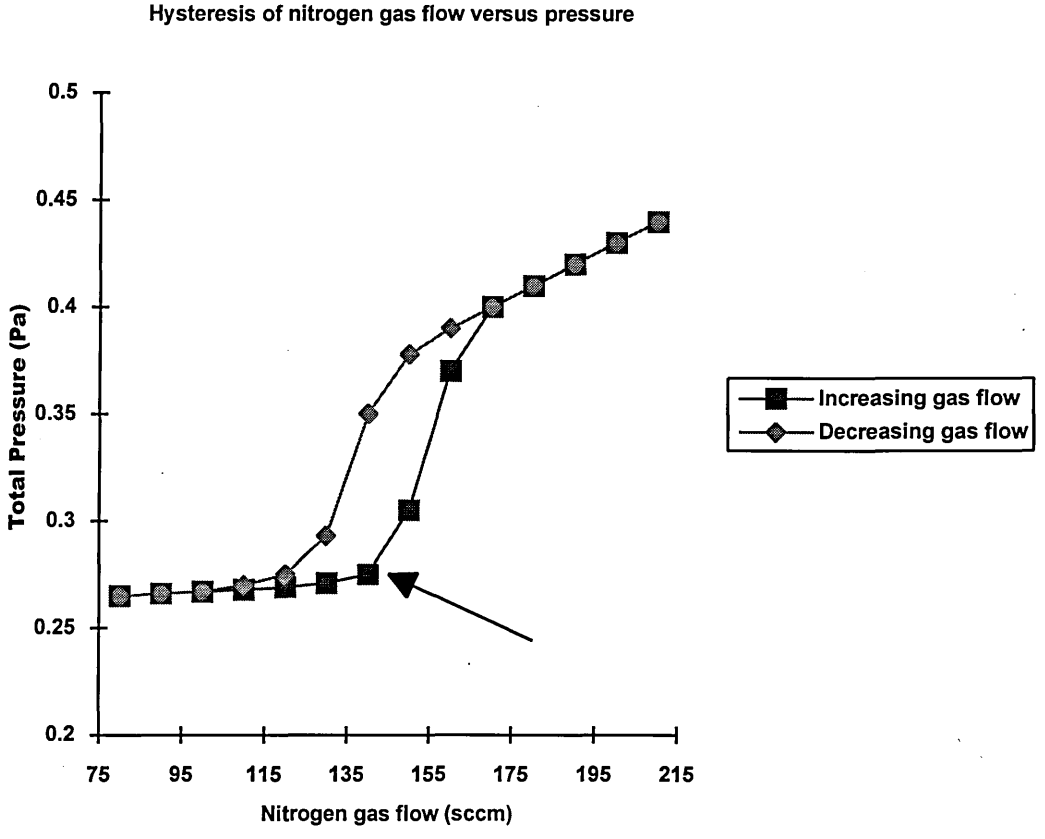

4.1.1 Deposition Conditions and Plasma Uniformity

All deposition runs began coating at a substrate temperature of approximately 450°C. Depending on the conditions during deposition, the substrate temperatures then either rose or fell to the final substrate temperatures shown below.

a. Steered-arc

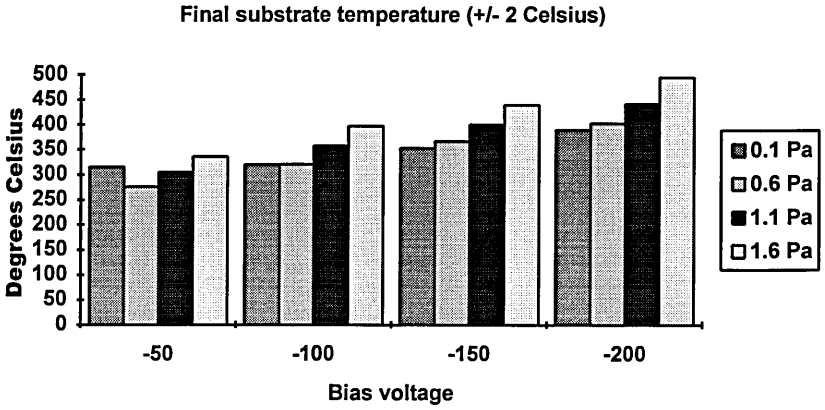

b. ABS Magnetron

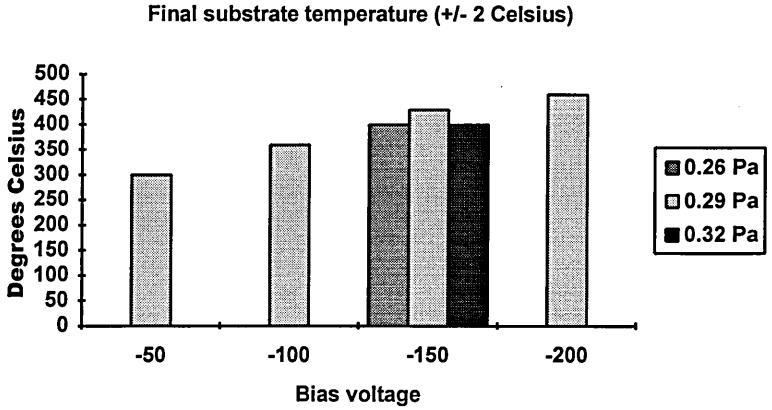

Monitoring of substrate temperature in the ABS magnetron process revealed a rapid temperature drop at the start of the coating phase in the lower biased coating runs, than for the optimum condition of -150 V.

Monitored process temperature at - 150 V bias

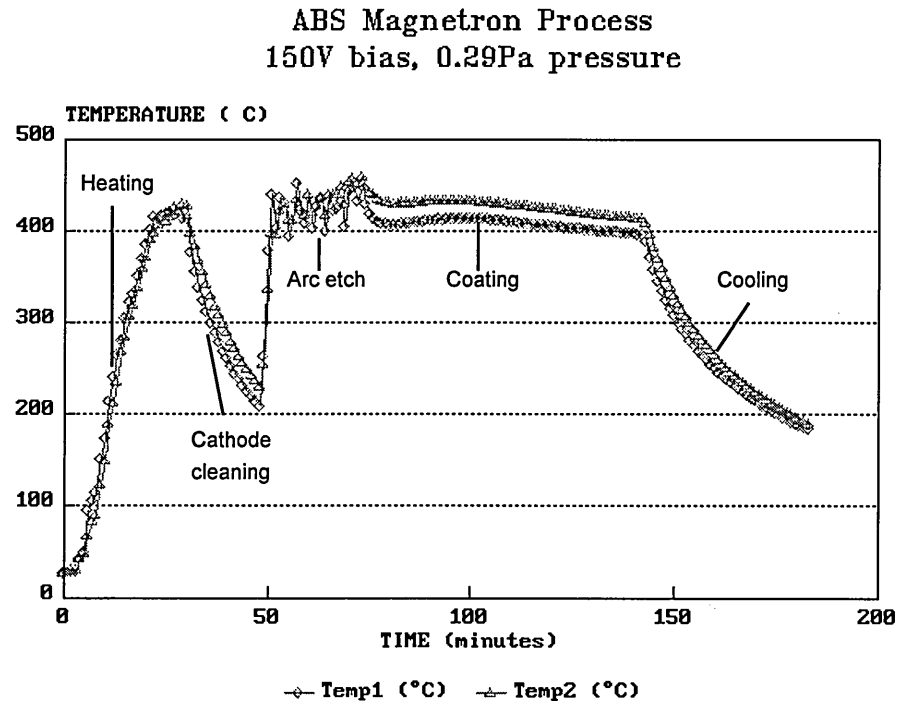

Monitored process temperature at - 100 V bias

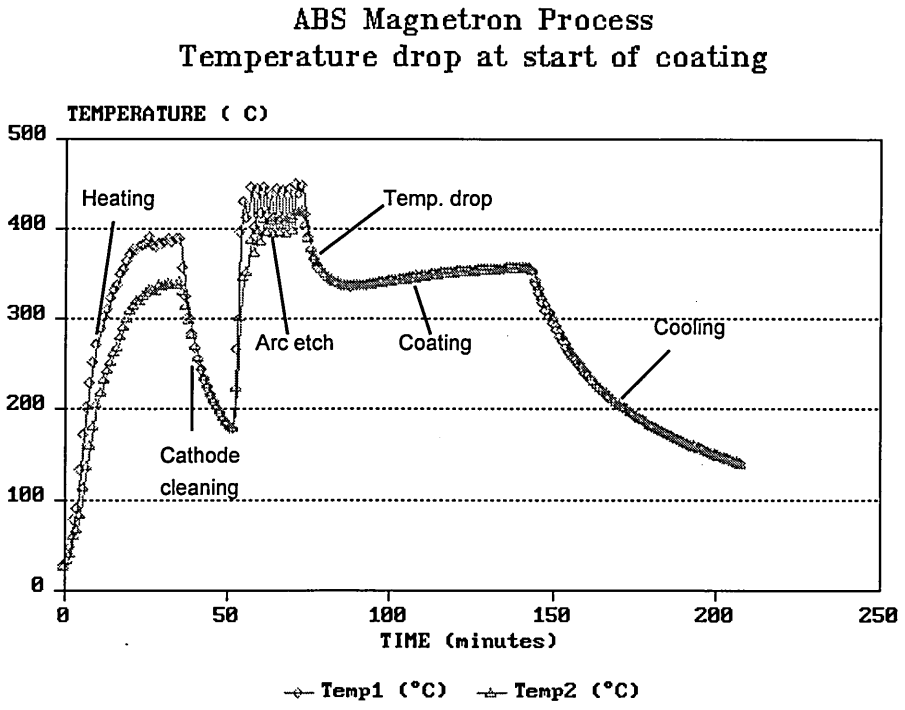

Substrates were placed at different positions in the chamber at various distances from the cathodes in a single coating run. The film thicknesses below give an indication of the ion bombardment intensity at those positions.

a. Steered-arc

Thickness (μm) after 180 minutes coating at 130A per cathode, -200V bias, 0.5 Pa.

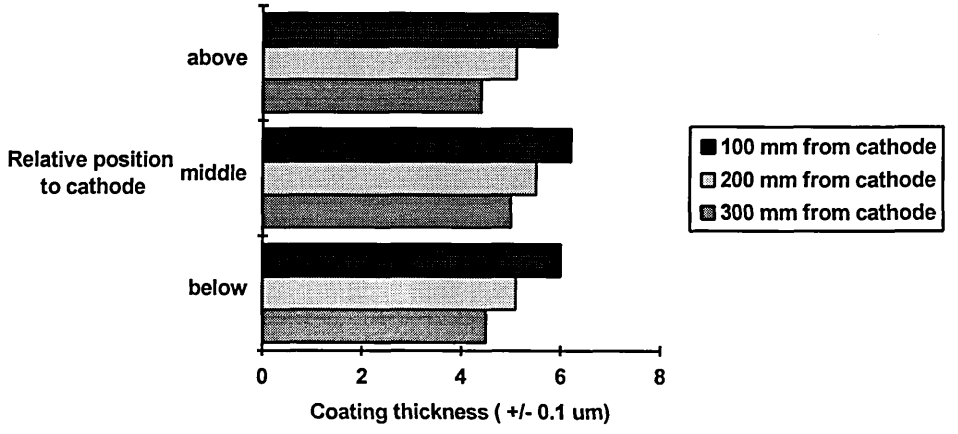

b. ABS magnetron

Thickness (μm) after 60 minutes coating at 10kW per cathode, -100V bias, 0.28 Pa.

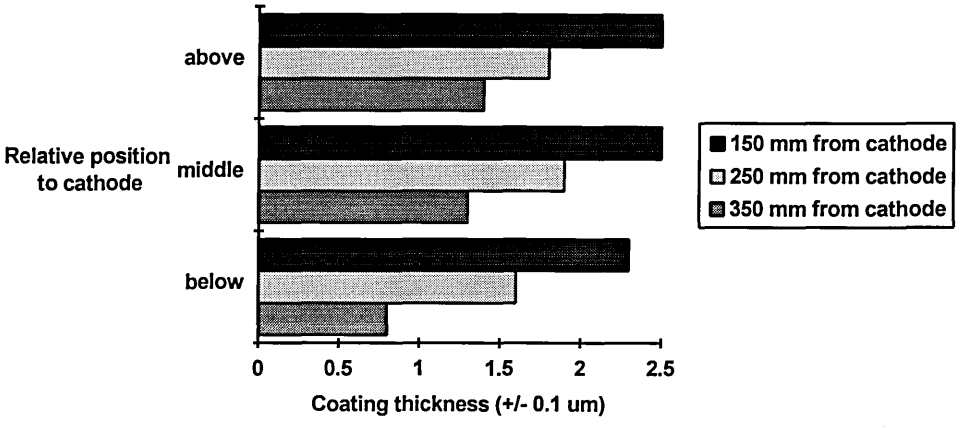

Bias current measurements were performed in the ABS magnetron chamber to determine the plasma uniformity with angle of rotation of the substrate turntable. This was done under sputter coating (table -100 V, cathodes -550 V) and glow discharge cleaning (table -1000 V, cathodes -200 V) conditions.

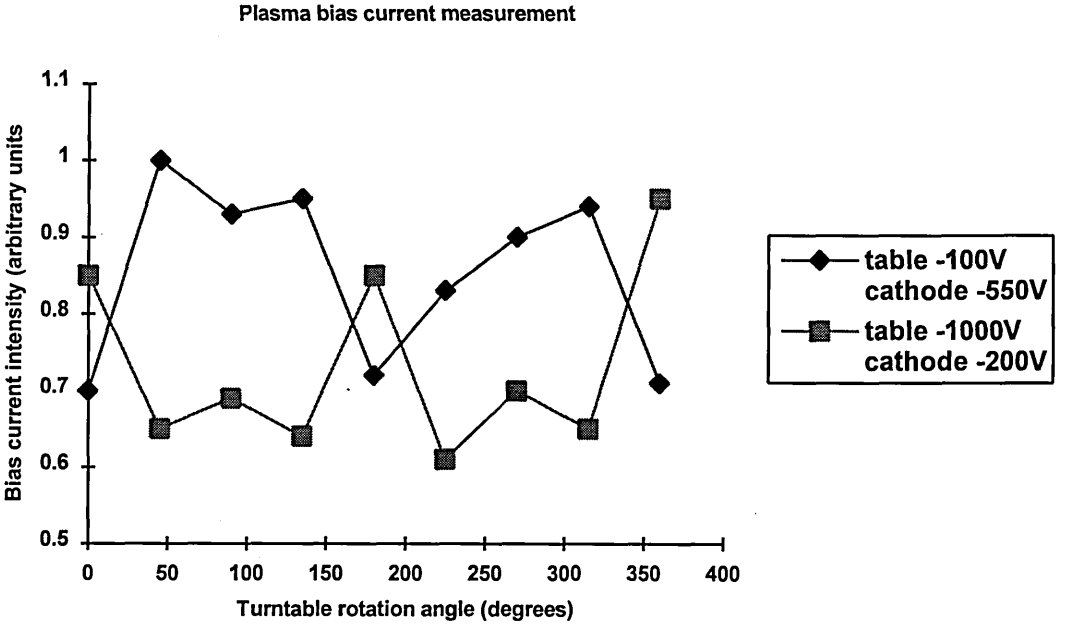

4.1.2 Colour

a. Steered-arc

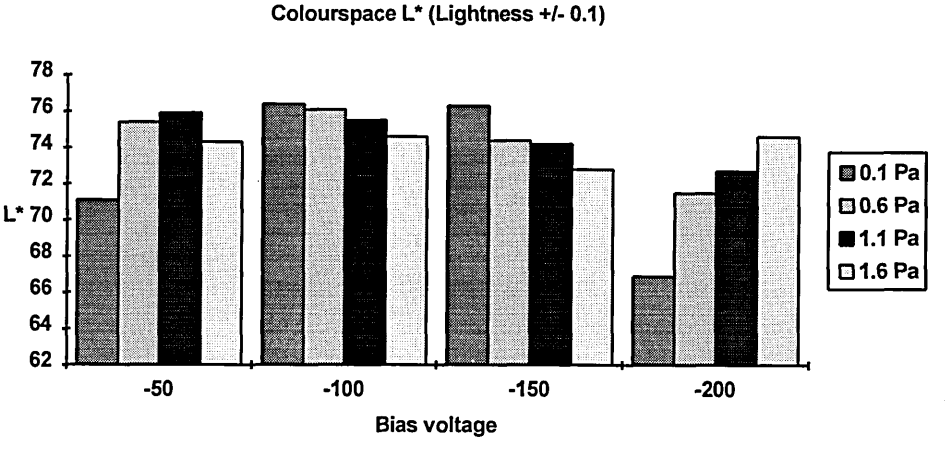

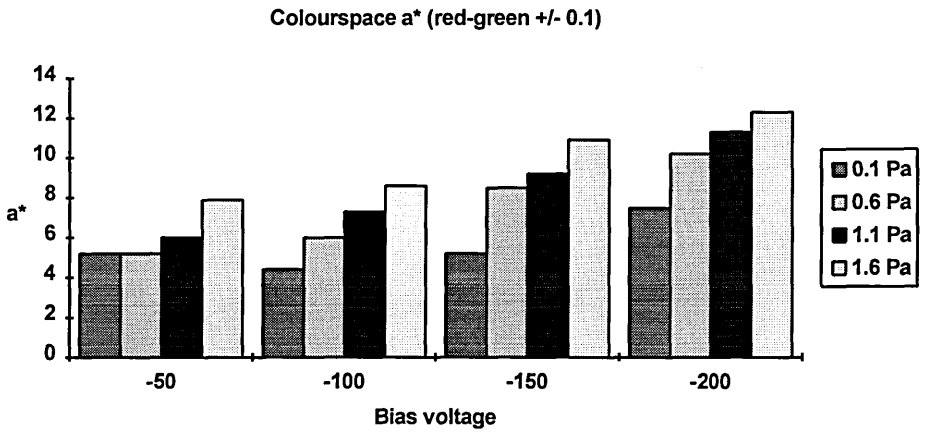

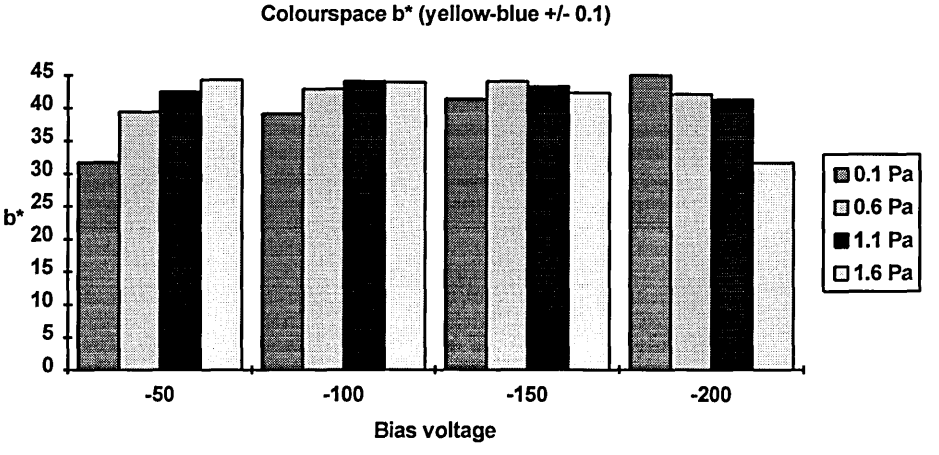

b. ABS magnetron

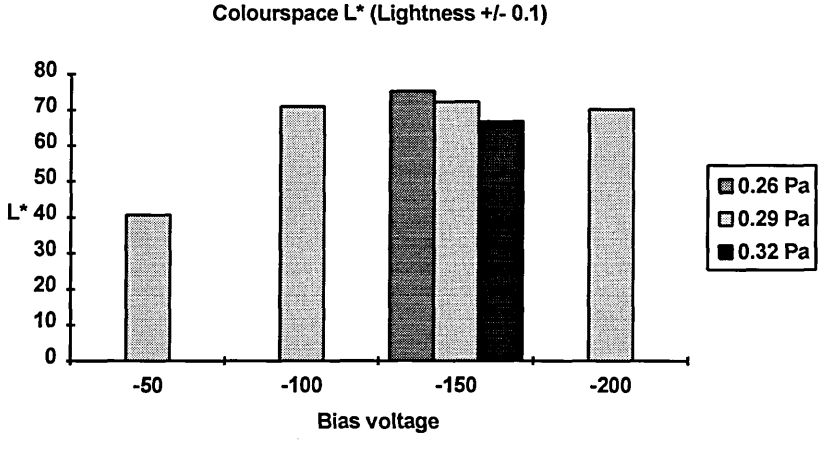

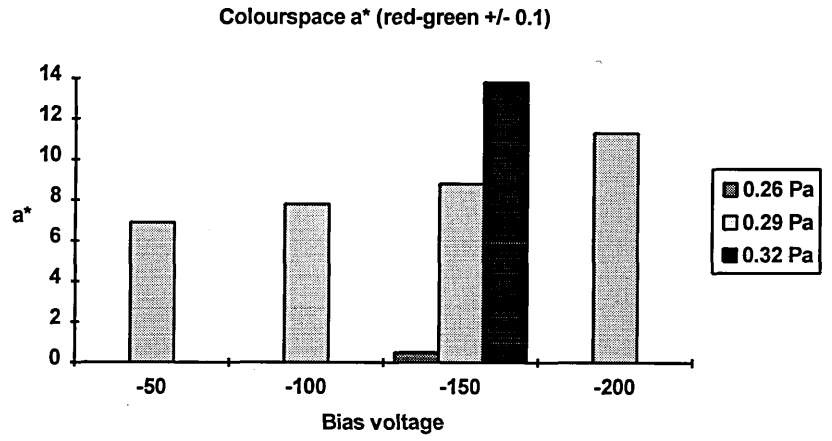

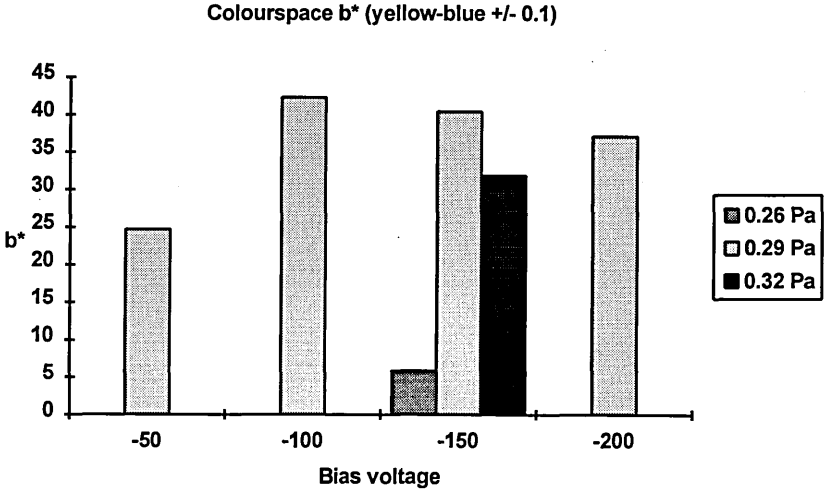

4.1.3 Surface Roughness and Droplets

a. Steered-arc

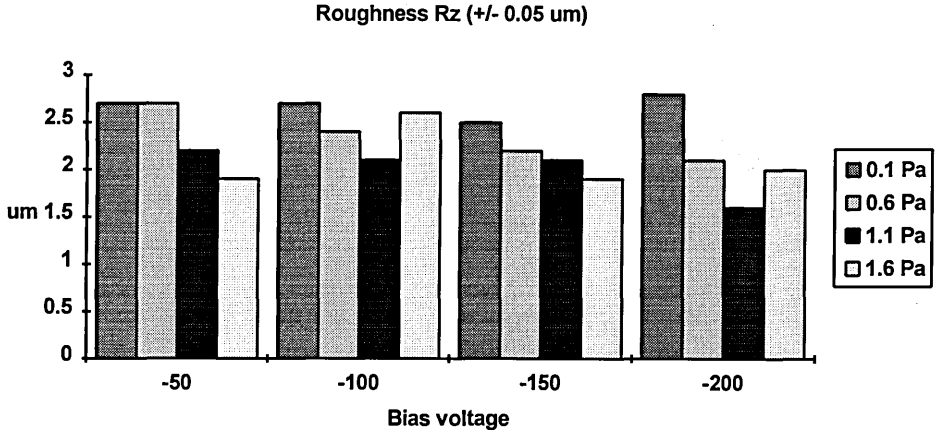

b. ABS magnetron

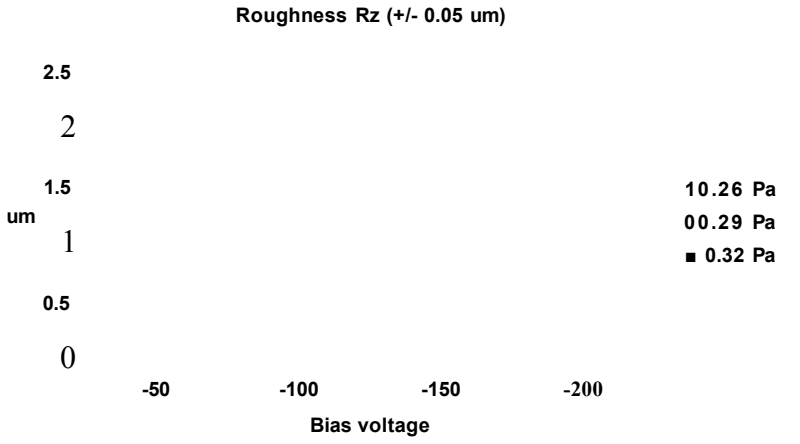

3-dimensional profile scans of 0.5 mm^ areas of the coating surfaces were performed using a "laser stylus" profilometer at the Forschungsinstitut fur Edelmetalle und Metallchemie. These were used to obtain an estimation of the droplet and crater count for the deposited films. The craters originated from removal of embedded droplets or from localised spallation of the coating. The counts were of objects greater in height or depth than 0.5 pm, and are presented below.

a. Steered-arc

-50 V bias 1.6 Pa pressure

-200 V bias 1.6 Pa pressure

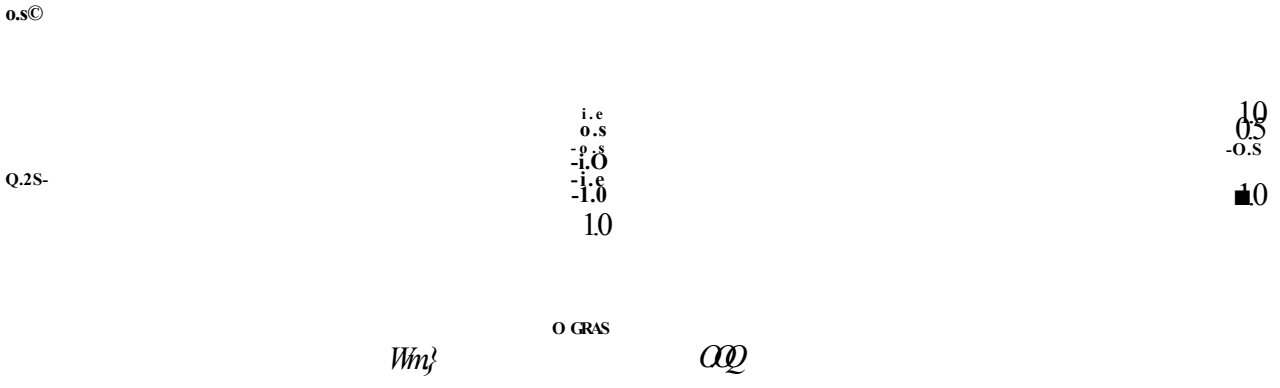

- 50 V bias 0.1 Pa pressure

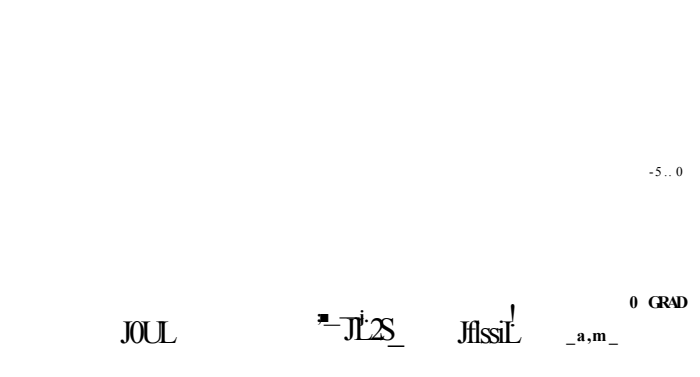

- 200 V bias 0.1 Pa pressure

Summary

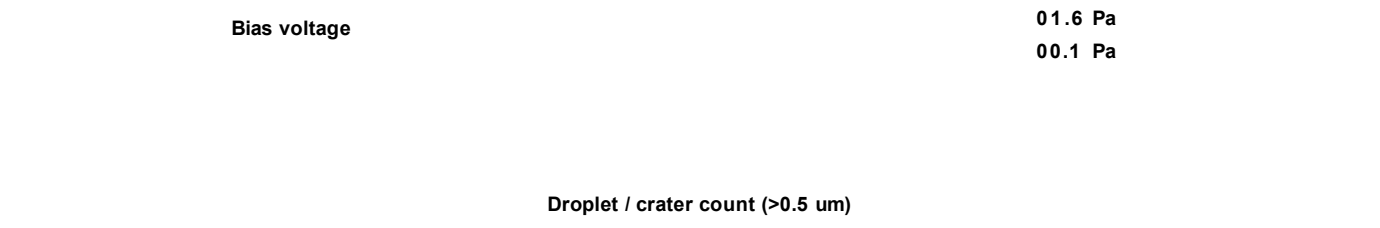

b. ABS magnetron

- 50 V bias 0.29 Pa pressure

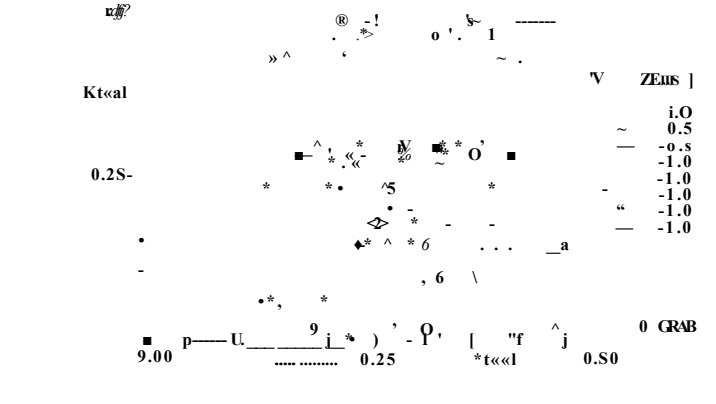

- 150 V bias 0.29 Pa pressure

-150V bias 0.26 Pa pressure

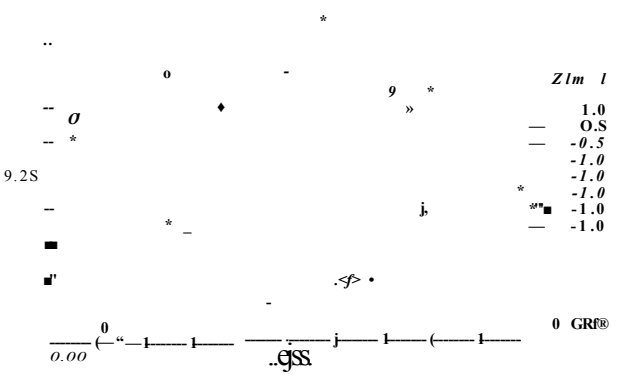

- 150 V bias 0.32 Pa pressure

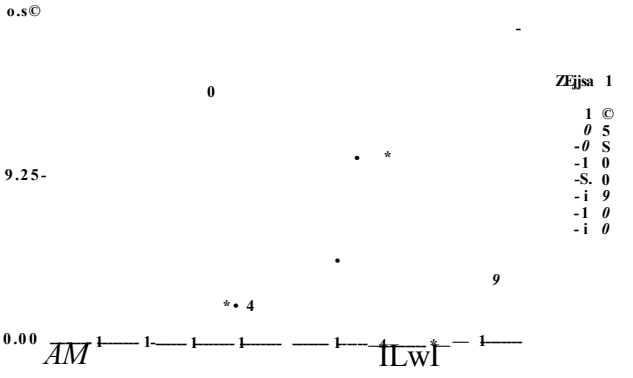

Summary :

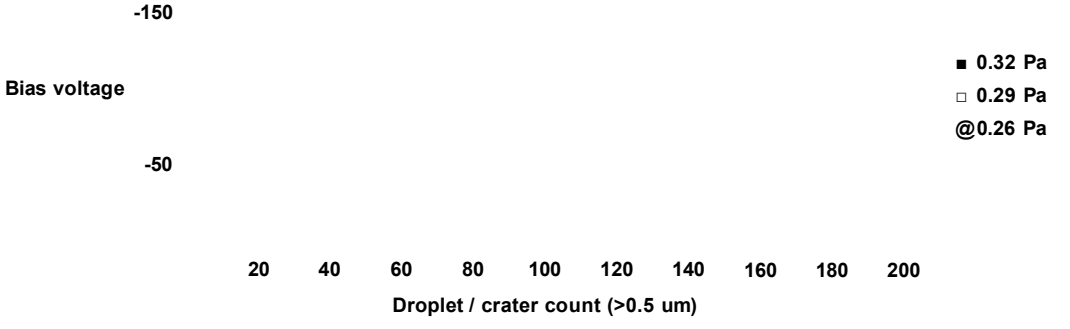

Arc etch only

4.1.4 Thickness / Deposition Rate

a. Steered-arc

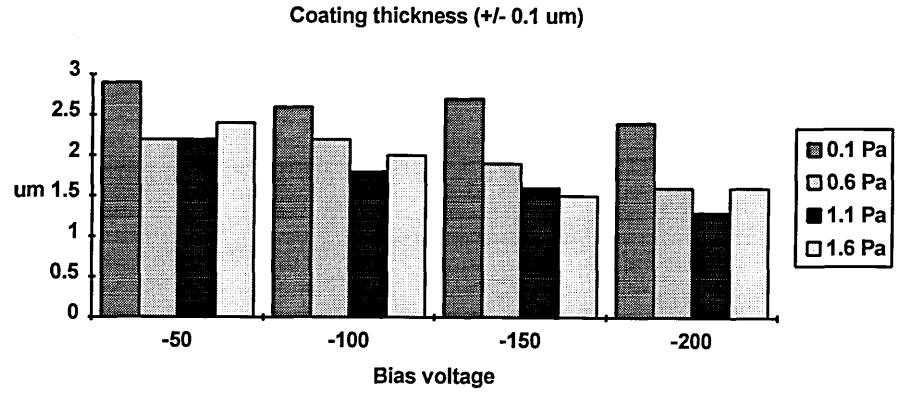

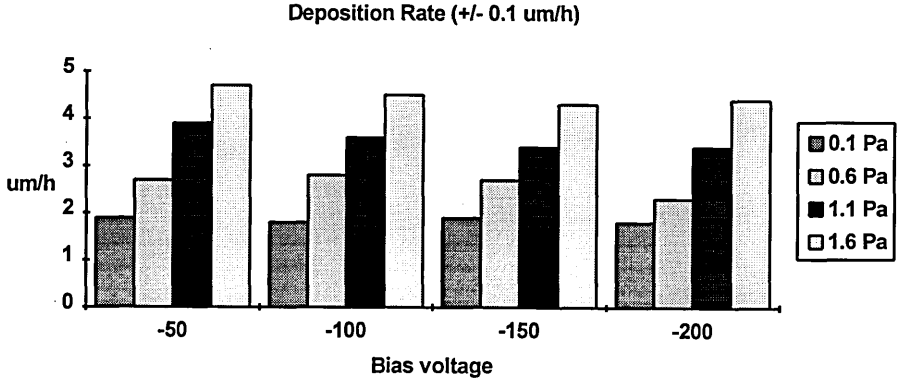

b. ABS magnetron

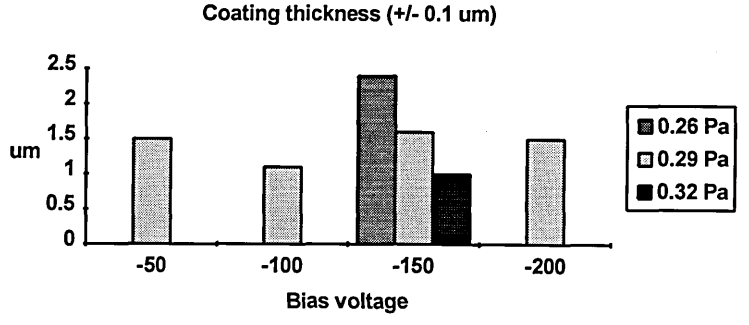

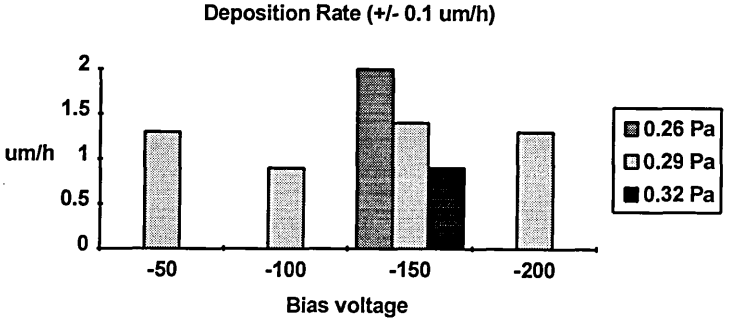

4.1.5 Microhardness and Ultra-microhardness

All microhardness test results are for coatings on HSS substrates as these gave the best support to the thin films.

a. Steered-arc

Coating hardness (+/- 50 kg mm^{-2}) using Knoop-50g load (uncoated = 800)

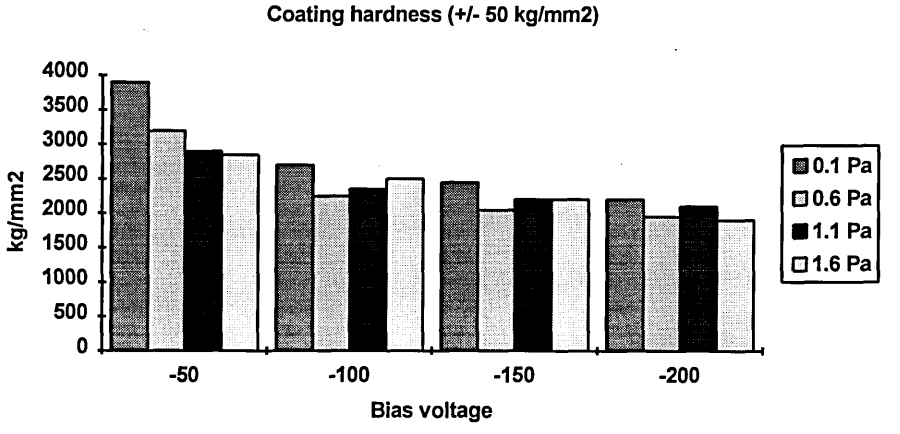

b. ABS magnetron

Coating hardness (+/- 50 kg mm^{-2}) using Knoop-50g load (uncoated = 1000)

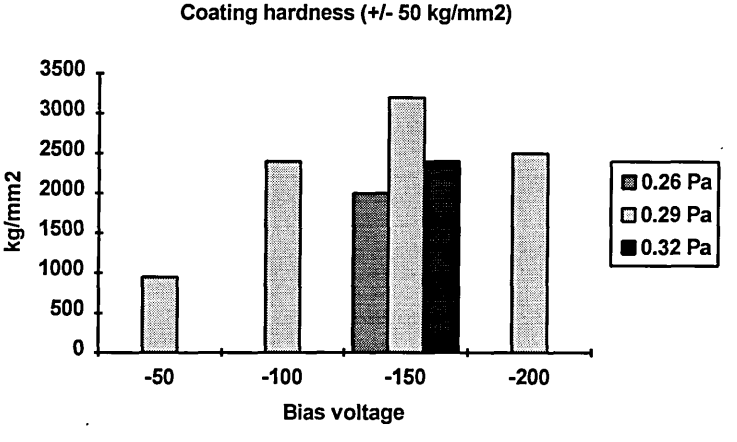

Using an ultra-microhardness indenter, a low-load measurement of the plastic hardness of the coatings was performed and the results are presented below.

a. Steered-arc

Coating hardness (+/- 30 $kg.mm^{-2}$) using 15g max. load (uncoated = 760)

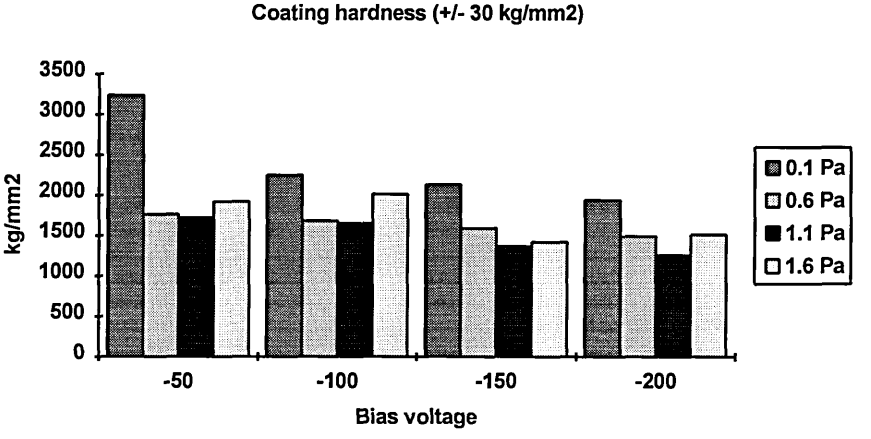

b. ABS magnetron

Coating hardness (+/- 30 $kg.mm^{-2}$) using 15g max. load (uncoated = 980)

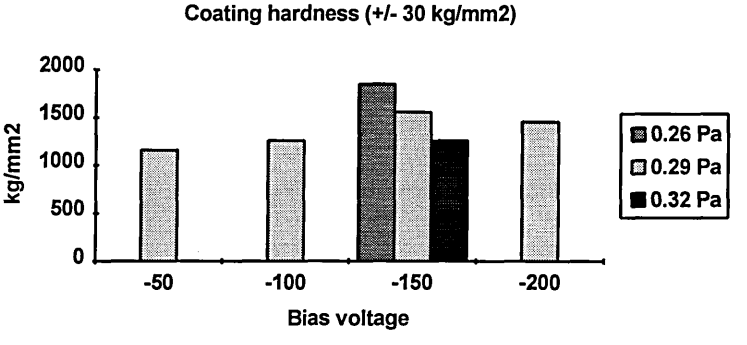

4.1.6 Adhesion

All adhesion results are for coatings on HSS substrates as these offered the best load bearing surfaces for this test. Generally, the adhesion of the film appeared better on the other substrates used (stainless steel, titanium and nickel alloy), but because of their lower bulk hardnesses, the apparent critical load was lower.

The Rockwell test consistently showed no cracking or spallation for all the coatings in the parameter study. Example indents are shown below :

Good adhesion (no cracking)

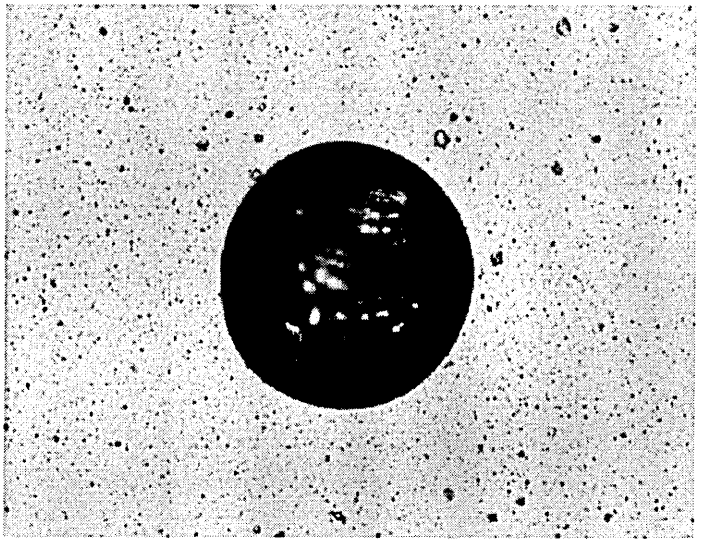

Deformation into indent on soft substrate (no cracking)

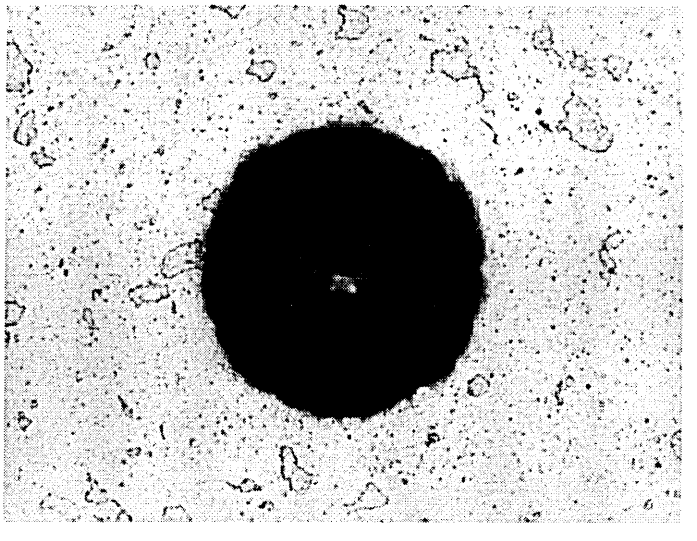

Example scratch tests at critical load and acoustic emission plots are shown below :

Edge chipping

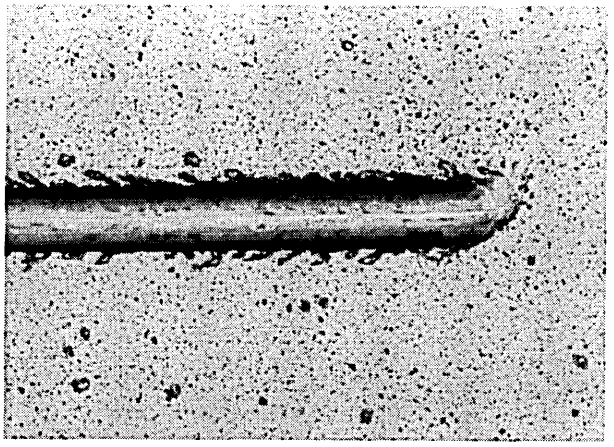

Coating spallation

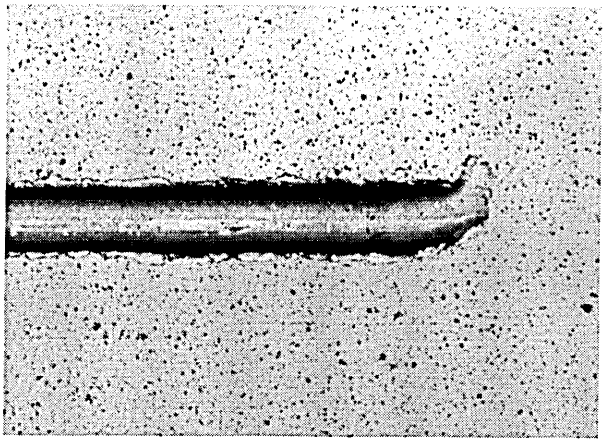

Gross coating failure

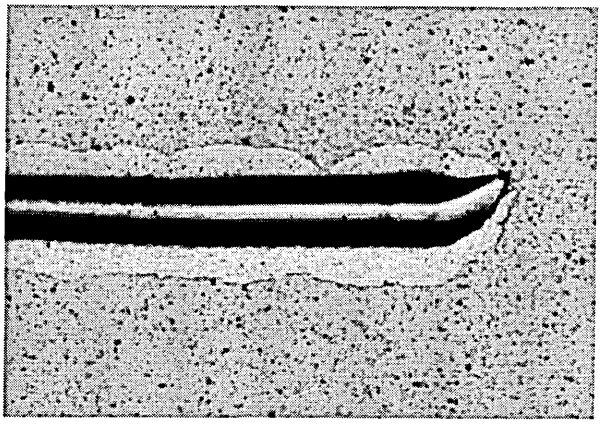

Acoustic emission at failure from a coating with low internal stress

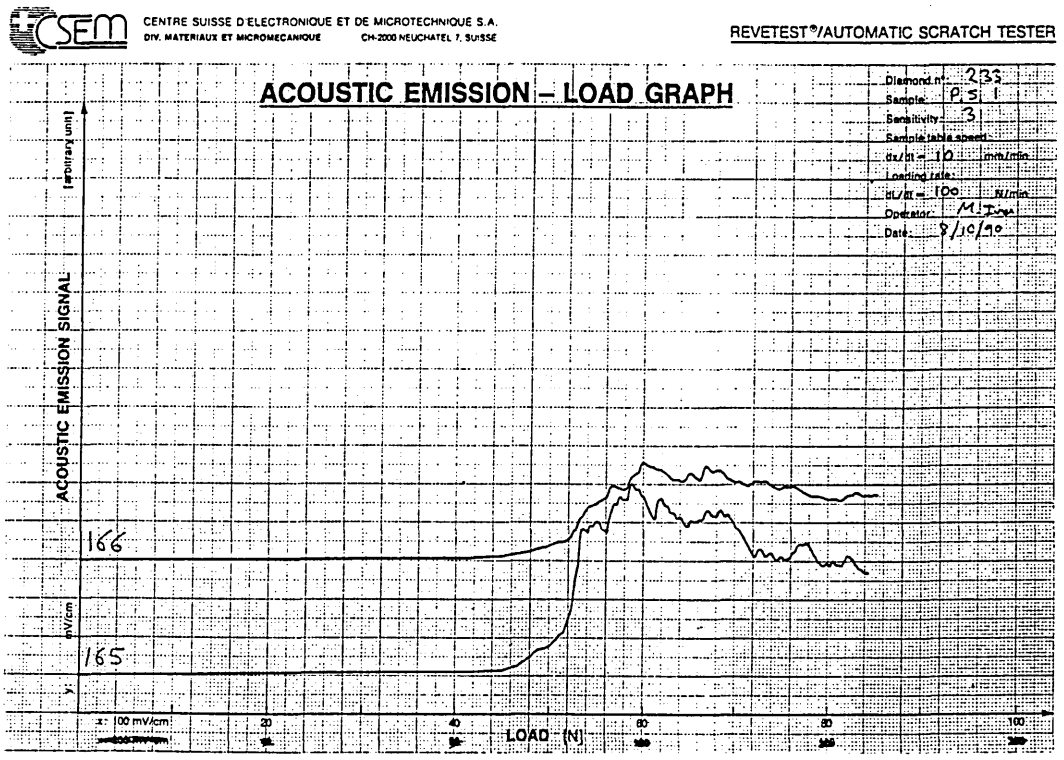

Acoustic emission at failure from a coating exhibiting high internal stress

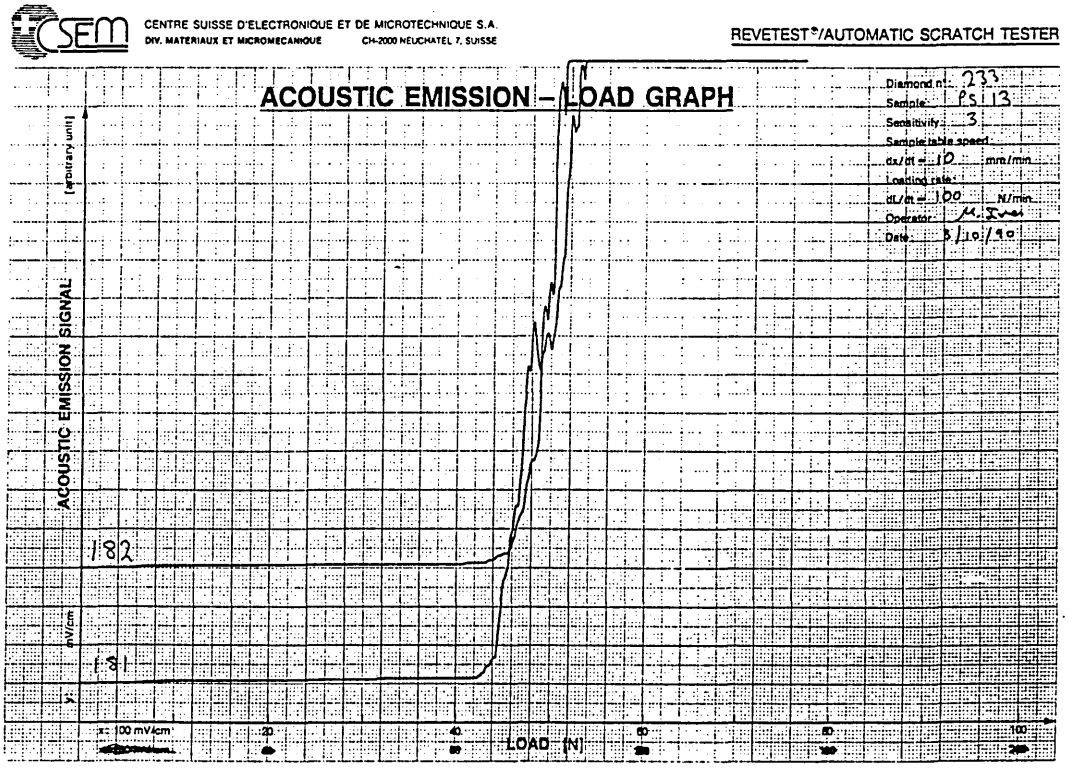

The scratch test critical load values given below correspond to spallation and failure of the coating and have been confirmed by optical microscopy.

a. Steered-arc

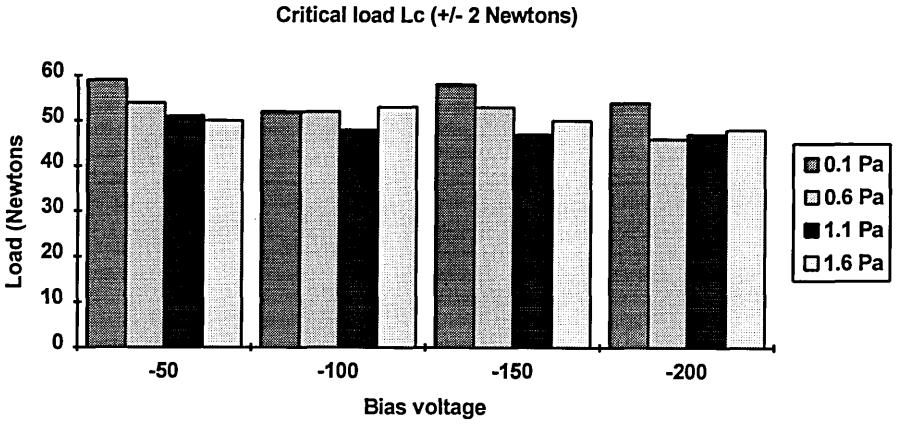

b. ABS magnetron

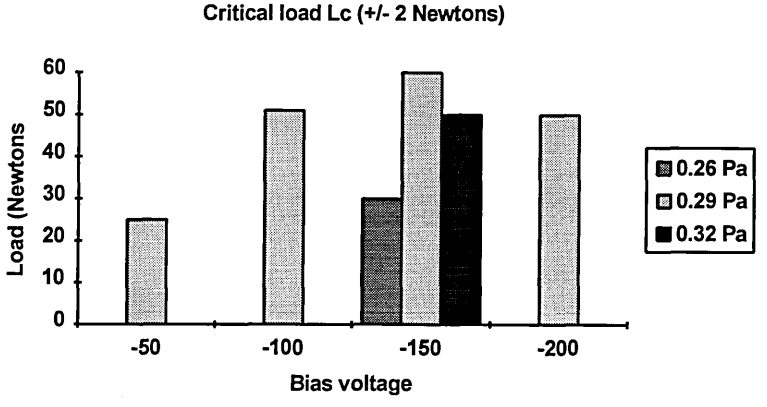

4.1.7 Structure

4.1.7.1 Scanning Electron Microscopy

a. Steered-arc

- 50 V bias 1.6 Pa pressure

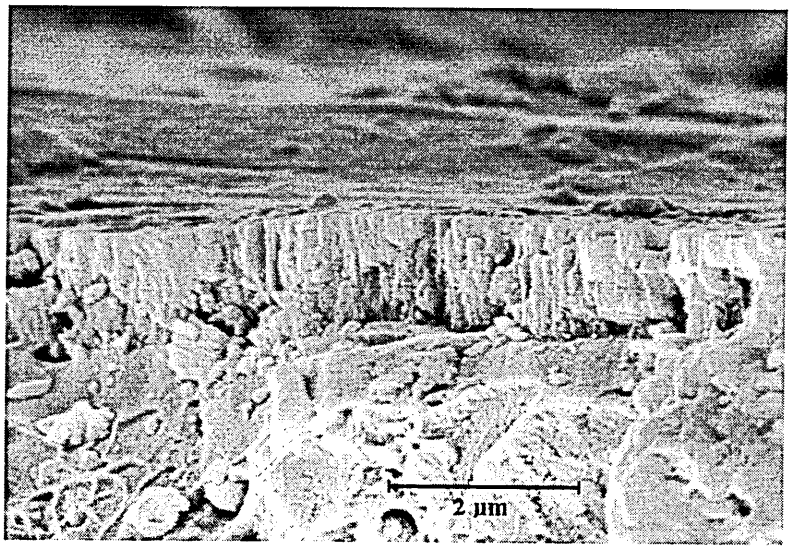

- 50 V bias 0.1 Pa pressure

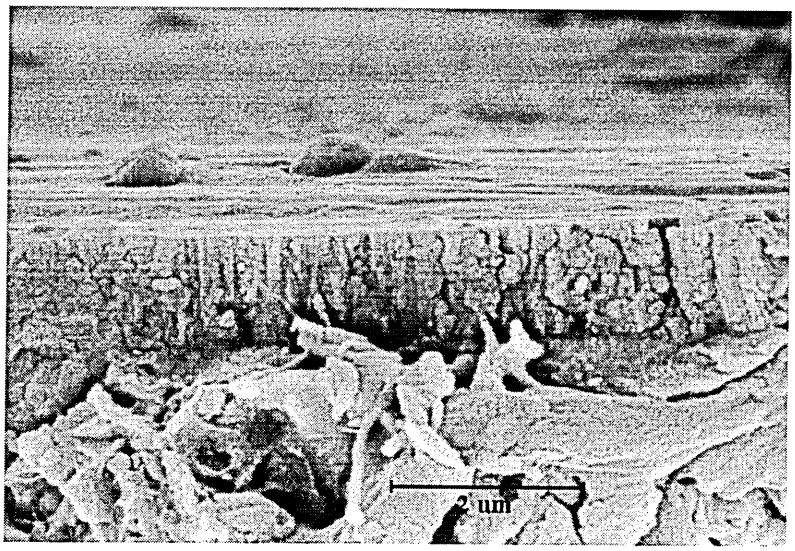

- 100 V bias 1.1 Pa pressure

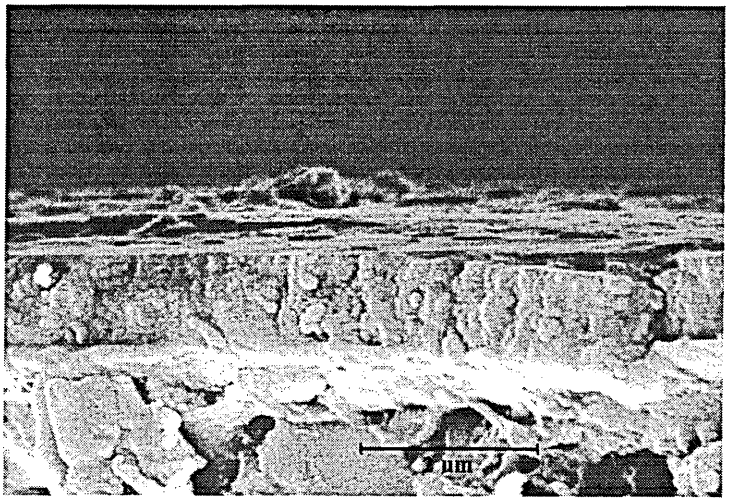

- 200 V bias 1.6 Pa pressure

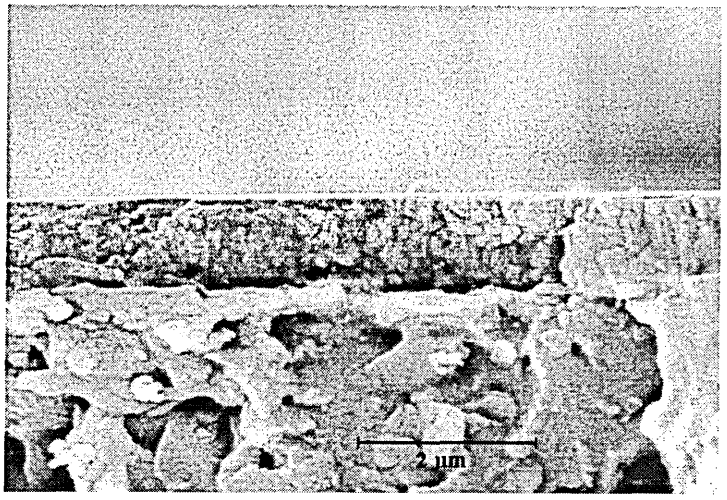

- 200 V bias 0.1 Pa pressure

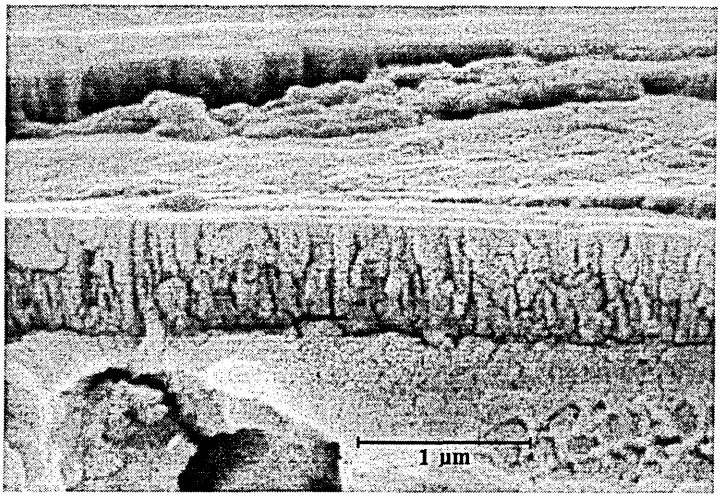

Summary of observed structure zones as depicted in the various structure-zone-models.

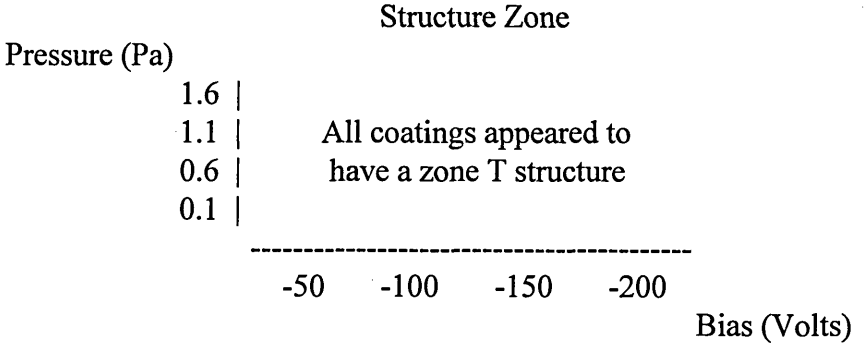

b. ABS magnetron

- 50 V bias 0.29 Pa pressure

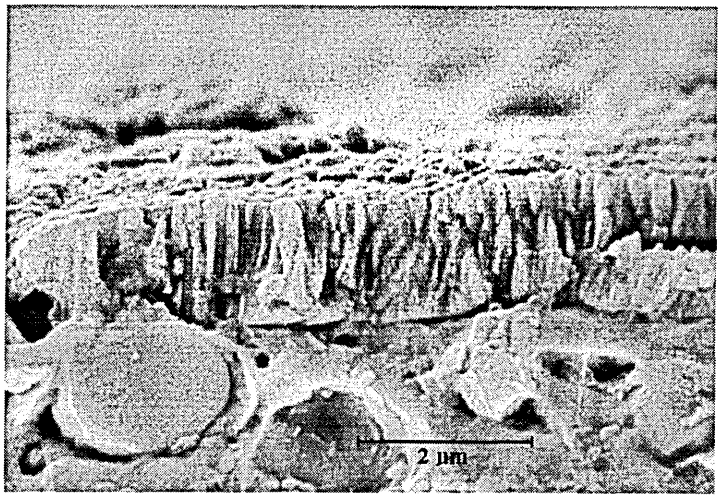

- 100 V bias 0.29 Pa pressure

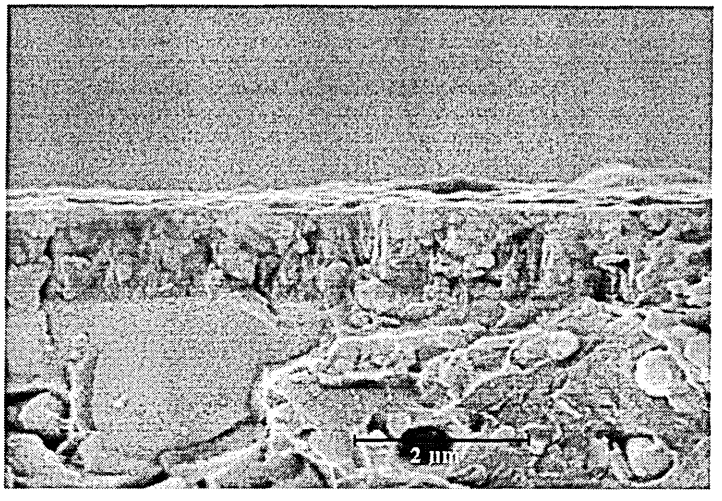

- 150 V bias 0.29 Pa pressure

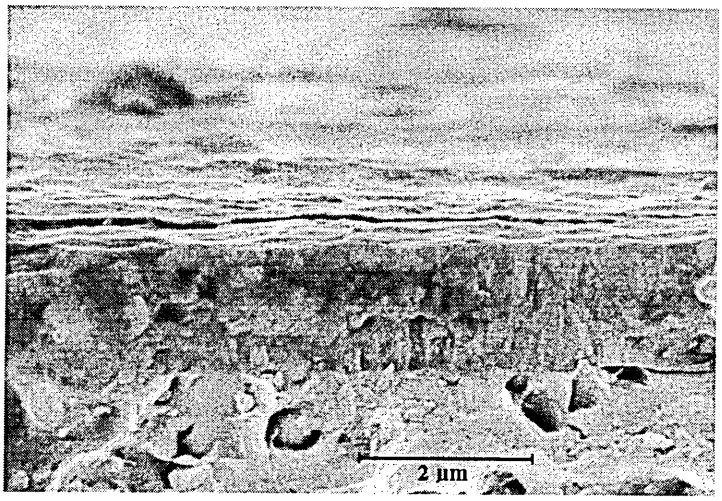

- 200 V bias 0.29 Pa pressure

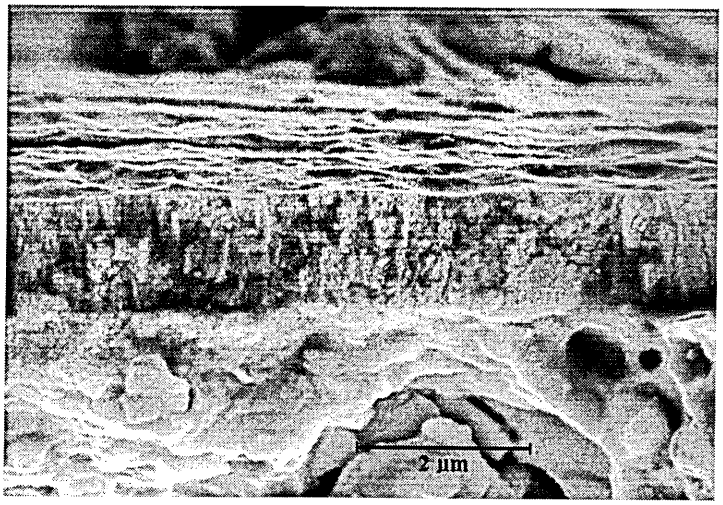

- 150 V bias 0.26 Pa pressure

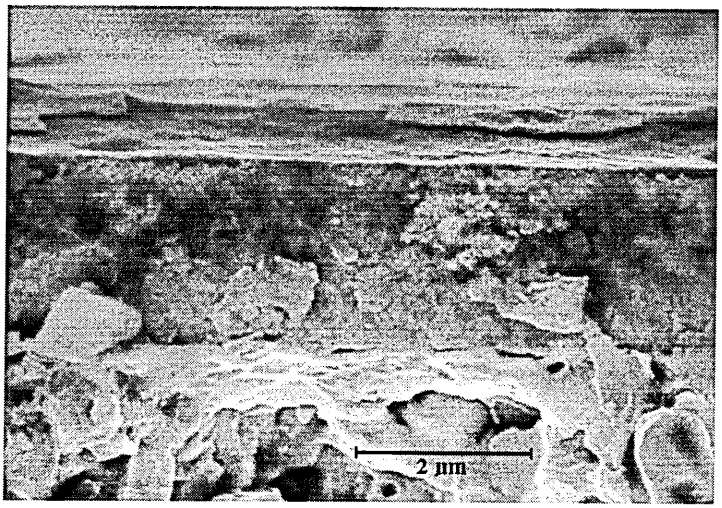

- 150 V bias 0.32 Pa pressure

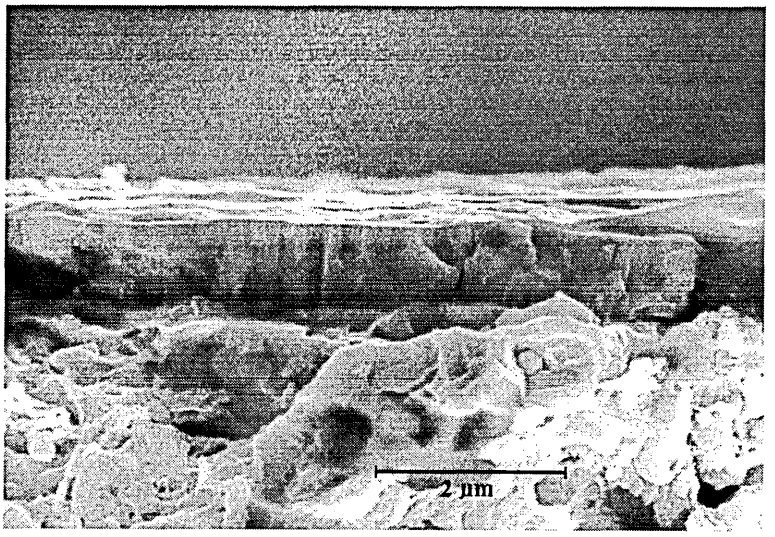

Summary of observed structure zones as depicted in the various structure-zone-models.

Structure Zone

Pressure (Pa)

0.32			zone T	
0.29	zone 1	zone T	zone T	zone T
0.26			zone 2	
	-50	-100	-150	-200

Bias (Volts)

Surface image of low pressure ABS magnetron coating showing droplets

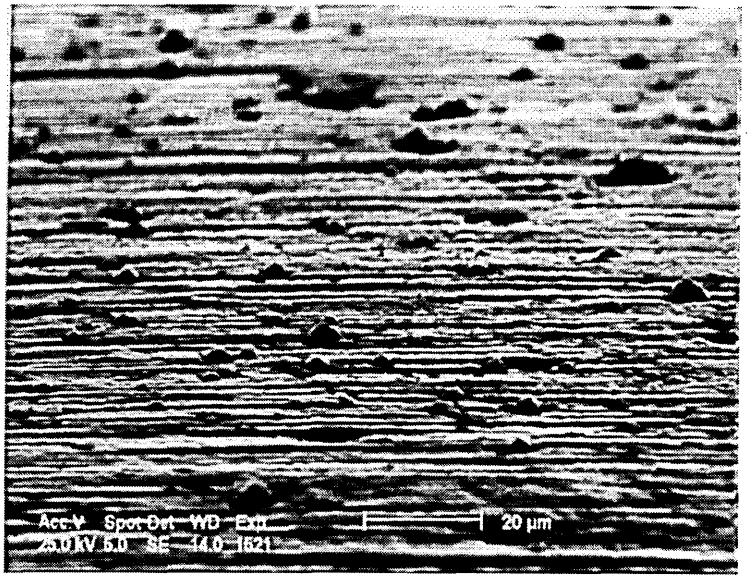

4.1.7.2 X-Ray Diffraction

a. Steered-arc

Varying bias voltage and pressure :

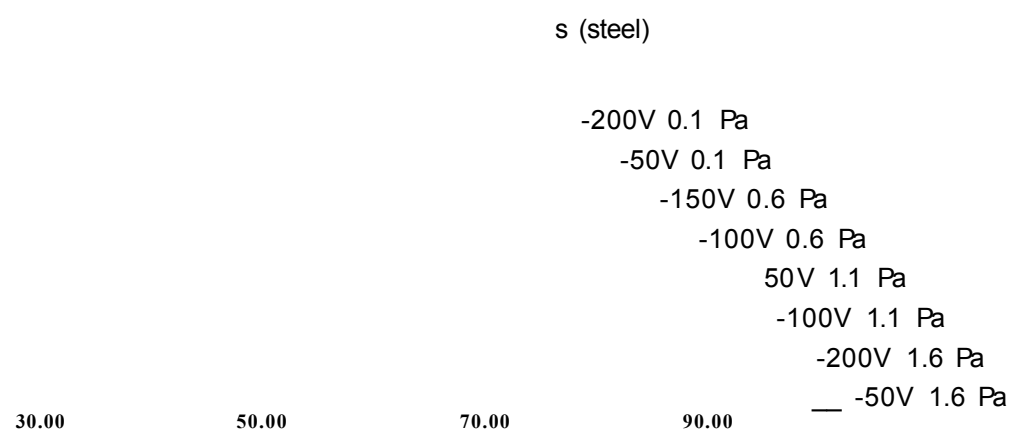

b. ABS magnetron

Varying bias voltage :

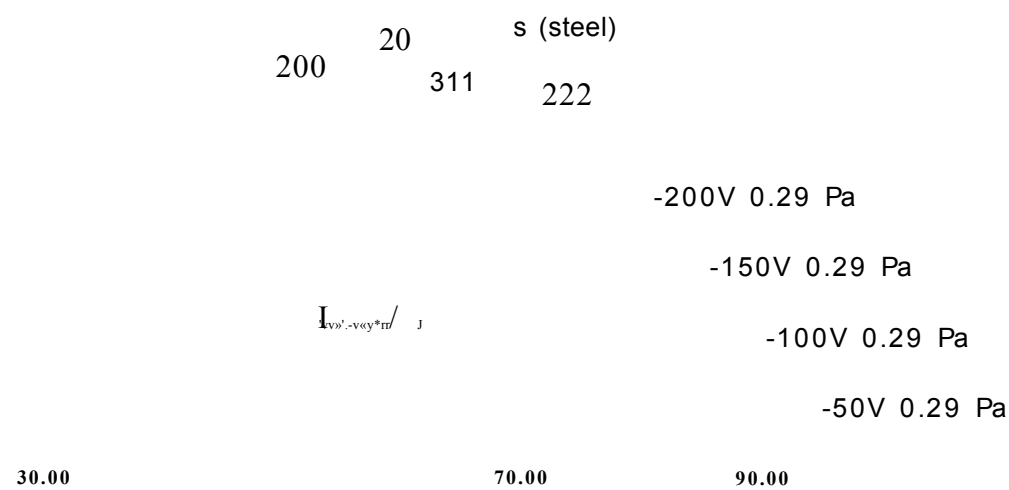

Varying pressure

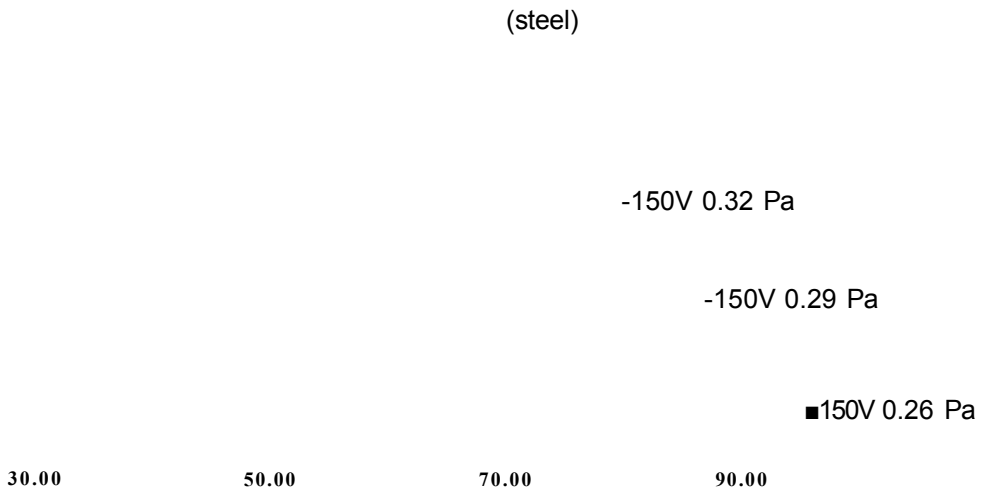

Texture Coefficients

When using a diffractometer in 0 - 20 mode (as in this work) diffraction takes place only from planes lying parallel to the sample surface, and so a sample exhibiting texture (or preferred orientation) will give greater X-ray peak intensities for those (hkl) planes than would be expected in a randomly orientated (or powder) sample. This may be quantified using the formula :

$$pM/= \frac{***hkl***/ \text{r M /}}{1/N \pounds \backslash ***hk[*** / ***Rhk/***} \qquad 0\ 5)$$

where ***l/jki*** is the measured (hkl) peak intensity of a textured sample, ***R/lkj*** is the (hkl) peak intensity from a randomly orientated sample and N is the number of peaks considered. Then ***Rflki*** = 1 signifies random orientation, P/7\/ < 1 signifies less planes lying in that orientation than would occur randomly, while ***P/lk/*** > 1 indicates preferred orientation in that planar direction.

a. Steered-arc

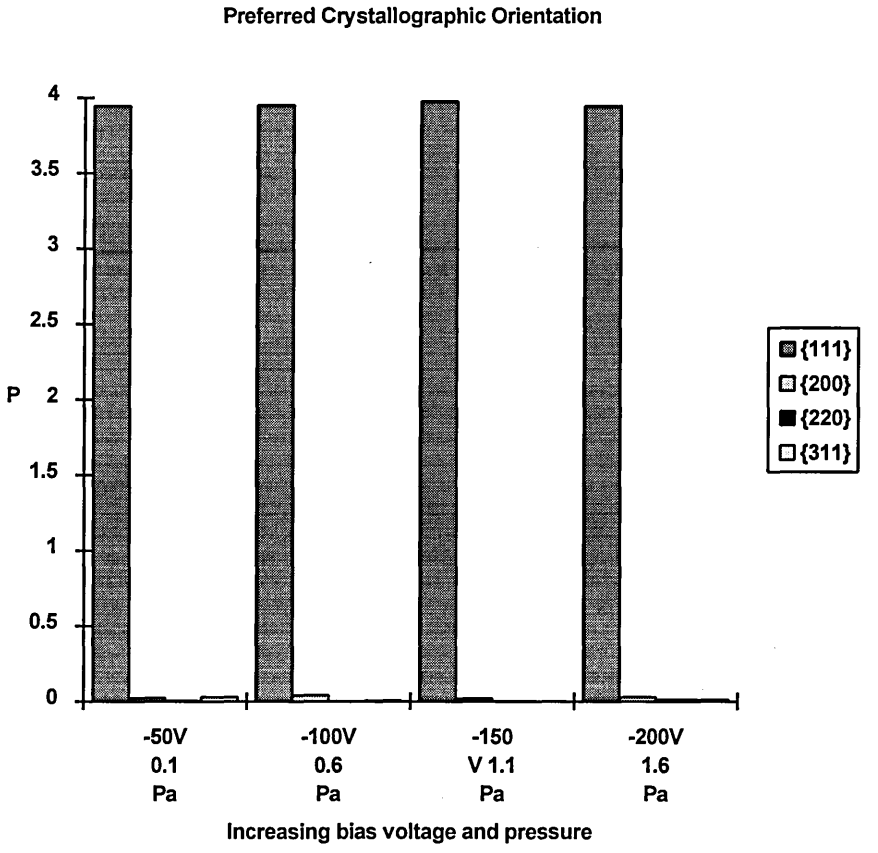

b. ABS magnetron

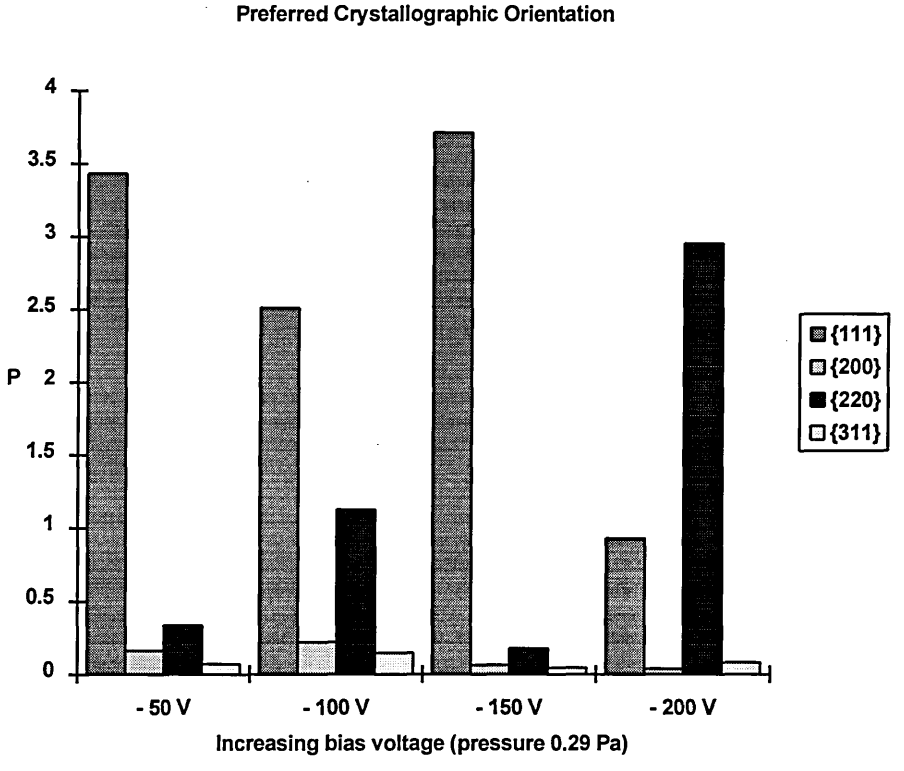

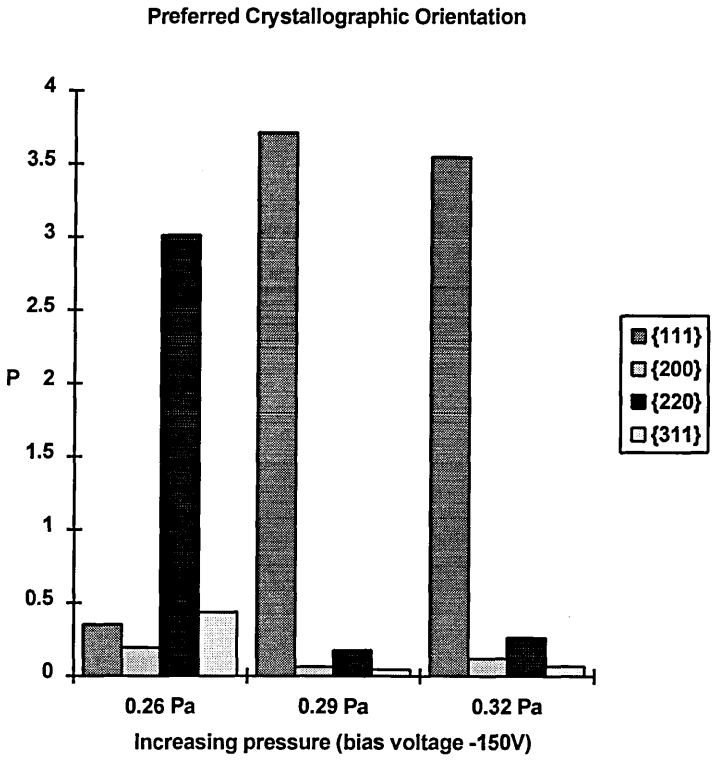

Lattice Parameters

Lattice parameter measurements were made using the formula :

$$a_{hkl} = d\,(h^2 + k^2 + l^2)^{0.5} \qquad \text{..... (16)}$$

where a_{hkl} is the lattice parameter for a particular set of planes (hkl) and d is the interplanar spacing according to the Bragg equation ($\lambda = 2d.\sin\theta$). Average lattice parameters a_0 were extrapolated for each coating from a linear plot of individual lattice parameters versus $\cos\theta\cot\theta$ (the diffractometer function), to eliminate systematic experimental error. The resulting increase in unit cell size from the JCPDS (Joint Committee for Powder Diffraction Standards) data value of 0.4240 nm gives an indication of the residual stress in the coating.

a. Steered-arc

Average lattice parameters

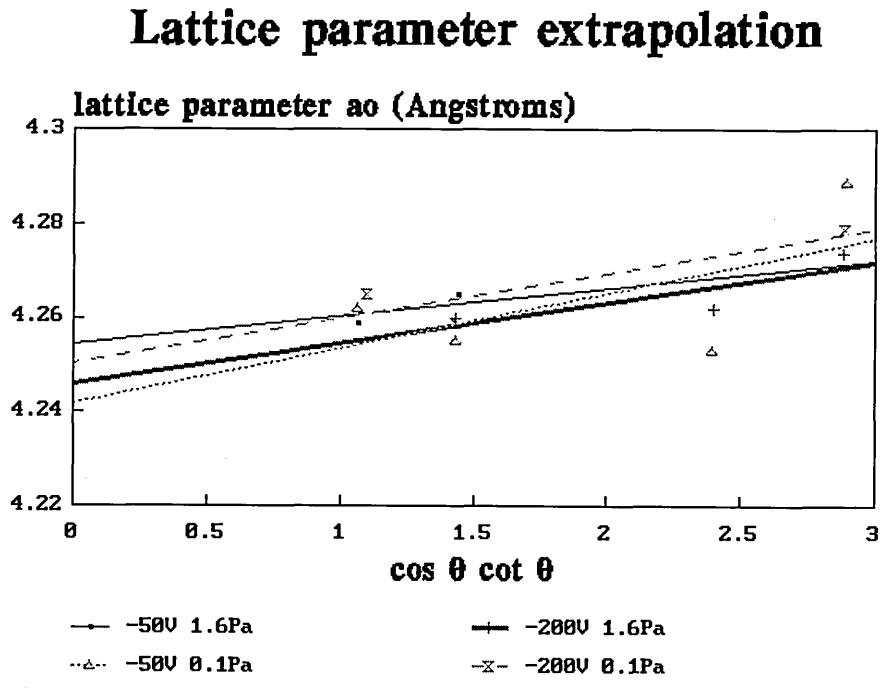

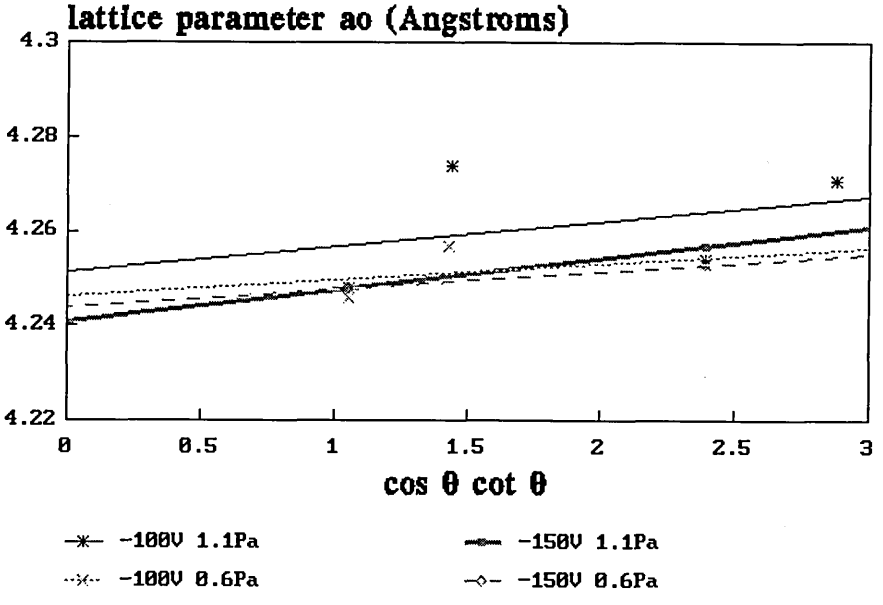

Summary :

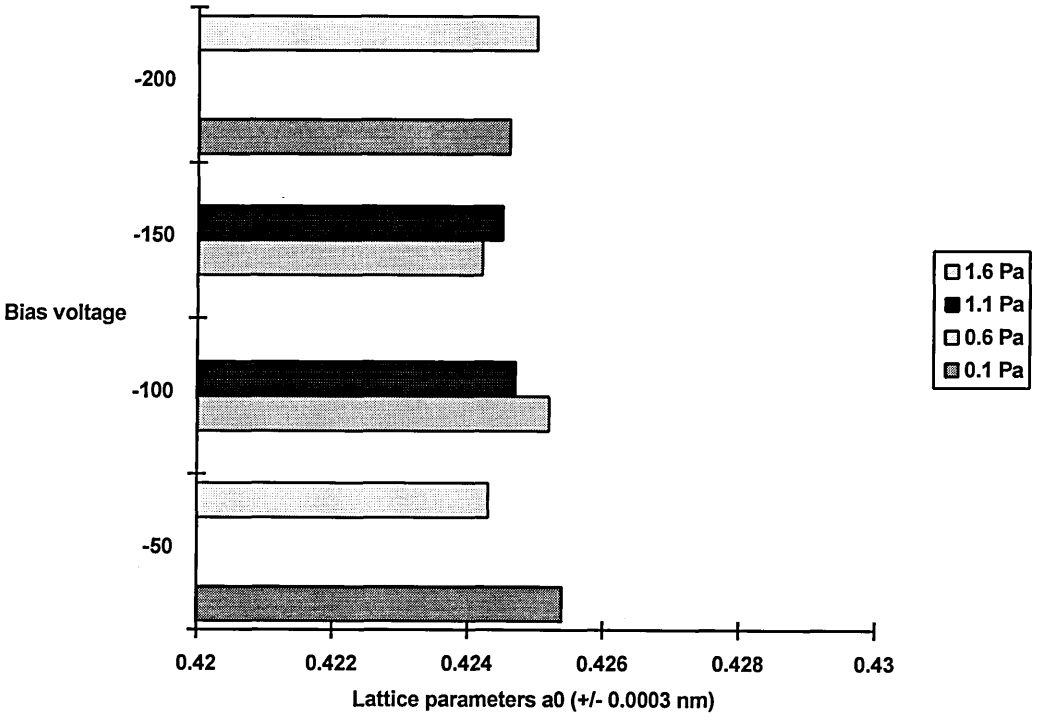

b. ABS magnetron

Average lattice parameters

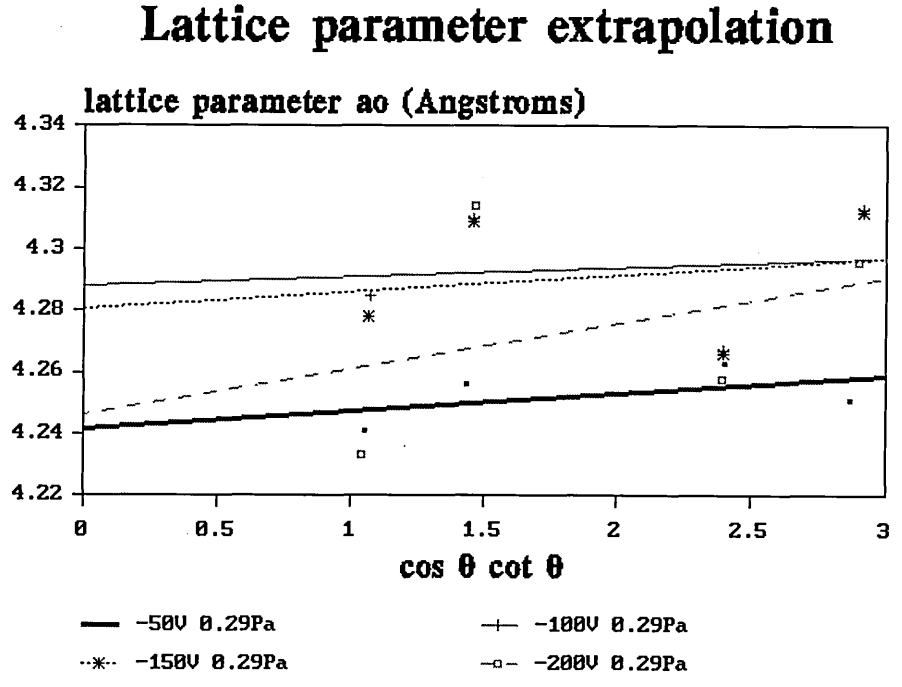

Lattice parameter extrapolation

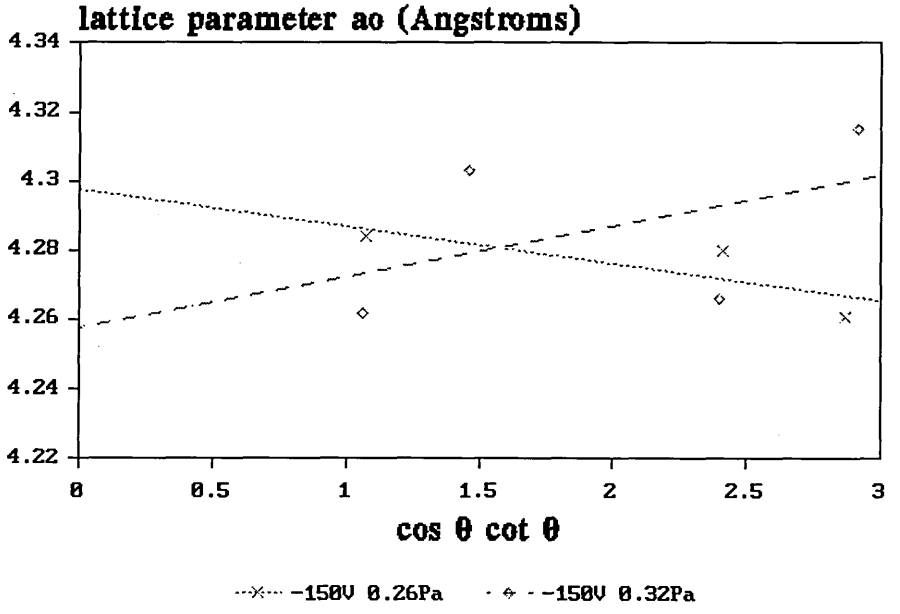

Summary :

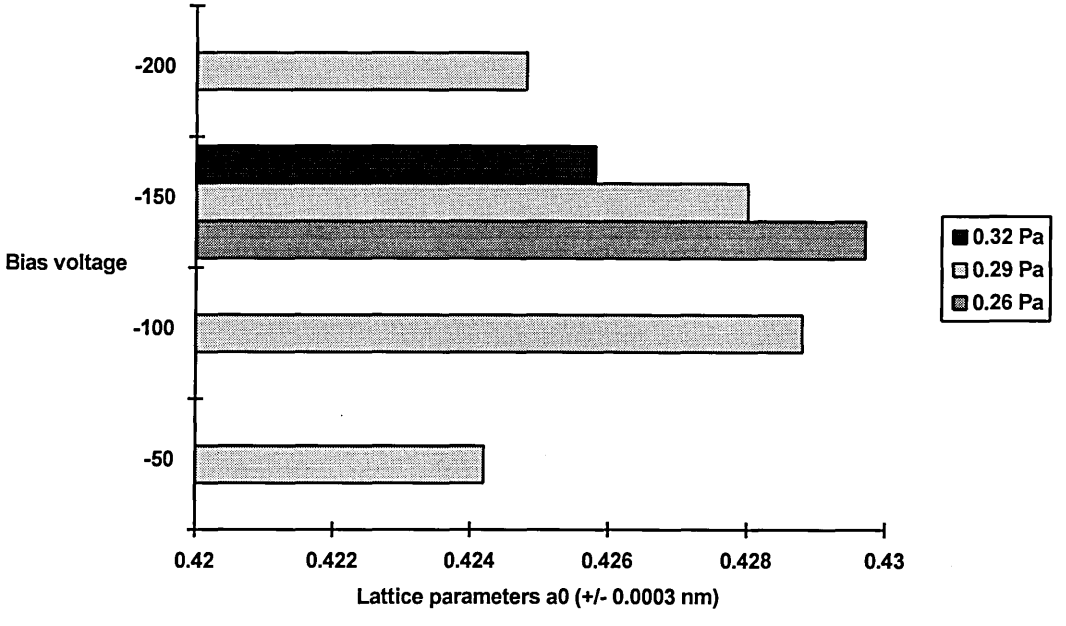

4.2 GDOES Technique

a. Steered-arc

-50 V bias 1.6 Pa pressure

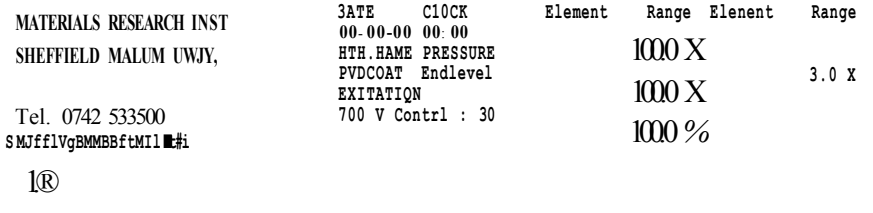

8 S

eo	6.7	1.4	2.1	2.7	S.4	4.1

- 50 V bias 0.1 Pa pressure

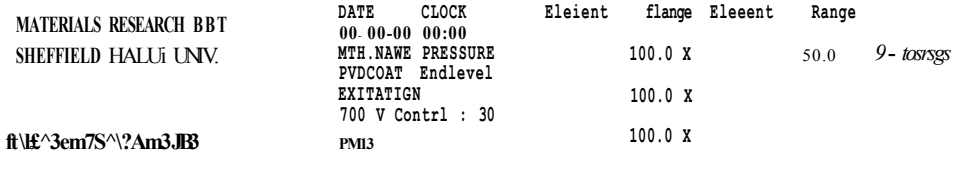

34 7.7

- 200 V bias 1.6 Pa pressure

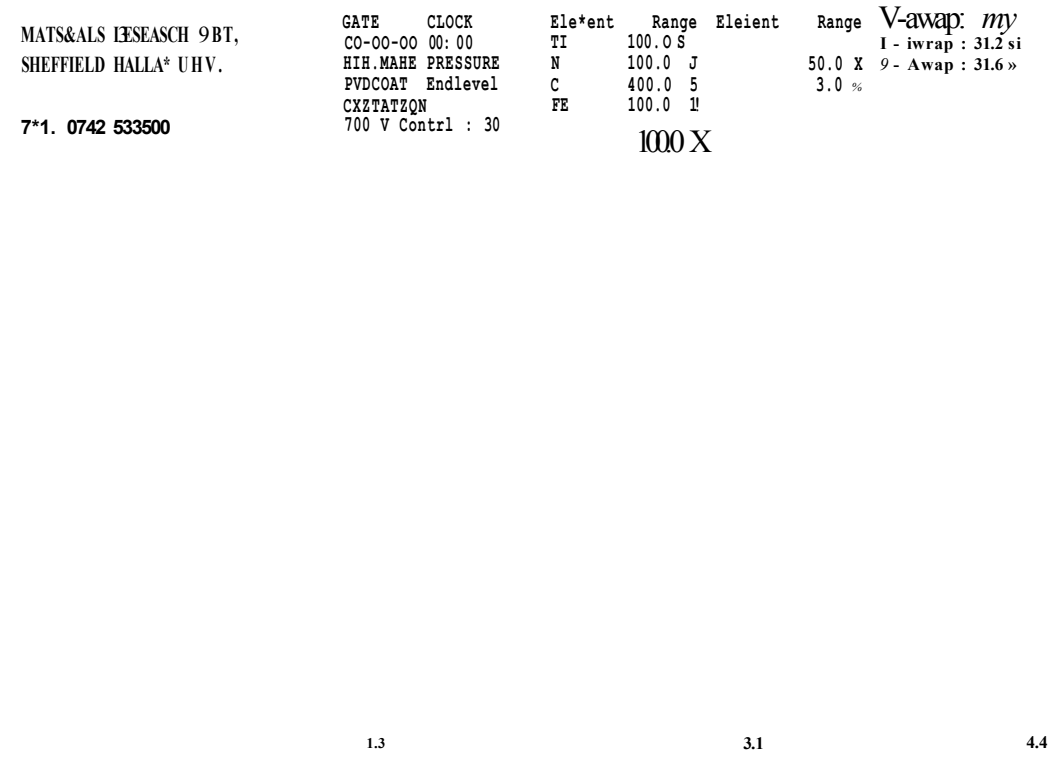

- 200 V bias 0.1 Pa pressure

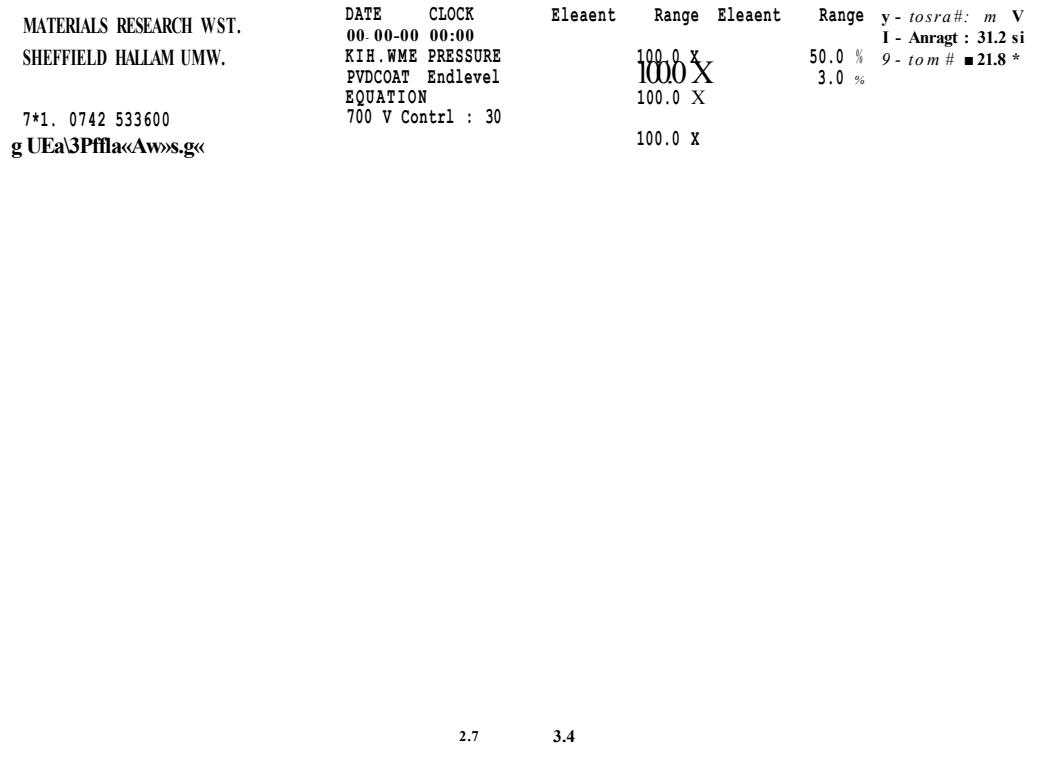

b. ABS Magnetron

-50 V bias 0.29 Pa pressure

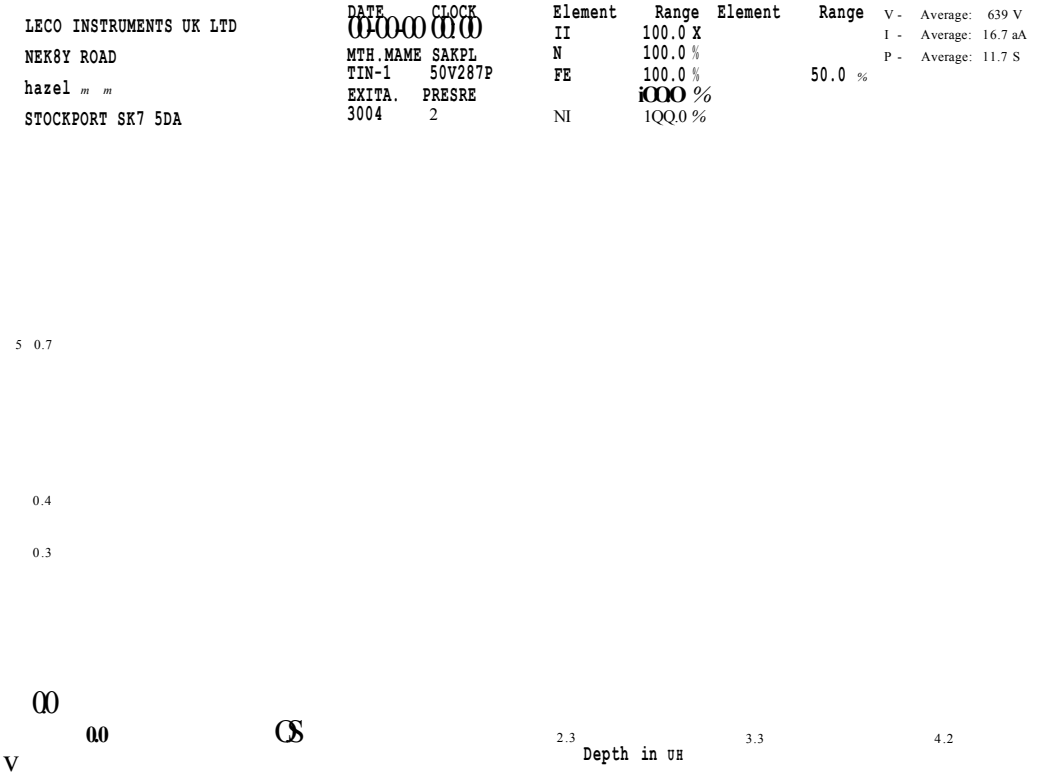

- 100 V bias 0.29 Pa pressure

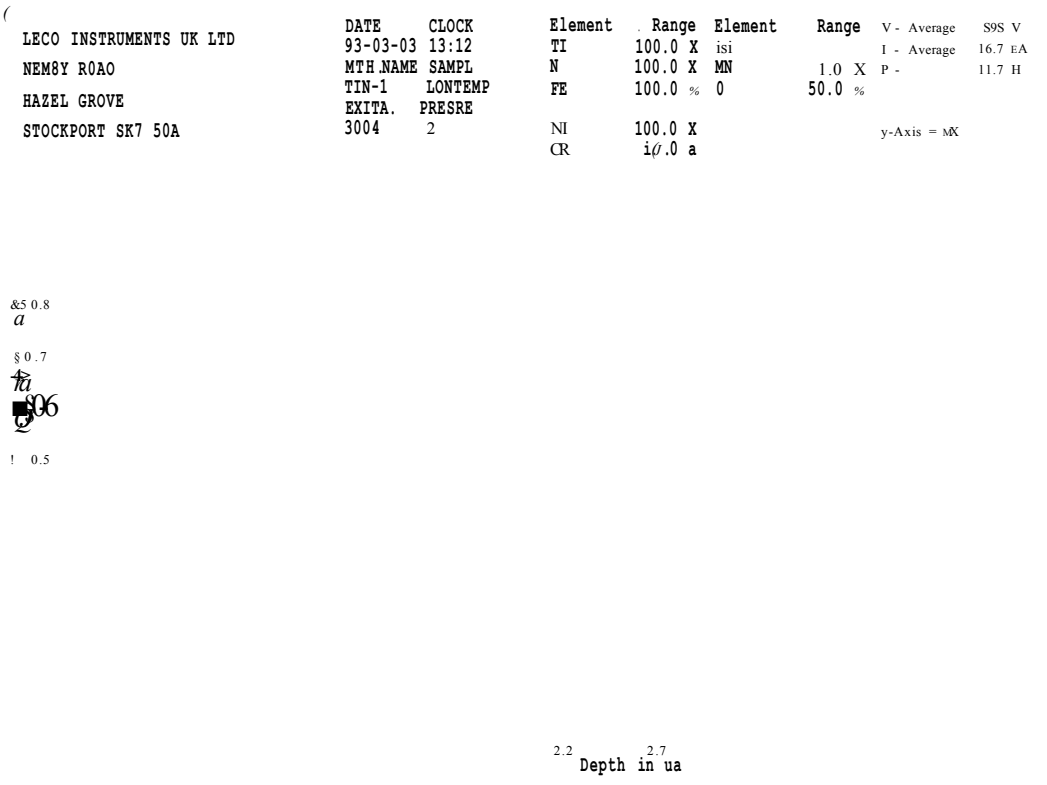

- 150 V bias 0.29 Pa pressure

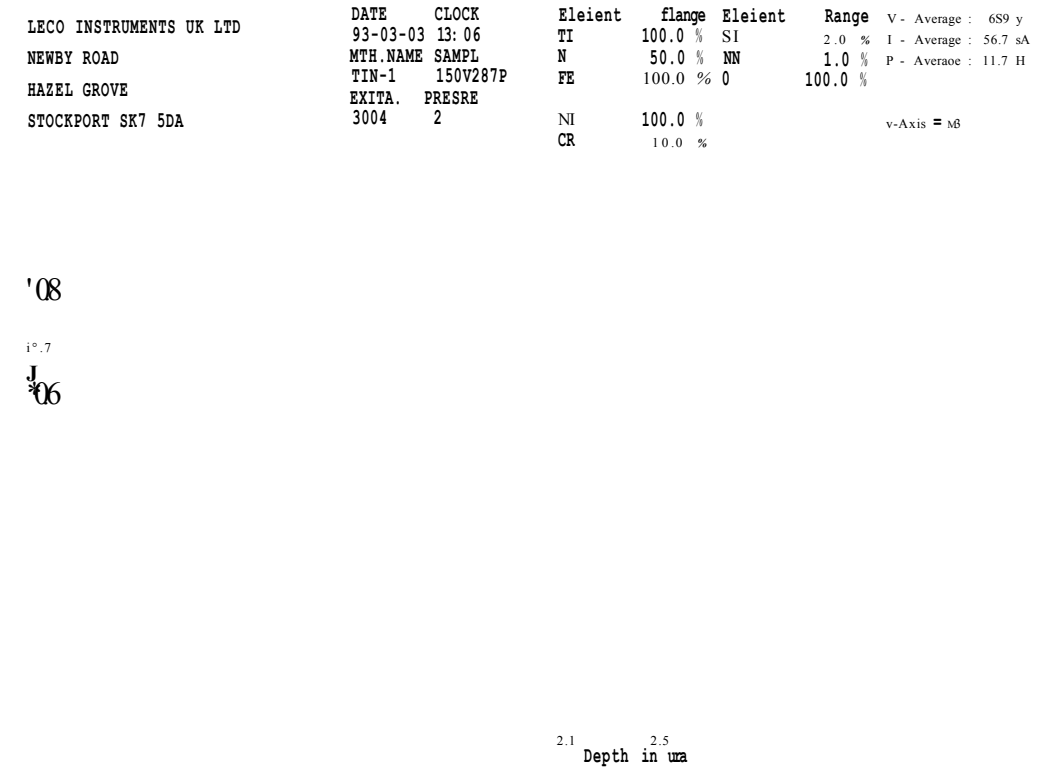

- 200 V bias 0.29 Pa pressure

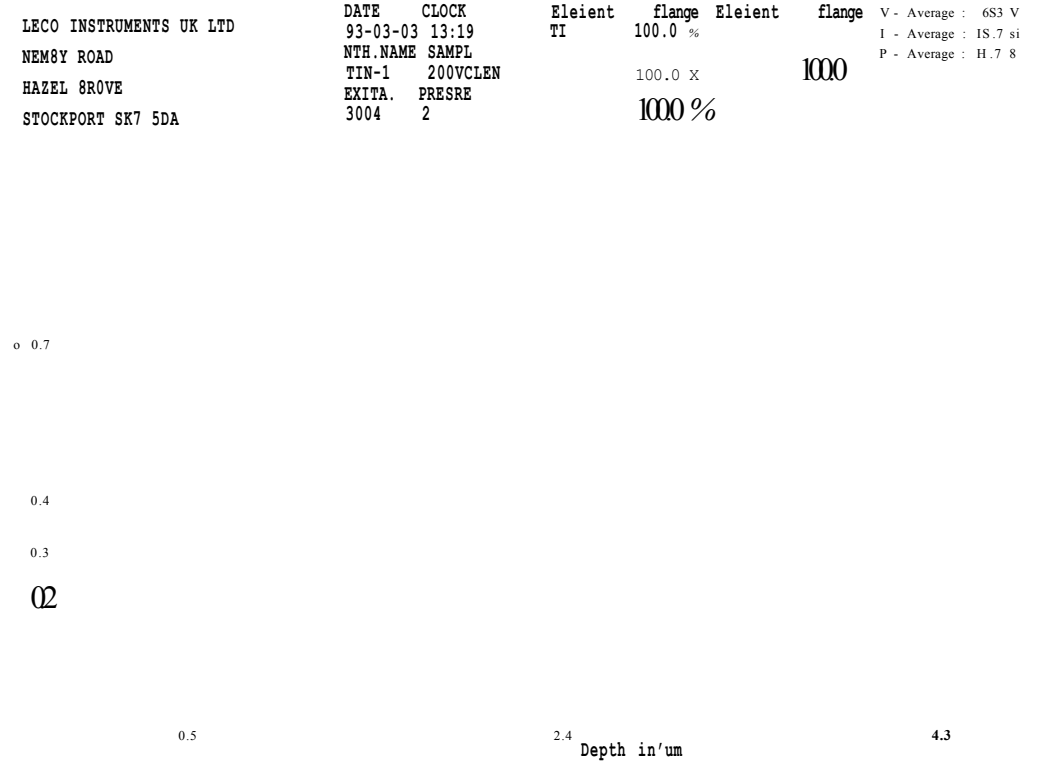

- 150 V bias 0.32 Pa pressure

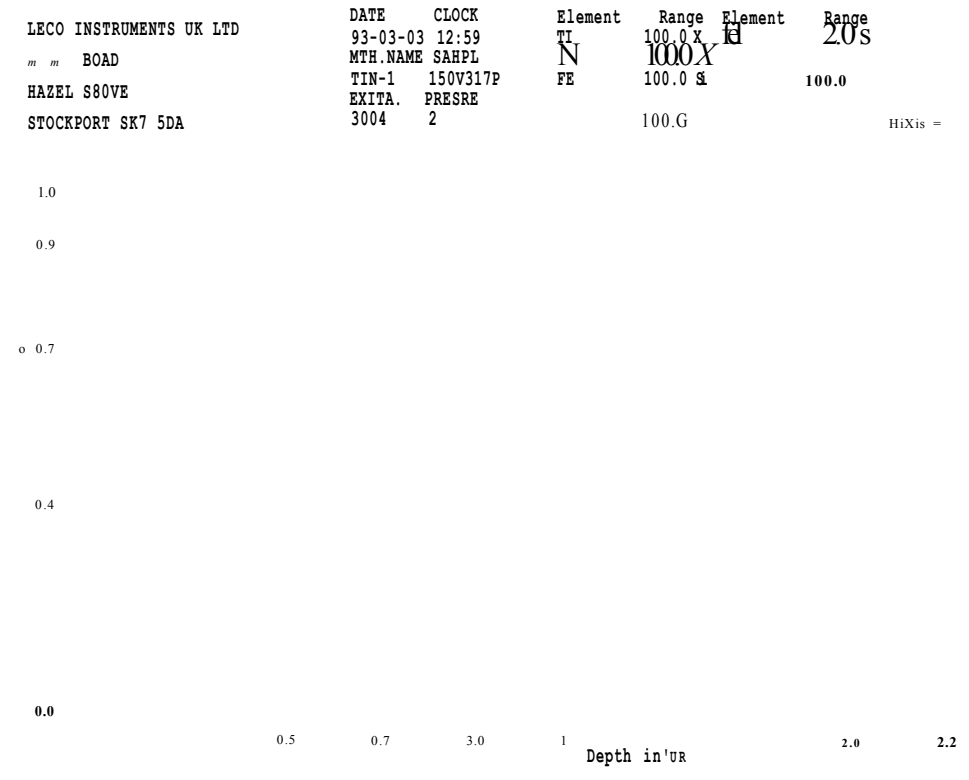

-150V bias 0.26 Pa pressure

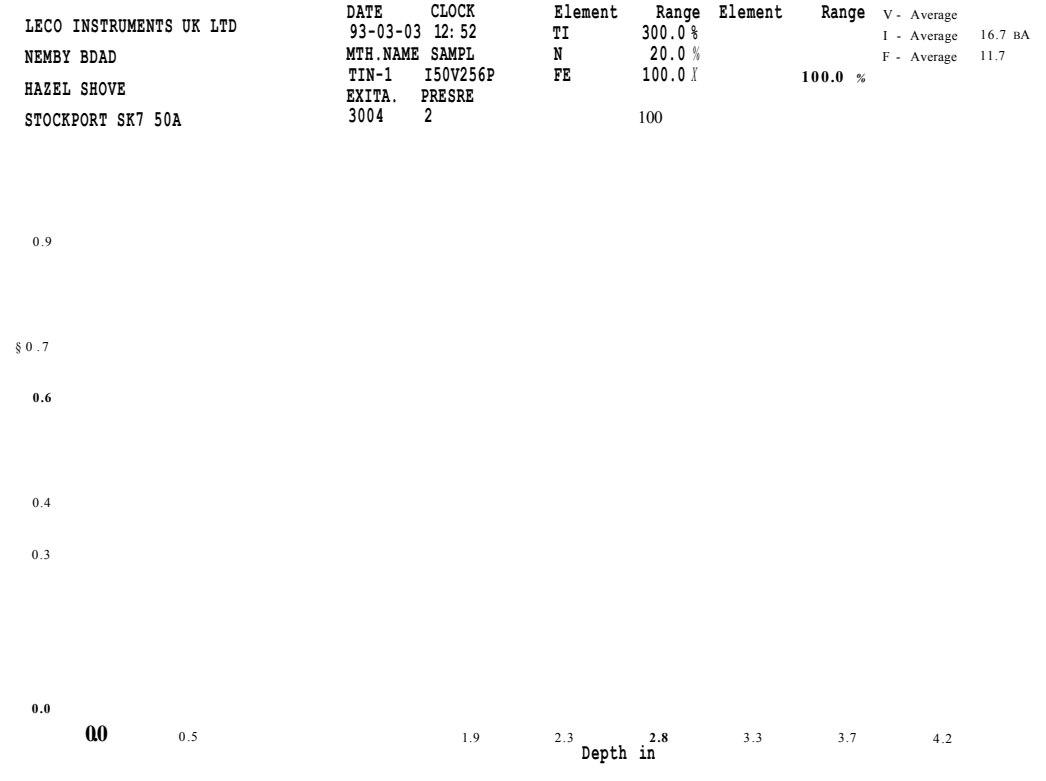

4.2.1 Composition

a. Steered-arc

Stoichiometry Ti : N ratio (+/- 5%)

Pressure (Pa)

1.6 |
1.1 | All coatings showed
0.6 | 1:1 stoichiometry
0.1 |

-50 -100 -150 -200

Bias (Volts)

b. ABS magnetron

Stoichiometry Ti : N ratio (+/- 5%)

Pressure (Pa)

0.32 | 4:5
0.29 | 2:3 1:1 1:1 1:1
0.26 | 5:3

-50 -100 -150 -200

Bias (Volts)

4.2.2 Coating Thickness

The coating thickness was assumed to be at the mid-point of the Ti and Fe profile lines falling to zero.

a. Steered-arc

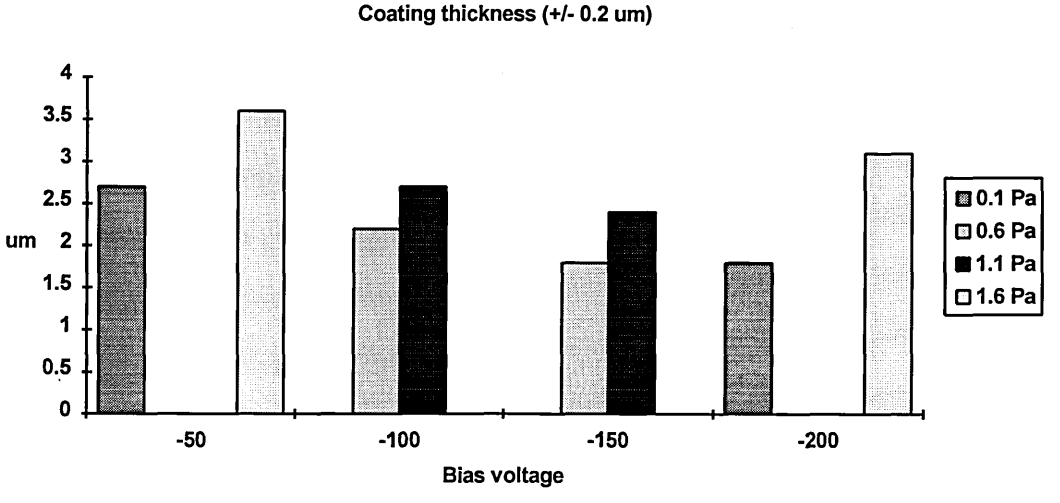

b. ABS magnetron

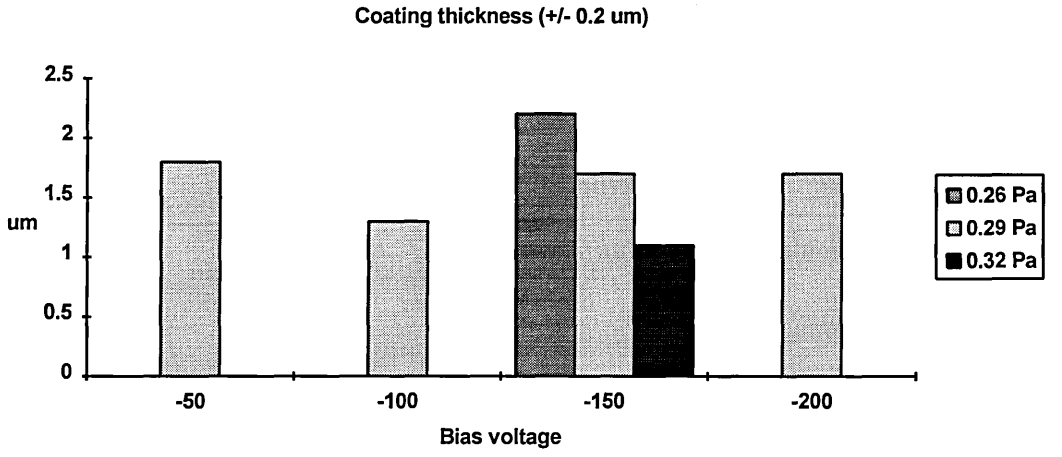

4.2.3 Sputter Crater Shapes

SEM image of a GDOES sputter crater

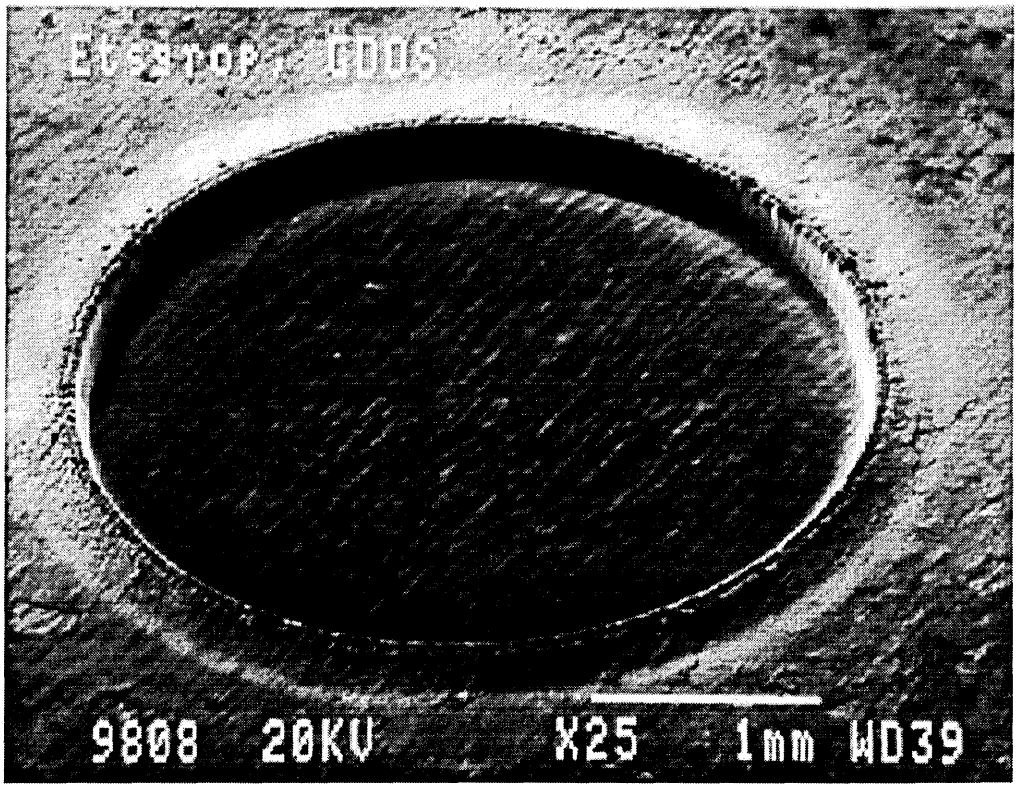

600 V 20 mA

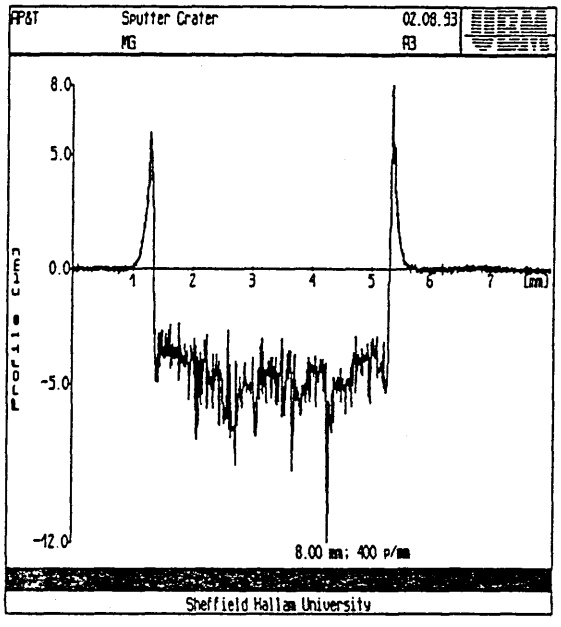

600 V 25 mA

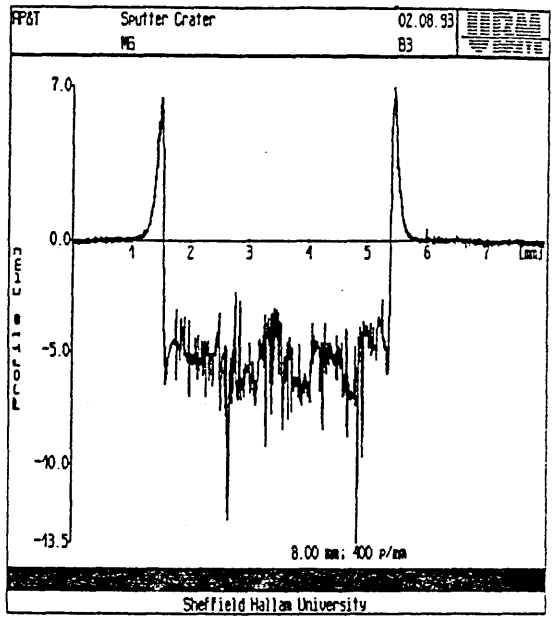

600 V 30 mA

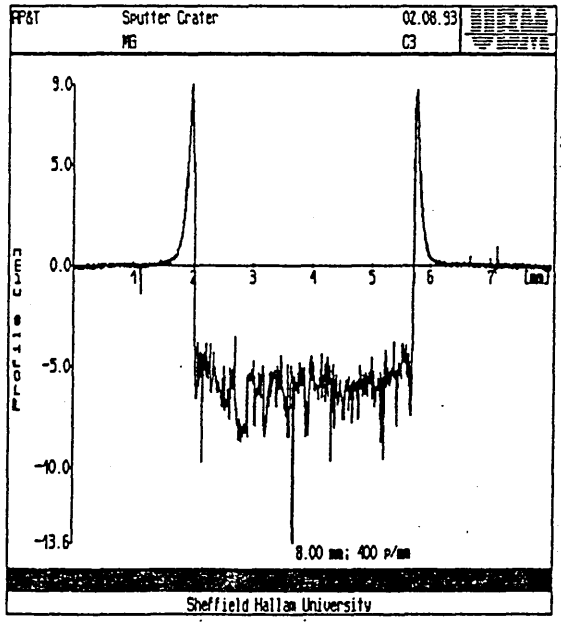

600 V 35 mA

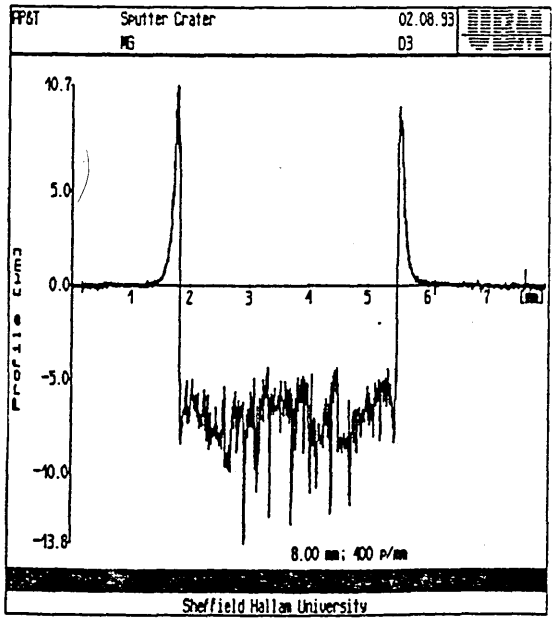

700 V 20 mA

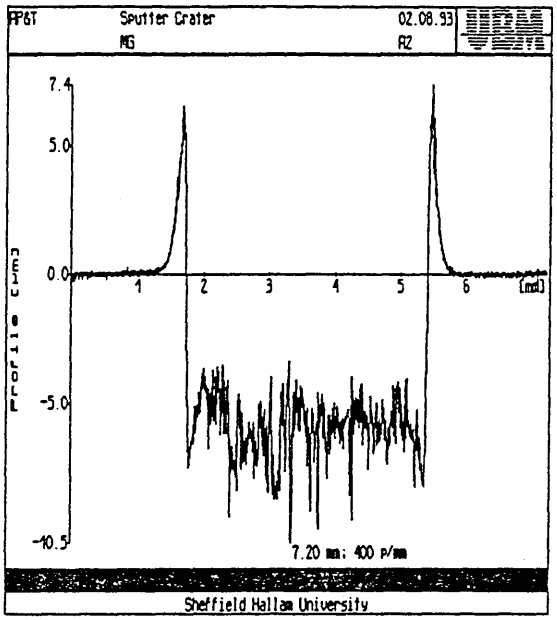

700 V 25 mA

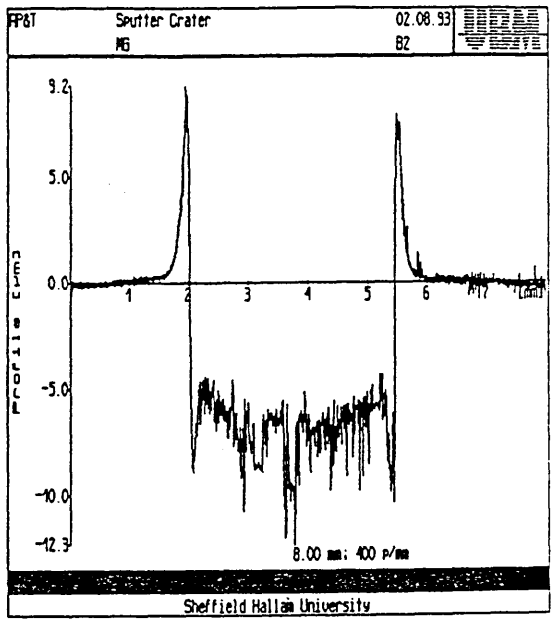

700 V 30 mA

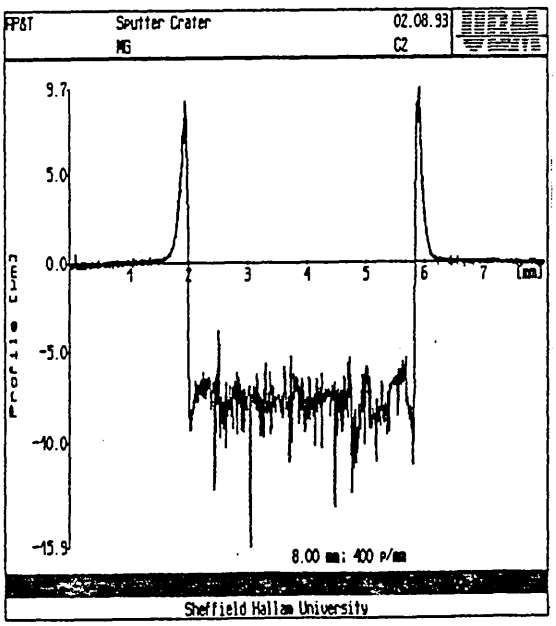

700 V 35 mA

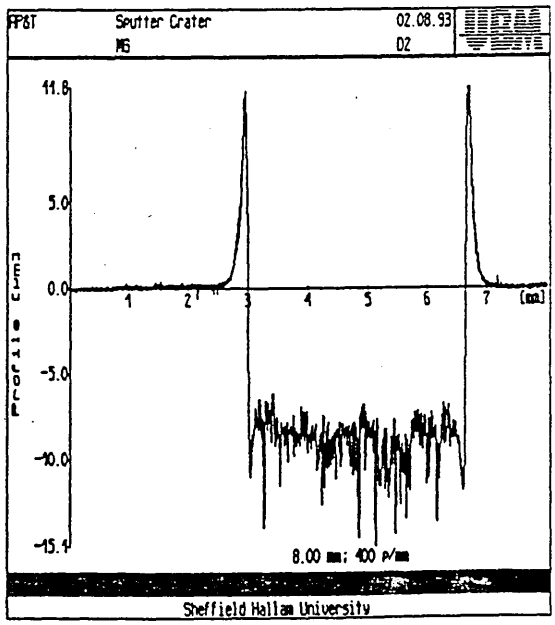

800 V 20 mA

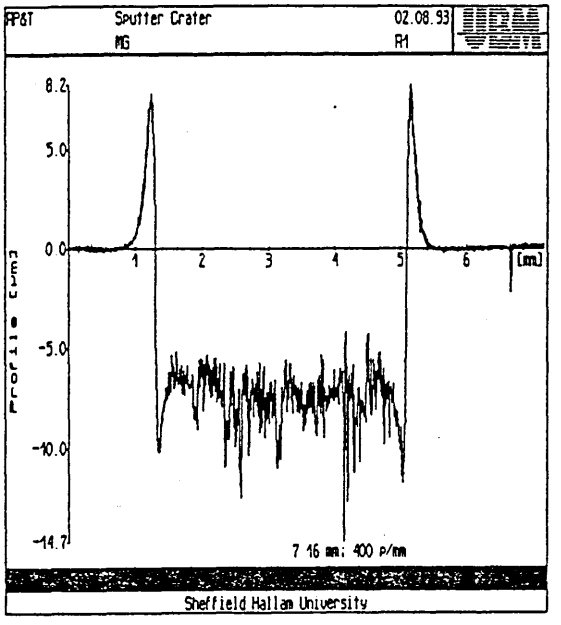

800 V 25 mA

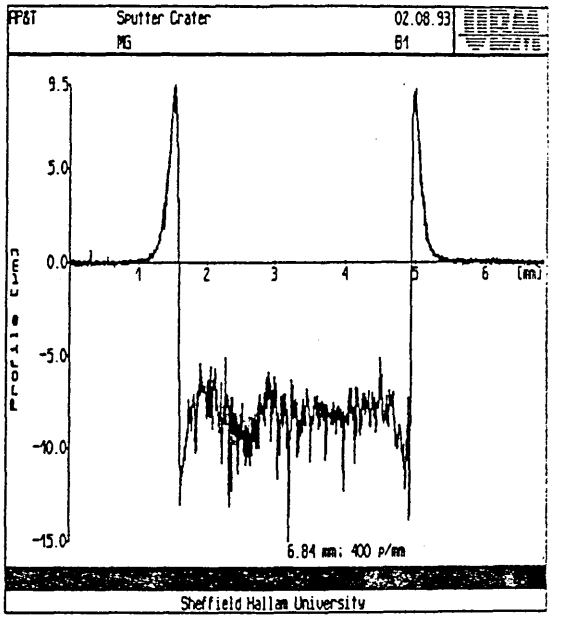

800 V 30 mA

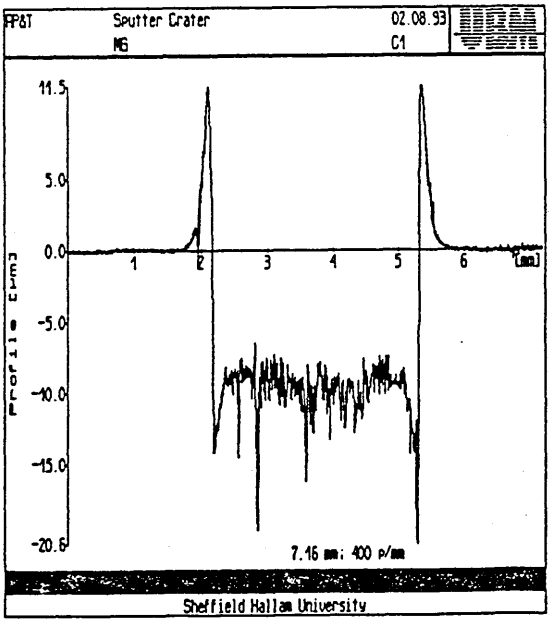

800 V 35 mA

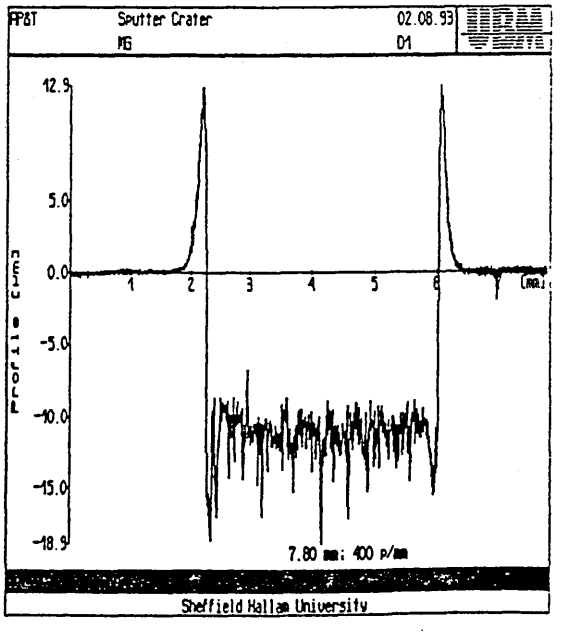

4.2.4 TiN Calibration

Steered-arc deposited TiN coating that was subject to step increased nitrogen flow

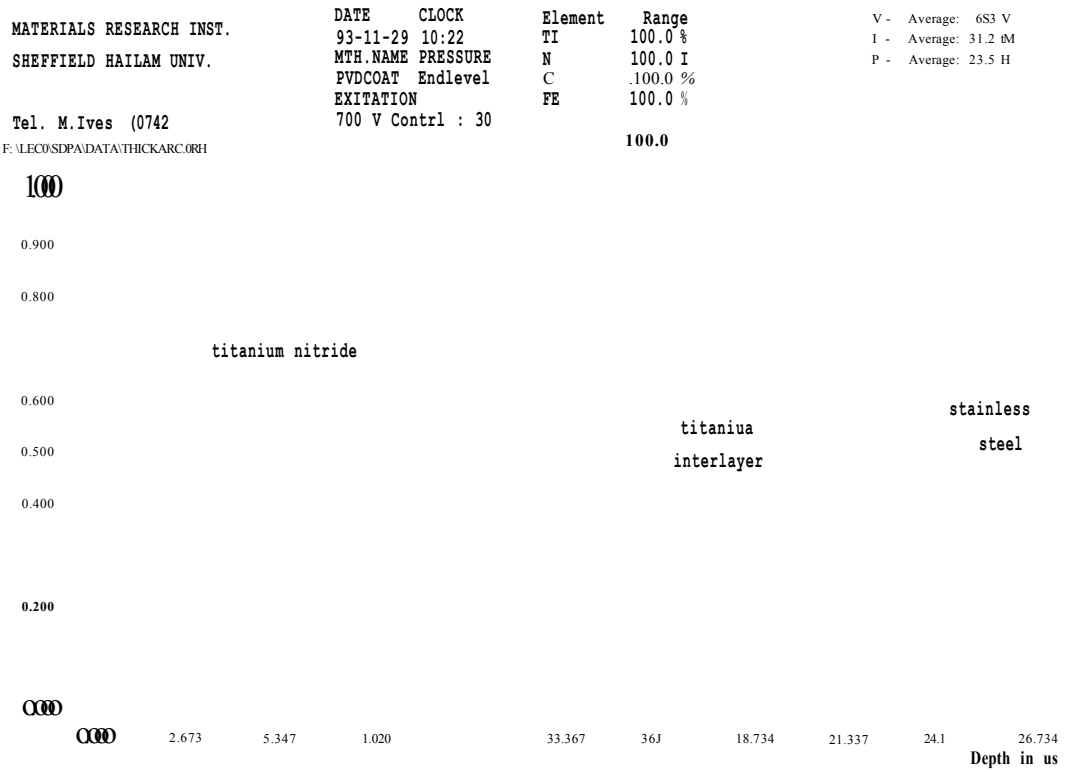

Straight line intensity versus Ti concentration calibration curve

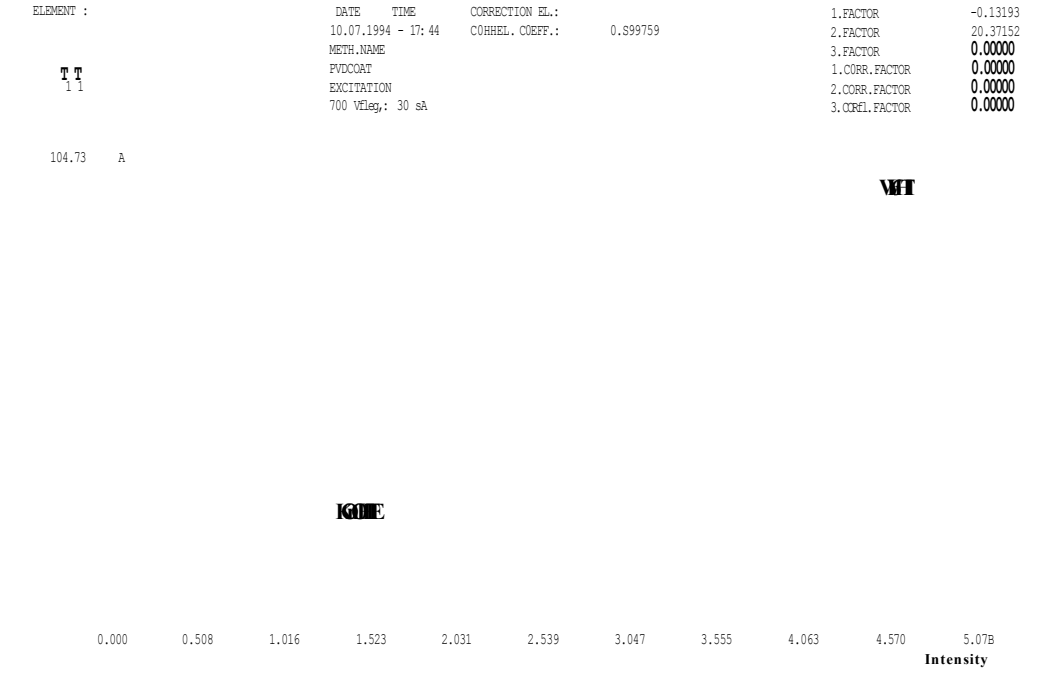

Straight line intensity versus N concentration calibration curve

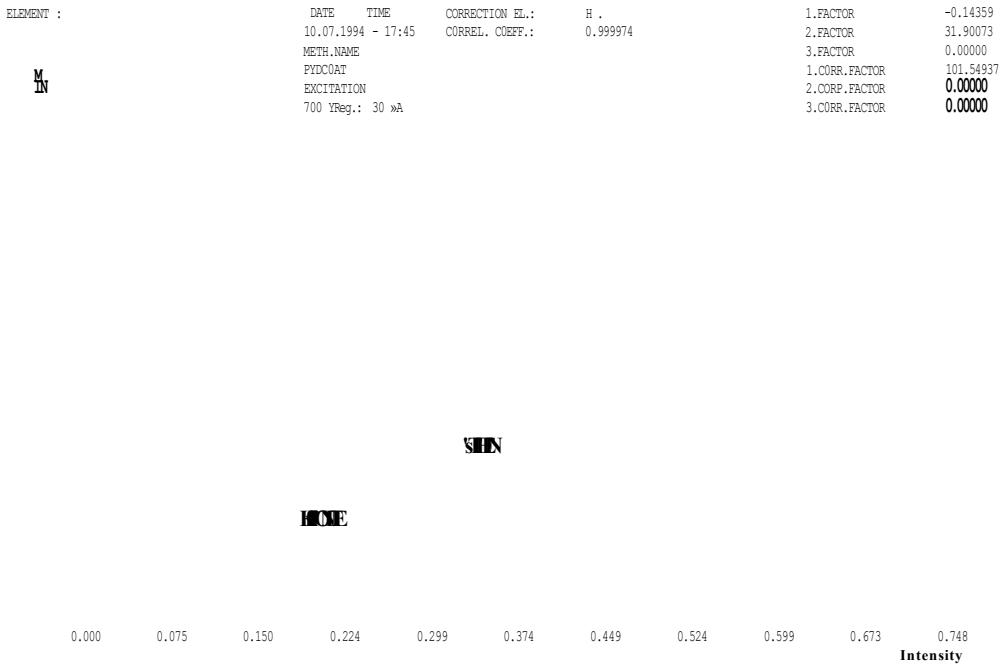

4.2.5 R.F. Depth Profile

Thermal barrier coating on turbine blade, to demonstrate the versatility of the GDOES technique for analysis of non-conducting coatings.

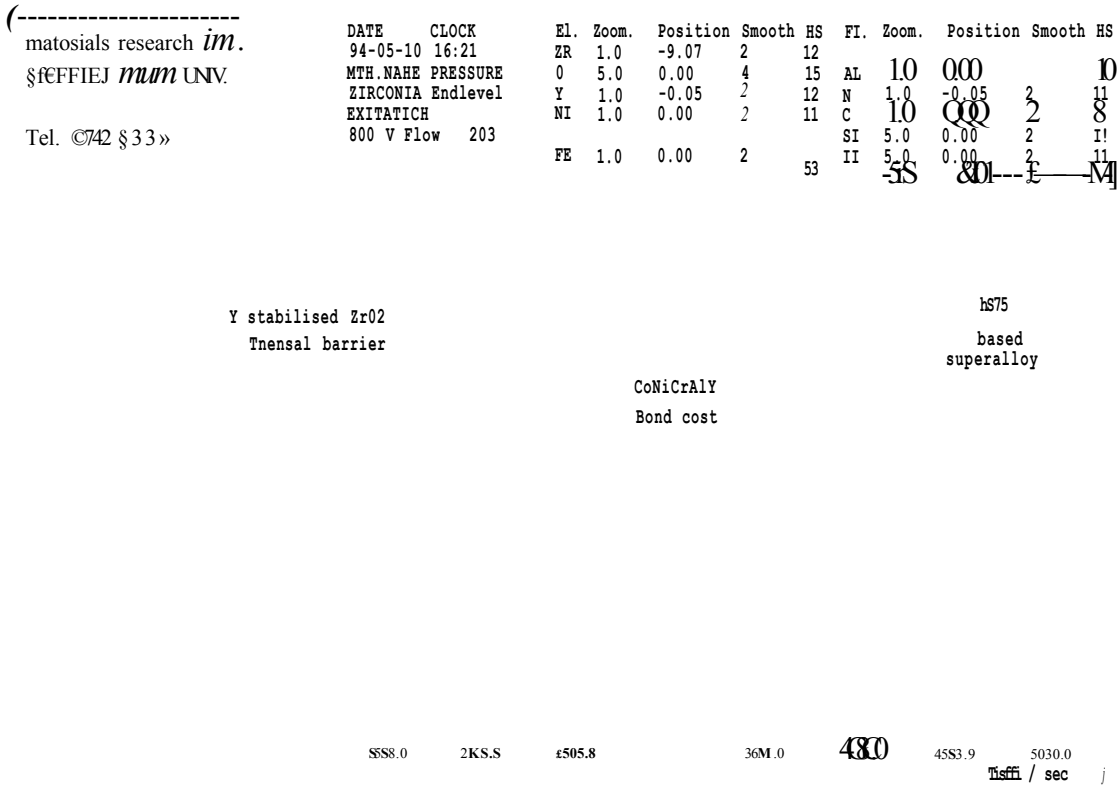

4.3 Interface Region

4.3.1 Glow Discharge Spectroscopy

Analysis to discover if nitrogen diffusion occurs after completion of the deposition process by examination of interface movement at normal deposition temperatures.

Ti-TiN-Ti-TiN multilayer coating before heat treatment (deposited at 350°C)

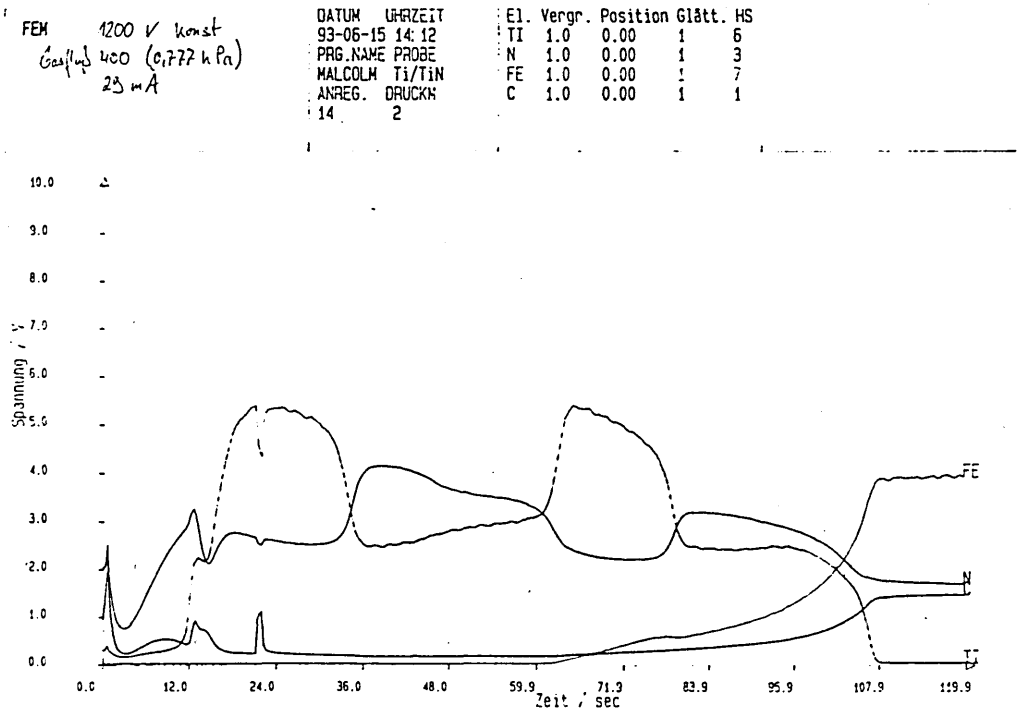

Ti-TiN-Ti-TiN multilayer coating after vacuum heat treatment for 1 hour at 450°C

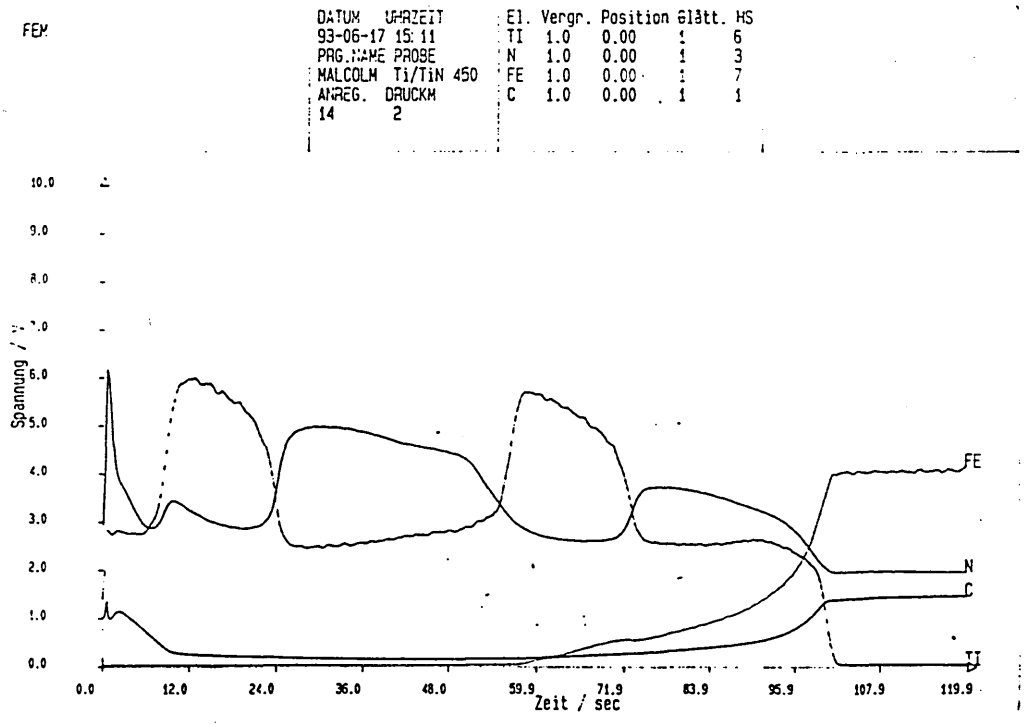

4.3.2 Scanning Transmission Electron Microscopy

STEM images of the arc etched coatings on HSS showing carbides from the underlying steel substrate protruding into the TiN film.

Separate STEM images

TIMGSTEN IRON

Overlaid STEM images

4.3.3 TRIM Program Calculations

Computer simulations of ion bombardment of surfaces using TRIM (TRansport of Ions in Matter) software based on Monte Carlo probability calculations.

Ti^{2+} ion implantation depth at -1000 V bias

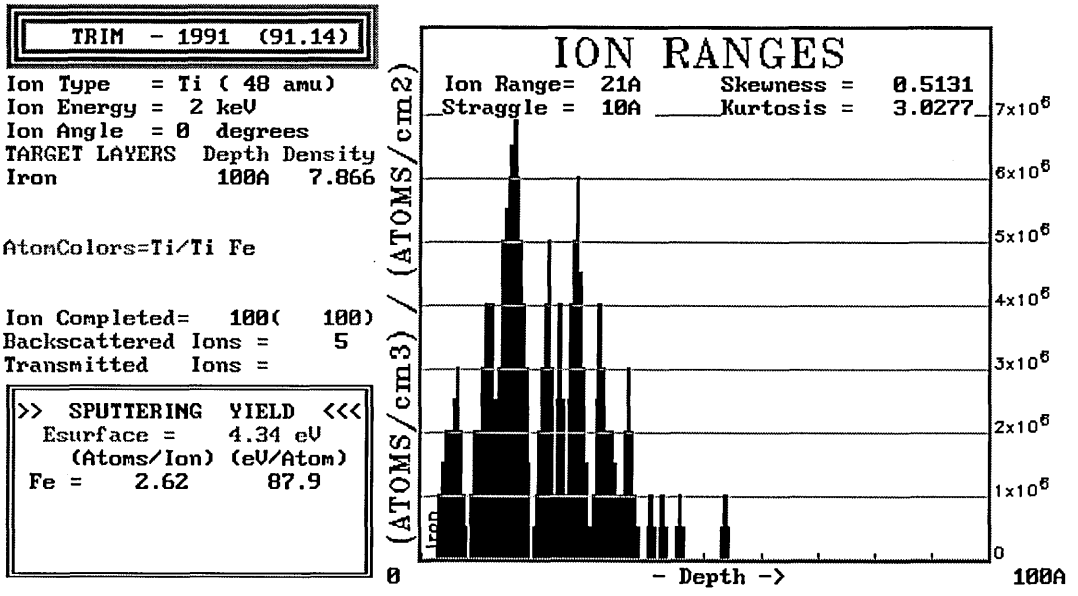

Fe sputter yield by Ar^{+} ions at -1000 V bias

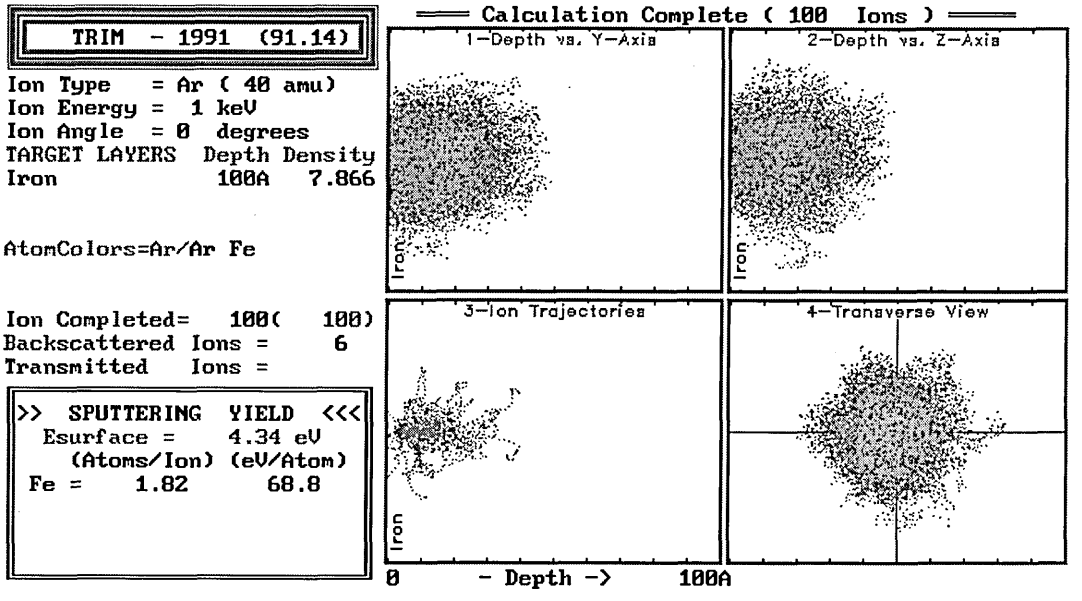

Fe sputter yield by Ti^{+} ions at -1000 V bias

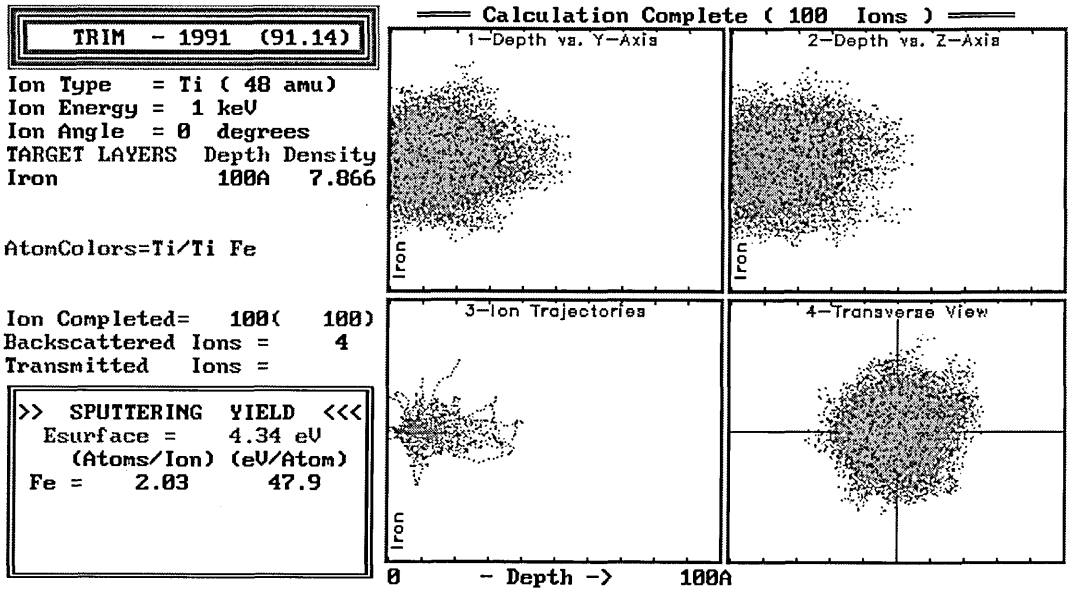

Fe sputter yield by Ti^{2+} ions at -1000 V bias

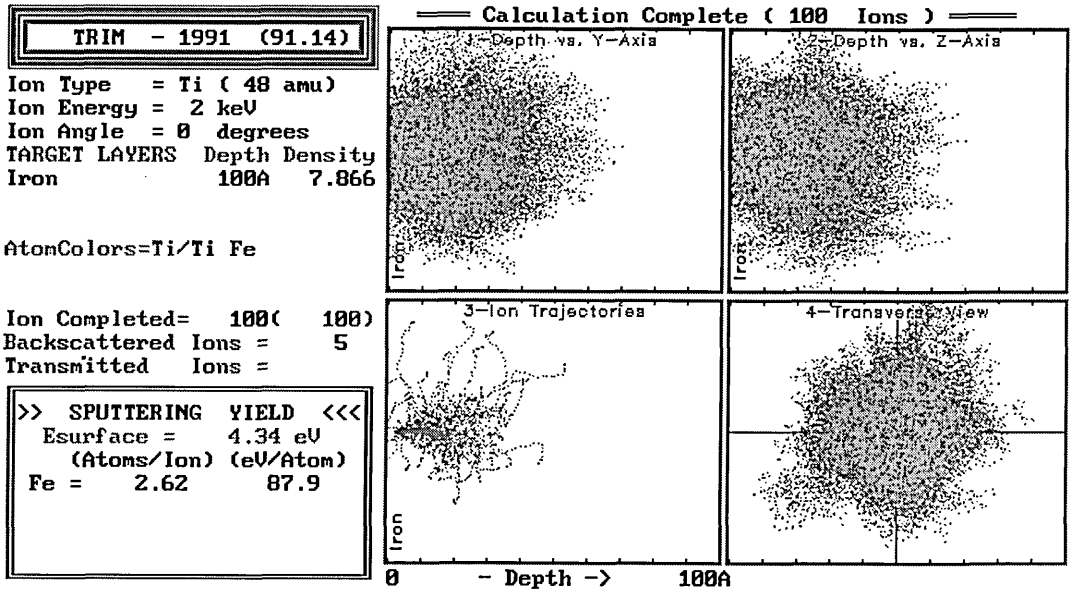

WC sputter yield by Ti^{+} ions at -1000 V bias

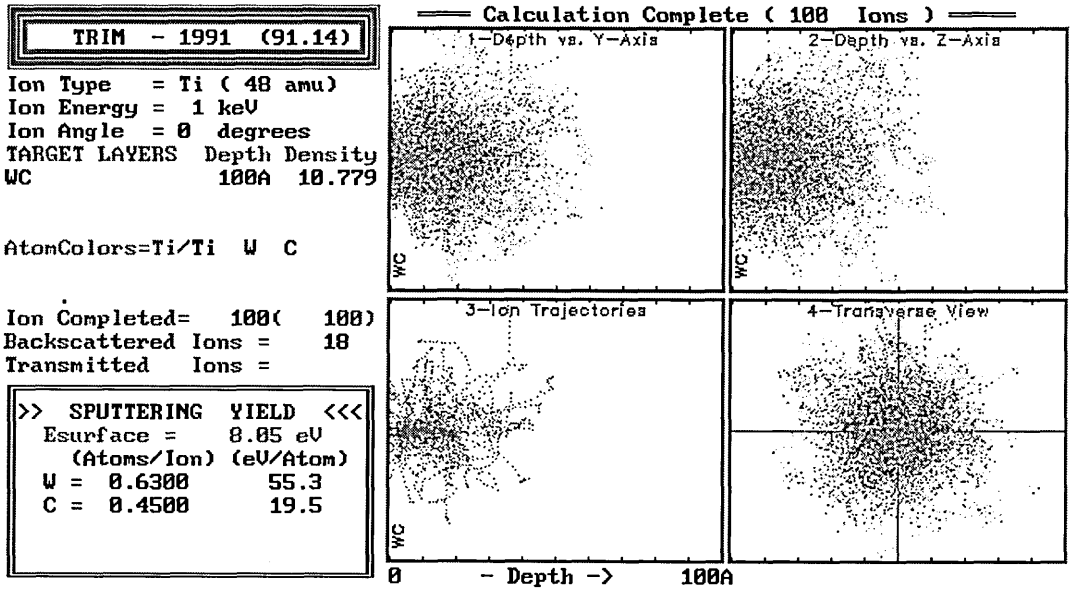

WC sputter yield by Ti^{2+} ions at -1000 V bias

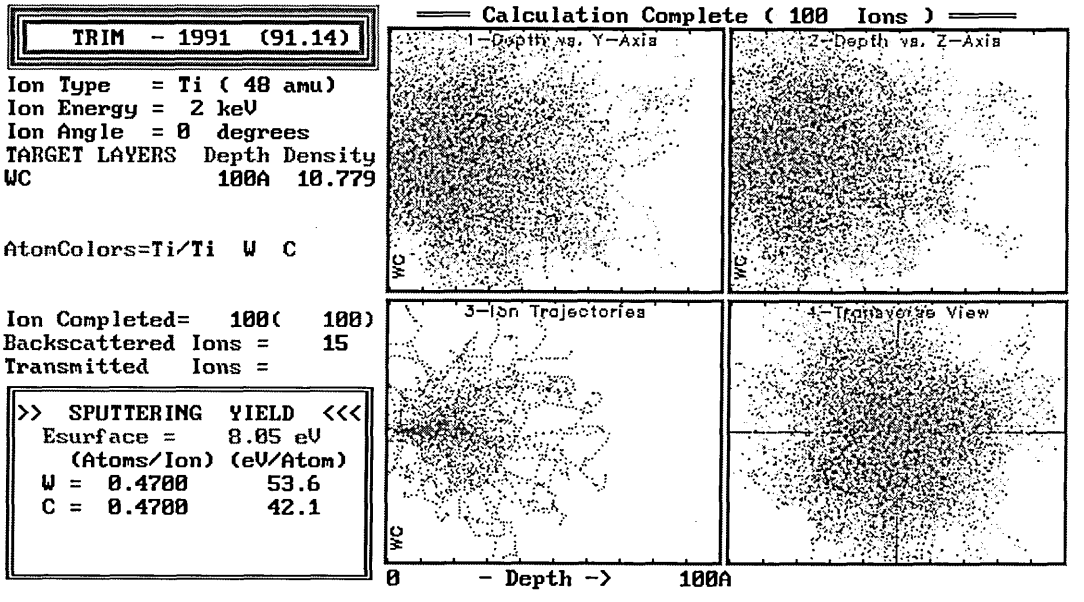

TiN sputter yield by Ar^+ ions at -100 V bias

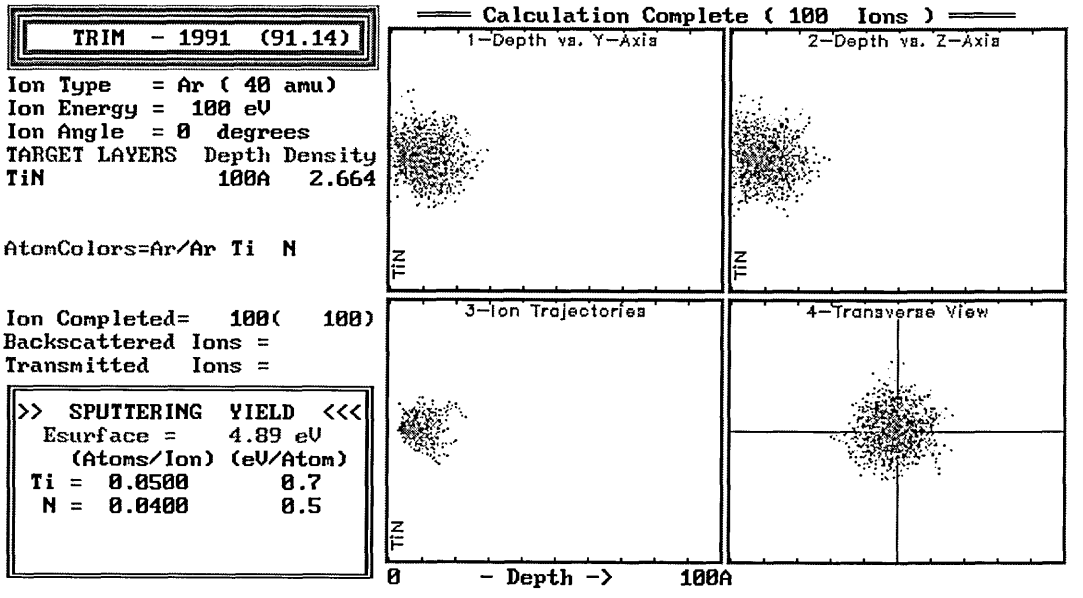

TiN sputter yield by Ar^+ ions at -200 V bias

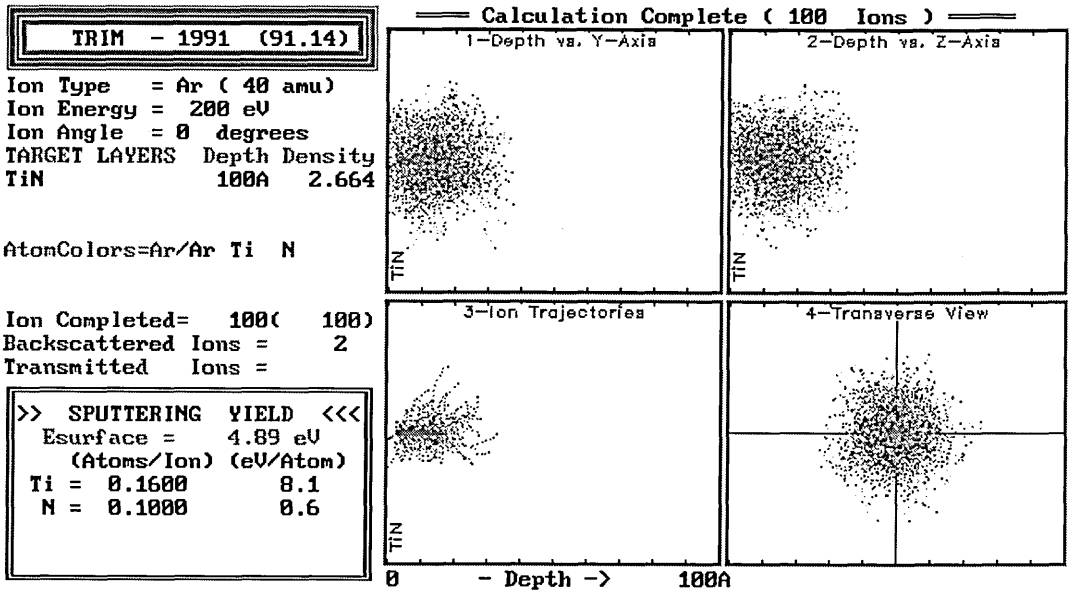

4.3.4 Sputter Depth Calculation

a. Steered Arc

Total substrate surface area = ~ 0.23 m^2

Substrate bias current at -1000 V with Ti ion bombardment = ~ 3 A

Therefore the ion current density = 13 A m^{-2}

Number of ions per second (amps x Coulombs) = 13 x 6.24 x 10^{18}

= 8.1 x 10^{19} ions m^{-2} s^{-1}

Typical sputtering time 5 minutes.

Number of incident ions during 5 mins. (5 x 60 secs.) = 2.4 x 10^{22} ions m^{-2}

b. ABS Magnetron

Total substrate surface area = ~ 1.2 m^2

Substrate bias current at -1000 V with Ti ion bombardment = ~ 10 A

Therefore the ion current density = 8.33 A m^{-2}

Number of ions per second (amps x Coulombs) = 8.33 x 6.24 x 10^{18}

= 5.2 x 10^{19} ions m^{-2} s^{-1}

Typical sputtering time 8 to 10 minutes.

Number of incident ions during 8 mins. (8 x 60 secs.) = 2.5 x 10^{22} ions m^{-2}

The number of incident Ti ions during the arc-etch phase of each deposition process is approximately the same : ~ 2.5 x 10^{22} ions m^{-2}.

The sputter yield of Fe by Ti ion bombardment at -1000 V is ~ 2 atoms per ion.

Therefore the number of sputtered Fe atoms is ~ 5 x 10^{22} atoms m^{-2}.

The density of Fe = 7870 kg m^{-3} = 7870000 g m^{-3}

The atomic weight of Fe = 55.85 g mol^{-1} , so the density of Fe = 140913 moles m^{-3}

Number of atoms per mole = Avogadro's constant (~ 6 x 10^{23} atoms mol^{-1})

Therefore the number of Fe atoms in a cubic metre = 8.5 x 10^{28} atoms m^{-3}

And the number of Fe atoms in a single atomic layer = 2 x 10^{19} atoms m^{-2}

The number of atomic layers sputtered during the arc-etch = 5 x 10^{22} / 2 x 10^{19}

= 2500 atomic layers Fe

The atomic diameter of Fe = 0.24 nm

Therefore the sputtered depth = 2500 x 0.24 = ~ 600 nm

4.3.5 X-Ray Photoelectron Spectroscopy

XPS analysis showed increased oxygen content in the lower bias coatings. Analysis of an unbiased coating (an extreme case) revealed large amounts of oxygen. The samples were subjected to sputter cleaning prior to analysis, so removing any oxide film from the surface and ensuring that the detected oxygen was in fact within the coating. Deconvolution of the collected data showed evidence of TiO_2 where the oxygen contamination appeared to be chemically bound to the titanium in the coating. The film colour of the unbiased coating was blue / black, also indicating the presence of titanium oxide.

Dense, fibrous coating - small oxygen 1s peak

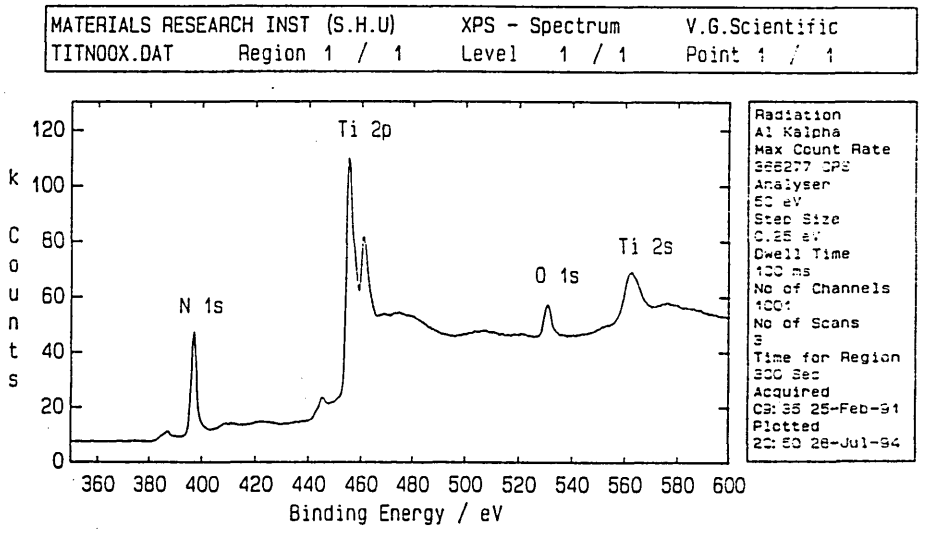

Porous columnar coating - large oxygen 1s peak

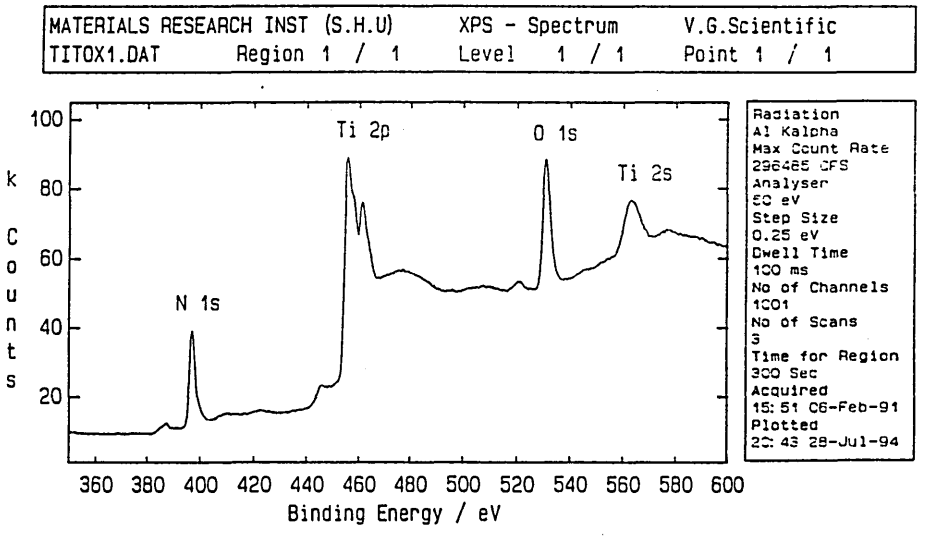

Dense, fibrous coating - Ti 2p peaks detail

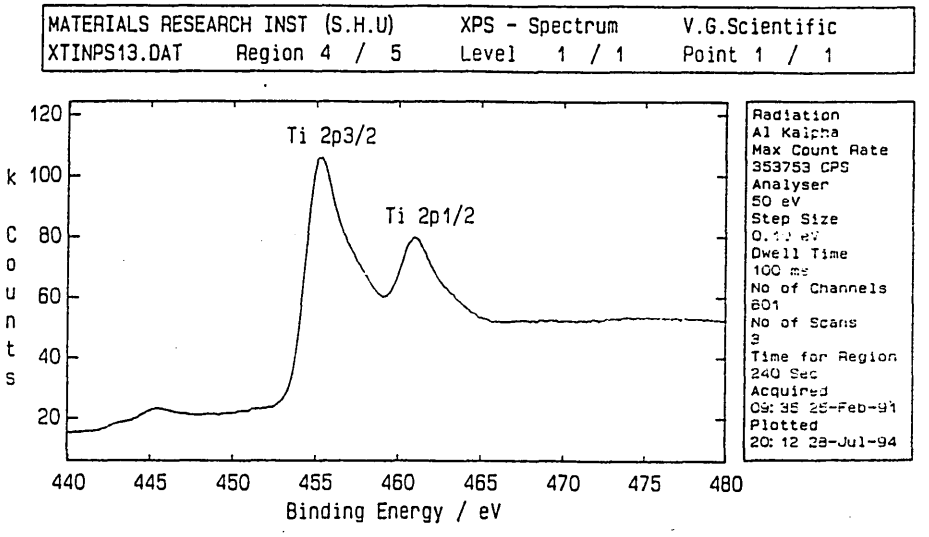

Porous columnar coating - Ti 2p peaks with overlapped O_2 peaks

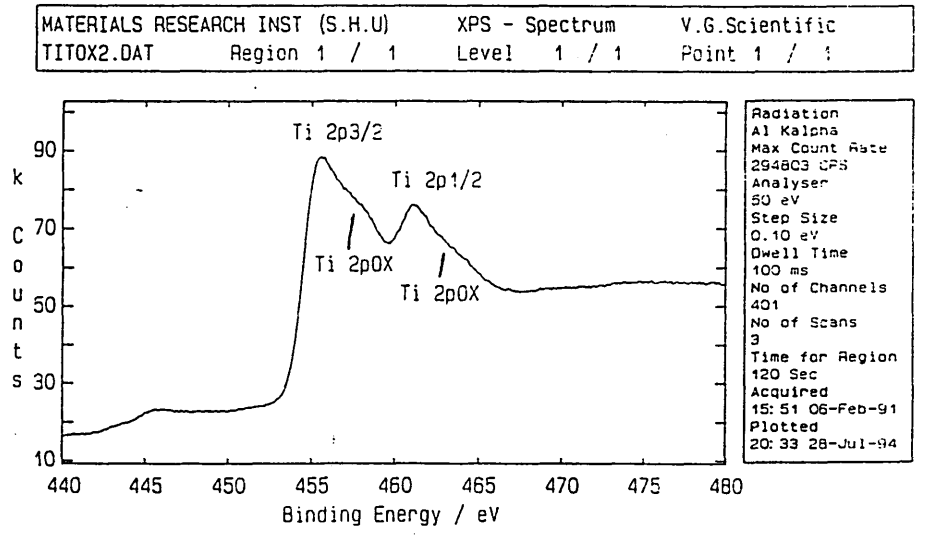

Overlapped peaks deconvolution

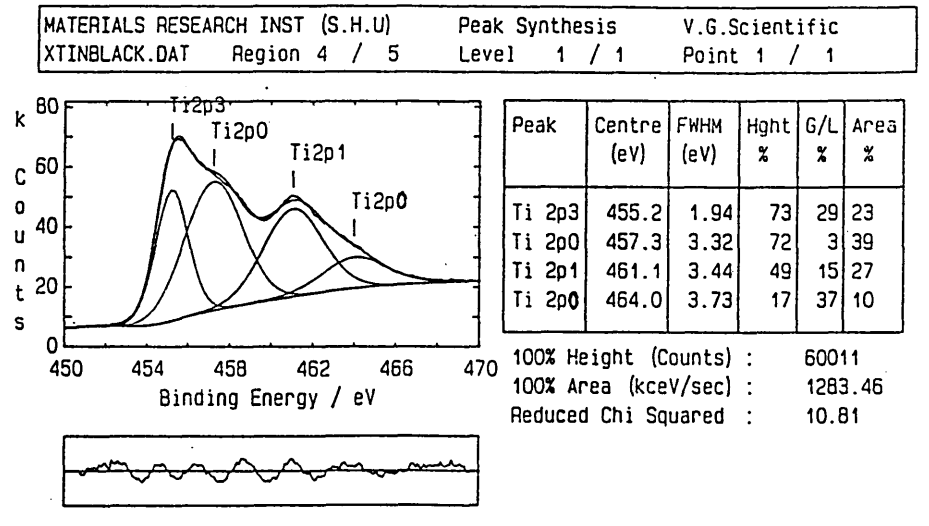

Peak	Centre (eV)	FWHM (eV)	Hght %	G/L %	Area %
Ti 2p3	455.2	1.94	73	29	23
Ti 2pO	457.3	3.32	72	3	39
Ti 2p1	461.1	3.44	49	15	27
Ti 2pO	464.0	3.73	17	37	10

100% Height (Counts) : 60011
100% Area (kceV/sec) : 1283.46
Reduced Chi Squared : 10.81

4.3.6 Adhesion vs Interlayer Thickness

Various interlayer thicknesses of titanium were deposited by the magnetron-only technique prior to 60 minutes of TiN deposition, to find the optimal layer thickness for maximum adhesion, and as a comparison with the ion-etch phase in the ABS magnetron technique. The scratch adhesion test was used to evaluate the coatings, optical microscopy was used to identify the initial type of failure - adhesive or cohesive, and acoustic emission was used for identification of the critical load at spallation and ultimate coating failure.

Interlayer deposition time (mins)	1	4	7	20
Interlayer thickness (mm)	0.02	0.1	0.2	0.6
Load at 1st adhesive failure (N)	10	33	36	29
Load at 1st cohesive failure (N)	20	21	18	13
Critical load for coating failure (N)	22	50	50	29

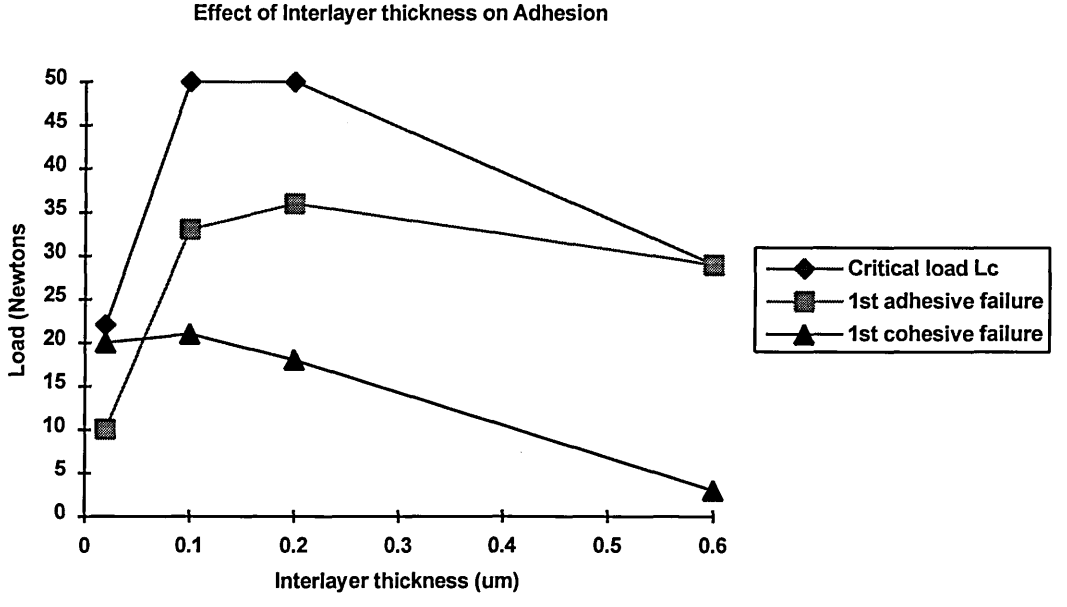

CHAPTER 5
Discussion

5.1 Parameter Study

5.1.1 Process Operation

Both the steered-arc and ABS magnetron processes were semi-automatic due to the extensive use of a PLC (programmable logic controller) in each system, to supervise all vacuum pumping and valve switching operations. PLC usage was greater in the ABS magnetron system, as it also controlled gas inlet valves and current and voltage switching to some extent. This would appear to make the ABS magnetron system easier to operate, but since this process was more complicated and entailed more steps, this apparent advantage was lost.

The two large doors of the ABS magnetron chamber caused a high susceptibility to water vapour contamination during substrate loading, and combined with the lower pumping speed, resulted in long pump-down times of several hours. Also, the PLC programming started running cooling water through the chamber walls as soon as pump-down began, instead of leaving hot water in them at first to aid outgassing and prevent water vapour adsorption. However, this problem could be alleviated by manually switching off the water pump during this period and ignoring the PLC error message. The large doors did have the advantage of providing unprecedented access to the chamber interior for cleaning and cathode maintenance.

The steered-arc process was very straight-forward, with a single heating / sputter-cleaning phase, followed by the coating phase. The ABS magnetron process entailed two heating / sputter-cleaning phases, a cathode cleaning phase and then the coating phase, making a longer overall processing time. Deposition rate was also lower with the ABS magnetron system, which also resulted in longer process times.

5.1.1.1 Deposition Conditions and Plasma Uniformity

Substrate temperature :

a. Steered-arc

Temperature increased with bias voltage due to greater ion bombardment of the substrate. Temperature also increased with gas pressure, due to increased arc stability resulting in a greater evaporation rate, and hence increased ion

bombardment of the substrate. This agrees with a corresponding increase in deposition rate (section 4.1.4).

b. ABS Magnetron

Once again temperature increased with bias voltage due to increased ion bombardment. Process monitoring of the temperature showed a rapid drop at the start of coating for the -50 V and -100 V bias coatings, as the ion bombardment could not sustain the high temperatures reached during the arc etch phase. This was seen to induce large thermal stresses that sometimes led to spallation (section 5.1.2.6.2).

No significant change was observed when varying the nitrogen pressure, which was expected, since substrate bombardment was predominantly by argon ions.

Coating (plasma) uniformity :

a. Steered-arc

The "fall-off" in coating thickness was linear with distance from the cathode showing a drop of 11% from 100 to 200 mm and 19% from 100 to 300 mm. As the cathodes were of small diameter (125 mm), there was a peak in thickness directly in front of the cathode (middle), while the top and bottom positions, corresponding to above and below the cathode plane respectively, were marginally less thick (5% less at 100 mm and 12% less at 300 mm).

Generally, the plasma produced in the steered-arc chamber, despite the small size of the cathodes, was stable and intense. This was born out by the high deposition rates attained throughout the chamber. However, the small cathodes tended to erode very quickly and resulted in reduced titanium flux with time and hence changes in the deposition rate and coating colour. This necessitated frequent cathode replacement. Typical cathode lifetime was 60 kWh which corresponded to approximately eight coating runs.

b. ABS magnetron

The large planar cathodes used with this process gave a more linear thickness distribution with height in the chamber, as the samples were always in front of the cathode. The decrease in thickness at the central position from 150 mm to 250 mm distance was 24% and to 350 mm distance was 48% showing a linear reduction with distance. The thickness in the bottom position was 8% less than the top and middle at 150 mm, increasing to 40% less at 350 mm distance. This decrease in the thickness near the bottom of the cathode was probably caused by the biased

turntable, which was only partially shielded from the plasma by an electrically isolated or "floating" skirt, and hence acted as a drain on the ion flux.

The large planar cathodes with uniform sputter erosion tracks resulted in a long lifetime of typically 1200 kWh, which corresponded to approximately 100 coating runs. The difference in cathode area compared to the steered-arc process makes the two erosion rates very similar, but the ABS magnetron system had the advantage of less frequent cathode replacement.

Generally, the plasma in the ABS magnetron chamber was weaker than in the steered-arc chamber, and showed a tendency to fluctuate as the substrate turntable rotated. There was also a split in the plasma, vertically down the centre of each cathode, such that one side constituted a higher substrate ion current than the other. This was thought to be due to the large metal bulk of the turntable being in close proximity to the linked magnetic fields.

The splitting can be explained as a fundamental problem arising when the cathode voltage and substrate bias voltage are unequal. There is a net current (electron) flow between them that is deflected up or down depending on the local magnetic linking field and the direction of the net current flow. The plasma ions generally follow the electron movement. The ions deflected upwards are lost to the chamber ceiling resulting in an apparently weakly ionized plasma region, while the ions deflected downwards are invariably caught by the large turntable bulk and appear as an intense area of plasma. Only when the cathode voltage and substrate bias voltage are equal is there no net current flow and hence a uniform plasma. If the relative magnitudes of the cathode voltage and substrate bias voltage are reversed, then so is the direction of net current flow and hence the positions of weak and intense plasma around the chamber. This effect can be observed from substrate ion current measurements (section 4.1.1) during the glow discharge cleaning phase (bias -1000V, cathode -200V) and the magnetron coating phase (bias -150V, cathode -550V). The use of a "top hat" on the turntable helped to confine the upwardly deflected ions to some extent but could not eliminate the problem as it is fundamental to the design and operation of the ABS chamber. However, it should not cause coating problems as long as the substrate turntable is rotated, though temperature fluctuations may induce thermal stresses.

5.1.2 Testing and Analysis

5.1.2.1 Colour

a. Steered-arc

The lightness parameter (L^* of the CIE standard) or reflectance of the coatings tended to peak in the mid to lower half of both the bias and pressure ranges, showing a general decrease with increasing bias and with increasing nitrogen pressure (except at -200V bias). This suggested a rougher surface finish, but the surface profile measurements did not substantiate this (section 4.1.3). The redness parameter ($+a^*$) of the coating increased with increasing bias and with increasing nitrogen pressure, possibly due to more nitrogen content in the film.

No particular parameter could be identified with the yellowness ($+b^*$) of the coating, but generally, like lightness, it peaked half way through the ranges of both nitrogen pressure and bias voltage, with increased yellowness at high bias and low pressure, and at low bias and high pressure combinations. This corresponds to a peak in yellowness and reflectance when :

$$\text{pressure} \,.\, \text{voltage} = \text{constant} \qquad \ldots\ldots\ldots (17)$$

and might be an indication of when the ideal combined deposition conditions are obtained.

b. ABS magnetron

At low bias the coating was dark brown and had a matte finish with all colourspace parameters low in value. This was due to an open columnar structure at the surface resulting in a high surface roughness. Increasing bias resulted in a paler yellow-gold colour and more reflective finish due to increased titanium flux, but dropped off at high bias. Thus the lightness parameter (L^*) peaked midway through the bias voltage range.

The lightness steadily decreased with increasing pressure due to cathode poisoning and gas scattering effects reducing the titanium flux at the substrate, resulting in a darker than normal golden colour. At low pressure the coating was silver in colour due to lack of nitrogen and a sub-stoichiometric composition. The redness parameter ($+a^*$) increased with both nitrogen pressure and bias voltage, again possibly corresponding to a higher nitrogen content.

Also, the yellowness ($+b^*$) of the coatings once again appeared to peak half way through both the pressure and voltage ranges studied along with the lightness, with

the maximum value appearing at the known optimum operating conditions for magnetron deposition. This reinforces the role of colour measurement as an indicator of ideal deposition conditions for TiN.

5.1.2.2 Surface Roughness and Droplets

Surface roughness measurements :

a. Steered-arc

There was no significant change in roughness with varying bias, a typical R_Z value was 2.5 μm for a coated sample, compared with 0.04 μm for an uncoated polished substrate.

As the nitrogen pressure was increased there was a reduction in the surface roughness (R_Z decreased to typically 1.9 μm). This was attributed to reduced macroparticle formation due to cathode poisoning. Cathode poisoning increases the melting point and arc velocity, and so smaller molten pools are formed which are the source of droplets.

b. ABS magnetron

Surface roughness versus bias was almost constant with an R_Z value of 1.2 μm compared with 0.05 μm for an uncoated polished substrate. At very low bias (-50 V), however, the R_Z value rose to 2.2 μm. At this bias, the coating structure was very porous and open with widely spaced columns. Thus the surface finish was rougher. Overall, the ABS magnetron process produced smoother coatings than the arc method, due to the reduction in macroparticles.

Reduced surface roughness with increasing pressure was observed as with arc coating where it is normally attributed to reduced macroparticle formation due to cathode poisoning. The same phenomenon has occurred with the ABS sputtering technique, and has been attributed to micro-arcs on the cathode surface due to an unstable power supply and possibly also to sputtering of atomic clusters. Cathode poisoning raises the energy input requirements for sputtering to occur, resulting in a lower sputter yield and smaller-sized clusters of atoms being liberated for a given ion bombardment (in effect, TiN was being sputtered instead of pure Ti). The droplets have not occurred during the arc-etch phase as confirmed by the surface profile scans.

Surface profile scans :

a. Steered-arc

The object count corresponded to 80% droplets and 20% craters. This count correlates well with the surface roughness results, showing a decrease in droplet number with increasing reactive gas pressure, due to cathode poisoning. There also appeared to be a slight increase in the number of droplets with increasing bias, due to electrostatic attraction.

b. ABS magnetron

The object count again corresponded to 80% droplets and 20% craters, except in the case of the low (-50V) bias coating in which the droplet to crater ratio was 50:50, and caused by the widely spaced columns of this structure. Of the other coatings, it is confirmed that the droplets originated during sputtering, rather than as macroparticles in the arc-etch phase, as demonstrated by a map of an etch-only surface which gave a droplet count of just 5.

5.1.2.3 Thickness / Deposition Rate

a. Steered-arc

Variations in the amount of substrate bulk within the chamber gave the following proportional relationship for coating thickness C_t , coating time T_c , substrate surface area A_s and bias current I_b (or flux of impinging titanium ions) :

$$C_t \propto T_c \cdot I_b / A_s \qquad \text{..... (18)}$$

Thus, in order to deposit the same thickness of coating on a substrate with 10 times more surface area, required 10 times longer coating or 10 times more bias current.

Deposition times were therefore adjusted according to the bias current reading on the instrument control panel in order to deposit similar thicknesses of coating. Thus, whilst most of the coatings were in the 1.5 - 2.5 μm range, the coating times were different, because of different deposition rates.

The deposition rates were highest at high pressure due to a more stable and intense arc discharge caused by the supportive background gas pressure. This resulted in greater titanium ion bombardment of the substrate and is in agreement with the observed higher substrate temperatures (section 4.1.1).

In general, there was no significant variation in deposition rate with bias, suggesting that all the available titanium flux was arriving at the substrate, even at

lowest bias. Thus the main effect of increasing the bias was to heat the substrate by increasing the kinetic energy of the arriving titanium ions, which may densify the growing film, but conversely may soften the substrate (section 4.1.5).

b. ABS magnetron

All the deposition times were kept constant (70 mins) so the coating thickness was a direct reflection of the deposition rate. Most of the coatings were approximately 1.5 μm thick. The deposition rate, and hence thickness, dropped off with increasing pressure, due to cathode poisoning.

The low pressure (0.26 Pa) sub-stoichiometric coating was considerably thicker as the cathode was not poisoned at all, and so was free to sputter at a much higher rate from all over its surface and not just from a well defined race-track. This indicates that even when operating at the optimum conditions on the hysteresis curve to give a stoichiometric film, the magnetron sputtering efficiency is severely reduced from its maximum which occurs when sputtering a pure metal only, with no reactive gas present.

Once again, there was no significant change in deposition rate with bias, as sputter deposition mainly involves neutrals and changes in bias only affect the amount of argon ion bombardment.

5.1.2.4 Microhardness and Ultra-microhardness

Conventional Knoop microhardness test :

a. Steered-arc

Microhardness decreased with increasing bias due to excess ion energy, resulting in surface over-heating and softening of the substrate. Microhardness was also lower at greater nitrogen pressure. This was due to more energy-loss collisions for the arriving titanium flux, resulting in a less dense structure and hence reduced coating hardness.

b. ABS magnetron

Microhardness increased with bias up to -150 V. This was due to a greater ion flux with higher bombardment energy, resulting in surface heating and increased adatom mobility, so densifying the growing film. At -200 V the increased ion bombardment at the surface resulted in a change in the preferred orientation to a less densely packed system, and hence a softer coating.

Microhardness peaked at a pressure of 0.29 Pa (the optimum deposition condition). At lower pressure the coating was predominantly titanium (signified by the metallic silver colour). The coating was substoichiometric, but appeared dense, and had bulk properties more like those of pure titanium, and hence was softer. At higher pressure, the cathodes started to become poisoned and their efficiency decreased, resulting in reduced titanium flux at the growing surface, and increased energy loss collisions for the bombarding argon ions. Deposition rate was lower, and adatom mobility was reduced, resulting in a less dense coating which was softer.

Ultra-microhardness indentation test :

a. Steered-arc

The ultra-microhardness results were consistently lower than those of the conventional Knoop hardness test, despite the lower applied load. This technique measured the plastic and elastic portions of strain and did not allow for elastic recovery of the coating to occur as the indenter remained in the coating during measurement. With no shrinkage of the indentation, this resulted in a lower apparent hardness. Because of the lower indentation load, there was less contribution from the substrate, and so the substrate softening with increasing bias was slightly less pronounced.

b. ABS magnetron

Once again, the plastic hardness values were generally lower than for the conventional hardness test. However, the low bias (-50 V, 0.29 Pa) coating and the low pressure (0.26 Pa, -150 V) coating both gave similar results to the conventional Knoop hardness test. This was due to the differing microstructures of these two films compared with the other coatings.

The low bias (-50 V) coating had a porous, open structure and thus there was little interaction between neighbouring columns within its bulk, hence it was in a tensile rather than a compressive stress state. The result was a very inelastic material, that behaved normally and deformed more under the greater load of the conventional hardness test. Thus the ultra-microhardness result was higher than the Knoop test result.

The low pressure (0.26 Pa, -150 V) coating was also very inelastic, but this time due to the ductility of its metallic nature. Its apparent high hardness, when compared to the other coatings, was due to the denser structure of this film.

5.1.2.5 Adhesion

a. Steered-arc

All the parameter study coatings showed good Rockwell adhesions with no visible spallation.

Scratch adhesion tests showed an almost uniform critical load of around 40-45 N for all bias and pressure combinations. However, the size of the acoustic emission peak at critical load was markedly larger at low nitrogen pressure (0.1 Pa) and is thought to signify high internal stress, causing catastrophic failure at penetration. This stress may have been induced by the extended coating times of the low pressure runs.

b. ABS magnetron

All the parameter study coatings showed good Rockwell adhesions, particularly those performed on stainless steel, nickel and titanium alloy substrates, where the coating deformed into the indentation without any visible spallation. Early coating runs that had obvious interfacial contamination were subject to gross spallation with the Rockwell test. The coatings most likely to show spallation appeared to be those deposited on flat HSS substrates. The good thermal conductivity [1] of HSS (40 to 50 $Wm^{-1}K^{-1}$ at 573K) appears to be responsible in setting up large thermal expansion mismatch stresses during deposition, by conducting heat quickly away from its surface and thus cooling and contracting more rapidly than the depositing coating. When the coatings were deposited onto other substrate materials (eg. stainless steel, titanium or nickel alloy) which have similar thermal conductivities to that of bulk TiN (25 $Wm^{-1}K^{-1}$) spallation due to thermal mismatch stress did not readily occur. The HSS drill blanks were less prone to spallation than the flat samples, possibly due to their smaller bulk, but also due to their convex surfaces, allowing for growing columns to expand naturally as they extended outwards, without generating such high compressive stresses that can lead to spallation (see figure 46).

Scratch adhesion versus bias was almost constant with critical loads of approximately 55 N, except at very low bias (-50 V). At this bias, microscopic examination of the scratch channel revealed ductile failure, in that the diamond actually penetrated through to the substrate without causing cracking or spallation of this softer coating. At higher biases, brittle failure, cracking and eventually spallation occurred every time. It would appear that the substrate bias had little or no effect on coating adhesion.

Scratch adhesion critical load peaked at a pressure of 0.29 Pa (the optimum operating condition) and reduced on either side. This result mirrored the variation of microhardness with pressure, and coating failure was due to the same reason (ie. a softer coating).

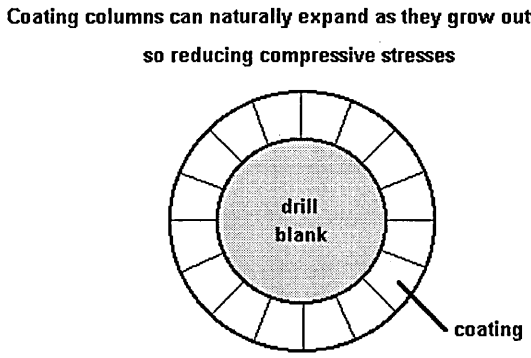

Figure 46. Cylindrical Drill Blank Geometry

5.1.2.6 Structure

5.1.2.6.1 Scanning Electron Microscopy

a. Steered-arc

A columnar (zone T) microstructure was evident in all the coatings produced in the parameter study. The film density appeared to be slightly greater at high bias and at low nitrogen pressure, which corresponded to less cathode poisoning and gas scattering effects, and therefore a high titanium flux at the substrate surface.

The surface of the coatings revealed fewer and smaller droplets at higher nitrogen pressure. This was due to cathode poisoning increasing the melting point and arc velocity, so resulting in smaller molten pools on the cathode surface, and hence reduced macroparticle emission.

The coating thicknesses of the fracture sections appeared less than those measured in section 4.1.4, and this was due to the orientation of the drills in the chamber during coating deposition. The drills were necessarily fractured part way down their flanks, and so the observed cross-sections were both further away and not directly facing the cathodes compared to the flat samples used for thickness and other measurements. However, the flat samples were representative of the tip of the drills (the main cutting edges).

b. ABS magnetron

The low bias (-50 V) coating appeared very porous and columnar with a rough surface finish, corresponding to a zone 1 microstructure. At higher bias, the film density increased and the surface finish became smoother, but some columnar growth was still evident (zone T).

The low nitrogen pressure coating appeared very dense and smooth due to its predominantly titanium only nature (zone 2 or possibly zone 3). However, the surface finish was spoilt by a high density of macroparticles, due to micro-arcing or sputtering of metallic clusters by the unpoisoned cathode. This could also be observed on the cathode surface as "pitting" near the centre of the racetrack erosion area.

At low temperatures, low biases or high pressures, the porous, open-columnar structure is prevalent. Low temperature gives rise to poor adatom mobility and the depositing species remain at or near the positions where they originally adsorbed. Re-arrangement into a more densely packed structure cannot readily occur before more depositing atoms arrive, hence all the voids are not filled and the structure is very porous. Similarly, low or no bias means that ion bombardment is minimal, so there is little kinetic energy input to increase adatom mobility and heat the film. High gas pressures also cause a reduction in the kinetic energy of all arriving species due to energy-loss collisions and scattering, but can appear denser, as observed here, due to the lower deposition rate allowing more time for adatom mobility before the next atoms arrive.

At higher temperatures, higher biases or lower pressures, inter-columnar voids decrease and a more dense, fibrous structure appears.

5.1.2.6.2 X-ray Diffraction

a. Steered-arc

XRD using Cu Kα radiation revealed a very strong {111} preferential texture in all the coatings, with no significant change over the whole parameter range. This is the normal result found with arc evaporated films and is thought to be due to the omission of argon ion bombardment during coating growth (section 5.4).

Lattice parameter measurements showed slight expansion due to titanium ion bombardment induced residual stress, but very little variation over the whole parameter range studied.

b. ABS magnetron

XRD using Cu Kα radiation revealed a very strong {111} preferential orientation in most of the coatings. As the bias voltage increased, or the pressure decreased, so the {111} texturing reduced, with an apparent anomaly in this trend at -150 V bias. At high bias (-200 V) and low pressure (0.26 Pa) the coatings both exhibited a dominant {110} preferred orientation. These deposition conditions both correspond to greater titanium flux and higher energy ions impinging on the substrate surface (high bias = high accelerating energy, low pressure = less poisoning and less gas scattering) (see section 5.4).

All coatings exhibited some lattice expansion, though this was minimal at low bias voltage. Generally, the lattice parameters increased with increasing ion bombardment, peaking under conditions of -150 V bias and low (0.26 Pa) nitrogen pressure. There appeared to be a marked increase in lattice parameter in the mid-bias range, particularly at -100 V. This is thought to originate from thermal stress caused by a temperature drop at the start of coating, from the 450°C peak temperature of the arc-etch phase down to the stable coating temperature of 360°C at -100 V bias (section 4.1.1). The effect of this thermal stress was particularly evident with the spallation of some of the coatings deposited on HSS substrates, which have a high thermal conductivity (40-50 $Wm^{-1}K^{-1}$ at 573 K) relative to the other substrate materials used (15-23 $Wm^{-1}K^{-1}$ for stainless steel, nickel and titanium [1]), and to bulk TiN itself (25 $Wm^{-1}K^{-1}$). As the temperature is steadily raised, the thermal conductivities of all the materials converge, until at CVD temperatures no such effects would be observed.

An even larger temperature drop at -50 V bias did not lead to such lattice expansion due to stress relief by the open columnar structure of this film.

The reduced lattice parameter size at -200 V bias is thought to be due to the higher temperature and adatom mobility causing an annealing effect that reduced the defect density in the coating and relaxed the stress.

5.2 GDOES Technique

5.2.1 Coating Composition and Thickness

a. Steered-arc

The GDOES depth profiles revealed all the coatings to approximately have a 1:1 stoichiometry, despite the variations in deposition conditions (stoichiometric TiN contains 77.4 mass% Ti and 22.6 mass% N). This indicates that all the deposition conditions studied had sufficient nitrogen to form fully filled interstitial TiN compounds. However, the profiles showed a slight drop in nitrogen concentration with depth through the coatings, due to water vapour contamination and outgassing at the start of coating, constituting a partial pressure that reduced as time went on. Any outgassing oxygen would be quickly ionized in the intense arc discharge and incorporated into the growing film preferentially to the nitrogen. Over saturation of nitrogen in the chamber would reduce this effect by increasing the chances of nitrogen incorporation instead.

The steered-arc process possesses remarkable tolerance to large variations in bias and reactive gas flow, with well-adhered, stoichiometric coatings being produced on almost every run, but offers little opportunity to vary the structure and properties of the coatings deposited. This is basically due to the omission of a working gas (argon) from the process, and to the ionization of the depositing species (titanium) by the arc. As a result, the ion bombardment intensity is not independent of the deposition rate, and so the adatom mobility cannot be significantly varied to enable a structural rearrangement and possible orientation change in the crystal structure, or at high mobility, resputtering of the deposited atoms.

Coating thicknesses were taken at the mid-point of the titanium and iron profiles falling to zero. This gave a consistently greater thickness measurement than with the conventional techniques by approximately 15 to 20%. The error in the depth quantification of the GDOES technique increased with depth, the cause of which will be discussed in section 5.2.3.

b. ABS magnetron

The ABS magnetron process was very sensitive to variations in reactive gas flow, resulting in significant changes in sputtering yield and hence in coating properties. This inherent instability required accurate and constant monitoring and control of the reactive gas pressure during a process. There was also a tendency for the coating process to demand more reactive gas as it progressed which was mimicked in the growing films. GDOES depth profiles generally showed a drop in nitrogen

concentration with depth through the coating. This was again because of water vapour contamination and outgassing at the start of coating. As the process continued, so the water vapour was dissociated and incorporated into the growing film or pumped away. This constituted a partial pressure in the chamber that gradually decreased as time went on, and was compensated for by the total pressure controller feeding in more reactive gas.

The low and high nitrogen pressure processes produced under and over stoichiometric films respectively. This was expected as the solid solubility of nitrogen in titanium is very high, and can easily accommodate the nitrogen concentrations observed here within the titanium lattice (see figure 47).

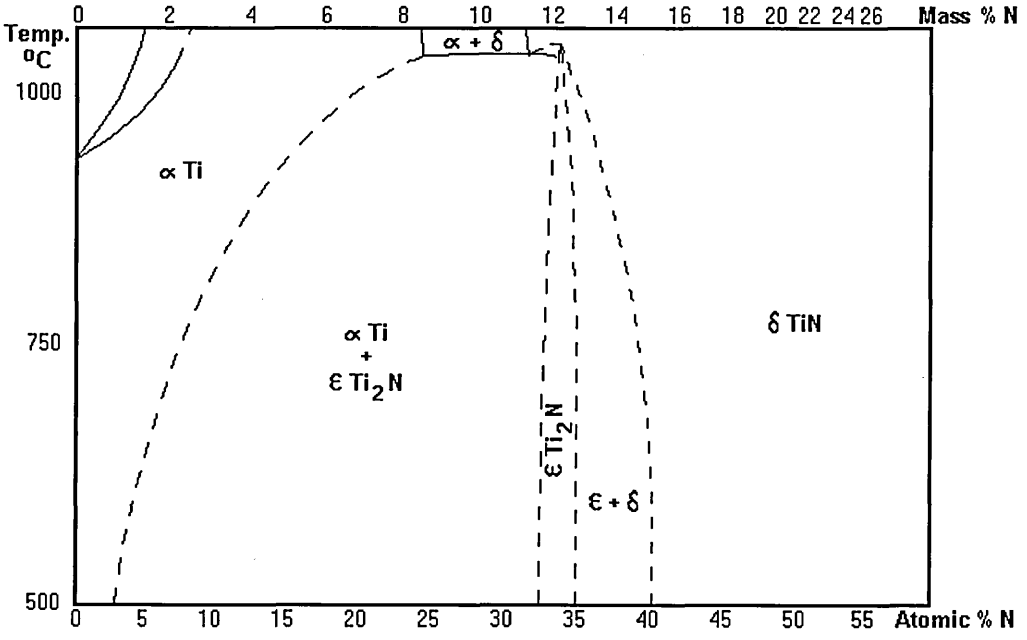

Figure 47. TiN Phase Diagram

Additionally, due to the inclusion of a working gas during deposition, the substrate bias voltage played a significant part in determining coating structure and properties due to ion bombardment effects. The low bias (-50 V) coating also showed a high nitrogen content, but additionally an excessive oxygen content (approximately 4 mass% compared to less than 1 mass% in the other coatings).

Above -50 V bias, a 1:1 stoichiometric TiN film was formed at all bias voltage values, when operated at the normal nitrogen pressure.

Coating thicknesses were again taken at the mid-point of the titanium and iron profiles falling to zero. The error in the thickness measurement was only 10% due to the thinner coatings, and so reduced depth of profiling.

5.2.2 Applicability of GDOES to Coating Analysis

The strategic importance of the GDOES technique for coating analysis is shown in this and other work [2 3]. The ability to provide information about coating thickness, stoichiometry, elemental distribution, layer structure and interfacial contamination, all with a single analysis and with such speed, cannot readily be matched by any other method.

The sensitivity of GDOES to light elements is essential for carbide and nitride coatings, and also for detection of contaminants, but the lack of readily available calibration materials for these elements can be a problem. There are also a few peculiarities with this technique that must be known for correct interpretation of results. These include the poor depth resolution regarding interfaces due to sputter crater shape, and the need to know all the elements present during analysis due to normalisation of compositions to 100%. These problems will be discussed further in the following sections.

5.2.3 Depth Resolution

Glow discharge sputtering is strongly dependent on the working gas, sample composition and the applied parameters: current, voltage and pressure. Careful adjustment and monitoring of these parameters is vital for controlling elemental sensitivity, and rate and resolution of depth profiling, as well as for quantification of the collected results.

An example of the effect of the discharge parameters is evident in the collected depth profiles (section 4.2). Large apparent coating-substrate "diffusion" zones were observed on the depth profiles through coatings, rather than abrupt step interfaces. This effect has also been observed in the literature [4], and is partially due to surface roughness, but also to an artefact produced by the GDOES technique, of a non-flat bottomed sputter erosion crater [5]. The crater shape ultimately dictates the depth resolution, and is caused by electric field variations and reflection or electrostatic attraction of the sputtering ions on the sidewalls of the erosion crater, resulting in a convex or concave crater bottom (see figure 48).

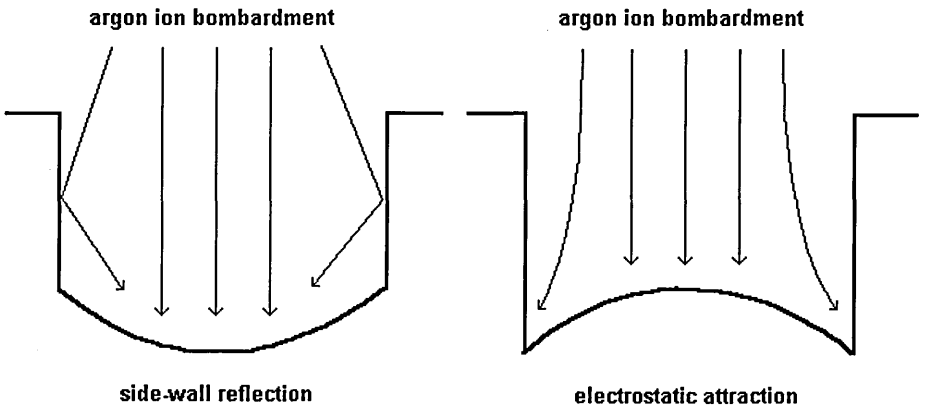

Figure 48. Glow Discharge Crater Shapes

This is illustrated further by surface profile measurements of a series of craters produced under varying discharge conditions (section 4.2.3). As the conditions change, so the crater shape changes as described above. The optimum conditions give a compromise between the two crater shape extremes, and these discharge conditions (-700 V and 30 mA) are currently used for coatings analysis.

5.2.4 Quantification

Quantification can only be as good as the calibration standards used, and the widest possible concentration range for each element is always desired. Calibration standards for all the common metallurgical materials (steels, bronzes, etc.) are readily available as they have been supplied for other spectroscopic techniques (XRF, EDX, etc.) for many years. However, glow discharge spectroscopy has the advantage over the X-ray techniques of easily detecting the light elements such as hydrogen, carbon and nitrogen. There is an acute lack of standards available for these elements, particularly in the high quantity ranges found in PVD coatings (e.g. 22.6 mass% N in stoichiometric TiN and 20 mass% C in stoichiometric TiC). The use of compacted powders for producing standards with high gas content has been attempted using commercially available powdered oxides [6 7] or by compacting a metal powder in a gas atmosphere so trapping the gas in pores. The compacted

powder is weighed and the composition calculated from the known density of the metal. This method clearly can be inaccurate and unreliable. An alternative method is to use PVD coatings as calibration standards. The problem is, of course, in guaranteeing the stoichiometry of the film when it can exist over a wide composition range (eg. 15 to 26 mass% N in TiN). This problem can be minimized by using a large number of coatings that are at or around stoichiometry and taking the average. Alternatively, coatings can be deposited that only exist over a very narrow compositional range such as Ti_2N (11-13 mass% N) and the single phase confirmed using X-ray diffraction. A third method is to grow a film under conditions of reactive gas saturation, but without argon plasma assistance, such that a fully filled {111} orientated interstitial lattice is formed with no sputtering effects that could change the stoichiometry. The mechanism of this technique is explained more fully in section 5.4. Reactive gas saturation in a magnetron sputtering process would lead to gross deposition inefficiency due to cathode poisoning, but the arc evaporation technique does not suffer so, and additionally it requires no argon plasma enhancement. This method is illustrated by a depth profile through an arc deposited TiN coating that was subjected to regular step increases in the nitrogen gas pressure throughout deposition (section 4.2.4). After the initial pure titanium layer the nitrogen concentration rose to a steady state, despite subsequent pressure increases. Similar depositions could be performed for other coating systems as required.

Ultimately the calibration could employ all the methods outlined here, and their validity confirmed by the fact that the various compositions will all sit on a straight line plot of glow discharge intensity versus composition (section 4.2.4).

5.2.5 Radio-Frequency Source

The use of a radio-frequency source allows the analysis of non-conductors by the GDOES technique. This extends the range of coating materials that can be depth profiled to include true ceramics, polymers and glasses. This will find particular application in the aero industry for depth profile analysis of thermal barrier coatings, which by definition are non-conductors (section 4.2.5).

Unfortunately, the operating parameters of the R.F. source are not yet as well understood as those for the D.C. source, and hence quantification is not currently possible, but often a qualitative comparison between good and bad coatings is all that is required to solve deposition problems.

5.3 Interface Region

5.3.1 Sputter Etching

Good adhesion is the most fundamental requirement for surface coatings in any application since, if the interfacial adhesion is poor, coating detachment will occur before any of the coating's other beneficial properties can be realised. The high temperatures used in CVD processes automatically lead to the removal of surface contaminants by reaction prior to deposition, and also promote some diffusion at the substrate-coating interface and elemental intermixing which leads to improved coating adhesion. Such interdiffusion is not so readily observed at the lower temperatures associated with PVD processes, and so additional adhesion-enhancing techniques have been employed, such as ion etching to sputter away contaminants and locally heat the surface layers to cause limited diffusion or implantation [8 9].

The GDOES depth profiles (section 4.2) showed large coating-substrate "diffusion" zones. These can be partly explained by the poor spatial resolution (1 μm) of the GDOES technique due to a non-flat bottomed sputter erosion crater, but there was also variation in the size of the diffusion zone from sample to sample that appeared to be related to deposition temperature. However, significant diffusion does not normally occur at the low temperatures involved in PVD. To illustrate this, a multilayered coating of the form Ti-TiN-Ti-TiN was deposited at low temperature (350^{o}C) and the compositional depth profile measured to see if diffusion of nitrogen into the titanium (nitriding) occurred. The coating was then vacuum heat-treated at the normal deposition temperature (450^{o}C) and another compositional depth profile measurement taken.

Results (section 4.3.1) showed no significant change in the interface positions, indicating that diffusion had not occurred, and the composition was fixed. The significance of this is that any change in the coating composition, by diffusion into the substrate or dissolution of contaminant adatoms, must take place during deposition and involve some form of atomic intermixing due to ion bombardment induced adatom mobility.

The deeper diffusion zones observed in some of the arc etched samples were probably due to the additional heat input aiding adatom mobility, and increased density of surface defects caused by the ion bombardment. The alternative explanation of direct ion implantation seems very unlikely at the bombardment energies involved. The TRIM program calculations support this, showing a titanium ion implantation range in iron of only 5 nm at 2 keV energy (section 4.3.3).

Ion etching can cause problems such as redistribution of sputtered material, overheating of the substrate, roughening of polished surfaces and generation of thermal stresses at the interface region. This clearly cannot be tolerated for decorative applications, but for industrial coating applications it may not be a problem, and the additional adhesion afforded by sputter etching the substrate surface is welcome.

STEM images of the arc etched coatings on HSS showed carbides from the underlying steel substrate protruding into the TiN film (section 4.3.2). This suggested that the arc-etch cleaning phase sputtered back the steel matrix, leaving the harder carbide particles sticking out. These carbides then provided a mechanical "keying" effect to enhance the coating adhesion, as well as providing additional nucleation sites for coating growth. They may also act as physical blocks to interfacial crack propagation that would, if unchecked, lead to gross coating spallation.

Computer modelling of ion bombardment of surfaces using the TRIM program (section 4.3.3), confirmed that at -1000 V bias, 1 and 2 keV (singly and doubly ionized) titanium ions would sputter the iron matrix significantly more than tungsten carbide particles (2.8 times more).

To see if the sputtered depth of >300 nm that was observed in the STEM images was possible to achieve during the arc-etch phase, a sputter depth calculation was performed for both deposition techniques (section 4.3.4).

This resulted in a sputter depth of approximately 600 nm, showing that it is quite feasible for the arc-etch phase of each process to sputter the substrate surface sufficiently to expose carbide particles in tool steels.

These results lead to the possibility of engineering the substrate surface to achieve the maximum level of adhesion for coatings deposited using an arc-etch stage. A series of experiments would find the optimal carbide particle size and distribution required, such that they could be precipitated during the steel production process.

5.3.2 Interlayers

Where surface roughening by sputtering is not acceptable, then the use of a metal interlayer (e.g. titanium) can also improve coating adhesion. Titanium interlayers have additionally been shown to improve the corrosion resistance of TiN coated substrates by forming a dense layer to block pinholes and intercolumnar porosity, and also by the formation of a passive oxide film (TiO_2) with high resistance to localised attack [10].

XPS results (section 4.3.5) showed an increased oxygen content in the lower bias arc coatings that was possibly due to water vapour contamination within the chamber. An unbiased coating that revealed large amounts of oxygen, was very porous such that free oxygen could have been trapped in voids in the open columnar structure. However, deconvolution of the collected data showed that the oxygen contamination was chemically bound to the titanium as TiO_2. It is thought that intercolumnar channels and pinholes in the porous low and unbiased coatings allow atmospheric interaction with the titanium interlayer which subsequently forms TiO_2.

The thickness of the interlayer is important, in that too thin a layer will have no beneficial effect due to insufficient stress relaxation and low solvent power. Conversely, too thick a layer will result in a large unreacted region with the relatively poor properties of the pure metal (when compared to the properties of the ceramic coating). The interlayer will thus be a weak point in the coating structure and subject to cohesive failure within the titanium bulk.

The experimental results illustrate this behaviour. From a plot of critical load versus interlayer thickness (section 4.3.6), the optimum interlayer thickness appeared to be between 0.1 and 0.2 μm. At less than this thickness the failure was predominantly adhesive, probably due to interfacial oxide contamination. Above this optimum thickness the failure was cohesive within the interlayer bulk.

The arc-etch phase of the ABS magnetron process resulted in a similar critical load value to that of the optimum interlayer thickness (approximately 50 N), showing a similar level of adhesion. Even better levels of adhesion may possibly be obtained by combining both arc-etching of the substrate with a titanium interlayer prior to coating deposition.

A further effect of introducing a titanium interlayer, is that it may dictate the crystallographic orientation of the nucleating TiN coating [11]. Bulk titanium has a hexagonal close packed (HCP) structure whose (0002) planes have almost identical lattice spacing as the (111) planes of face-centred cubic (FCC) TiN. Thus condensation of {111} orientated TiN is favoured from the outset. Crystallographic orientation will be discussed further in section 5.4.

5.4 Crystallographic Orientation

5.4.1 Preferred Orientation

In an ideal polycrystalline material, each grain will have a crystallographic orientation different from that of its neighbours and the orientation of all the grains will be randomly distributed. However, it is usual for the grains to cluster to a greater or lesser degree about some particular non-random orientation, and this is known as "preferred orientation" or "texture", the importance of this resulting anisotropy lies in the effect it has on the macroscopic properties of the material [12].

A possible explanation of preferred orientation in coating growth can be made by consideration of the surface defect structure (steps) of the growing film, the adsorption of incident metal atoms, the chemisorption of reactive gas atoms and the bombardment energy of working gas ions and to a lesser extent of metal ions.

5.4.2 Film Growth

Firstly it must be established that coatings such as titanium nitride can only form as a solid and not as a gas phase. This is confirmed from the hysteresis test of gas flow versus pressure (section 4.1), in which a sharp increase in total pressure is observed when the flux of titanium atoms reduces due to cathode poisoning. Clearly, there is no longer sufficient titanium available to combine with the nitrogen present and remove it from the gas phase. Thus the nitrogen stays as a gas and the system pressure rises.

When there are sufficient quantities of reactive gas and metal atoms, then they will combine to form a solid, but because there are no strong attractive forces this can only occur by nucleation upon a solid surface such as the substrate.

The rate of nucleation (and hence growth) is determined by the density of nucleation sites on the surface, which is directly related to the density of surface defects (steps) which are the source of strong adsorption sites [13]. Therefore, it is speculated, that a particular crystallographic orientation, that presents the maximum number of such sites to the surface of a solid, will be the orientation that is most likely to nucleate and so dominate the overall structure.

For titanium nitride the unit cell crystal structure is face-centred-cubic (FCC) (the Na-Cl structure, see figure 49) and a TiN film must always grow with this periodically repeating structure.

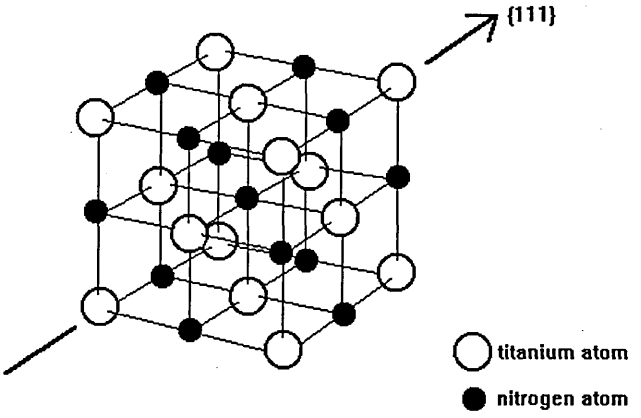

Figure 49. TiN Crystal Structure (FCC)

Since a film grows by deposition of monatomic layers then in order to increase the number of nucleation sites in the depositing atomic plane the unit cell crystal must be tilted with respect to the incident flux of depositing atoms in order to present the most densely packed plane to the surface. A (100) or (110) plane will present only a few interatomic nucleation sites, whilst a (111) plane will present a much larger number of possible sites (see figure 50). This last tilt orientation gives the maximum nucleation site density on the growing surface, and corresponds to a body-diagonal orientation of the FCC unit cell, ie. the {111} direction.

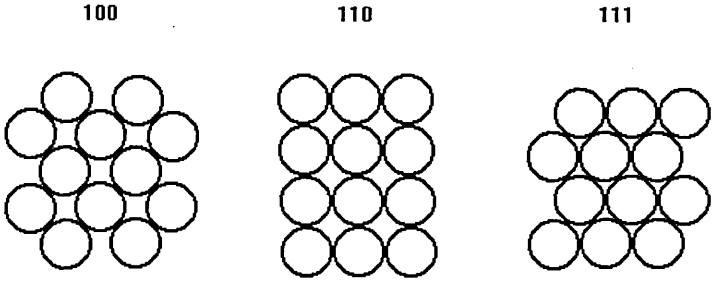

Figure 50. Surface Atomic Packing Structure for the Major Orientations

This tilting of the unit cell in the {111} direction is also replicated by the surface crystallite shape of the growing columns. Under low ion bombardment conditions a pyramidal surface structure is commonly observed [14] (consider the corner of a cube).

Higher ion bombardment conditions probably destroy this structure by sputtering.

Therefore, under favourable deposition conditions, a {111} orientated coating will always prevail for a cubic structure.

It is now necessary to consider what these favourable deposition conditions are, and what will cause the orientation to vary from {111}.

5.4.3 Crystallite Growth

An examination of the TiN unit cell in the {111} direction (see figure 49) reveals a layered structure consisting of alternate monolayers of titanium atoms and nitrogen atoms. This alternating layered structure reflects the deposition sequence and gives an insight into the bonding involved in a TiN film and why 1:1 stoichiometry is not normally exceeded in {111} orientated films (except by substitution or by trapping of free nitrogen at intercolumnar grain boundaries, point defects or dislocation sites).

Consider a monolayer of titanium atoms. Incident atoms of reactive gas (nitrogen) impinge directly upon unoccupied adsorption sites and fill them. Providing there is a sufficient partial pressure of nitrogen in the atmosphere, then a monolayer of nitrogen atoms will be adsorbed until no further sites are available. At this point the "sticking coefficient" reduces to zero and adsorption of nitrogen will stop (see figure 51). At normal PVD operating pressures a monolayer will form in 10^{-3} seconds.

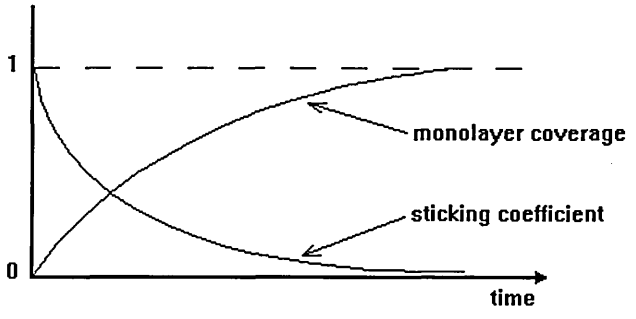

Figure 51. Sticking Coefficient and Monolayer Coverage

Under normal conditions this monolayer will be bound to the surface by very weak Van der Waals type bonds involving no charge transfer. This is known as "physisorption" and the attractive force is provided by the instantaneous dipole

moments of the adatom and its nearest neighbour surface atom. The residence time of such adsorbed atoms is typically 10^{-12} seconds. However, during a PVD process there is also a transfer of thermal energy which allows physisorbed atoms to surmount an energy barrier and electron exchange will occur between substrate and adatom. The adatom is now much more strongly bound with the surface and is said to be "chemisorbed" (see figure 52). The type of bonding depends on the atoms involved and will be discussed later.

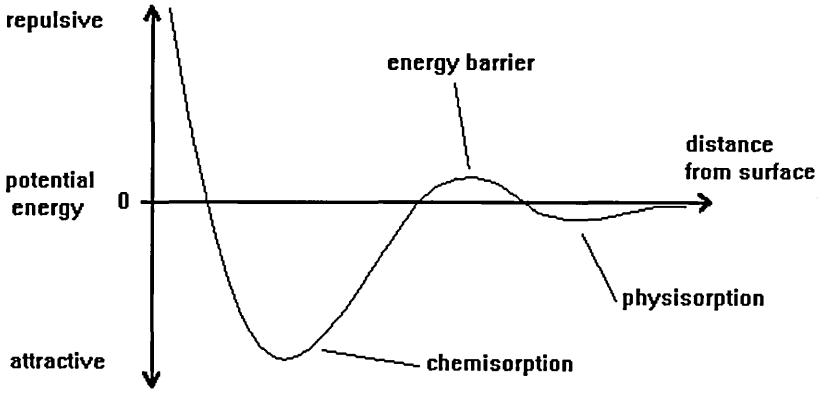

Figure 52. Adsorption

Thus a monolayer of nitrogen atoms is quite strongly bound, and will require bombardment by relatively high kinetic energy particles in order to dislodge it. The sputtered titanium atoms are not accelerated by the substrate bias voltage and so do not have sufficient kinetic energy to sputter away a significant number of strongly bound nitrogen atoms (although some may be removed, resulting in interstitial vacancies in the coating microstructure and a substoichiometric film or, as will be demonstrated later, an orientation change). Therefore a monolayer of titanium atoms will be deposited once more.

It must be noted that this layer-by-layer growth is an idealised consideration, whilst in reality the incident flux of titanium and nitrogen atoms is continuous. At sufficient nitrogen pressure, the instant a monolayer of titanium is deposited, whether as a single atom, cluster or entire film, then a monolayer of nitrogen will adsorb onto it before the next titanium atoms arrive. If there is insufficient nitrogen pressure then the titanium atoms will readily deposit onto the previous titanium monolayer and build up a pure metal or mixed lattice. However, an excess of nitrogen will not result in a lattice of pure nitrogen building up, since the attractive

forces for nitrogen cease once all adsorption sites on the titanium surface are filled (see figure 51).

Thus the alternate atomic layers build up, and since they must conform to the FCC Na-Cl structure, then the {111} orientated crystallite appears.

XRD results from the ABS magnetron coatings (section 4.1.7.2) revealed a very strong {111} preferential orientation in most of the coatings. However, the high bias (-200 V) and low pressure (0.26 Pa) coatings both exhibited a {110} preferred orientation. In the sputter deposition process there is also a working gas present (argon), and these deposition conditions both correspond to greater ion flux and higher energy ions impinging on the substrate surface (high bias = high accelerating energy, low pressure = less poisoning and less gas scattering).

The situation discussed so far has assumed low bias conditions in which the argon ions do not play a significant sputtering role. However, argon ions under high bias conditions will have sufficient kinetic energy to sputter away the more loosely bound adatoms from the depositing surface (the more loosely bound atoms will be those that are not in positions conforming to other orientations of the FCC Na-Cl structure). TRIM program calculations (section 4.3.3) show a 2.9-fold increase in the sputter yield of TiN when the bias voltage increases from -100V to -200V under argon ion bombardment. Any vacancies produced in the titanium layer will be readily filled by adsorbing nitrogen atoms and any vacancies in the nitrogen layer will be filled by incident titanium ions. Thus a mixed atomic layer will be created. The next atomic layer will also be mixed, but in a different arrangement favoured by the layer below and the overall drive to form the thermodynamically stable FCC Na-Cl lattice structure. Thus a differently orientated crystal appears.

A similar process occurs at low reactive gas pressures. Now the probability of forming a complete nitrogen monolayer is lowered, leaving a greater number of vacancies that could possibly be filled by titanium atoms. Also, the lower gas pressure means a longer mean free path and less energy-loss collisions for the incident argon ions. Thus there is increased ion energy and an improved probability of sputtering the surface atoms.

Under sputtering conditions that produce a 50 % nitrogen and 50 % titanium layer, the crystallographic orientation could be either {110} or {100}(see figure 53).

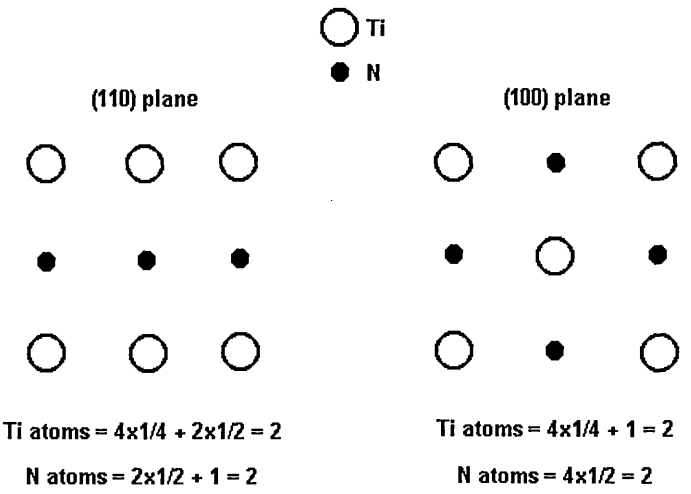

Figure 53. (110) and (100) FCC Lattice Planes

The exact orientation depends on the surface mobility of the atoms, which is dictated by the ion bombardment energy and rate of arrival of depositing atoms (ion to atom ratio). Higher ion energy or ion numbers increases adatom mobility, while higher depositing atomic flux decreases mobility time. A high ion to atom ratio will allow the 50:50 TiN atomic layer to rearrange itself into its lowest energy, most thermodynamically stable state. This will correspond to evenly distributed Ti and N atoms which results in the {100} orientation. Less adatom mobility due to lower energy or time will result in a less evenly distributed layer and a {110} orientated or, more likely, a mixed orientation layer.

This orientation change with increasing ion bombardment corresponds to a reduction in the tilt of the unit cell crystal with respect to the coating surface, until the {100} orientation presents flat faces to the surface. This is in agreement with the observed surface smoothing effect encountered with increasing bias [3]. Also, since the growing columns now also have flat sides, they can pack more closely together forming an overall more dense columnar structure than is possible with {111} orientated columns. This agrees with the published structure-zone-diagrams [15 16 17].

For one of these alternative orientations to dominate there must be a continuous flux of high energy ion bombardment throughout the whole deposition process. If there is not, then a complete titanium or nitrogen monolayer may form and the film orientation will revert back to {111}. It may thus be possible to deposit a film with no overall preferential texturing by periodically cycling the bias level (and hence bombardment energy) during the deposition process.

5.4.4 Bombardment Energy

It should be possible to determine the bombardment energy required to cause an orientation change, by considering the ion to atom ratio arriving at the substrate. The bias level will allow the ion bombardment to be varied, while the atomic flux will be fixed for a given magnetron operating power. The titanium atoms are not affected by the bias voltage because, in general from a sputter source, they are neutral and so are not subject to acceleration across the dark space (sheath) formed around the negatively biased substrate (this does not apply to arc evaporated coatings, however, in which the titanium arrives as ions, such that bombardment energy and deposition rate increase simultaneously, and as a result no orientation change readily occurs unless there is insufficient nitrogen to form a monolayer).

Clearly the ion bombardment energy must be sufficient to partially sputter surface atoms at a rate comparable to the rate of adsorption, such that an equilibrium condition can be established. The partial monolayer coverage will then be "locked" in place by the next atomic monolayer deposited.

In general we see just three dominant orientations : {111}, {110}, {100}. The {100} orientation is only seldom seen and corresponds to conditions of high bombardment energy, to promote adatom mobility, without excessive sputtering of more than 50% of the surface monolayer, as this will result in a substoichiometric film. It is likely that many PVD systems cannot generate the required ion flux density to deposit this structure, or cannot maintain it continuously, such that other orientations appear. The {110} orientation is then likely to be observed as part of a mixed orientation film, when the {100} orientation is not achieved. The {111} orientation corresponds to the widest ion energy band and so is most easily obtained. Other orientations - eg. {311}, {211}, etc. do not appear to show the same dominance because they present less step defects (and hence adsorption sites) at the surface, and so their nucleation probability is reduced by comparison.

5.4.5 Arc Evaporated Coatings

The arc evaporation process is a special case because the depositing species is highly ionized, and hence deposition and ion bombardment are inextricably linked.

Arc evaporated TiN coatings almost always exhibit {111} preferred orientation, no matter what the deposition conditions.

XRD results from the steered-arc coatings (section 4.1.7.2) revealed a very strong {111} preferential texture in all the coatings, with no significant change over the

whole parameter range.

This can be explained by two suppositions. Firstly, in the arc evaporation process, the pre-coating (sputter cleaning) phase always deposits a film of pure titanium onto which the TiN film must grow. Pure α-phase titanium has a hexagonal close packed (HCP) structure which is closely related to the FCC structure because of its high atomic packing density. More importantly, the hexagonal arrangement of atoms on the (0002) planes ({0001} direction) of the HCP structure exactly match the hexagonal arrangement of atoms on the (111) planes ({111} direction) of the FCC structure (see figure 54). Thus the probability of nucleation at these sites and {111} orientated growth is enhanced.

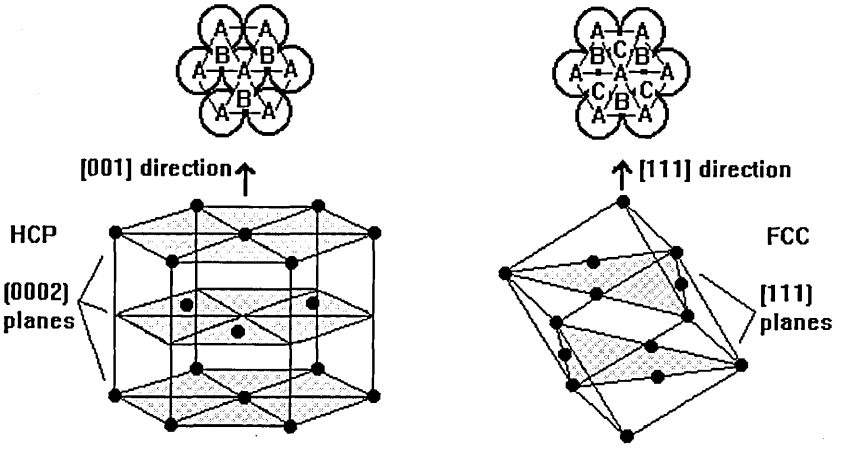

Figure 54. Comparison of HCP and FCC structures

Secondly, during the coating phase, the arc evaporation process does not use a working gas and hence the growing film surface cannot be bombarded by high kinetic energy argon ions independently of the depositing titanium. Thus any increase in bias which would result in a greater energy input per incident atom, is paralleled by an increase in the number of depositing particles, assuming there is sufficient flux available. Any gain in adatom mobility which might lead to an orientation change is lost by the associated increase in rate of deposition, so limiting the time for adatom movement.

Only at very high bias, insufficient nitrogen, or close proximity to the cathode, might an orientation change occur, due to the high flux density of titanium ions present in the arc discharge causing surface heating, and so aiding adatom mobility.

The exception to the rule is at zero bias, when the ionic charge on the titanium no longer plays a part in the deposition process and as a result an orientation change might again occur, driven only by the relative amounts of titanium and nitrogen present, and by the orientation of the underlying substrate.

Providing there is sufficient nitrogen available, arc deposited coatings will also invariably be stoichiometric because there is no working gas used during deposition, and hence little sputtering of atoms from the depositing TiN lattice. The only substrate bombardment that occurs is by the depositing titanium atoms themselves, which in turn provide adsorption sites for the nitrogen. Thus an increase in bombardment only serves to increase the rate of deposition.

5.5 Atomic Bonding

The coatings deposited by PVD processes are generally chosen for their extreme properties of low friction, high hardness, chemical inertness and wear resistance. Such properties can only be explained by very strong internal bonding. The bonding explanation given here is not based on any practical work, but combines existing metallurgical solid solution mechanisms with chemical theories on transition metal electron shell structure and applies them specifically to PVD coatings such as TiN.

5.5.1 Interstitial Solid Solutions

The transition metal nitrides and carbides belong to a class of compounds known as "interstitial solid solutions" [18]. That is, a homogeneous mixture of two or more kinds of atoms in the solid state, where the solute atom (eg. nitrogen) enters into the interstices between the solvent atoms (eg. titanium) (see figure 55).

Clearly, the solute atoms must be small in size relative to the solvent atoms, and indeed interstitial solid solutions only occur if the solute atom has an apparent radius smaller than 0.59 that of the solvent. The five most important interstitial atoms are hydrogen, boron, carbon, nitrogen and oxygen, all of which are small.

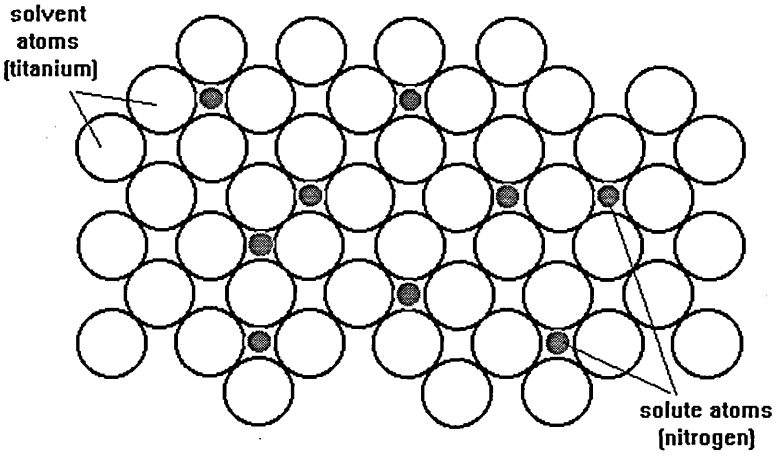

Figure 55. Interstitial Solid Solution

The exact nature of the bonding in interstitial solid solutions is unclear. The stability of interstitial compounds was thought to depend entirely on the ratio of the radii of the constituent atoms. This ratio should be such that the metal atoms are nearly in mutual contact and that the solute atoms are distributed over the interstices between them so that they are in contact with the metal atoms, and cause only a

slight expansion of the metal lattice. In order to achieve this atomic contact, there is also a minimum size for the solute atoms, allowing them to bond in the interstices. The solute atoms will occupy the largest interstices in the metal lattice structure that allows them to achieve this contact. Thus, in a face centred cubic (FCC) structure which has both tetrahedral and octahedral sites, the solute atoms, if sufficiently large, will occupy the larger octahedral interstices (see table 1). If all these sites are occupied then the structure is that of Na-Cl and corresponds to the stoichiometric composition MX, as with titanium nitride.

TABLE 1 : Interstitial Sites and Radius Ratios

Metal structure	Interstitial site	Min. Radius ratio	Max. Radius ratio
FCC	octahedral	0.41	0.59
	tetrahedral	0.23	---
HCP	octahedral	0.41	0.59
	tetrahedral	0.23	---
BCC	tetrahedral	0.29	---

Atomic radius of titanium = 0.1467 nm
Atomic radius of nitrogen = 0.0739 nm
Radius ratio N/Ti = 0.504

However, atomic size is not the only factor that determines whether or not an interstitial solid solution will form. Small interstitial solute atoms dissolve much more readily in transition metals than in other metals and this is believed to be due to their unusual electronic structure. The transition metals all have an incomplete electron shell inside the outer valence shell, while other metals all have fully filled inner shells. As a result, two shells of the transition metals can contribute to the electrical and thermal properties, instead of just the valency shell as with other metals. This means that while one shell is used in bonding with the interstitial atoms, the other shell can contribute to the free electron "gas" that makes the "ceramic" compound conductive.

5.5.2 Covalent-Ionic Bonding

Because the interstitial atoms generally choose interstices that are exactly or nearly a perfect fit, the metal lattice atoms and interstitial atoms are in mutual contact [19]. The outer electron shells of the metal and non-metal atoms overlap, and because the

transition metal atom contains a partly empty inner shell, the nuclei share electrons, resulting in a covalent bond. This covalent bonding in the transition metal is much stronger than normal covalent bonding because it involves an inner electron shell. In the case of TiN, the 3d shell of titanium only contains 2 electrons out of a maximum possible of 10. The 2p (valence) shell of nitrogen contains 3 electrons, which is half-filled and therefore a stable state. However, if the nitrogen shares these 3 electrons with the 3d shell of the titanium, then this shell will also now be half-full (5 electrons) and thus stable. There then still remains 2 valence electrons in the 4s shell of titanium, that are free to conduct (see figure 56).

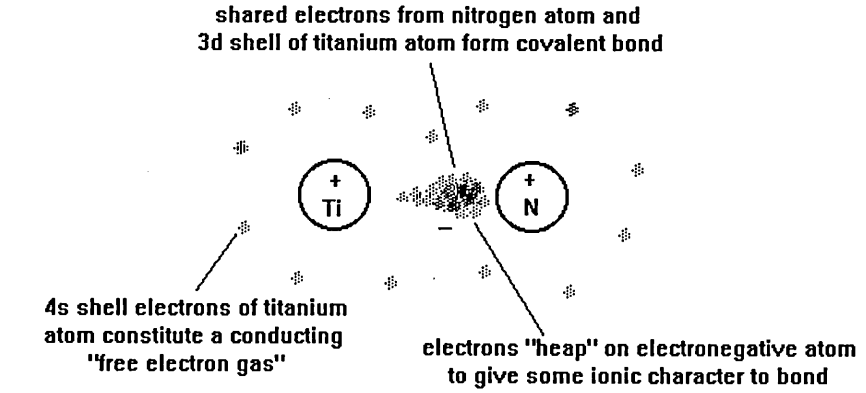

Figure 56. Covalent-Ionic Bonding

Because the metal and non-metal atoms have different ionization energies and electron affinities, the covalent bond does not form symmetrically between them [20]. The shared electrons tend to be "heaped up" on the more electronegative atom, so making the bond somewhat ionic in character.

In general, the presence of some ionic character strengthens a covalent bond. The amount of ionic character in a bond can be approximately deduced from the relative electronegativities of the constituent elements by the following formula :

$$ic\% = 35.(en_1 - en_2) - 20 \qquad \text{..... (19)}$$

where $ic\%$ is the percentage ionic character of the bond, and en_1, en_2 are the relative electronegativities according to Pauling's electronegativity scale [21] (see table 2).

TABLE 2 : Electronegativity Scale

F	3.9	Ag, Cu	1.7
O	3.5	Ga, Ti	1.6
N, Cl	3.0	Al, In, Zn, Zr	1.5
Br	2.8	Be, Cd, Tl	1.4
C, S, I	2.5	Sc, Y	1.3
Se	2.4	Mg	1.2
Au, H, P, Te	2.1	Ca, Li, Sr	1.0
As, B	2.0	Ba, Na	0.9
Hg, Sb	1.9	K, Rb	0.8
Bi, Ge, Pb, Si, Sn	1.8	Cs	0.7

For example, transition metals such as titanium have relative electronegativities of 1.6, while nitrogen has a relative electronegativity of 3. This gives a 29% ionic character for the covalent bonds in titanium nitride. This ionic character may be a little greater for "ionic" crystal structures, such as the Na-Cl structure of TiN, because each "ion" has several "ions" of the opposite sign as its immediate neighbours.

References

[1] G.W.C. Kaye and T.H.Laby, *Tables of Physical and Chemical Constants*, 1986, Longman Group Ltd., London.

[2] V.Hoffmann, *Fresenius J.Anal.Chem.*, 1993,346,165.

[3] M.Y.Jaroudi, H.T.G.Hentzell, S.E.Hornstrom and A.Bengston, *Thin Soilid Films*, 1989,182,153.

[4] W.B.Teo and K.Hirokawa, *Surface and Interface Analysis*, 1988,11,421.

[5] Y-M.Pak, T.Tanaka and H.Kawaguchi, *Analytical Sciences*, 1993,9,137.

[6] H.Nickel, W.Fischer, D.Guntur and A.Naoumidis, *Journal of Analytical Atomic Spectrometry*, 1992,7(3),239.

[7] G.Ehrlich, U.Stahlberg, V.Hoffmann and H.Scholze, *Spectrochimica Acta*, 1991,46B(2),115.

[8] W.D.Munz, D.Schulze and F.J.M.Hauzer, *Surf.Coat.Technol.*, 1992,50,169.

[9] W.D.Sproul, P.J.Rudnik, K.O.Legg, W.D.Munz, I.Petrov and J.E.Greene, *Surf.Coat.Technol.*, 1993,56,179.

[10] Y.Massiani, A.Medjahed, J.P.Crousier, P.Gravier and I.Rebatel, *Surf.Coat.Technol.*, 1991,45,121.

[11] Y.I.Chen and J.G.Duh, *Surf.Coat.Technol.*, 1991,46,371.

[12] B.D.Cullity, *Elements of X-Ray Diffraction*, 1978, Addison-Wesley, Massachusetts.

[13] J.A.Thornton, *Metal Finishing*, 1979,5,83.

[14] D.S.Rickerby, A.Matthews and P.R.Chalker, *Advanced Surface Coatings*, 1991, Blackie & Son Ltd., Glasgow.

[15] B.A.Movchan and A.V.Demchischin, *Fiz.Met.Metalloved.*, 1969,28,653.

[16] J.A.Thornton, *Ann.Rev.Mater.Sci.*, 1977,7,239.

[17] R.Messier, A.P.Giri and R.A.Roy, *J.Vac.Sci.Technol.*, 1984,A(2),500.

[18] J.D.Fast, *Interaction of Metals and Gases, Vol.2*, 1971, Macmillan, London.

[19] A.H.Windle, *A First Course in Crystallography*, 1977, G.Bell & Sons, London.

[20] A.H.Cottrell, *An Introduction to Metallurgy*, 1967, Edward Arnold, London.

[21] H.O.Pritchard and H.A.Skinner, *Chem.Rev.*, 1955,55,745.

CHAPTER 6
Conclusions and Future Work

The overall conclusion of the parameter study is that each of the deposition processes examined has advantages and disadvantages when used in different coating applications. For applications involving the deposition of simple single metal (mono) nitrides and carbides with a consistently repeatable microstructure and stoichiometric composition, with minimal process control requirements, the steered-arc technique is the obvious choice, provided that macroparticle inclusion is acceptable. If macroparticles are a problem, such as in decorative applications, then the use of some additional filtering, such as a plasma duct, might be the answer.

For applications where it is desirable to change compositions and microstructures, and hence colours and mechanical performances, then the ABS magnetron technique is the better choice. It is also the obvious choice for decorative applications, though can still be prone to some droplets (or sputtered clusters) as shown in the work presented here. The process additionally allows the relatively easy use of segmented cathodes for alloy coatings, and the possibility to deposit non-conductors using r.f. power supplies. The main drawback appears to be the more complicated process control and unstable operation which limit reliability and reproducibility in a commercial environment.

The unstable process operation of the ABS magnetron is an inherent feature of all magnetron systems, where the gas flow / pressure must be balanced at the "knee" of a hysteresis curve (a fine line between stoichiometric coating deposition and cathode poisoning). The use of pressure feedback control will always lead to instability in gas flow and hence composition due to desorption and outgassing within the chamber. Water vapour that desorbs from the chamber walls, fixturing and cathodes during the deposition process will constitute a partial pressure in the chamber that the pressure measurement system cannot differentiate from the reactive gas pressure. As a result it will compensate by varying the reactive gas flow to maintain a constant pressure, thus upsetting the fine balance of the system. There will always be some water vapour contamination in the chamber as it is not a closed vacuum system (sample loading and unloading necessitates opening to atmosphere). Thus, the only reliable feedback system would appear to be optical spectroscopy of the metal and reactive gas emission lines in the plasma in the vicinity of the substrates.

The steered arc process is, of course, equally susceptible to this problem if operated by a constant pressure controller with just enough reactive gas for

stoichiometry. However, there is a simple, though wasteful, remedy for this technique, which is to saturate the chamber with excess reactive gas such that any contribution from water vapour contamination becomes insignificant. The arc will still run relatively efficiently on the poisoned cathode, with the added advantage of reduced macroparticle emission. To try the same remedy with a magnetron system , whose efficiency is only 1% at best, would reduce the sputter yield to a negligible amount and be economically unviable, as well as altering the coating properties.

The problem of water vapour contamination is exacerbated in the Hauzer ABS magnetron chamber by the two large doors which effectively split the chamber into three slices, and while allowing unprecedented access for cleaning and sample loading, also allow a through stream of moist air. A de-humidified work place and only opening one door at a time would no doubt help reduce this initial contamination. The ABS magnetron chamber also tended to be very cluttered, both with a large turntable assembly and many blanked-off feed-throughs, which are potential sites for trapping water vapour. The use of infrared heating within the chamber during pump-down and sputter cleaning would result in a marked improvement. Also, upgrading of the pumping system, might be considered in the future, especially if process turn-around time became an important issue. An increase in pumping speed would reduce pumping times and levels of contamination, and additionally would flatten out the pressure-flow hysteresis curve, thus allowing more stable operation [1].

The plasma in the ABS magnetron chamber showed a tendency to fluctuate as the substrate turntable rotated. Crude plasma intensity measurements performed by monitoring the substrate bias current as a single sub-turntable was rotated in the chamber, showed the plasma to be split down the centre of each cathode into quadrants, such that one side was more intense than the other. This splitting can be explained as a fundamental problem affecting any linked field, unbalanced magnetron system. It arises when the cathode voltage and substrate bias voltage are unequal (the normal situation), as there is then a net current (electron) flow between them that is deflected up or down depending on the local magnetic linking field and the direction of the net current flow. The plasma ions generally follow the electron movement, and the ions deflected upwards are lost to the chamber ceiling resulting in an apparently weakly ionized region, while the ions deflected downwards are invariably caught by the large turntable bulk and appear as an intense region of plasma. Only when the cathode voltage and substrate bias voltage are equal is there no net current flow and hence a uniform plasma. If the relative magnitudes of the

cathode voltage and substrate bias voltage are reversed, then so is the direction of net current flow, and hence the regions of weak and intense plasma around the chamber reverse positions. As long as the turntable, and hence substrates, are rotated, the overall bombardment should be evenly distributed and the effect negligible, though temperature fluctuations may induce thermal stresses.

The Rockwell indentation test can only realistically be used as an absolute minimum guideline to coating adhesion, as it is such a crude and unquantifiable test. All the coatings produced in these parameter studies passed the Rockwell test and were indistinguishable from one another. However, the Rockwell tester is useful for measuring the bulk hardness of the substrate material before and after coating to ensure no annealing has occurred due to overheating.

The scratch adhesion test remains the only useful method for measuring coating adhesion, but must be combined with visual inspection of the scratch channel by optical microscopy to identify the type of failure.

The arc etch appears to achieve a similar or better level of adhesion as that of a titanium interlayer of ideal thickness. Sputter cleaning with multiply ionized titanium ions is also more effective than using argon ions, due to the greater mass and hence bombardment energy ($\frac{1}{2}mv^2$). This is clear from the fact that the substrate is not properly clean after the glow discharge phase - an un-etched sample showed a very poorly adhered coating. The question thus arises, why not just use the arc etch phase from the start ? The steered arc process certainly does this, but with the risk of arcing on the substrate surface if very dirty, so a gentle preclean is recommended.

The good adhesion achieved by the arc etch phase has been reported to be due to ion implantation or diffusion into the substrate giving rise to an intermetallic phase that bridges the interface boundary of unlike materials [2]. The ion bombardment energies involved do not achieve any great implantation depth [3], and diffusion at PVD temperatures was also discounted by analysis using GDOES before and after heat treatment of a coated sample. However, sputtering of the substrate surface atoms during the etch phase is possible, along with their redeposition and mixing with the nucleating cathode metal atoms.

Only TEM imaging can adequately resolve the interface region, and the TEM work performed here suggests another possibility for the good adhesion of the arc etched coatings. STEM images show that the substrate is sputtered preferentially leaving carbide particles standing proud of the surface, and the coating deposited

around them. These provide a mechanical "keying" effect with the coating, and may also act as physical blocks to crack propagation along the interface, thus reducing the possibility of gross spallation. The science of steel production is very mature, such that it is possible to very accurately precipitate carbide particles of predetermined size and distribution within a steel matrix. It follows that a series of experiments to find the optimal carbide size and distribution density will allow the engineering of surfaces that provide the highest possible level of adhesion for coatings deposited in this manner.

The inclusion of macroparticles at the interface (and within the bulk of an arc deposited film) may have a similar effect, thus explaining the good adhesion of arc coatings despite the apparent high internal stresses. Macroparticles at the interface region would also aid the adhesion of coatings to substrates that do not possess any hard carbides to block crack propagation. It may be that macroparticles are a beneficial artefact of the arc evaporation process, and the quest should not be to remove them, but to ensure that they are evenly distributed and of the optimum size.

The dangers of spallation due to thermal expansion mismatch stress were evident also during the parameter study, in which one of the process runs endured a large temperature drop at the start of the coating phase. The resulting film on a HSS substrate promptly delaminated on cooling to room temperature, while coatings on stainless steel, titanium and a nimonic alloy remained well adhered. An examination of the thermal conductivity's [4] of the materials involved found the HSS to have a considerably different thermal conductivity to those of the other materials, which were all similar to that of titanium nitride itself.

The deposited films showed peaks in both the reflectance (or Lightness L^*) and the yellowness ($+b^*$) that appeared to coincide with the optimum deposition conditions for both processes and hence the ideal coating compositions. The optimum conditions were determined either from the measured properties of the coatings, or in the case of the ABS magnetron pressure value, from the "knee" position of the gas flow-pressure hysteresis curve. It would appear that the measurement of coating colour might be used as a post-deposition quality control technique.

The GDOES technique would appear to be of considerable importance for coating analysis. The ability to provide information about coating thickness, stoichiometry, elemental distribution, layer structure and interfacial contamination, all with a single

technique and with such speed, cannot readily be matched by any other method.

The sensitivity of GDOES to light elements is essential for carbide and nitride coatings, and also for detection of contaminants, but the lack of readily available calibration materials for these elements is a problem. However, by working closely with the production side of PVD coatings, then calibration materials of acceptable accuracy can be produced.

In respect of some of the points raised with regards to the ABS magnetron process, it is interesting to note that the latest PVD system to be developed by Hauzer Techno Coatings B.V. (the HTC 625 Multilab) [5] has the following features as standard :

1. Smaller dimensions with fewer feed-throughs.
2. Integral infrared heating.
3. Higher possible arc currents (up to 150 A)

The theory on crystallographic orientation in thin films goes some way to explaining an area of the subject that has never been properly addressed in the past. By considering the atomic arrangements of the different orientations of TiN obtained under various deposition conditions, combined with the sequence of arrival of atoms and ions during coating growth, a workable theory has been produced. Development and refinement of the theory with extension to coatings other than TiN, and to actual calculation of the conditions required to bring about an orientation change would prove useful in the development of coatings for applications requiring specific microstructural properties.

With regards to future work, the parameter study and practical work might also be repeated in the ABS magnetron system with additional infrared heating fitted, in order to see if this does indeed cure the problems of water vapour contamination and thermal expansion mismatch stress, which have lead to unstable composition and poor adhesion. Further TEM work is also required to show if the crystallographic orientation at nucleation is influenced by the underlying substrate, and how the orientation changes under different bias conditions. This might be achieved by depositing the film on silicon substrates, which can be grown with specific orientations.

References

[1] W.D.Sproul, *Surf.Coat.Technol.*, 1987, 33, 73.

[2] W.D.Munz, D.Schulze and F.J.M.Hauzer, *Surf.Coat.Technol.*, 1992, 50, 169.

[3] S.Kadlec, J.Musil and J.Vyskocil, *Surf.Coat.Technol.*, 1992, 54-55, 287.

[4] G.W.C.Kaye and T.H.Laby, *Tables of Physical and Chemical Constants*, 1986, Longman Group Ltd., London.

[5] W.D.Munz, K.Vannisselroy, R.Tietema, T.Hurkmans and G.Keiren, *Surf.Coat.Technol.*, 1993, 58, 205.

ACKNOWLEDGEMENTS

The author would like to thank everyone who has been involved in the work towards this thesis, particularly the staff of the Materials Research Institute at Sheffield Hallam University. Additional thanks to the collaborating bodies listed below and to Rolls-Royce plc and the Science and Engineering Research Council for funding with a CASE award.

Interatom/Multi-Arc GmbH, Bergisch-Gladbach, Germany.
Hauzer Techno Coating Europe BV, Venlo, Netherlands.
Philips Analytical, Eindhoven, Netherlands.
LECO Instruments plc, Stockport, England.
Research Centre for Surface Engineering, Hull University, England.
Atomic Energy Authority, Harwell, Oxford, England.
IBM Research, Yorktown, New York, USA.
Forschungsinstitut für Edelmetalle und Metallchemie, Schwäbisch Gmünd, Germany.

APPENDIX 1
Process Monitor

The requirement to monitor certain process parameters during a coating run and record them for future reference is fundamental, whether it is for research or production purposes. For research, it is quite clearly vital to know what happened during the deposition process in order to make any sense of test results, and in order to be able to repeat a coating run. For production purposes, it is necessary to be able to check deposition records to see if there were any problems or unusual eventualities that may have caused a coated component to fail in use and the customer to return it. This is equally important if the customer reports outstanding results from the coating. It is necessary to know if the process was the cause or something else, eg. substrate material, cleaning, usage, lubricant, etc.

Ideally, during a process, every variable should be continuously monitored. This will, of course, be impossible, so the most important parameters should be taken into account. For a PVD process these would include pressure, gas flows, temperatures, voltages and currents of cathodes and substrates. The voltages and currents of the cathodes are likely to be preset for each phase of a coating process. If this is so, and the power supplies are reasonably stable, then the monitoring of these may be omitted. So for a typical process, it will be necessary to monitor temperature from one or more thermocouples, at least two gas flows (working and reactive), and one or more pressure gauges.

Continuous monitoring might be possible on a chart recorder, but would lead to cumbersome amounts of data. Manual monitoring might be every five or ten minutes, during which time, a lot could happen. Data sampling and storage every minute by computer would seem to be a suitable compromise, and would allow the data to be subsequently manipulated and plotted.

The process monitor listed here, for the ABS magnetron system, collects data every five seconds, but averages over each minute for storage onto disk. Three gas flows, two temperatures, and three pressures are recorded. Three pressure gauges are used as follow :

1. A Pirani gauge to measure up to atmospheric pressure during pump-down and venting operations.
2. An ion gauge to measure down to the base pressure and used during leak-testing.
3. A Viscovac pressure monitor that is sensitive to fluctuations in the mid-range coating pressures, and provides feedback to the reactive gas flow controller.

The analogue voltages from these sensors are connected via an eight-way full

differential input multiplexer to an analogue to digital converter (ADC) and data acquisition board of an IBM PC or compatible.

The monitoring software was written in BASIC for simplicity, since high speed was not a necessity as there is no real-time graphical output. Data is stored in an array during run-time, then dumped to disk and/or printer at the end of the process. From disk, the data can be accessed by a spreadsheet or graphics package for manipulation or production of plots of parameters versus process time.

During run-time, the software also performs a leak-test function and gives visible and audible warning of over-temperature and/or incorrect working gas flow, to aid the user.

Program Breakdown

Lines 1-8

Title and screen set-up.

Lines 10-98

Set up arrays and zero flag variables.

Arrays:

TEMPOR : temporary array for holding and accumulating 5 second data from RAWDATA array before dumping into main DATALOG array after each minute.

VOLTAGE : array to hold voltage values from each ADC channel after every sample and then average over three samples.

RAWDATA : array to hold converted VOLTAGE value as its proper format value.

DATALOG : main logging array updated every minute from TEMPOR. .

Channel identification :

0 - Viscovac pressure gauge.

1 - nitrogen flow rate.

2 - methane flow rate.

3 - argon flow rate.

4 - temperature of thermocouple one.

5 - temperature of thermocouple two.

6 - Pirani pressure gauge.

7 - ion pressure gauge.

Flag variables : COATING : signals coating in progress if=1.
COATEND : signals coating has finished if=1.
COATFLAG : signals start of coating if=1.
ERRORTRAP : confirms start of coating if=1.

variable COATSTART : updated in minutes since coating began.

Lines 100-498

Start of program.

Clears screen.
Calls ADC set-up routine at line 1000.
Calls intro screen/details/leaktest at line 5000.
Clears screen.

Lines 500-998

Main run-time execution loop.

During data acquisition this loop calls all other subroutines, returning here each time.

5 second interrupt timer is set up - this jumps to the datalogger routine at line 1500 every 5 seconds.

Variables :

MINUTES : time in minutes since process began.

FLAG : updated every 5 seconds in datalogger to signal when to dump data to main array.

START$: starting time of process run.

Zero minutes data is put directly into DATALOG array now.
Call ADC 8 channel acquisition routine at line 1100.
Call voltage to data conversion routine at line 2000.
Call real-time screen display routine at line 3000.
Call screen messages routine at line 4000.

Repeat if not end of coating process (COATEND=1).

If end of process (COATEND=1 or END key pressed) then stop interrupt timer and jump to End Menu at line 6000.

Lines 1000-1098

Analogue to digital converter board set-up.

ADDRESS = base address of ADC board.

First do a conversion with channel number equal to 255 so that next conversion in acquisition routine will be channel 0. Reset status bit.

Enable auto channel incrementing, starting with channel 0.

RETURN.

Lines 1100-1498

ADC board acquisition routine - reading 8 channels.

Clear VOLTAGE array and dimension.

Start conversion of first channel.

Pause loop until conversion finished (checks status bit).

Read in low and high bytes.

Convert to voltage by dividing by 2^{12} (4096) (12-bit ADC).

Loop back to start conversion for next channel.

Loop back to start conversion to average over 3 readings.

Loop to truncate all channel voltages to 3 d.p.

RETURN.

Lines 1500-1998

Interrupt handler routine.

Load channel data into an accumulating temporary array TEMPOR.

Error trap to confirm start of coating phase.

Increment 5 second FLAG counter - when this reaches 12 then a minute has passed (12 x 5 seconds = 60 seconds).

If FLAG does not equal 12 then RETURN.

If minute has passed then get contents of TEMPOR array and divide by 12 to average values over 1 minute.

Store average in DATALOG array.

LOOP to truncate non-pressure parameters to 1 d.p.

Assign pressure parameters key values if over- or under-range.

RETURN.

Lines 2000-2998

Voltage to data value conversion routine.

Each parameter is taken in turn.

All process parameters are linearly related to the output voltages except for the Pirani gauge. This one can be approximated by three separate linear relationships.

By measuring voltages and corresponding parameter data values, a series of x and y values are obtained that can be plotted against each other. The gradient m and y-intercept c can be found thus giving the voltage and data relationship. Linear regression of the values gives a straight line equation fit $y = m.x + c$, corresponding to $data = m.voltage + c$

Out of range voltages are given appropriate values.

RETURN.

Lines 3000-3998

On-screen real-time data display routine.

This routine is self explanatory.

COATING TIME is derived from total process time minus the coating start time.

Over- or under-range messages are printed accordingly.

There is an automatic switch between printing of the Pirani gauge or the ion gauge output, depending on the pressure (ie. whether the ion gauge is active or not).

RETURN.

Lines 4000-4998

On-screen real-time message display.

Reset message flag MESS.

Check RAWDATA array for over-temperature, if too high then set message flag MESS=1. Temperature limits can be set here.

If in coating phase, check RAWDATA for incorrect argon flow. If not 11% (220 sccm +/-10) then set message flag MESS=2 if too low, MESS=3 if too high. Argon flow rate can be set here. (Also change error message below !)

Check for start of coating phase and set flag COATFLAG=1 (Coating started if nitrogen or methane gas flows are above 20 sccm). If COATING=0 (ie. start of coating) then COATSTART is given current process time.

Check for end of coating phase and set flag COATEND=1 (Coating ended if argon flow less than 20 sccm and pressure less than 10^{-4} mbar). Also force coating end if process time equals 4 hours, so as to prevent error when DATALOG array is full.

Print on-screen messages :

If MESS=0 print default message "Press END to end process"

If MESS=1 print error message "Temperature too high"

If MESS=2 print error message "Argon flow below 11%"

If MESS=3 print error message "Argon flow above 11%"

Also provide audible BEEP to alert operator of error messages.

RETURN.

Lines 5000-5298

Introduction screen routine.

This is the start-up screen that is first seen at switch-on.

Software name, version, date and greeting depending on time of day are printed.

Operator name is entered.

Process number/disk filename is entered.

Process details are entered.

Ignition resistance status is entered.

Option given to re-enter all details if incorrect.

Lines 5300-5998

Leak-test routine.

Reset BASEPRESS variable to maximum.

First the active pressure gauge is selected (GAUGE) and the current pressure reading loaded into BASEPRESS for display. This is repeated continuously while the GAUGE reading is less than the pervious BASEPRESS value, such that BASEPRESS will decrease and always shows the minimum or base pressure value during pump down. (Note - if the pressure (GAUGE) should rise, the BASEPRESS value will stay fixed at its last minimum reading and will not rise with it).

Print message to close high vacuum valves.

Check continuously for a key press to begin leak testing.

Take pressure reading by calling ADC set-up and acquisition, and load value into variable P1.

Start TIMER for 60 seconds.

Print time on screen.

At end of minute, take another pressure reading and load value into variable P2.

Reset LEAKRATE variable to maximum (1).

Calculate LEAKRATE using formula (P2-P1).800/60

Print LEAKRATE.

If LEAKRATE greater than $3.5x10^{-3}$ mbar.l.s^{-1} then print failure message, or else print "Leak rate OK".

Option given to repeat leak test or continue with process.

RETURN.

Lines 6000-6088

End menu routine.

List of available options at end of process run.

PRINTOUT - program jump to line 6090.

DISKSAVE - program jump to line 7000.

LEAKTEST - program jump to line 8000.

NEW PROCESS - program jump to line 9000.

EXIT - program jump to line 9500.

Lines 6090-6998

Hardcopy printout routine.

Produces printout of logged data, with operator name, date, process details etc. in tabular form.

Jumps back to end menu routine at line 6000.

Lines 7000-7400

Disk save routine.

Saves logged data, with operator name, date, process details etc. to disk in same format as the hardcopy printout routine, for retrieval by a spreadsheet software package.

Displays destination directory and filename on screen.

Lines 7500-7900

Disk save routine (continued).

Saves logged data only to disk in format accessible by the "import" facility of the Harvard Graphics software package. This allows graphs of process parameters versus time to be produced with minimal user manipulation.

Displays destination directory and filename on screen.

Jumps back to end menu routine at line 6010 (no CLS).

Lines 8000-8998

Leak-test routine.

Another leak-test routine, identical to the one at line 5300, but without storage and printout of results. Allows leak-testing immediately at end of process to be performed if desired.

Jumps back to end menu routine at line 6000.

Lines 9000-9498

Program restart routine.

Confirms command to re-run program as all stored data (in arrays) will be lost.

Runs program or jumps back to end menu routine at line 6000.

Lines 9500-9610

Program exit routine.

Confirms command to exit program as all stored data (in arrays) will be lost.

Exits program, then exits BASIC and returns to DOS, or else jumps back to end menu routine at line 6000.

```
1 'PVD Process monitor
2 'Version 2.1
5 KEY OFF
6 SCREEN 0
8 '
9 'set up arrays
10 DIM TEMPOR(11,7)
20 DIM VOLTAGE(7)
30 DIM RAWDATA(7)
40 DIM DATALOG(300,7)
50 '0=viscovac, 1=nitrogen flow, 2=methane flow, 3=argon flow
60 '4=temp1, 5=temp2, 6=pirani gauge, 7=ion gauge
70 COATING=0: COATSTART=0: COATEND=0
80 COATFLAG=0: ERRORTRAP=0
98 '
99 'start of program
100 CLS
110 GOSUB 1000
120 GOSUB 5000
130 PRINT "  READY TO BEGIN PROCESS - HIT ANY KEY  "
140 BEEP
150 A$=INPUT$(1)
490 CLS
498 '
499 'main runtime execution loop
500 ON TIMER(5) GOSUB 1500
510 TIMER ON
520 MINUTES=0: FLAG=0
530 START$=TIME$
540 FOR PAR=0 TO 7
550 DATALOG(MINUTES,PAR)=RAWDATA(PAR)
560 NEXT PAR
570 GOSUB 1100
580 GOSUB 2000
590 GOSUB 3000
600 GOSUB 4000
700 IF COATEND=1 THEN 750
710 A$=INKEY$
720 IF A$="" THEN 570
730 IF LEN(A$)=2 THEN A$=RIGHT$(A$,1)
740 IF A$<>CHR$(79) THEN 570
750 TIMER OFF
760 BEEP: CLS
800 GOTO 6000
998 '
999 'A/D set up routine
1000 ADDRESS=1808
1010 OUT ADDRESS+4,128
1020 OUT ADDRESS+5,255
1030 OUT ADDRESS+6,0
1040 IF INP(ADDRESS+4) < 128 THEN 1040
1050 X=INP(ADDRESS+6)
1060 OUT ADDRESS+4,0
1070 OUT ADDRESS+5,0
1080 RETURN
1098 '
1099 'A/D 16 channel acquisition routine
1100 ERASE VOLTAGE
1110 DIM VOLTAGE(15)
1140 FOR AV=1 TO 3
```

```
1150 FOR CHAN=0 TO 7
1160 OUT ADDRESS+6,0
1170 IF INP(ADDRESS+4) < 128 THEN 1170
1180 LOW=INP(ADDRESS+5)
1190 HIGH=INP(ADDRESS+6)
1200 TOTAL=(256*HIGH+LOW)
1210 VOLTAGE(CHAN)=VOLTAGE(CHAN)+(TOTAL/409.6)
1220 NEXT CHAN
1230 NEXT AV
1250 FOR CHAN=0 TO 7
1260 VOLTAGE(CHAN)=VOLTAGE(CHAN)/(AV-1)
1270 VOLTAGE(CHAN)=(FIX((VOLTAGE(CHAN)+.0005)*1000!))/1000!
1280 NEXT CHAN
1400 RETURN
1498 '
1499 '5 second interrupts driving datalog every minute
1500 FOR PAR=0 TO 7
1510 TEMPOR(FLAG,PAR)=RAWDATA(PAR)
1520 NEXT PAR
1530 IF COATFLAG=1 AND ERRORTRAP=1 THEN COATING=1
1540 IF COATFLAG=1 THEN ERRORTRAP=1 ELSE ERRORTRAP=0
1580 FLAG=FLAG+1
1590 IF FLAG<>12 THEN RETURN
1600 MINUTES=MINUTES+1
1610 FLAG=0
1620 FOR PAR=0 TO 7
1630 FOR LOOP=0 TO 11
1640 DATALOG(MINUTES,PAR)=DATALOG(MINUTES,PAR)+TEMPOR(LOOP,PAR)
1650 NEXT LOOP
1660 DATALOG(MINUTES,PAR)=DATALOG(MINUTES,PAR)/12
1670 NEXT PAR
1680 FOR PAR=1 TO 5
1690 DATALOG(MINUTES,PAR)=(FIX((DATALOG(MINUTES,PAR)+.5)*10))/10
1700 NEXT PAR
1710 IF DATALOG(MINUTES,0)<0 THEN DATALOG(MINUTES,0)=-999
1720 IF DATALOG(MINUTES,0)>10 THEN DATALOG(MINUTES,0)=999
1730 IF DATALOG(MINUTES,7)>10 THEN DATALOG(MINUTES,7)=999
1900 RETURN
1998 '
1999 'voltage to data conversion routine
2000 'Viscovac
2010 RAWDATA(0)=(VOLTAGE(0))/1000
2020 IF VOLTAGE(0)>=9.8 THEN RAWDATA(0)=999
2030 IF VOLTAGE(0)<=.02 THEN RAWDATA(0)=-999
2100 'Nitrogen flow
2110 RAWDATA(1)=FIX(VOLTAGE(1)*200)-2
2120 IF RAWDATA(1)<0 THEN RAWDATA(1)=0
2200 'Methane flow
2210 RAWDATA(2)=FIX(VOLTAGE(2)*200)-2
2220 IF RAWDATA(2)<0 THEN RAWDATA(2)=0
2300 'Argon flow
2310 RAWDATA(3)=FIX(VOLTAGE(3)*400)-4
2320 IF RAWDATA(3)<0 THEN RAWDATA(3)=0
2400 'Temp 1
2410 RAWDATA(4)=FIX((VOLTAGE(4)*88.67299)+5.59339)
2500 'Temp 2
2510 RAWDATA(5)=FIX((VOLTAGE(5)*91.51)+5.106417)
2600 'Pirani gauge
2610 IF VOLTAGE(6)<7 THEN RAWDATA(6)=10^((VOLTAGE(6)*.484643)-2.65224)
2620 IF VOLTAGE(6)>=7 AND VOLTAGE(6)<=9.5 THEN RAWDATA(6)=10^((VOLTAGE(6)*.50477
```

```
5)-3.00212)
2630 IF VOLTAGE(6)>9.5 THEN RAWDATA(6)=10^((VOLTAGE(6)*2.643083)-23.4497)
2640 IF VOLTAGE(6)=0 THEN RAWDATA(6)=-999
2700 'Ion gauge
2710 RAWDATA(7)=10^((VOLTAGE(7)*.603072)-6.01065)
2720 IF VOLTAGE(7)>=9.8 THEN RAWDATA(7)=999
2990 RETURN
2998 '
2999 'real-time data display routine
3000 LOCATE 1,1:PRINT"PVD PROCESS MONITOR V2.1"
3010 LOCATE 1,70:PRINT DATE$
3020 LOCATE 5,12:PRINT "PROCESS TIME =";MINUTES;
3030 IF MINUTES=1 THEN PRINT "minute   " ELSE PRINT "minutes  "
3040 LOCATE 5,46:PRINT "COATING TIME =";MINUTES-COATSTART;
3050 IF MINUTES-COATSTART=1 THEN PRINT "minute   " ELSE PRINT "minutes  "
3500 LOCATE 8,13:PRINT "TEMPERATURE 1 =";RAWDATA(4);"°C      "
3510 LOCATE 8,47:PRINT "TEMPERATURE 2 =";RAWDATA(5);"°C      "
3520 LOCATE 11,13:PRINT "NITROGEN FLOW =";RAWDATA(1);"sccm     "
3530 LOCATE 11,47:PRINT "METHANE FLOW =";RAWDATA(2);"sccm     "
3540 LOCATE 15,31:PRINT "ARGON FLOW =";RAWDATA(3);"sccm     "
3550 LOCATE 19,11
3560 IF RAWDATA(7)<>999 THEN PRINT "ION GAUGE = ";:PRINT USING "#.######";RAWDA'
A(7);
3565 IF RAWDATA(7)=999 THEN PRINT "PIRANI GAUGE = ";:PRINT USING "###.####";RAWI
ATA(6);
3570 PRINT " mbar       "
3580 LOCATE 19,45:PRINT " VISCOVAC = ";
3590 IF RAWDATA(0)<>-999 AND RAWDATA(0)<>999 THEN PRINT USING "#.######";RAWDAT/
(0);
3600 IF RAWDATA(0)<>-999 AND RAWDATA(0)<>999 THEN PRINT " mbar  "
3610 IF RAWDATA(0)=999 THEN PRINT "Over-range      "
3620 IF RAWDATA(0)=-999 THEN PRINT "Under-range     "
3900 RETURN
3998 '
3999 'on screen messages
4000 MESS=0
4010 'LOCATE 23,28: PRINT "                              "
4100 'over temperature message
4110 IF RAWDATA(4)>450 OR RAWDATA(5)>450 THEN MESS=1
4200 'incorrect argon flow message
4210 IF COATING=1 AND RAWDATA(3)<210 THEN MESS=2
4220 IF COATING=1 AND RAWDATA(3)>230 THEN MESS=3
4300 'coating start
4310 COATFLAG=0
4320 IF RAWDATA(1)>20 OR RAWDATA(2)>20 THEN COATFLAG=1
4330 IF COATING=0 THEN COATSTART=MINUTES
4400 'coating end
4410 IF COATING=1 AND RAWDATA(3)<20 AND RAWDATA(7)<.0001 THEN COATEND=1
4420 IF MINUTES=299 THEN COATEND=1
4500 LOCATE 23,28
4510 IF MESS=0 THEN PRINT " Press END to end process "
4520 IF MESS=1 THEN COLOR 31,0: PRINT "   TEMPERATURE TOO HIGH   ": BEEP
4530 IF MESS=2 THEN COLOR 31,0: PRINT "   ARGON FLOW BELOW 11%   ": BEEP
4540 IF MESS=3 THEN COLOR 31,0: PRINT "   ARGON FLOW ABOVE 11%   ": BEEP
4800 COLOR 7,0
4900 RETURN
4998 '
4999 'intro screen
5000 CLS:BEEP
5010 LOCATE 1,1:PRINT"PVD PROCESS MONITOR V2.1"
```

```
5020 LOCATE 1,70:PRINT DATE$
5030 T$=LEFT$(TIME$,2)
5040 V=VAL(T$)
5050 IF V<12 THEN MESSAGE$="GOOD MORNING !"
5060 IF V>=12 AND V<18 THEN MESSAGE$="GOOD AFTERNOON !"
5070 IF V>=18 THEN MESSAGE$="GOOD EVENING !"
5080 LOCATE 5,34:PRINT MESSAGE$
5090 LOCATE 10,1
5100 INPUT;"Enter operator name : ",OP$
5110 PRINT:PRINT
5120 INPUT;"Enter process number/filename (8 chars max) : ",NUM$
5125 PRINT:IF LEN(NUM$)>8 THEN 5120
5130 PRINT
5140 INPUT;"Enter process details : ",DETAIL$
5150 PRINT:PRINT
5160 INPUT;"Ignition resistance status ";IGN$
5170 PRINT:PRINT
5180 PRINT:PRINT
5190 PRINT "          Hit R to REDO this screen, or ANY OTHER KEY to START PROCI
SS"
5200 A$=INPUT$(1)
5210 IF A$="R" OR A$="r" THEN 5000
5298 '
5299 'leaktest
5300 CLS:BEEP:BASEPRESS=999
5310 LOCATE 1,1:PRINT"PVD PROCESS MONITOR V2.1"
5320 LOCATE 1,70:PRINT DATE$
5330 LOCATE 15,11:PRINT "SHUT HIGH VACUUM VALVES AND PRESS A KEY TO BEGIN LEAK T
EST"
5340 GOSUB 1100: GOSUB 2000
5350 IF RAWDATA(7)=999 THEN GAUGE=RAWDATA(6) ELSE GAUGE=RAWDATA(7)
5360 IF GAUGE<BASEPRESS THEN BASEPRESS=GAUGE
5370 LOCATE 10,24:PRINT "BASE PRESSURE = ";:PRINT USING "###.#######";BASEPRESS;
: PRINT " mbar      "
5380 A$=INKEY$
5390 IF A$="" THEN 5340
5400 GOSUB 1100: GOSUB 2000
5410 P1=RAWDATA(7)
5420 START=TIMER
5430 LOCATE 10,24: PRINT "                                        ": LOCATE 15,11: PRIN
T "                                                                "
5440 LOCATE 10,36: PRINT "LEAK  TEST"
5450 FINISH=TIMER
5460 LOCATE 15,39: PRINT FIX(FINISH-START)
5470 IF FINISH<START+60 THEN 5450
5480 GOSUB 1100
5490 GOSUB 2000
5500 P2=RAWDATA(7)
5510 BEEP:LEAKRATE=1
5520 LEAKRATE=((P2-P1)*800)/60
5530 LOCATE 10,36: PRINT "          ": LOCATE 15,39: PRINT "    "
5540 LOCATE 10,5: PRINT "BASE PRESSURE = ";:PRINT USING "###.##";(BASEPRESS*1000
00!);: PRINT " E-05 mbar "
5545 LOCATE 10,48: PRINT "LEAKRATE = ";:PRINT USING "#.##";(LEAKRATE*1000);: PRI
NT " E-03 mbar.l/s"
5550 LOCATE 15,35
5560 IF LEAKRATE>=.0035 THEN PRINT"OOPS - FAILED !" ELSE PRINT " LEAK RATE OK"
5570 BEEP
5580 LOCATE 20,8
5590 PRINT "      Press R to REPEAT leak test or any other key to continue    "
```

```
5600 A$=INPUT$(1)
5610 IF A$="r" OR A$="R" THEN 5300
5620 LOCATE 20,8
5630 PRINT "                                                                    "
5640 LOCATE 20,22
5650 BEEP
5900 RETURN
5998 '
5999 'end menu
6000 CLS:BEEP
6010 LOCATE 1,1:PRINT"PVD PROCESS MONITOR V2.1": LOCATE 1,70: PRINT DATE$
6020 LOCATE 5,23:PRINT "Press P for PRINTOUT of process details"
6030 LOCATE 8,23:PRINT "Press D for DISKSAVE of process details"
6040 LOCATE 11,23:PRINT "Press L for LEAKTEST measurement"
6050 LOCATE 14,23:PRINT "Press N for NEW PROCESS"
6060 LOCATE 17,23:PRINT "Press X for EXIT to DOS"
6070 A$=INPUT$(1): BEEP
6080 IF A$="P" OR A$="p" THEN 6090
6081 IF A$="D" OR A$="d" THEN 7000
6082 IF A$="L" OR A$="l" THEN 8000
6083 IF A$="N" OR A$="n" THEN 9000
6084 IF A$="X" OR A$="x" THEN 9500
6085 GOTO 6070
6088 '
6089 'hardcopy
6090 BEEP
6100 LPRINT"PVD PROCESS MONITOR V2.1"
6110 LPRINT
6120 LPRINT
6130 LPRINT"Date : ";DATE$
6140 LPRINT"Operator : ";OP$
6150 LPRINT"Process number/filename : ";NUM$
6160 LPRINT"Process details : ";DETAIL$
6170 LPRINT
6180 LPRINT"Ignition resistance status : ";IGN$
6190 LPRINT"Base pressure :";: LPRINT USING "###.##";(BASEPRESS*100000!);: LPRI
T" E-05 mbar"
6200 LPRINT"Leak rate :";: LPRINT USING "#.##";(LEAKRATE*1000);: LPRINT " E-03 m
bar.l/s"
6210 LPRINT
6220 LPRINT"Process start time : ";START$
6230 LPRINT
6240 LPRINT
6250 LPRINT"Viscovac    Ion gauge     Nitrogen   Methane   Argon    Temp 1   Tem
p 2    Time "
6260 LPRINT" (mbar)      (mbar)        (sccm)    (sccm)    (sccm)    (°C)     (°
C)    (min)"
6270 LPRINT: FOR LOOP=0 TO MINUTES
6280 IF COATING=1 AND LOOP=COATSTART+1 THEN LPRINT: LPRINT"////////////////////
/////// Start of coating cycle ////////////////////////////"
6290 IF DATALOG(LOOP,0)>-450 AND DATALOG(LOOP,0)<450 THEN LPRINT USING "#.######
   "; DATALOG(LOOP,0); ELSE LPRINT "########    ";
6300 IF DATALOG(LOOP,7)<>999 THEN LPRINT USING "#.######  "; DATALOG(LOOP,7); EL
SE LPRINT "########  ";
6310 LPRINT TAB(28) DATALOG(LOOP,1);
6320 LPRINT TAB(38) DATALOG(LOOP,2) TAB(48) DATALOG(LOOP,3) TAB(57) DATALOG(LOOP
,4);
6330 LPRINT TAB(66) DATALOG(LOOP,5) TAB(74);
6340 LPRINT USING "###";LOOP
6350 NEXT LOOP: LPRINT
```

```
6360 LPRINT"////////////////////////////// End of process ////////////////////
////////////": LPRINT
6400 GOTO 6000
6998 '
6999 'disksave
7000 BEEP
7010 CLS
7020 IF NUM$="" THEN NUM$="NO NAME"
7060 FILE$="C:\PVD\DATA\"+NUM$+".PVD"
7070 LOCATE 22,4: PRINT "DATA FILENAME IS : ";NUM$+".PVD"
7080 LOCATE 22,43: PRINT "FULL DATA STORED AT   C:\PVD\DATA\"
7090 OPEN "O",#1,FILE$
7100 WRITE #1,"PVD PROCESS MONITOR V2.1"
7130 WRITE #1,"Date : ";DATE$
7140 WRITE #1,"Operator : ";OP$
7150 WRITE #1,"Process number/filename : ";NUM$
7160 WRITE #1,"Process details : ";DETAIL$
7180 WRITE #1,"Ignition resistance status : ";IGN$
7190 WRITE #1,"Base pressure :";BASEPRESS;"mbar"
7200 WRITE #1,"Leak rate :";LEAKRATE;"mbar.l/s"
7220 WRITE #1,"Process start time : ";START$
7230 WRITE #1,"Time";"Viscovac";"Ion gauge";"Nitrogen";"Methane";"Argon";"Temp1"
;"Temp2"
7240 WRITE #1,"(mins)";"(mbar)";"(mbar)";"(sccm)";"(sccm)";"(sccm)";"(°C)";"(°C)
"
7290 FOR LOOP=0 TO MINUTES
7300 PRINT #1,LOOP;",";
7310 IF DATALOG(LOOP,0)>-450 AND DATALOG(LOOP,0)<450 THEN PRINT #1,USING "#.####
##,";DATALOG(LOOP,0); ELSE PRINT #1,"    ,";
7320 IF DATALOG(LOOP,7)<>999 THEN PRINT #1,USING "#.######,";DATALOG(LOOP,7); EL
SE PRINT #1,"    ,";
7330 WRITE #1,DATALOG(LOOP,1);DATALOG(LOOP,2);DATALOG(LOOP,3);DATALOG(LOOP,4);DA
TALOG(LOOP,5)
7340 NEXT LOOP
7400 CLOSE #1
7500 BEEP
7510 FILE$="C:\PVD\HGDAT\"+NUM$+".PVD"
7520 LOCATE 23,4: PRINT "DATA FILENAME IS : ";NUM$+".PVD"
7530 LOCATE 23,40: PRINT "HARVARD DATA STORED AT   C:\PVD\HGDAT\"
7540 OPEN "O",#1,FILE$
7550 WRITE #1,"Time (mins)";"Viscovac (mbar)";"Ion gauge (mbar)";"Nitrogen (sccm
)";"Methane (sccm)";"Argon (sccm)";"Temp1 (°C)";"Temp2 (°C)"
7560 FOR LOOP=0 TO MINUTES
7570 PRINT #1,LOOP;",";
7580 IF DATALOG(LOOP,0)>-450 AND DATALOG(LOOP,0)<450 THEN PRINT #1,USING "#.####
##,";DATALOG(LOOP,0); ELSE PRINT #1,"    ,";
7590 IF DATALOG(LOOP,7)<>999 THEN PRINT #1,USING "#.######,";DATALOG(LOOP,7); EL
SE PRINT #1,"    ,";
7600 WRITE #1,DATALOG(LOOP,1);DATALOG(LOOP,2);DATALOG(LOOP,3);DATALOG(LOOP,4);DA
TALOG(LOOP,5)
7610 NEXT LOOP
7620 CLOSE #1
7900 GOTO 6010
7998 'leaktest again
7999 '
8000 CLS:BEEP:BPRESSURE=999
8010 LOCATE 1,1:PRINT"PVD PROCESS MONITOR V2.1"
8020 LOCATE 1,70:PRINT DATE$
8030 LOCATE 15,11:PRINT "SHUT HIGH VACUUM VALVES AND PRESS A KEY TO BEGIN LEAK T
EST"
```

```
8040 GOSUB 1100: GOSUB 2000
8050 IF RAWDATA(7)=999 THEN GAUGE=RAWDATA(6) ELSE GAUGE=RAWDATA(7)
8060 IF GAUGE<BPRESSURE THEN BPRESSURE=GAUGE
8070 LOCATE 10,24:PRINT "BASE PRESSURE = ";:PRINT USING "###.#######";BPRESSURE;
: PRINT " mbar      "
8080 A$=INKEY$
8090 IF A$="" THEN 8040
8100 GOSUB 1100: GOSUB 2000
8110 P1=RAWDATA(7)
8120 START=TIMER
8130 LOCATE 10,24: PRINT "                                        ": LOCATE 15,11: PRI
T "                                                                "
8140 LOCATE 10,36: PRINT "LEAK  TEST"
8150 FINISH=TIMER
8160 LOCATE 15,39: PRINT FIX(FINISH-START)
8170 IF FINISH<START+60 THEN 8150
8180 GOSUB 1100
8190 GOSUB 2000
8200 P2=RAWDATA(7)
8210 BEEP:LRATE=1
8220 LRATE=((P2-P1)*800)/60
8230 LOCATE 10,36: PRINT "          ": LOCATE 15,39: PRINT "    "
8240 LOCATE 10,5: PRINT "BASE PRESSURE = ";:PRINT USING "###.##";(BPRESSURE*1000
00!);: PRINT " E-05 mbar "
8245 LOCATE 10,48: PRINT "LEAKRATE = ";:PRINT USING "#.##";(LRATE*1000);: PRINT
" E-03 mbar.l/s"
8250 LOCATE 15,35
8260 IF LRATE>=.0035 THEN PRINT"OOPS - FAILED !" ELSE PRINT " LEAK RATE OK"
8270 BEEP
8280 LOCATE 20,8
8290 PRINT "      Press R to REPEAT leak test or any other key to continue    "
8300 A$=INPUT$(1)
8310 IF A$="r" OR A$="R" THEN 8000
8320 LOCATE 20,8
8330 PRINT "                                                                  "
8340 LOCATE 20,22
8350 BEEP
8360 GOTO 6000
8998 '
8999 'restart
9000 LOCATE 20,34
9010 COLOR 31,0
9020 PRINT "ARE YOU SURE ?"
9030 COLOR 7,0
9040 BEEP
9050 A$=INPUT$(1): BEEP
9060 IF A$="Y" OR A$="y" THEN RUN
9070 LOCATE 20,34
9080 PRINT "               "
9090 GOTO 6000
9498 '
9499 'exit to dos
9500 LOCATE 20,34
9510 COLOR 31,0
9520 PRINT "ARE YOU SURE ?"
9530 COLOR 7,0
9540 BEEP
9550 A$=INPUT$(1): BEEP
9560 IF A$="Y" OR A$="y" THEN 9600
9570 LOCATE 20,34
9580 PRINT "               "
9590 GOTO 6000
9600 CLS
9610 SYSTEM
```

Process monitor output of gas flow

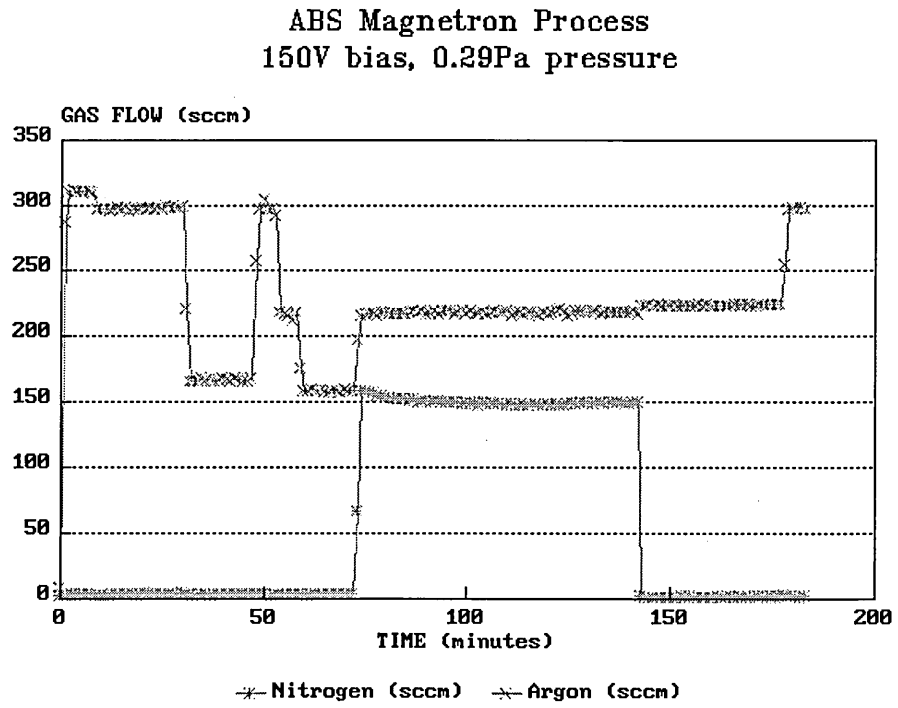

Process monitor output of chamber pressure

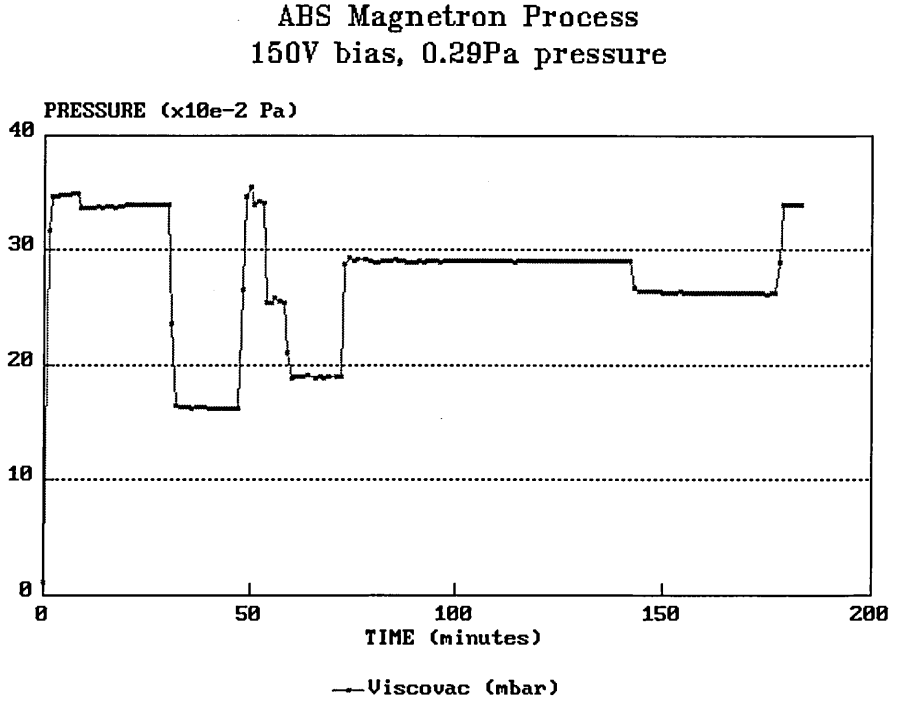

Process monitor output of substrate temperature

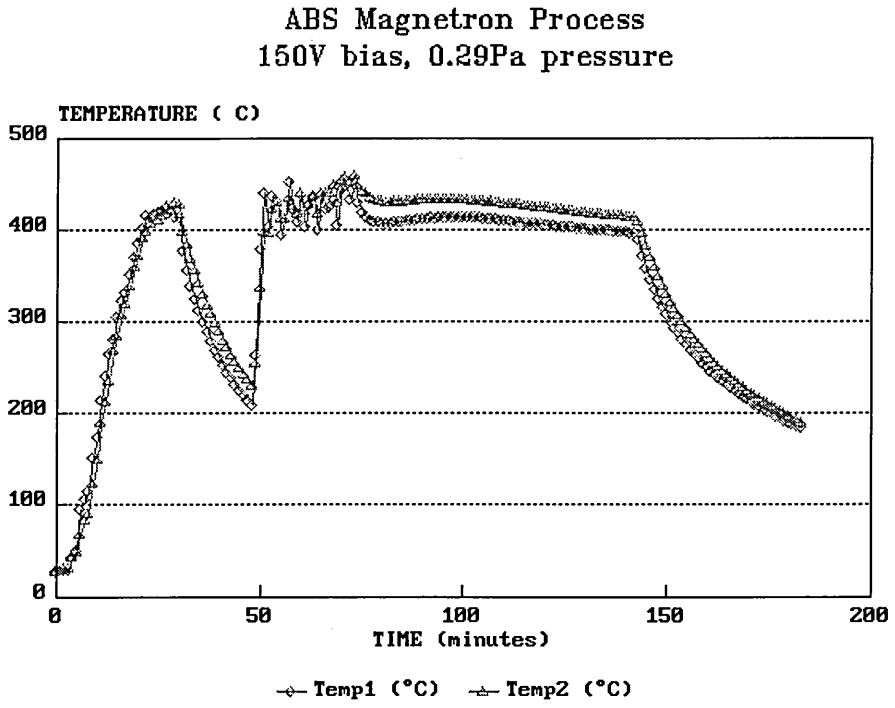

APPENDIX 2
Courses and Conferences Attended

"*Short Course in Analytical Scanning Electron Microscopy for Scientists and Engineers*", May 1990, Sheffield City Polytechnic.

"*Workshop on Current Topics in Advanced PVD Technology for Optical and Wear Resistant Applications*", April 1991, San Diego, California.

"*19th International Conference on Metallurgical Coatings and Thin Films*", April 1991, San Diego, California.

"*Hard Coatings by PVD Methods Workshop*", July 1991, Hull University.

"*3rd International Conference on Advances in Coatings and Surface Engineering for Corrosion and Wear Resistance*", May 1992, Newcastle Polytechnic.

"*Hard Coatings by PVD Methods and Evaluation Techniques Workshop*", October 1992, Sheffield Hallam University.

APPENDIX 3
Publications

"Fundamental Studies of the Steered Arc Technique"
M.Ives, J.S.Brooks, J.Cawley and W.Burgmer, *Surf.Coat.Technol.*, 1991,49, 244.
Presented at the International Conference on Metallurgical Coatings and Thin Films, April 1991, San Diego, California.

"Fundamental Studies of the ABS Enhanced Magnetron Technique"
M.Ives, J.Cawley and J.S.Brooks, *Surf.Coat.Technol.*, 1993,61,127.
Presented at the International Conference on Metallurgical Coatings and Thin Films, April 1993, San Diego, California.

Surface and Coatings Technology, 49 (1991) 244–252

Fundamental studies of the steered arc technique

M. Ives, J. S. Brooks and J. Cawley
Materials Research Institute, Sheffield City Polytechnic, Pond Street, Sheffield S1 1WB (U.K.)
W. Burgmer
Multi-Arc GmbH, Bergisch Gladbach (F.R.G.)

Abstract

Studies were carried out on the physical vapour deposition of titanium nitride wear-resistant coatings by cathodic arc evaporation, incorporating magnetic arc steering. Coatings were laid down under a range of carefully controlled conditions with two process parameters varied, the substrate bias voltage and nitrogen partial pressure. The resulting array of coated samples was subjected to a series of characterization techniques. Test results show the process to be stable over the operating range studied, with several clear trends relating to process parameters. These include a colour shift, a change in microhardness, a change in microstructure and a change in internal stress.

1. Introduction

Physical vapour deposition (PVD) of titanium nitride wear-resistant coatings by cathodic arc evaporation is a tried and tested process that has been successfully used in industry for several years. It is signified by its low deposition temperature (below 500 °C) coupled with a high degree of ionization, which enhances coating density and adhesion [1–4].

However, in a minority of applications, the conventional arc technique is also typified by macroparticle, or droplet, formation which increases surface roughness and can sometimes cause premature failure of the coating [5–7]. Macroparticle formation occurs mainly in the heating–sputtering phase and alternative heating techniques can eliminate this problem.

A recent development of this conventional process is the ability to steer the arc in a predetermined path by means of a magnetic field [8, 9].

This has been reported [10–13] to reduce the frequency and size of macroparticle formation by increasing the speed at which the arc traverses the cathode, so limiting crater size. (Macroparticles are produced when the arc is stationary on the cathode for any length of time, eroding a large crater and forming a large molten pool.)

The purpose of this study is to evaluate the steered arc process, its performance and how the coatings produced change, if at all, with varied process parameters.

2. Experimental details

Coating deposition was performed in a prototype steered arc PVD coating plant produced by Multi-Arc GmbH. This consisted of a diffusion pumped vacuum chamber of 740 l capacity fitted with two steered arc evaporators mounted on adjacent walls. The cathodes were discs of pure titanium, 125 mm in diameter. To ensure consistent starting conditions, the cathodes were replaced at regular intervals to eliminate any variation in Ti^+ emission caused by surface erosion effects.

Substrates were 8 mm high speed steel (HSS) twist drills and polished HSS blocks $9 \times 18 \times 18$ mm^3. These were cleaned and ultrasonically degreased in alkali and freon baths and mounted at a distance of 250 mm from the cathode in a rotating holder in the chamber. They were then sputter cleaned in the vacuum chamber at the start of the coating procedure. Sputtering was carried out in an argon atmosphere with the substrates biased at −1000 V and evaporators operating at 130 A each. The sputtering time was typically 3.5 min and substrates were raised to a temperature of approximately 450 °C, as measured by an IR pyrometer.

The process variables explored were substrate bias voltage (−50 to −200 V) and nitrogen partial pressure (0.1–1.6 Pa). (Reference throughout the text to high and low substrate bias voltages imply absolute values, *i.e.* high bias is −200 V, and low bias is −50 V.) All other parameters remained constant except for coating time which was varied to obtain similar coating thicknesses for comparison. See Table 1 for deposition conditions.

The resulting array of coated samples was subjected to a series of characterization tests involving the following: colour difference measurements (L*a*b* CIE standard test using a Minolta CR-100 colorimeter); surface roughness profiling (using a Mahr Perthen profilometer); microhardness measurements (using a Tukon (model MO) microhardness tester with a Knoop

0257-8972/91/$3.50

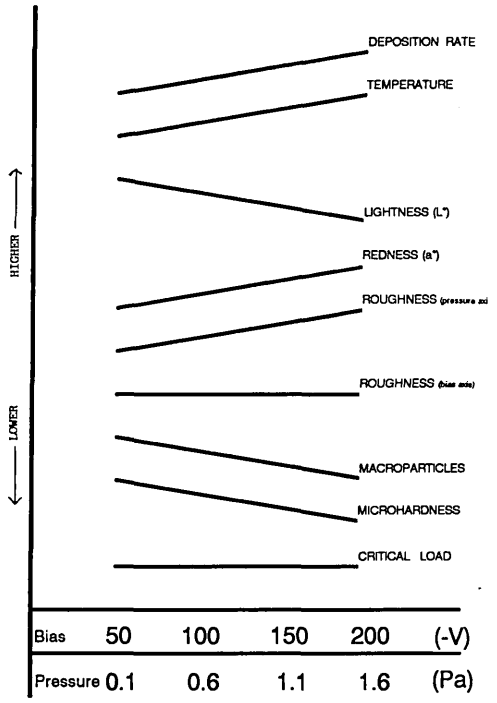

Fig. 1. Coating trends.

diamond indenter under an applied load of 50 g); scratch adhesion testing (on a CSEM Revetest automatic scratch tester, diamond tip radius $R = 0.2$ mm, scratching speed $dx/dt = 10$ mm min^{-1}, loading rate $dL/dt = 100$ N min^{-1}, sensitivity 3 scale units); X-ray diffraction (XRD) analysis; scanning electron microscopy (SEM) examination of microstructure with wavelength dispersive X-ray (WDX) analysis; X-ray photoelectron spectroscopy (XPS) analysis.

3. Results and discussion

The results are summarized in Table 2. Several clear trends are apparent from these results and are shown in Fig. 1 and discussed below.

3.1. Coating colour

The lightness (parameter L* of CIE standard) or reflectance of the coatings decreased with increasing bias and with increasing nitrogen pressure. This suggested a rougher surface finish, but the surface profile measurements did not substantiate this.

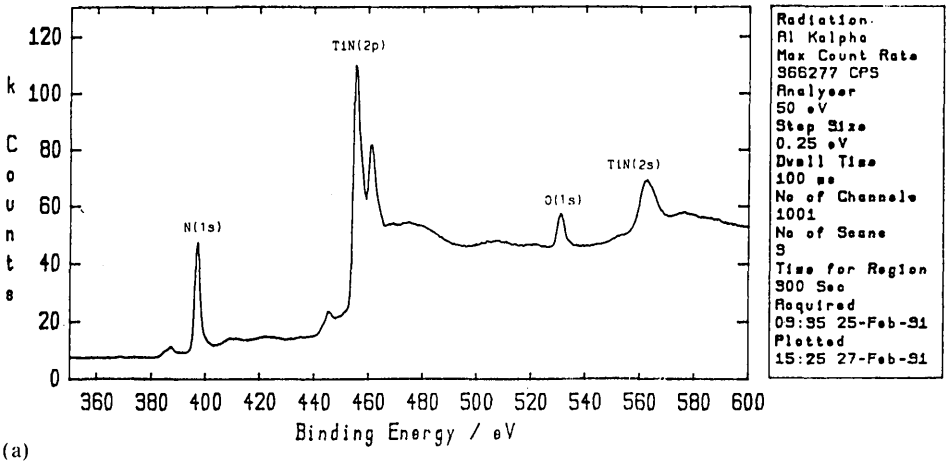

(a)

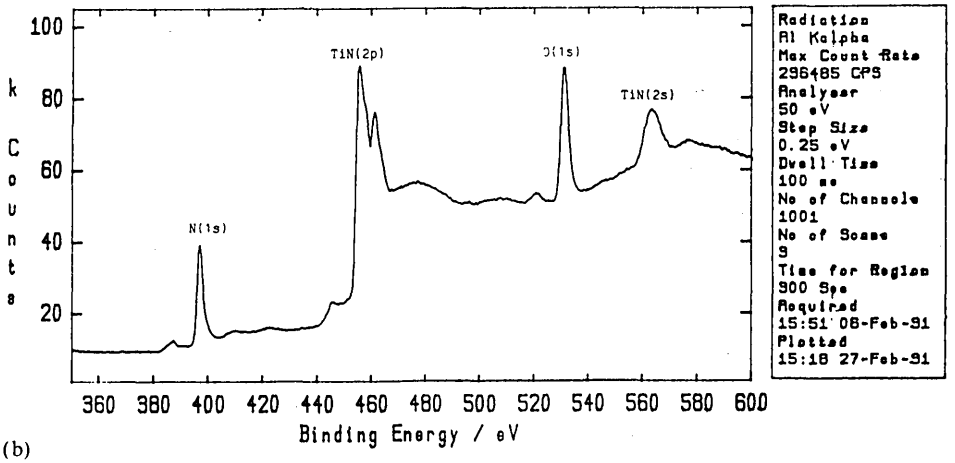

(b)

Fig. 2 (*continued*).

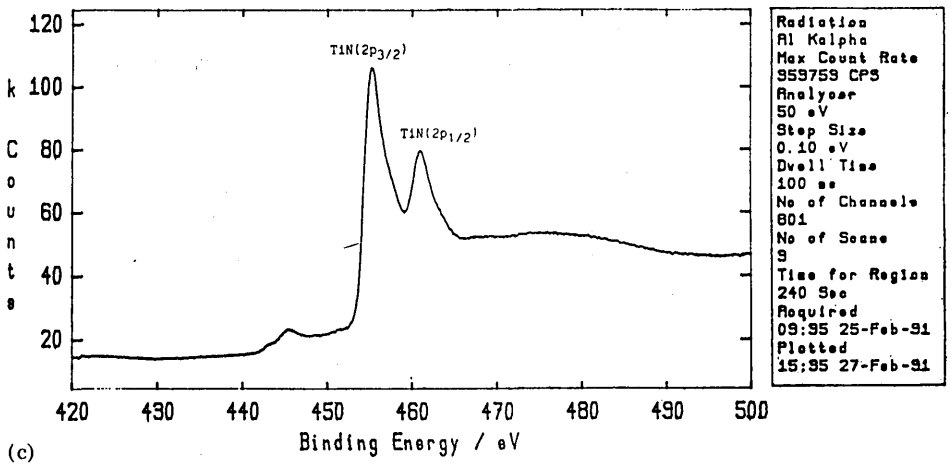

(c)

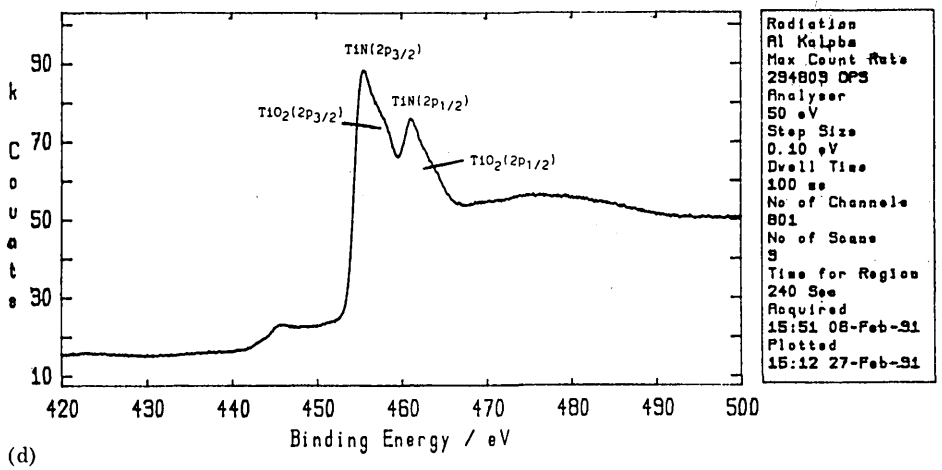

(d)

Fig. 2. XPS results: (a) dense, fibrous coating, small oxygen 1 s peak; (b) porous columnar coating large oxygen 1 s peak; (c) dense, fibrous coating, TiN(2p) peaks detail; (d) porous columnar coating, TiN(2p) peaks with overlapped TiO_2 peaks.

TABLE 1. Deposition conditions

Arc current (A)	130
Number of evaporators	2
Substrate distance (mm)	250
Nitrogen partial pressure (Pa)	0.1–1.6
Substrate bias voltage (−V)	50–200
Coating time (min)	20–90
Substrate temperature during coating (°C)	300–500

Coating times (min)

N_2 (Pa)	Bias (−V)			
	50	100	150	200
1.6	30	27	23	20
1.1	33	30	27	24
0.6	50	47	43	40
0.1	90	86	83	80

Substrate temperatures (°C)

N_2 (Pa)	Bias (−V)			
	50	100	150	200
1.6	336	397	440	495
1.1	305	357	400	442
0.6	276	321	367	403
0.1	315	320	353	390

TABLE 2. Results

Sample number	Thickness (μm)	Colour			Roughness R_z (μm)	Hardness (HK)	Scratch load (N)
		L*	a*	b*			
1	3.0	80.5	−1.9	43.7	1.9	2840	42
2	2.9	79.5	−1.1	43.3	2.6	2510	45
3	2.5	78.5	1.2	42.0	1.9	2220	44
4	2.6	78.6	1.3	43.2	2.0	1870	40
5	3.2	81.5	−3.0	41.3	2.2	2900	42
6	3.5	80.9	−1.8	42.9	2.1	2330	40
7	3.2	79.8	−0.4	43.0	2.1	2210	40
8	2.0	78.1	1.2	41.7	1.6	2110	41
9	2.6	80.0	−2.6	36.3	2.7	3210	40
10	2.6	81.8	−3.0	41.6	2.4	2230	40
11	2.3	80.9	−1.2	43.3	2.2	2040	40
12	2.3	79.0	0.8	40.9	2.1	1950	39
13	3.2	81.8	−3.7	31.3	2.7	3910	42
14	3.0	82.9	−3.9	35.4	2.7	2720	37
15	2.9	83.4	−2.9	40.1	2.5	2470	42
16	2.2	81.2	−2.1	43.5	2.8	2180	40
Standard deviation	0.25	0.2	0.2	0.2	0.4	400	1.5
Uncoated	–	84.4	−2.3	−2.0	0.04	800	–

Key to sample numbers

N_2(Pa)	Bias (−V)			
	50	100	150	200
1.6	1	2	3	4
1.1	5	6	7	8
0.6	9	10	11	12
0.1	13	14	15	16

At the same, time, the redness (parameter a* of CIE standard) of the coating increased with increasing bias and with increasing nitrogen pressure.

Although XRD and WDX failed to reveal any significant compositional change relating to this, XPS did detect some oxygen content in the coating, with increased oxygen levels as the coatings became darker. Indeed, as an extreme example, XPS of a porous black coating found on the vacuum chamber walls showed high oxygen content (Fig. 2). Similar findings have been reported in the literature [14, 15].

3.2. Surface roughness

There was no significant change in roughness with increasing bias. An R_z value of 2.7 μm for the coated surface, compared with 0.04 μm uncoated polished HSS was typical at low nitrogen partial pressure. However, as the partial pressure was increased, surface roughness R_z decreased to 1.9 μm.

This has been reported elsewhere [4, 5, 12] and attributed to cathode poisoning by the nitrogen which reduces macroparticle formation. Micrographs of the coating surfaces (Fig. 3) show larger droplets at low nitrogen partial pressure. At high nitrogen partial pressure, an increase in bias voltage results in fewer droplets. However, it is the smaller droplets that have gone, leaving the large droplets which contribute the same R_z figure.

3.3. Microhardness and structure

The microhardness testing showed lower hardness at higher bias voltage and at higher nitrogen partial pressure.

In relation to the structure zone model [16], microstructural examination of fractured drills (Fig. 4) showed the coatings deposited at high nitrogen partial pressure and bias to have a zone 2 columnar structure changing to the ideal and harder zone T tightly packed

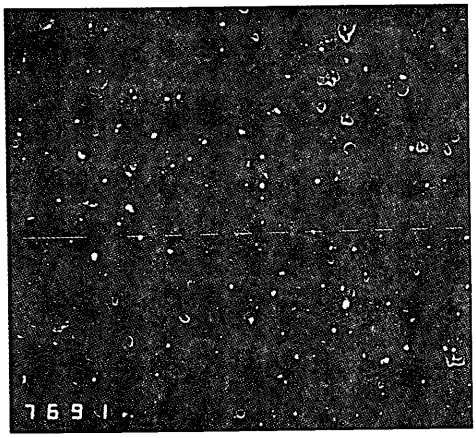

(a)

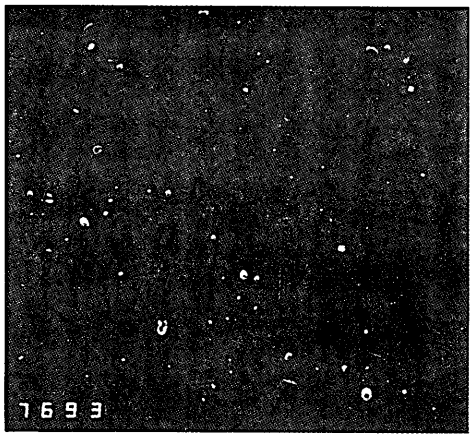

(b)

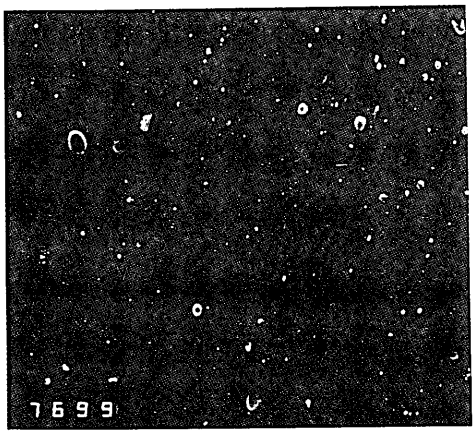

(c)

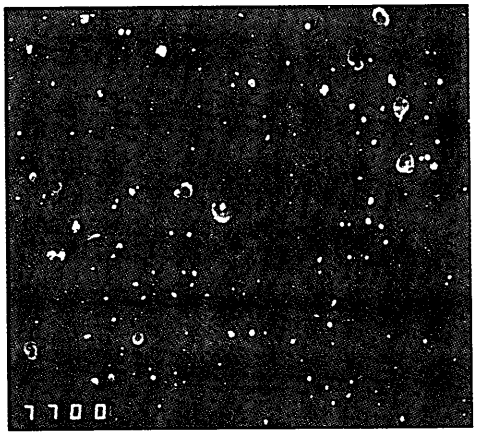

(d)

Fig. 3. Macroparticle micrographs (400×, all to same scale, markers on micrograph (a) represent 10 μm): (a) bias −50 V, N_2 1.6 Pa; (b) bias −200 V, N_2 1.6 Pa; (c) bias −50 V, N_2 0.1 Pa; (d) bias −200 V, N_2 0.1 Pa.

fibrous structure at low pressure and bias. A similar change is reported [17] for TiC films.

This would agree with the observed coating times (inverse of deposition rate) in which the columnar structure was laid down much more quickly than the fibrous structure and also with the observed substrate temperature which tended to remain higher at high N_2 pressure and bias.

It was found that the operating range investigated in this work was (in terms of N_2 pressure, bias voltage and hence temperature) in excess of that required for maximum coating hardness (zone T), though this could be altered by reducing arc current and thus ion energy.

A denser and harder equiaxed (zone 3) structure is attainable but only at much higher deposition tempertures outside the normal operating range and with the possibility of substrate softening.

3.4. Scratch adhesion

Scratch test critical load results showed a fairly uniform failure level at between 40–45 N which is average for TiN on HSS. However, the size of the acoustic emission peak at critical load showed a marked increase at the lowest nitrogen partial pressure (Fig. 5). This is thought to indicate high internal stress in the coating, causing catastrophic failure at penetration. This is not the case at higher nitrogen partial pressures and is probably related to the much shorter coating times.

3.5. X-ray diffraction

XRD using Cu Kα radiation (Fig. 6) reveals a very strong {111} preferential texture in all coatings with no significant change over the parameter range. The composition appears to be TiN–TiC—a small amount of

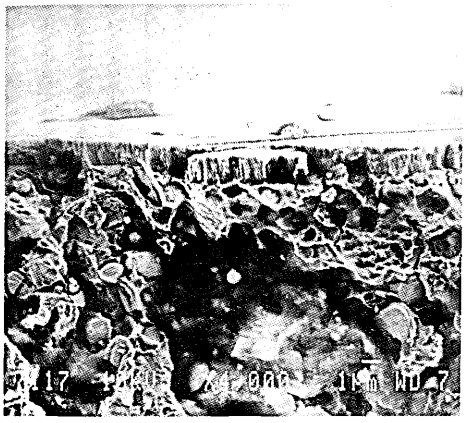

(a)

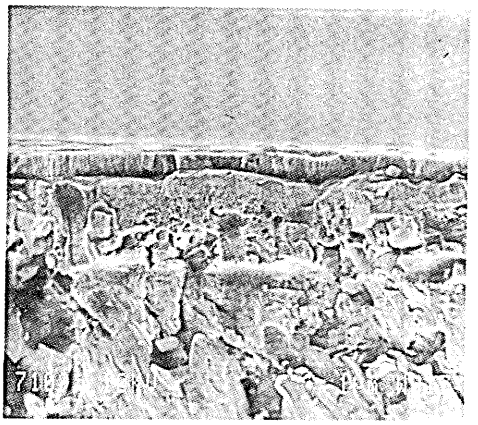

(b)

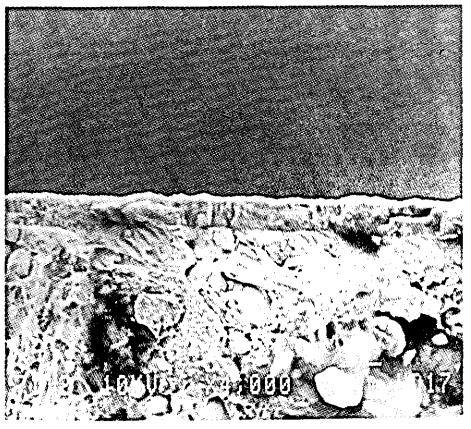

(c)

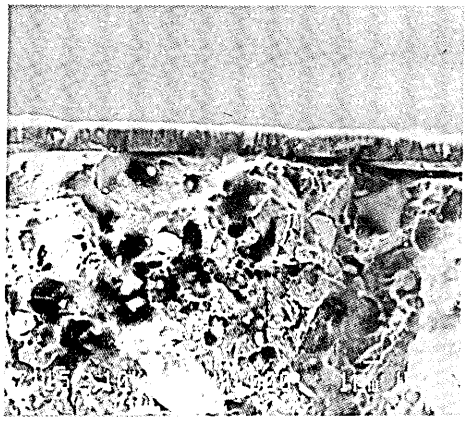

(d)

Fig. 4. Fracture micrographs (4000×): (a) bias −50 V, N_2 1.6 Pa, zone 2; (b) bias −200 V, N_2 1.6 Pa, zone 2; (c) bias −50 V, N_2 0.1 Pa, zone T; (d) bias −200 V, N_2 0.1 Pa, zone 2.

TiC probably forming by diffusion of carbon at the interface from within the steel substrate.

The lattice parameter for the TiN was determined to be 4.28 Å which is in agreement with that found by Roos *et al.* [18] in their steered arc coatings.

3.6. Scanning electron microscopy microstructural and compositional analysis

This was performed using a JEOL 840A scanning electron microscope on drill fracture sections (Fig. 4). These showed a fibrous zone T structure at low bias and low nitrogen pressure and a more columnar zone 2 structure at the higher parameter values.

WDX revealed no significant change in the ratio of titanium to nitrogen throughout the range of coatings produced (Fig. 7). This suggests the coating composition is stable and independent of nitrogen partial pressure above a certain threshold value.

3.7. X-ray photoelectron spectroscopy surface characterization

XPS was carried out in a VG Scientific Microlab 500. Samples were sputter cleaned for 15 min at 4 kV, 150 μA by argon bombardment and then analysed using an aluminium X-ray source at 15 kV, 20 mA.

Results show the oxygen content to be greater in more columnar structured coatings. Some evidence was also found for the presence of TiO_2 where the oxygen contamination appears to be chemically bound to the titanium in the coating (Fig. 2).

4. Conclusion

In general, all the coatings over the parameter ranges tested appeared very similar. There was only a slight detectable variation in the normal yellow–gold colour

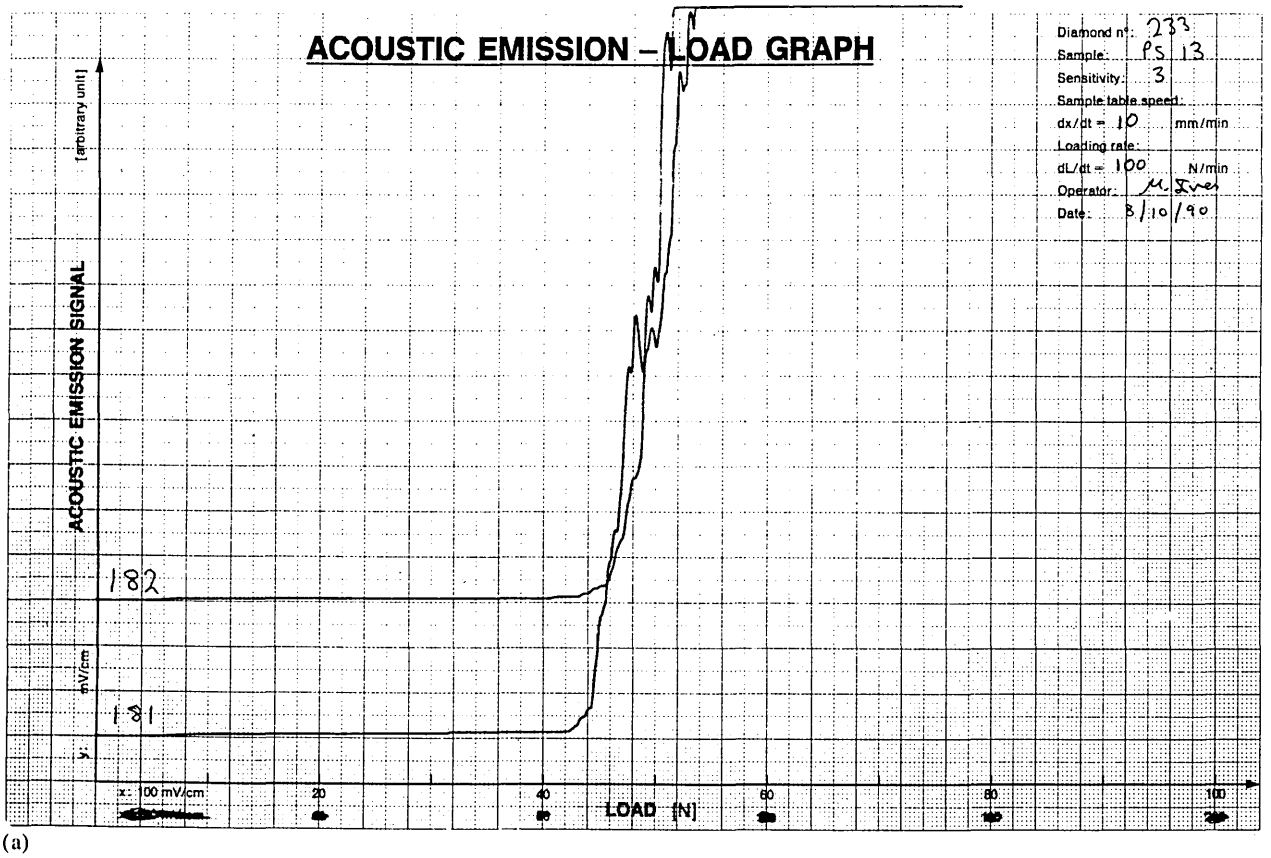

(a)

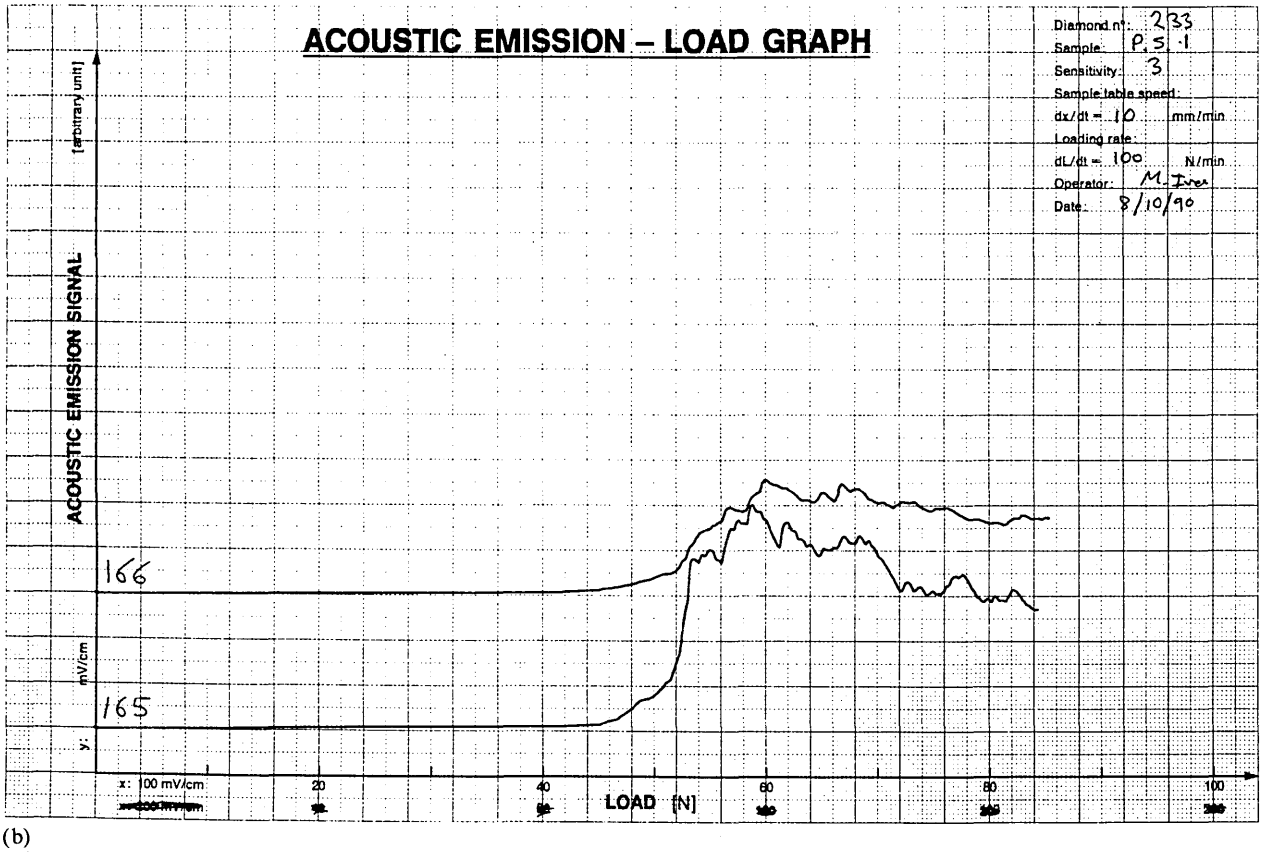

(b)

Fig. 5. Scratch test results: (a) bias −50 V, N_2 1.6 Pa, small acoustic emission peak, limited coating delamination, low residual stress; (b) bias −50 V, N_2 0.1 Pa, large acoustic emission peak, catastrophic coating failure, high residual stress.

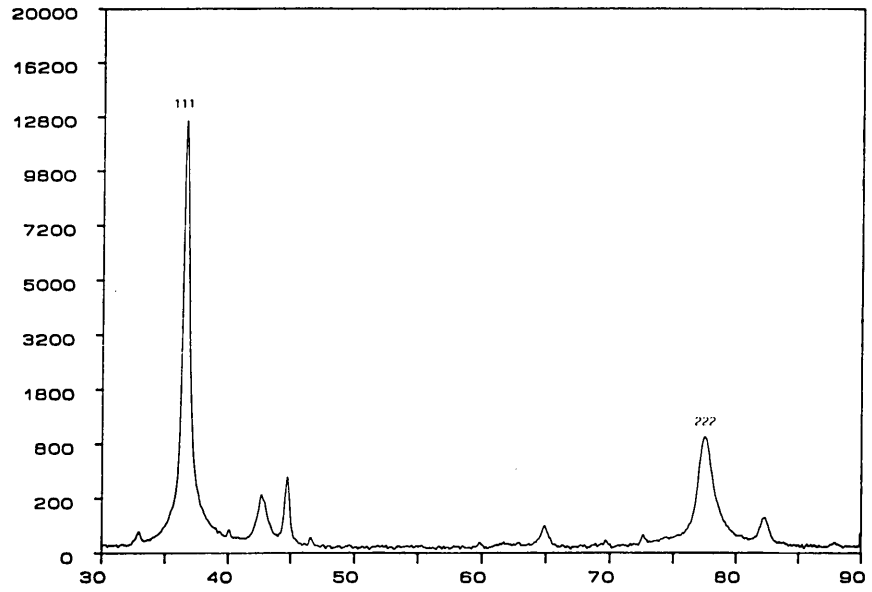

Fig. 6. XRD results: typical trace showing strong 111 peak.

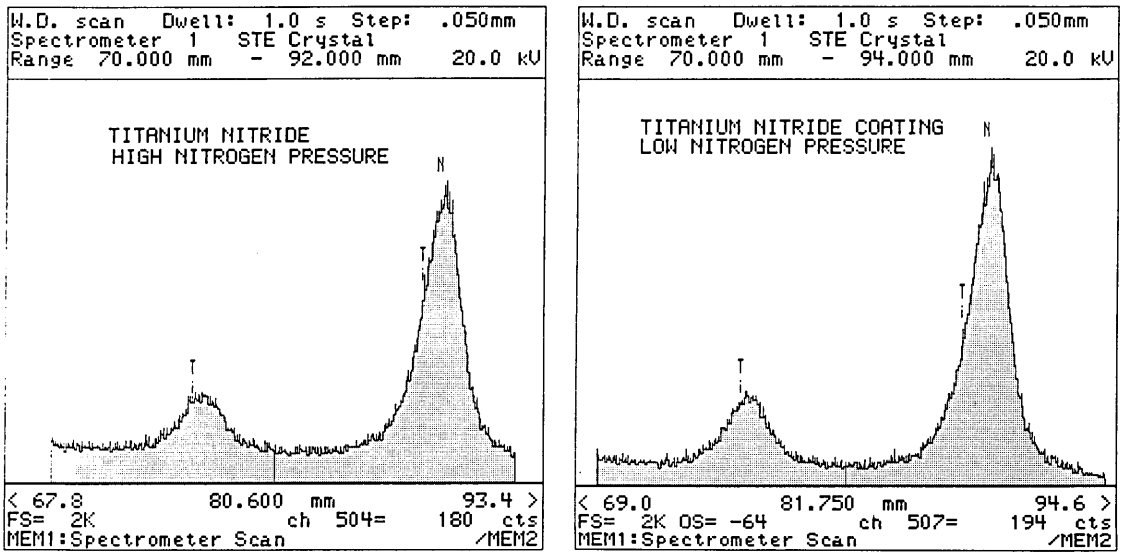

Fig. 7. WDX results.

that is typical of TiN coatings, and scratch tests were virtually identical. Nitrogen pressure, whilst affecting substrate temperature during deposition, did not appear to influence significantly the coating composition. This suggests that the steered arc coating process is stable and quite tolerant over a wide range of operating conditions.

The operating conditions chosen for this work, in general, exceeded those required for maximum coating hardness (maximum hardness only being obtained at low bias and low nitrogen pressure). A reduction in evaporator current to 100 A or less should, by reducing ion energy, result in the desired zone T microstructure-over this same range of substrate bias and nitrogen partial pressure. A softer coating may also be desirable for many uses with its associated reduction in brittleness.

Some bound oxygen was detected, especially in the columnar structured coatings. It has been reported [19] that oxygen at the interface increases the adhesion of TiN coatings to polycarbonate plastic though no increase in adhesion to HSS was observed in this work. However, the presence of oxygen did appear to affect coating colour, and so may be desirable to give an "old gold" or bronze, or even a blue–black colour for the decorative industry.

Acknowledgments

The authors wish to thank Dr. H. J. Heuvel and Mr. H. G. Dederichs for their assistance with coating production, and Dr. B. Lewis and Mr. G. E. Gregory for their help with the analysis techniques and interpretation. Also thanks to Multi-Arc GmbH for use of coating facilities, and the Science and Engineering Research Council for funding with a CASE award.

References

1 B. Rother, *Surf. Eng.*, *4* (4) (1988) 335–341.
2 P. Jacquot, F. Grosset and O. Ribet, *Proc. Int. Seminar on Plasma Heat Treatment Sciences for Technology*, Senlis, France, 21–23 September, 1987, PYC Edns., Paris, 1987, vol. 1, pp. 483–493.
3 P. W. Hatto and D. G. Teer, *Vacuum*, *36* (1–3) (1986) 67–69.
4 C. Bergman, *ASM Conf. on Ion Plating and Implantation*, *1986*, American Society for Metals, Metals Park, OH, 1986, pp. 115–122.
5 P. C. Johnson, *Phys. Thin Films*, *14* (1989) 129–199.
6 C. N. Tai, E. S. Koh and K. Akari, *Surf. Coat. Technol.*, *43–44* (1990) 324–335.
7 P. A. Lindfors, *ASM Conf. on Ion Plating and Implantation*, *1986*, American Society for Metals, Metals Park, OH, 1986, pp. 161–167.
8 S. Ramalingam, C. B. Qu and K. Kim, *U.S. Patent 4,673,477*, 1987.
9 P. Jewsbury, S. Ramalingam and R. F. Chang, *Conf. on Engineering Materials for Advanced Friction and Wear Applications*, Gaithersburg, MD, 1–3 March, 1988, American Society for Metals, Metals Park, OH, 1988, pp. 107–112.
10 D. M. Sanders, *J. Vac. Sci. Technol. A*, *7* (3) (1989) 2339–2345.
11 J. Vyskocil and J. Musil, *Surf. Coat. Technol.*, *43–44* (1990) 299–311.
12 E. Erturk, H. J. Heuvel and H. G. Dederichs, *Surf. Coat. Technol.*, *39–40* (1989) 455–464.
13 S. Boelens and H. Veltrop, *Surf. Coat. Technol.*, *33* (1987) 63–71.
14 B. Zega, *Surf. Coat. Technol.*, *39–40* (1989) 507–520.
15 D. S. Rickerby and S. J. Bull, *Surf. Coat. Technol.*, *39–40* (1989) 315–328.
16 J. A. Thornton, *J. Vac. Sci. Technol.*, *11* (1974) 660.
17 R. F. Bunshah and C. Deshpandey, *Phys. Thin Films*, *13* (1987) 59–107.
18 J. R. Roos, J. P. Celis, E. Vancoille, H. Veltrop, S. Boelens, F. Jungblut, J. Ebberink and H. Homberg, *Proc. Int. Conf. on Metallurgical Coatings*, *1990*, *Thin Solid Films*, *193/194* (1990) 547–556.
19 M. Ahern, *Surf. Coat. Technol.*, *43–44* (1990) 279–287.

Surface and Coatings Technology, 61 (1993) 127–132

Fundamental studies of the ABS-enhanced magnetron sputter technique

M. Ives, J. Cawley and J. S. Brooks

Materials Research Institute, Sheffield Hallam University, City Campus, Pond Street, Sheffield S1 1WB (UK)

Abstract

Studies have been carried out on the physical vapour deposition of titanium nitride wear-resistant coatings by ABS-enhanced magnetron sputtering. This technique incorporates arc etching of the substrates prior to coating; and magnetic unbalancing and field-linking of the cathodes when used in the magnetron mode. Coatings have been deposited under a range of carefully controlled conditions with variations in two of the process parameters: substrate bias voltage and nitrogen partial pressure. The resulting coatings were subjected to a series of characterization techniques. Results show the need for accurate gas flow control in sputtering processes; the problems with maintaining substrate temperature in biased systems; and the benefits to coating adhesion and the interface region from ion bombardment.

1. Introduction and background

Physical vapour deposition (PVD) of wear resistant coatings has been successfully performed using various techniques for several years. It is widely recognised that plasma enhancement within these processes gives a marked improvement to coating quality owing to increased ionization and adatom mobility of the depositing species. Also, lower deposition temperatures (typically below 500 °C) can be realized, which is vital for the coating of heat-sensitive components, such as tool steels, without loss of hardness. Two of the most popular PVD techniques are cathodic arc evaporation and magnetron sputtering.

The cathodic arc evaporation process is signified by its intense degree of ionization and high flux density of evaporating material. The dense plasma produced never requires any secondary ionization enhancement and hence the coatings formed are normally very well adhered [1–4].

However, the process suffers from inefficient cathode utilization, uneven (non-stoichiometric) evaporation of multi-component targets, and most fundamentally, the production of macroparticles (droplets) which increase surface roughness and can lead to premature coating failure [5–7].

Macroparticle formation can be reduced (but not eliminated) by increasing the speed at which the arc traverses the cathode surface by magnetic confinement or steering, or by filtering the produced plasma using a magnetic coil [8–14].

The conventional magnetron sputtering process is signified by its ability to deposit a wide range of materials, both conducting (d.c. mode) or non-conducting (r.f. mode), and by its more uniform cathode erosion track (planar magnetron) when compared with the erosion profile of an arc cathode.

The magnetron itself, already employs a magnetic field to confine secondary electrons and so enhance the degree of ionization, but nevertheless produces a weaker plasma and lower deposition rate than the arc process. Also, it suffers from a very poor "throwing distance" of typically only a few centimetres [15, 16].

By unbalancing the magnetron, in which the outer poles of the existing magnetron magnets are strengthened, it is possible to extend the plasma region (and "throwing distance") out towards the substrate [17]. A further enhancement is to use several such unbalanced magnetrons in an opposed magnet geometry, where the fields are linked and closed (in the x–y plane) around the substrate, so confining and intensifying the plasma in this region [18–21]. Plasma density and ionization by this method are still lower than by a similar cathodic arc arrangement, but more reasonable deposition rates are possible at a cathode-to-substrate distance of 20–30 cm.

The confined arc and unbalanced planar magnetron cathode constructions are technically similar and readily lend themselves to integration into a single cathode unit. Such a unit is capable of operating in either mode, with just a magnetic rearrangement and different power supply characteristics [22].

This is the principle behind the Hauzer ABS (Arc Bond Sputter) system. This claims to offer a "hybrid" coating process utilizing the confined arc mode to "etch" the substrate prior to coating. Thus "implantation" of

0257-8972/93/$6.00

the depositing species is caused and adhesion is enhanced, followed by the droplet-free versatility of an unbalanced magnetron coating [23].

The purpose of this study is to evaluate the ABS process, its performance and how the coatings produced change, if at all, with varied process parameters.

2. Experimental details

Coating deposition was performed in a production HTC 1000-4 ABS PVD coating unit produced by Hauzer Techno Coating Europe B.V. This consisted of a turbo-pumped vacuum chamber of 800 l capacity fitted with four rectangular cathodes of 600 mm × 190 mm working area.

For this study, the standard TiN coating system was chosen, and hence the cathodes were fabricated from 99.98% purity titanium. The reactive gas used was nitrogen (99.999%) and for sputtering the working gas was argon (99.999%).

Reactive gas flow was automatically controlled by a proportional integrating differential controller with feedback of total pressure (argon flow kept constant). Optimal coating pressure was determined manually from a hysteresis plot of nitrogen gas flow *vs.* total pressure, and set at a value just prior to the onset of cathode poisoning (*i.e.* the "knee" of the increasing pressure side of the loop in Fig. 1).

A realistic substrate load of 12 sub-turntable assemblies was used throughout the study. For analysis, 30 mm diameter stubs of polished M2 high speed steel (HSS), 20 × 50 mm strips of 316 stainless steel, and 6 mm HSS drill blanks were used. These were ultrasonically cleaned and degreased in alkali and freon baths, and mounted on the rotating sub-turntable assemblies at a nominal distance of 250 mm from the cathodes.

After pumpdown to a base pressure of typically 8×10^{-4} Pa, with a leak rate better than 5×10^{-2} Pa $l\,s^{-1}$ and water vapour partial pressure less than one-tenth that of nitrogen, the process was begun.

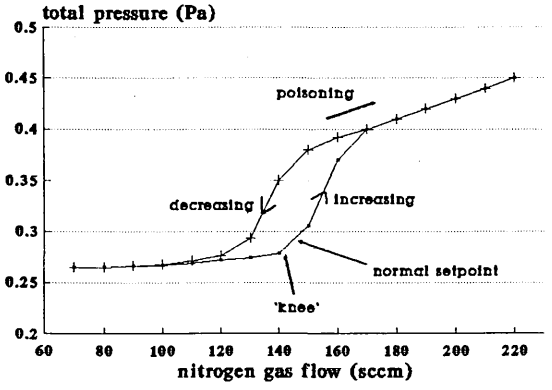

Fig. 1. Nitrogen gas flow *vs.* pressure.

A process run consisted of 30 min argon glow discharge, during which the substrates would be heated to 400 °C and sputtered clean of any residual surface contaminants. This would be followed by 15 min of sputter cleaning of the cathodes themselves, during which shutters would be closed to protect the already cleaned substrates. Normally the arc etching mode would follow, using two alternate cathodes operated at 100 A each and heating the substrates in ten cycles to 450 °C with alternate cooling cycles to 400 °C. Finally, coating in unbalanced magnetron mode, as described earlier with the cathodes operating at 10 kW each, deposited a 1.5–2 μm coating in approximately 60 min. Normal operating pressure was 2.9×10^{-1} Pa (60% Ar, 40% N_2).

During most stages, the substrates were negatively biased to enhance ion bombardment: −1000 V in glow discharge mode, −1200 V in arc etch mode, and normally −150 V in coating mode. References throughout the following text to high and low substrate bias voltages imply absolute values, *i.e.* low bias is −50 V and high bias is −200 V.

The process variables explored were substrate bias voltage (−50 to −200 V) and nitrogen partial pressure (in fact, total pressure was the controlled factor, but since the argon gas flow was kept constant, it was the nitrogen partial pressure that was effectively altered). Pressures of 2.6×10^{-1} Pa and 3.2×10^{-1} Pa were chosen either side of the optimal pressure, but within a feasible operating range for coating deposition.

The resultant coated samples were subjected to a series of characterization tests involving the following:

(i) microhardness measurement using a Tukon (model M0) microhardness tester with a Knoop diamond indenter under an applied load of 50 g;

(ii) surface roughness profiling using a Rank–Taylor Hobson Form Talysurf-120L;

(iii) scratch adhesion testing on a VTT Technology Inc. scratch tester (type ST105) with Rockwell-C diamond tip radius 200 μm, $dl/dx = 10\ N\ mm^{-1}$;

(iv) X-ray diffraction (XRD) analysis on a Philips 1710 based automated powder diffractometer;

(v) glow discharge optical spectroscopy (GDOS) depth profiling using a Leco GDS-750 quantitative depth profiler glow discharge spectrometer;

(vi) scanning electron microscope fractography on a Philips XL40 analytical scanning electron microscope.

3. Results and discussion

The results are summarized in Table 1 and discussed below.

TABLE 1. Summary of results

Pressure (10^{-1} Pa) (±0.05)	Bias (V) (±10)	Temperature (°C) (±20)	Hardness (KHN 50 g) (±50)	Roughness (μm)			Scratch L_c (N) (±5)	XRD				GDOS Ti:N ratio
				R_a (±0.005)	R_z (±0.05)	R_{max} (±0.05)		{111} ratio	{200}	{220}	a_0 (±0.005)	
Arc-etched samples												
2.9	−50	300	950	0.11	2.2	3.1	25	100:	9:	10	4.240	2:3
2.9	−100	360	2400	0.03	1.1	1.9	50	100:	12:	32	4.318	1:1
2.9	−150	430	3200	0.04	1.3	2.2	60	100:	3:	4	4.298	1:1
2.9	−200	460	2500	0.03	1.0	1.5	50	42:	6:	100	4.298	1:1
2.6	−150	400	2000	0.03	1.5	2.9	30	19:	18:	100	4.240	5:3
2.9	−150	430	3200	0.04	1.3	2.2	60	100:	3:	4	4.298	1:1
3.2	−150	400	2400	0.03	1.9	1.5	50	100:	6:	7	4.318	4:5
Non-etched sample												
2.9	−150	400	2400	0.06	1.0	1.3	45	100:	2:	3	4.279	3:4
Uncoated sample												
—	—	—	1000	0.006	0.05	0.05	—	—	—	—	—	—

Coating thickness: 2 μm ± 0.2; substrate material: HSS (M2) except for XRD; XRD substrate material: stainless steel (316).

3.1. Microhardness

Microhardness increases with bias up to −150 V. This is due to greater ion flux with higher bombardment energy, resulting in surface heating and increased adatom mobility, so densifying the growing film. At −200 V there is a change in the preferred orientation of the film (see Section 3.4) owing to the increased ion bombardment, and the resultant structure is softer.

Microhardness peaks at a pressure of 2.9×10^{-1} Pa (the optimum operating pressure as calculated from the hysteresis plot of gas flow). At lower pressure the coating is sub-stoichiometric and predominantly titanium (signified by its metallic silver colour). The coating is dense (see Section 3.6), but has properties more like those of pure titanium and so is softer. At higher pressure, the cathodes start to become poisoned and their efficiency decreases, resulting in reduced titanium flux at the growing surface. Deposition rate is lower and the coating less dense, and hence softer.

3.2. Surface roughness

Surface roughness *vs.* bias is almost constant, except at very low bias (−50 V). At this bias, the coating structure is very porous and open with large-spaced columns (see Section 3.6). Thus the surface finish is rougher and visibly duller.

Reduced surface roughness with increasing pressure is a phenomenon observed in arc coating and normally attributed to reduced macroparticle formation due to cathode poisoning (cathode poisoning increases melting point and arc velocity). Equally, with a sputtering technique, cathode poisoning raises the energy input requirements for sputtering to occur, resulting in lower sputter yield for a given ion bombardment (in effect, sputtering TiN instead of pure Ti). It would appear that droplets or atomic clusters can also emanate from a sputtering cathode (the cathode surface appearing pitted near the centre of the "racetrack"), and this is again reduced by increasing nitrogen pressure and hence poisoning. Too much poisoning will, of course, reduce the sputtering rate to an impracticably low level, hence the need for reactive gas control.

3.3. Scratch adhesion

Scratch adhesion critical load peaks at a pressure of 2.9×10^{-1} Pa (the optimum operating pressure) and falls off on either side. This result mirrors the variation of microhardness with pressure, and coating failure is due to the same reason, *i.e.* a softer coating.

Scratch adhesion *vs.* bias is almost constant, except at very low bias (−50 V). At this bias, the scratch test result as a measure of coating adhesion comes into question, and the limits of the test become apparent.

Microscopic examination of the scratch channel reveals that at −50 V bias, the softer coating suffers ductile failure and the indenter actually penetrates through to the substrate without causing cracking or spallation. At the higher biases, brittle failure, cracking and eventually spallation of the coating occur each time. It would appear that substrate bias has little or no effect on coating adhesion within the range of values studied.

3.4. X-Ray diffraction

XRD using Cu Kα radiation reveals a very strong {111} preferential texture in most of the deposited coatings. The high bias (−200 V) and low pressure (2.6×10^{-1} Pa) coatings, however, both exhibit a {220} preferred orientation (Figs. 2 and 3). Both of these

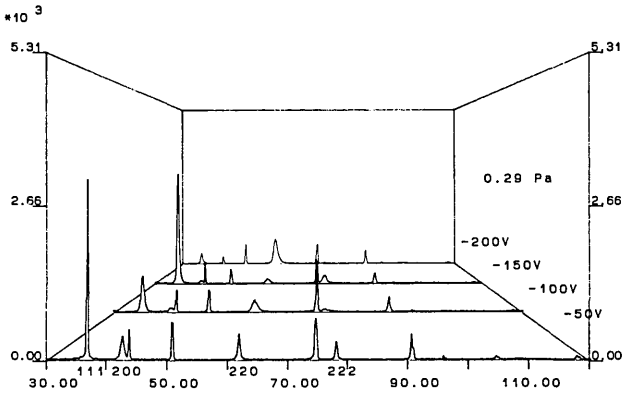

Fig. 2. XRD plots at various bias voltages.

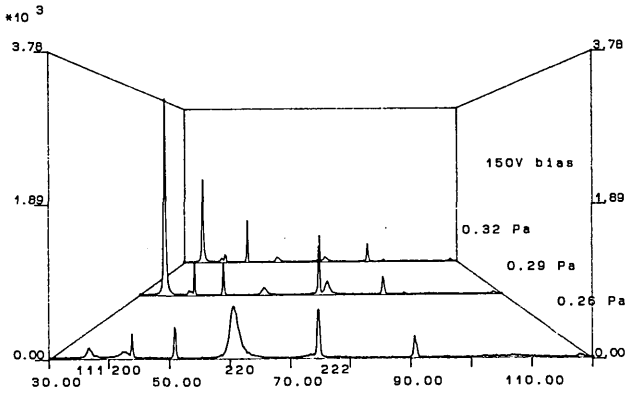

Fig. 3. XRD plots at various pressures.

deposition conditions correspond to an increased ion bombardment flux density (high bias = greater accelerating potential, low pressure = less gas scattering) and a denser film structure (see Section 3.6).

Lattice parameter (a_0) measurements show that at low bias (−50 V) or at low pressure (2.6×10^{-1} Pa), the unit cell is the same size as that quoted in the *JCPDS Powder Diffraction File* data [24]. With increasing bias or pressure, the unit cell distorts and there is lattice expansion due to residual stresses in the coating.

The −100 V coating exhibits an abnormally large unit cell size, and this is due to thermally induced stresses originating from a temperature drop at the start of the coating cycle. The −50 V coating, which also endures a temperature drop, does not suffer the same fate as a result of stress relaxation by the porous structure.

3.5. Glow discharge optical spectroscopy

The GDOS depth profiles were performed after completion of the deposition process. They show a drop in nitrogen concentration with depth through the coating, possibly as a result of increasing density of structure with fewer intercolumnar voids and less nitrogen entrapment (Fig. 4).

The low and high pressure processes produce under- and over-stoichiometric films respectively, as might be expected. Entrapment of nitrogen within the porous structure of the high-pressure film is assumed, since it is very difficult to form an over-stoichiometric chemical compound in an interstitial solid solution.

The low bias (−50 V) coating shows excessive oxygen content (4 wt.% compared with less than 1 wt.% in the other coatings); this is due to the open porous nature of this film (see Section 3.6), and agrees with previous results from X-ray photoelectron spectroscopy of low or un-biased coatings [25]. The −50 V coating also appears to have a high nitrogen to titanium ratio, again possibly a result of nitrogen entrapment in the porous structure.

In the higher bias range (−100 to −200 V), a 1:1 stoichiometric TiN film is formed at optimum pressure (2.9×10^{-1} Pa).

The GDOS results show large coating/substrate diffusion zones rather than abrupt interfaces. This can partly be explained by poor spatial resolution (1 μm) of the GDOS technique owing to a non-flat bottomed erosion crater. However, there is variation in the size of the diffusion zone from sample to sample, and it appears to be related to process temperature. The deeper diffusion zones in some of the arc-etched samples are probably due to the additional heat input and increased density of surface defects caused by the ion bombardment rather than as a result of direct ion implantation [16, 26].

3.6. Scanning electron microscope fractography

Scanning electron microscopy (SEM) examination of fracture sections revealed that the low bias (−50 V) coating had a very porous columnar structure, with a rough surface. At −100 V and above, the columnar structure was denser, and became less well defined (though still present) with increasing bias, indicating possible transition to the fibrous Zone T structure.

The high pressure (3.2×10^{-1} Pa) coating appeared slightly more columnar than that at the optimum pressure, although nothing like the low bias (−50 V) coating.

The low pressure (2.6×10^{-1} Pa) coating appeared very dense, with no discernable columnar structure. The surface of the coating was, however, covered with micrometre-sized droplets, despite deposition by magnetron sputtering. At first this was assumed to have emanated from the arc etch phase, but SEM investigation of an "etch only" sample showed only a few such droplets, indicating that they were indeed produced during the sputtering phase.

4. Conclusion

As far as operation of the ABS process is concerned, it is generally very similar to other PVD systems, but

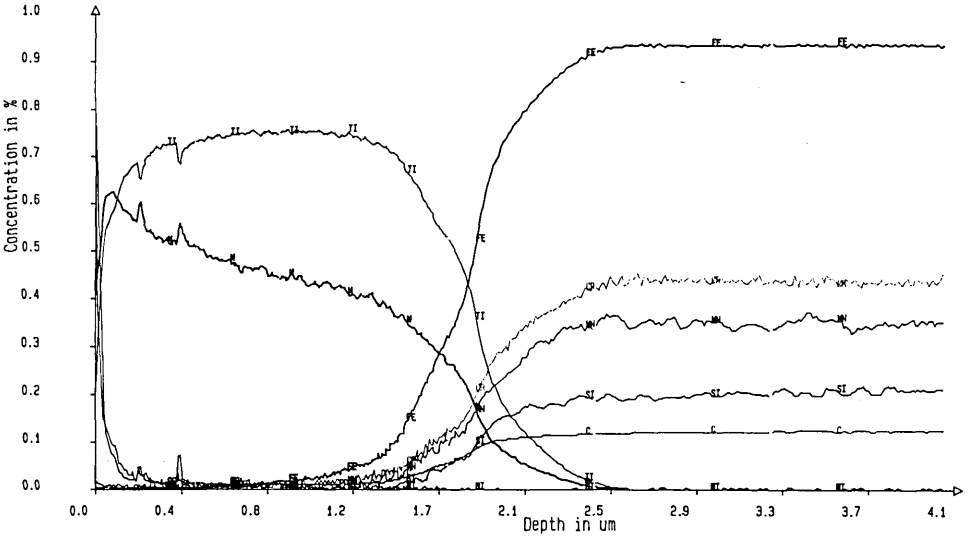

Fig. 4. GDOS depth profile of coating deposited at −150 V bias, 0.29 Pa pressure.

with two heating/cleaning phases instead of one (*i.e.* glow discharge and arc etch stages).

The arc etch phase certainly appears beneficial to the interface region, and hence to coating adhesion, owing to the deposition of a titanium interlayer, the increase in density of surface defects and the additional heat energy input [16]. The rise in surface temperature aids adatom mobility and increases diffusion of titanium into the substrate. Whether titanium ions are actually implanted more than 5 nm into the substrate during this stage is unresolved, but this seems unlikely at the relatively low bombardment energies involved (2400 eV for doubly ionized species) [26].

During the coating phase, problems with maintaining substrate temperature at lower biases or with large loads can lead to thermal stresses in the coating that cause spallation as soon as the substrates cool down. This becomes particularly apparent for coating–substrate combinations with considerably differing thermal conductivities, as in the case of TiN on HSS. This problem can be solved by operating the entire process at lower temperature, or, ideally, by providing additional radiation heating within the vacuum chamber. The latter has the advantage of improving adatom mobility in the growing film and possibly leading to a denser and better structure.

Apart from the −50 V coating, within the range of values studied, bias voltage appears to have little or no effect on stoichiometry, adhesion or surface roughness. It does, however, affect the growing film structure, and hence the crystallographic orientation and microhardness values.

Variations in reactive gas pressure have a much greater effect on all coating properties owing to the inherently sensitive nature of the reactive magnetron sputtering technique. Quite clearly, it is vital to operate the process with an accurately controlled reactive gas partial pressure in order to maintain coating properties and stoichiometry throughout the entire deposition process [27, 28].

Acknowledgments

The authors wish to thank Dr. John Murphy and Leco Instruments for the use of the GDOS facilities, and Rolls Royce plc and the Science and Engineering Research Council (SERC) for funding with a CASE award.

References

1 B. Rother, *Surf. Eng., 4* (4) (1988) 335.
2 P. Jacquot, F. Grosset and O. Ribet, *Proc. Int. Seminar on Plasma Heat Treatment Sciences for Technology*, Vol. 1, 1987, pp. 483–493.
3 P. W. Hatto and D. G. Teer, *Vacuum, 36* (1–3) (1986) 67.
4 C. Bergman, *ASM Conf. on Ion Plating and Implantation, 1986*, American Society for Metals, Metals Park, OH, 1986, pp. 115–122.
5 P. C. Johnson, *Phys. Thin Films, 14* (1989) 129.
6 C. N. Tai, E. S. Koh and K. Akari, *Surf. Coat. Technol., 43–44* (1990) 324.
7 P. A. Lindfors, *ASM Conf. on Ion Plating and Implantation, 1986*, American Society for Metals, Metals Park, OH, 1986, pp. 161–167.
8 D. M. Sanders, *J. Vac. Sci. Technol. A, 7* (3) (1989) 2339.
9 J. Vyskocil and J. Musil, *Surf. Coat. Technol., 43–44* (1990) 299.
10 E. Erturk, H. J. Heuvel and H. G. Dederichs, *Surf. Coat. Technol., 39–40* (1989) 455.
11 S. Boelens and H. Veltrop, *Surf. Coat. Technol., 33* (1987) 63.
12 K. Akari, H. Tamagaki, T. Kumakiri, K. Tsuji, E. S. Koh and C. N. Tai, *Surf. Coat. Technol., 43–44* (1990) 312.
13 P. Sathrum and B. F. Coll, *Surf. Coat. Technol., 50* (1992) 103.
14 P. J. Martin, R. P. Netterfield, A. Bendavid and T. J. Kinder, *Surf. Coat. Technol., 54–55* (1992) 136.

15 R. K. Waits, *J. Vac. Sci. Technol., 15* (2) (1978) 179.
16 J. A. Thornton, *Metal Finishing, 77* (5) (1979) 83.
17 N. Savvides and B. Window, *J. Vac. Sci. Technol. A, 4* (3) (1986) 504.
18 S. L. Rohde, I. Petrov, W. D. Sproul, S. A. Barnet, P. J. Rudnik and M. E. Graham, *Thin Solid Films, 193–194* (1990) 117.
19 W. D. Sproul, P. J. Rudnik, M. E. Graham and S. L. Rohde, *Surf. Coat. Technol., 43–44* (1990) 270.
20 W.-D. Münz, *Surf. Coat. Technol., 48* (1991) 81.
21 W. D. Sproul, *Surf. Coat. Technol., 49* (1991) 284.
22 P. Robinson and A. Matthews, *Surf. Coat. Technol., 43–44* (1990) 288.
23 W.-D. Münz, D. Schulze and F. J. M. Hauzer, *Surf. Coat. Technol., 50* (1992) 169.
24 *JCPDS Powder Diffraction File*, Set 6–10 (1967) 135.
25 M. Ives, J. S. Brooks and J. Cawley, *Surf. Coat. Technol., 49* (1991) 244.
26 S. Kadlec, J. Musil and J. Vyskocil, *Surf. Coat. Technol., 54–55* (1992) 287.
27 W. D. Sproul, *Surf. Coat. Technol., 33* (1987) 73.
28 W. D. Sproul, *Surf. Coat. Technol., 39–40* (1989) 499.